REPORT DOCUMENTATION PAGE

Form Approved
OMB NO. 0704-0188

1. AGENCY USE ONLY (Leave Blank)	2. REPORT DATE	3. REPORT TYPE AND DATES COVERED
	January 2004	Final Report 01-Jun-2003 to 30-Nov-2003

4. TITLE AND SUBTITLE
Research Study Towards a MEFFV Electric Armament System

5. FUNDING NUMBERS
N00014-03-1-0834

6. AUTHOR(S)
J.A. Pappas, J.R. Kitzmiller, G.A. Wedeking, M.D. Werst, G.B. Frazier, W. Smith, D. Milner, A. Toepfer, and M. Erengil

7. PERFORMING ORGANIZATION NAME(S) AND ADDRESS(ES)
Center for Electromechanics, The University of Texas at Austin, 1 University Station, R7000, Austin, TX 78712

8. PERFORMING ORGANIZATION REPORT NUMBER
RF-220

9. SPONSORING / MONITORING AGENCY NAME(S) AND ADDRESS(ES)
Office of Naval Research
Ballston Centre Tower One
800 North Quincy Street
Arlington VA 22217-5660

10. SPONSORING / MONITORING AGENCY REPORT NUMBER

11. SUPPLEMENTARY NOTES

12 a. DISTRIBUTION / AVAILABILITY STATEMENT
Approved for public release; distribution unlimited.

12 b. DISTRIBUTION CODE

13. ABSTRACT (Maximum 200 words)

The U.S. Marine Corps Marine Family of Fighting Vehicles (MEFFV) Program is focused on developing a fighting vehicle that is survivable and lethal on the battlefield of 2020 and beyond. One vehicle variant seeks to exploit synergies between electric mobility and electric armament systems by employing a hybrid electric mobility propulsion system and an electric gun for an all Electric MEFFV.

The objective of this project was to determine the feasibility, benefits, and technical challenges associated with the E-MEFFV. A point design approach was used to accomplish the program objective. This entailed developing an array of options for some major vehicle subsystems. It also entailed accepting results of other relevant studies (e.g., results of the Army Electric Gun Program) and developing an array of options for principle performance specifications (e.g., lethality requirements, silent watch requirements, or vehicle speed). Various combinations of component and performance options were evaluated in order to identify a small subset of viable components worthy of more detailed investigation. Investigations evolved through increasingly more detailed performance simulation, packaging studies, and vehicle configuration studies as the subset of viable components became smaller. The process resulted in a concept design that includes vehicle configuration, weight estimates, and performance simulations, top-level design specifications, and a technology development roadmap to enable realization of the E-MEFFV.

14. SUBJECT TERMS
electric gun, railgun, pulsed alternator, high power converter, MEFFV, hybrid electric vehicle; wound composite materials

15. NUMBER OF PAGES
204

16. PRICE CODE

17. SECURITY CLASSIFICATION OR REPORT	18. SECURITY CLASSIFICATION ON THIS PAGE	19. SECURITY CLASSIFICATION OF ABSTRACT	20. LIMITATION OF ABSTRACT
UNCLASSIFIED	**UNCLASSIFIED**	**UNCLASSIFIED**	**UL**

NSN 7540-01-280-5500

Standard Form 298 (Rev.2-89)
Prescribed by ANSI Std. 239-18
298-102

Research Study Towards a MEFFV Electric Armament System

Final Report

submitted to:

Michael S. Byerly
Office of Naval Research

Submitted by:
J.G. Pappas, J.R. Kitzmiller G.A. Wedeking, and M.D. Werst
UT-CEM

G.B. Frazier, WilfordSmith, David Milner, and Al Toepfer
SAIC

M. Erengil
UT-IAT

RF 220

Center for Electromechanics
The University of Texas at Austin
1 University Station
R7000
Austin, TX 78712
(512) 471-4496 fax (512) 471-0781

January 2004

Contents

Tables

Figures

I. Introduction and Summary

The U.S. Marine Corps Marine Family of Fighting Vehicles (MEFFV) Program is focused on developing a fighting vehicle that is survivable and lethal on the battlefield of 2020 and beyond. One vehicle variant seeks to exploit synergies between electric mobility and electric armament systems by employing a hybrid electric mobility propulsion system and an electric gun for an all Electric MEFFV. The objective of this project was to determine the feasibility, benefits, and technical challenges associated with the E-MEFFV.

A point design approach was used to accomplish the program objective. This entailed developing an array of options for some major vehicle subsystems. It also entailed accepting results of other relevant studies (e.g., results of the Army Electric Gun Program) and developing an array of options for principle performance specifications (e.g., lethality requirements, silent watch requirements, or vehicle speed). Various combinations of component and performance options were evaluated in order to identify a small subset of viable components worthy of more detailed investigation. Investigations evolved through increasingly more detailed performance simulation, packaging studies, and vehicle configuration studies as the subset of viable components became smaller. The approach allowed the team to quickly move to a nearly optimized system that, at the very least, represents a good choice of subsystem and component technologies for the final and most detailed quantitative analysis and simulations. The process resulted in a concept design that includes vehicle configuration, weight estimates, and performance simulations, top-level design specifications, and a technology development roadmap to enable realization of the E-MEFFV.

The vehicle, hybrid motive drive system, and electric armaments system concepts are shown in figures I-1 and I-2. The vehicle has a top speed of 90 km/h and cruises at 50 km/h. The installed prime power is 1 MW. The electric gun system is capable of firing a five round burst of 9 MJ launch packages at 2.9 km/s with shot rate limited by the autoloader. The thermal management system is sized to reject heat from all systems and auxiliaries at 600 kW. The overall mass of the entire vehicle weapons system and primary armor is approximately 35 metric tons. The mass is 38 metric tons if active armor is included.

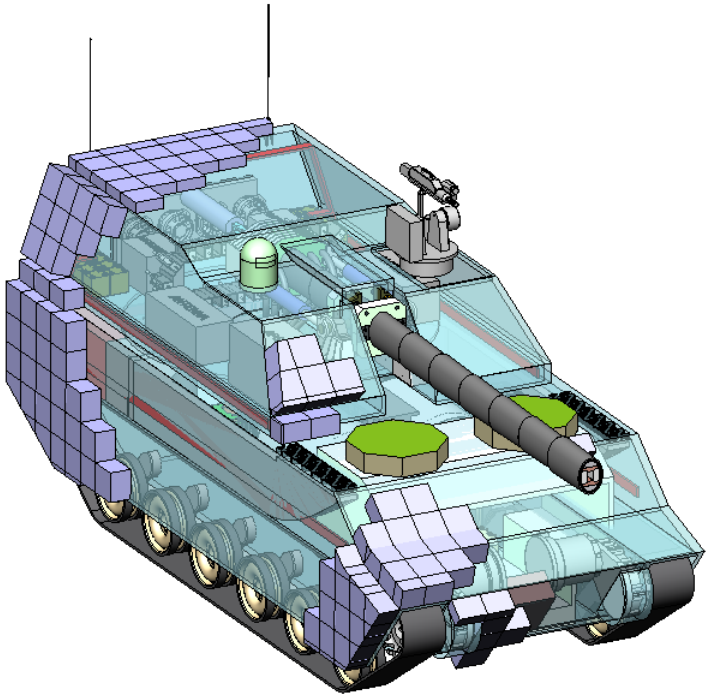

Figure I-1. Solid model of electric MEFFV concept (front view) - including electric weapons, active armor tiles, hybrid electric drive and auxiliary systems.

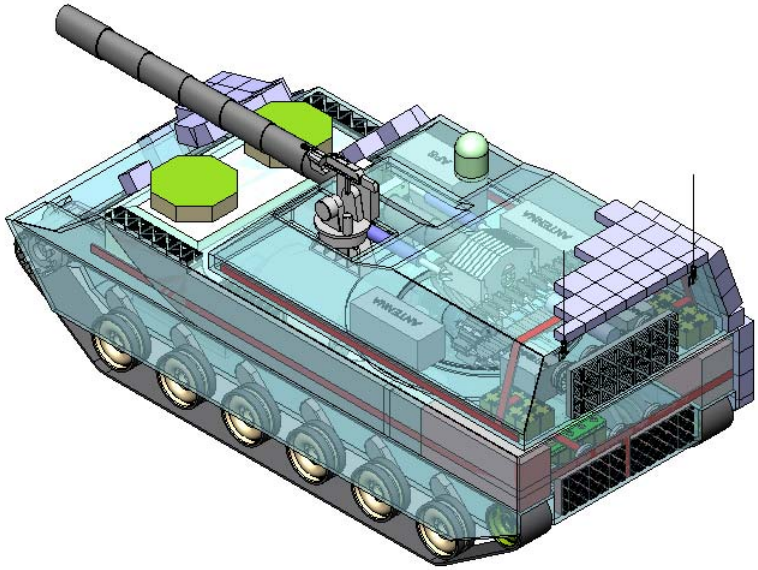

Figure I-1. Solid model of electric MEFFV concept (rear view, turret partially cut away)

An IPT management structure was used to incorporate the expertise of the five stakeholders in this project: The Office of Naval Research, the MEFFV program office, the Center for Electromechanics, the Institute for Advanced Technology, and Science Applications International Corporation. SAIC led the effort to develop the mission and vehicle requirements. The IAT led the effort in launch package design and lethality. The launch package and lethality sections were submitted directly to the sponsor by the IAT as a separate annex to this report. CEM led the design of the electric gun and pulsed power supply and produced the vehicle configuration concept.

ONR provided system performance requirements directly as well as through the MEFFV program office and Booz Allen as part of an overall MEFFV system study. The contractor team incorporated the requirements information as the bases for the trade analyses and studies.

Power requirements for the MEFFV vehicle presented in this study are based on force-on-force simulations using the M30 Assault Variant as a surrogate for the MEFFV. The power requirement for the M30's mobility and gun firing were determined using two independent analyses. Power requirements for vehicle movement were calculated with two modeling programs: JCATS and CHPSPerf. The former, JCATS, is a force-on-force simulation program that provides data from individual tanks in a simulated combat setting between two large multi-unit forces. The latter, CHPSPerf, is a model that determines the power demands and energy management information for a hybrid electric vehicle based upon that vehicle's movement and energy loads. The vehicle movement output from the JCATS model was input to the CHPSPerf program to determine the power demands in the JCATS simulation. In addition, the gun firing output from the JCATS model was input to a second model to calculate power demands with respect to time for the unit's firing during the simulation.

A detailed study of the MEFFV system mobility and weapon and defensive armaments power requirements was performed. Results of the analyses were used to develop and select the power system solution for the MEFFV. The trades led to a series hybrid solution as the logical choice for powering a system with high sustained non-mobility electrical power loads characteristic of EM gun equipped direct fire vehicles. The series hybrid power system envisioned for this application will provide power to multiple electric loads with diverse power

requirements. Integration of the power consuming and power producing components was accomplished through a re-configurable hierarchical control system that automatically selects the best component or combination of components for providing load power demands. This architecture makes possible high-power weapons systems operation, hyper-mobility, hill-climbing, and limited silent watch/mobility in a system weight class unachievable with conventional power architecture technologies.

Lethality requirements were derived from the Booz Allen mission studies and the launch package design is based on the launch requirements of the penetrator. Mass and velocity from the lethality and launch package trade studies and designs were incorporated as input parameters to the pulse power supply and vehicle design trade studies and point designs. Because most of the lethality and launch package trade studies are classified, the report on these topics was submitted by the IAT as a separate annex.

The pulsed alternator trades have resulted in a concept design that the team believes will define the entry-level machine for integration into a main battle. If adequately funded, this prototype could be realized by 2010. While a prototype of this alternator has not been built, the technology assumptions used in the design is supported by extensive engineering analysis and some hardware development. The basic trades and alternator concept design was accomplished by employing, for the first time, CEM-UT's sizing algorithm called the Advanced Pulsed Alternator Design System (APADS). APADS is a combination of MATLab scripts and FORTRAN source code that together define an accurate solid model of the pulsed alternator best suited to drive a given railgun load. Output from APADS defines the PA critical design parameters and generates a solid model containing basic dimensions and material properties. APADS also generates input files for the system performance simulation.

The power converters control power flow between the pulsed alternator and gun and control the alternator's charge sequence. Both the gun switch converter (GSC) and the field coil converter (FCC) are bi-directional converters. That is, they both operate as rectifier and inverter. The basic requirements for the converters come from the pulse power system design and detailed performance simulation.

Both the GSC and FCC handle extremely large peak power at voltage on the order of 15 kV. The extreme operating conditions drive the designer toward switching devices that can handle high current and voltage. While lower-power devices can be used, the mass, volume, and reliability penalties associated with packaging large numbers of small devices quickly become apparent. Therefore, the device most often chosen is a symmetrical thyristor, or SCR. Even large thyristors cannot handle the entire discharge power. As a result, the SCRs are arranged in appropriate series- and parallel-connected arrangements. The thyristors control the power flow, must share and withstand voltage, turn on under relatively extreme rates of current rise, and turn off when current flow through them reverses. In addition, because the devices are arranged in series-parallel arrays, the SCRs must share current and voltage well; no single device can handle the thermal or voltage loads impressed by the alternator.

No existing device can meet the operating requirements of the MEFFV system in the space allotted. Therefore, devices were extrapolated from existing technology with development requirements that range from those realizable in the near term to those requiring longer-term development. In either case, given appropriate support, there is a reasonable chance that any of the forecast devices could be produced by 2010. Both advanced silicon and silicon-carbide devices were considered in the power converter trades.

The vehicle concept design presented in this report is based on assumptions used in the electric gun and vehicle subsystem trade studies and concept designs. Technology development is required in each of the major subsystems of the electric gun system and vehicle drive train. The impact of the design assumptions and the technology development requirements are contained in the requirements and technology development subsections for each major subsystem and together constitute the team's recommendations for investment in electric gun and vehicle technology development for an electric MEFFV.

II. Mission Requirements Analysis

Introduction and Requirements

Power requirements for the MEFFV vehicle presented in this study are based on force-on-force simulations using the M30 Assault Variant as a surrogate for the MEFFV. The power requirement for the M30's mobility and gun firing were determined using two independent analyses. Power requirements for vehicle movement were calculated with two modeling programs: JCATS and CHPSPerf. The former, JCATS, is a force-on-force simulation program that provides movement and firing data (among other things) from individual tanks in a simulated combat setting between two large multi-unit forces. The latter, CHPSPerf, is a model that determines the power demands and energy management information for a hybrid electric vehicle based upon that vehicle's movement and energy loads. The vehicle (or unit) movement output from the JCATS model was input to the CHPSPerf program to determine the power demands in the JCATS simulation. In addition, the gun firing output from the JCATS model was input to a second model to calculate power demands with respect to time for the unit's firing during the simulation.

The analysis revealed that with a prime power capability in the 1 MW class the vehicle should be able to handle most of the power loads required in the battle. The vehicle had no problem with movement, never needing more than 600 kW of power even for periods of peak acceleration. The vehicle did have some difficulty firing all shots in the scenario, since the CPA's bus power draw occasionally peaked around 1.500 MW. These peaks only occurred during long bursts of shots in short periods of time, and much less power was required for most other portions of the battle.

Methods Employed and Assumptions Used

Booz Allen conducted a Lethality Study [II-1] to examine unit movements and gun firing in a simulated battle scenario. The scenario was composed of seven different operational vignettes between two large forces. The vignettes for one force are shown as arrows or lines and numbered in figure II-1. Each vignette was modeled discreetly, but was linked chronologically to

the larger integrated scenario. In order, these were "Movement to Contact", "Hasty Attack", "Screen", "Defend", "Counter-Attack", "Urban Raid", and "Deliberate Attack with Breach" for the overall conflict. Each unit in the battle conducted autonomous move, wait or fire tasks during each vignette. Each gun firing task for a unit was denoted as an "engagement". The actions of all units in the battle scenario were based on modern tactics of warfare that were integrated into the JCATS model to make the simulation as realistic as possible. We obtained the output data from this study by Booz Allen and conducted the power analyses on it using CHPSPerf and Excel.

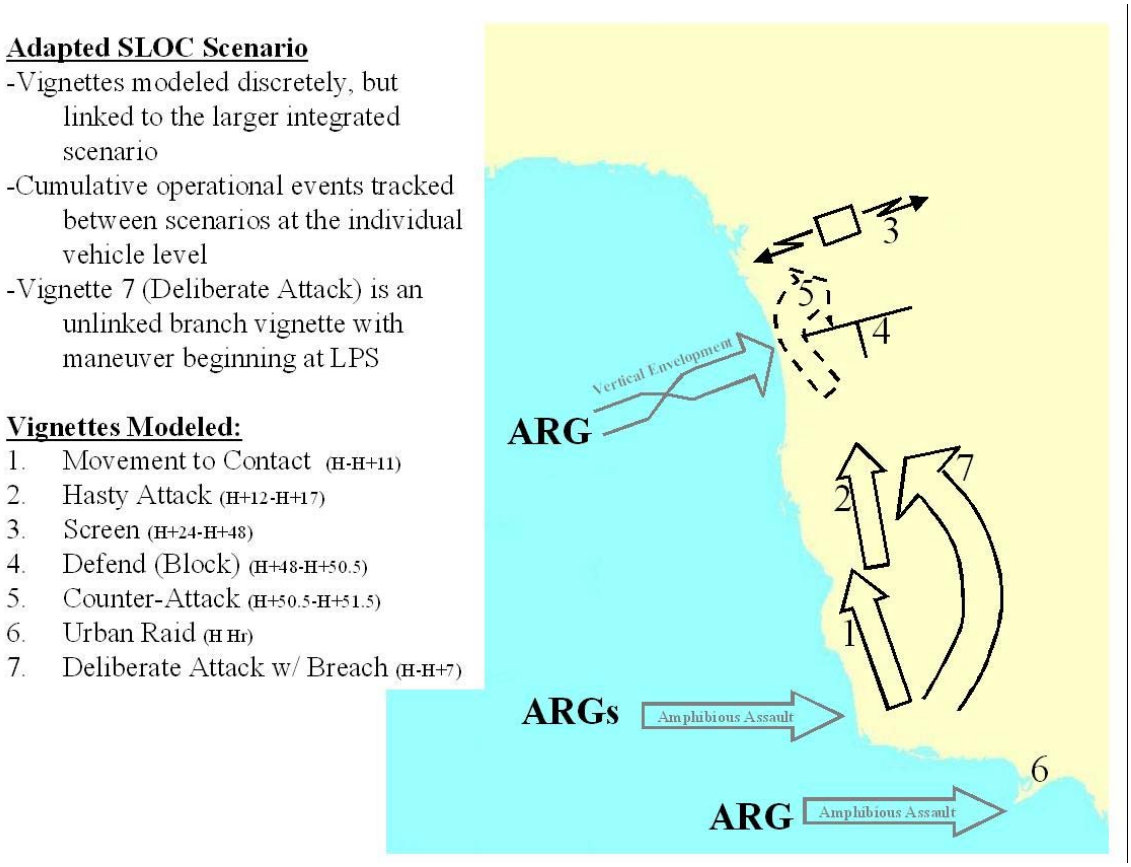

Figure II-1. Battle scenario comprised of multiple vignettes of operation
(Booz Allen lethality study)

The JCATS battle simulation from Booz Allen provided unit-level movement and firing details on 28 units in the scenario. Five units were selected by Booz Allen to represent the spectrum of combat intensity: Units 7, 83, 88, 504, and 793. The output movement data was

tabulated for each unit with respect to time, unit name, coordinates (position in X, Y, and Z coordinates), speed, directional heading, terrain type, slope, grade, and distance traveled. Firing data for each unit was tabulated with respect to time, scenario name (vignette), unit shooting, engagement number, number of shots taken, number of targets fired upon, engagement duration, and rate of fire. Tables II-1 and II-2 show samples of the movement and firing data respectively for unit 83 (M30A_83).

Table II-1. Unit 83 movement data sample (move to contact vignette)

Seconds	CLOCK	UNITNAME	XCOORD	YCOORD	ZCOORD	SPEED	DIRCTN	Terrain Type	Slope	%Grade	Distance
1520	25.33	M30A_83	43.576	34.33	0.015	16	9	Rugged Terrain with Numerous Rocky Outcrops	0.000	0.000	0.012
1521	25.35	M30A_83	43.576	34.33	0.015	16	9	Rugged Terrain with Numerous Rocky Outcrops	0.000	0.000	0.000
1522	25.37	M30A_83	43.576	34.33	0.015	16	9	Rugged Terrain with Numerous Rocky Outcrops	0.000	0.000	0.000
1523	25.38	M30A_83	43.577	34.346	0.016	25	338	Rugged Terrain with Numerous Rocky Outcrops	0.062	6.238	0.016
1524	25.4	M30A_83	43.577	34.346	0.016	25	338	Rugged Terrain with Numerous Rocky Outcrops	0.000	0.000	0.000
1525	25.42	M30A_83	43.577	34.346	0.016	25	338	Rugged Terrain with Numerous Rocky Outcrops	0.000	0.000	0.000
1526	25.43	M30A_83	43.569	34.365	0.016	25	338	2 Lane Hard Surface	0.000	0.000	0.021
1527	25.45	M30A_83	43.569	34.365	0.016	25	338	2 Lane Hard Surface	0.000	0.000	0.000
1528	25.47	M30A_83	43.569	34.365	0.016	25	338	2 Lane Hard Surface	0.000	0.000	0.000
1529	25.48	M30A_83	43.562	34.384	0.016	25	338	2 Lane Hard Surface	0.000	0.000	0.020

Table II-2. Unit 83 firing data sample (move to contact vignette)

Scenario Name	Shooter Name	Engmnt Number	Scenario Start Time (Min)	Scenario End Time (Min)	# Shots Taken	# of Distinct Targets	Engmnt Duration (Min)	Engmnt Rate of Fire	Scenario Time Since Last Engmnt (Minutes)
Movement to Contact	M30A_83	1	76.72	77.14	2	1	0.42	4.762	N/A
Movement to Contact	M30A_83	2	77.21	78.14	3	1	0.93	3.226	0.070
Movement to Contact	M30A_83	3	78.76	78.95	1	1	0.19	5.263	0.620
Movement to Contact	M30A_83	4	78.96	81.06	10	1	2.1	4.762	0.010
Movement to Contact				Total Shots	16				
Hasty Attack	** M30A_83 does not have a main gun engagement during this run								
Hasty Attack	M30A_83			Total Shots	0				
Tactical Roadmarch	M30A_83	N/A	N/A	N/A	N/A	N/A	N/A	N/A	N/A
Screen	M30A_83	N/A	N/A	N/A	N/A	N/A	N/A	N/A	N/A
Defend/ Counter-Attack	M30A_83	1	195.56	195.81	1	1	0.25	4.000	N/A
Defend/ Counter-Attack	M30A_83	2	196.81	197.64	3	1	0.83	3.614	1.000

We selected Unit 83 from the JCATS model for the analysis with CHPSPerf to calculate its movement power requirements over time. This selection was based upon its relatively average movement and firing loads compared to the mission profiles of the other five units provided. Data from each vignette was input separately into CHPSPerf and run for the first 1000 s.

The tabular movement data for Unit 83 had to be modified for use in CHPSPerf. The data for each vignette was reformatted into an abridged data table with fewer rows of data. Using Excel and C++ code, consecutive rows of data with similar values of speed, facing, grade, and terrain were grouped into single rows of simplified input data for CHPSPerf. Consecutive rows of data with the above terms being within a specified variation (i.e. 20%, 9%, 9%, and terrain type resp.) were averaged into these single rows. For example, if the velocity of the vehicle changed by 21% from one row to the next, the rows before and after this change would be split up into two separate groups of rows. Furthermore, a numerical value of rolling resistance was applied to each different description of terrain in the abridged table as listed in table II-3. The procedure of table abridgement was completed for Unit 83 in each vignette. The vignettes for unit 83 included “Move to Contact”, “Hasty Attack”, “Tactical Road-March”, “BEZ to ‘Deliberate Attack’ Attack Position”, and “Deliberate Attack”). Unit 83 did not move during the Screen and the Defend/Counter Attack vignettes and so these were not included in this analysis.

Table II-3. Rolling resistance applied for terrain descriptions

Terrain Description	Rolling Resistance Applied (lb/ton)
2 Lane Hard Surface	0.4410
Trail	0.4410
2 Lane Loose Surface	0.4410
Background Description (general)	0.6125
Dry River Bed	0.6125
Scrub	0.6125
Highly Dissected	0.9800
Rugged Terrain with Numerous Rocky Outcrops	0.9800
Cultivated Land (Wheat)	0.9800
Fair/Dry Weather Surface	0.9800
Faux River	0.9800
Flowing River	1.2250

The columns of the abridged data table were sorted in an appropriate order to be a compatible input for CHPSPerf. The CHPSPerf model was run for each vignette using the appropriate abridged data tables. The vehicle was defined as a 30-ton series hybrid with the following set of input parameters (different from the defaults) shown in table II-4. The output figures from CHPSPerf were then used to view the power requirements for the vehicles motion in each vignette.

Table II-4. CHPSPerf Inputs

Parameter	Setting
Engine Power (kW)	500 per engine
Generator Power (kW)	500/generator
Traction Motors Power (kW)	500/side
# Battery Pack Cells in Parallel	2
# Motors in Drive Train	2
Max Power of Traction Motors	200
Minimum Engine Power (kW)	50
Optimum Engine Power (kW)	750
Stop Time	1000 s
Duty Cycle/ Mission	*One of the vignettes in an abridged data table*

The vehicular power requirements for gun firing were calculated in Excel. All five units from the JCATS model were selected for the analysis. No units were left out because it was thought the EM gun firing would require relatively greater amounts of power than would movement. The higher power draw of the gun would be more sensitive to differences in encounters on the battlefield and therefore would vary more than the power draw for vehicle movement. Furthermore, the variation in power requirements from unit to unit and from vignette to vignette could be found and analyzed.

Some assumptions were made for the analysis of the firing data. The units were assumed to be capable of holding up to 5 shots at a given time. Each shot was assumed to be equivalent to 30,000 kJ of energy, meaning the unit could store up to 150,000 kJ of energy for firing its gun. Furthermore, both the stored energy and the number of shots could not drop below zero. Finally, the unit was assumed to have a constant rate of energy regeneration at all times including within and between engagements. Basically this meant that the unit would attempt to take all the shots as depicted in the JCATS model, but would fail to do so if it ran out of shots during the

engagement. However, the constant rate of energy regeneration could provide sufficient energy to enable some or all of the remaining shots to be fired in an engagement. Therefore the analysis focused on the required rate of energy regeneration, or power, which was necessary for the unit to fire all the shots described in the battle.

Multiple power settings were independently analyzed for each unit. The power setting was set to a constant at 500 kW, 800 kW, 1000 kW, or 1500 kW for each unit's firing profile. The actual number of shots taken in each engagement was calculated in Excel based upon the number of stored shots at each given time and the number of regenerated shots with respect to time. The number of "missed shots" was defined as the difference between the calculated number of shots taken and the number of shots taken in the JCATS simulation. The required power level is simply the power setting that provides zero missed shots in all engagements.

Results of Analyses, Simulations, Trade Studies and Designs

The results from CHPSPerf indicated that the power demands for unit mobility in each vignette were easy to achieve with power to spare. Unit 83 traversed a wide variety of terrains, some with significant values of rolling resistance, at nominal speeds between 0 and 39 kph. Figures II-2 to II-6 graphically show the tank's motion in the first 1000 s of the "Move to Contact", "Hasty Attack", "Tactical Road-March", "BEZ to 'Deliberate Attack' Attack Position", and "Deliberate Attack" vignettes respectively. As shown in the figures, terrain rolling resistance, and grade varied significantly over the time modeled, while velocity was varied occasionally. The maximum positive grade was up to 0.08 (rise/run) in the Tactical Roadmarch and Deliberate Attack vignette. Rolling resistance ranged from 80 lb/ton to 200 lb/ton in almost every vignette.

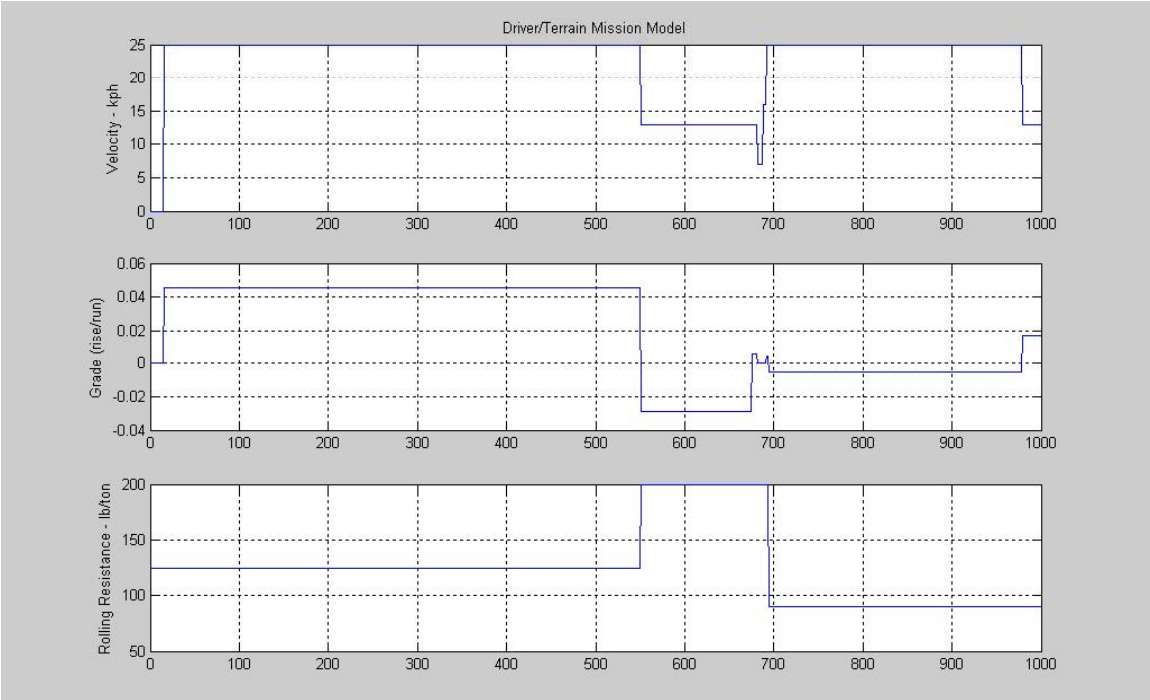

Figure II-2. Unit #83 environment profile for “movement-to-contact” vignette

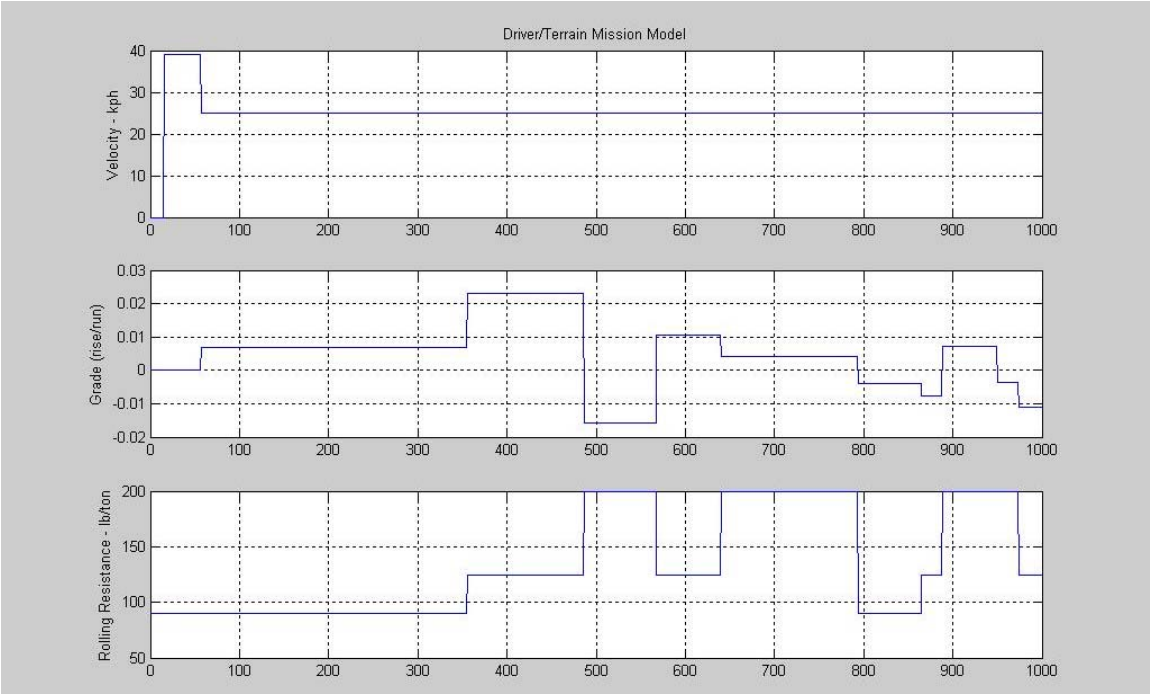

Figure II-3. Unit #83 environment profile for “hasty attack” vignette

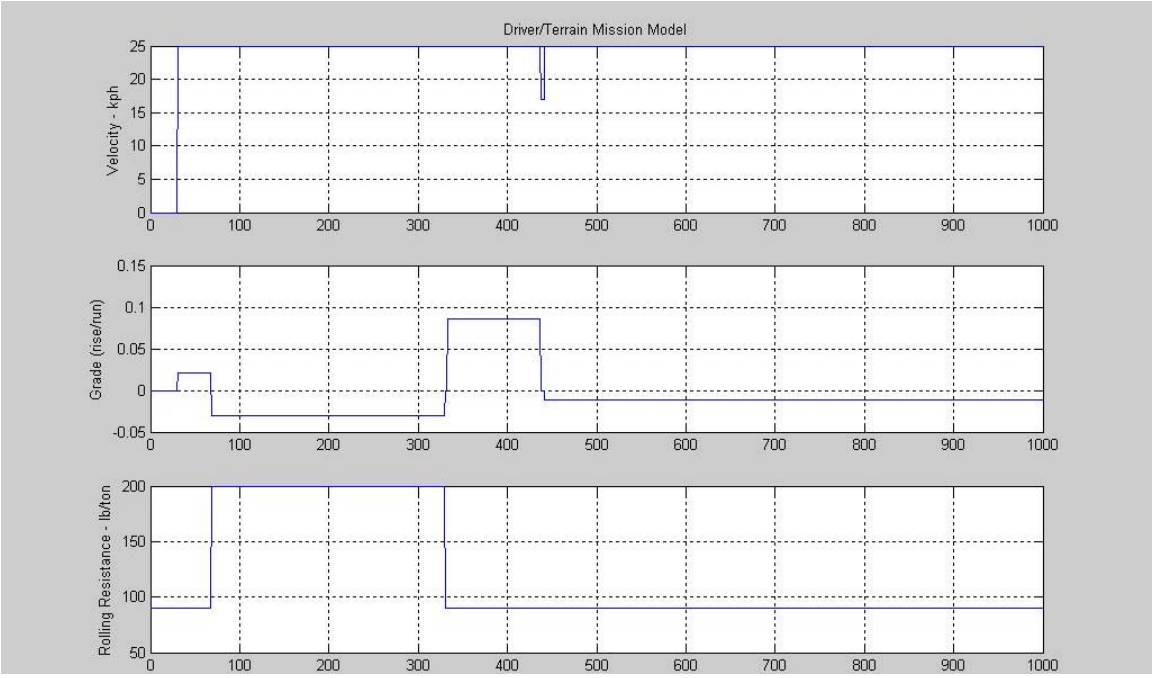

Figure II-4. Unit #83 environment profile for “tactical roadmarch” vignette

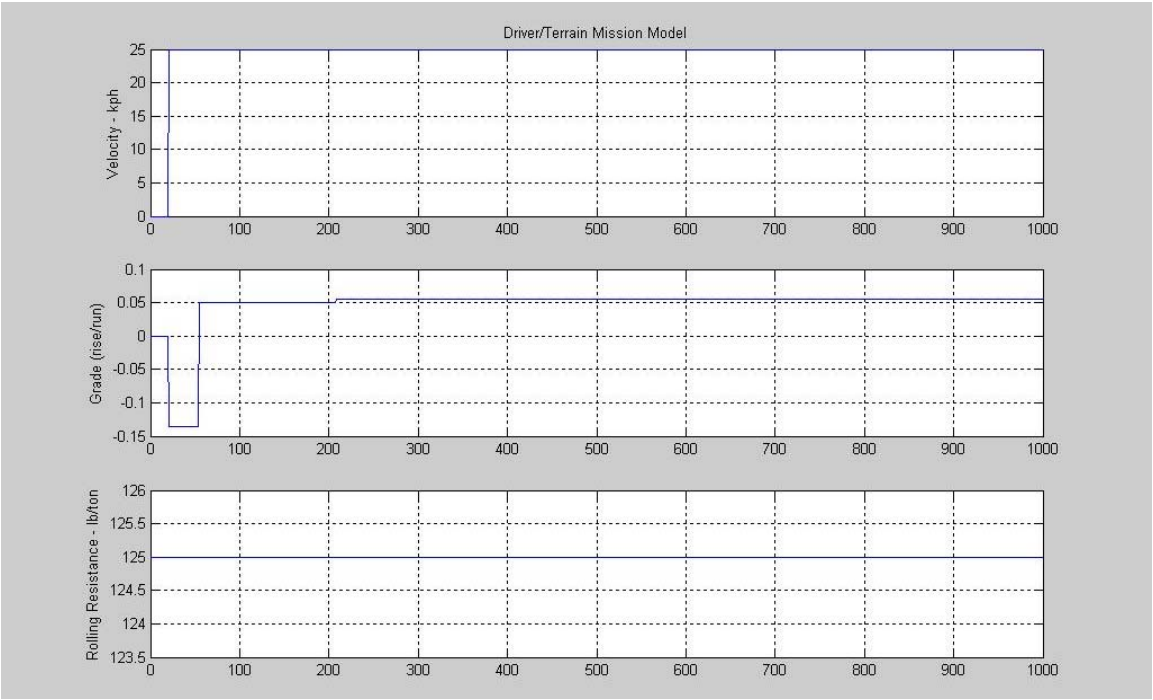

Figure II-5. Unit #83 environment profile for “beach exit zone to ‘deliberate attack’ attack position” vignette

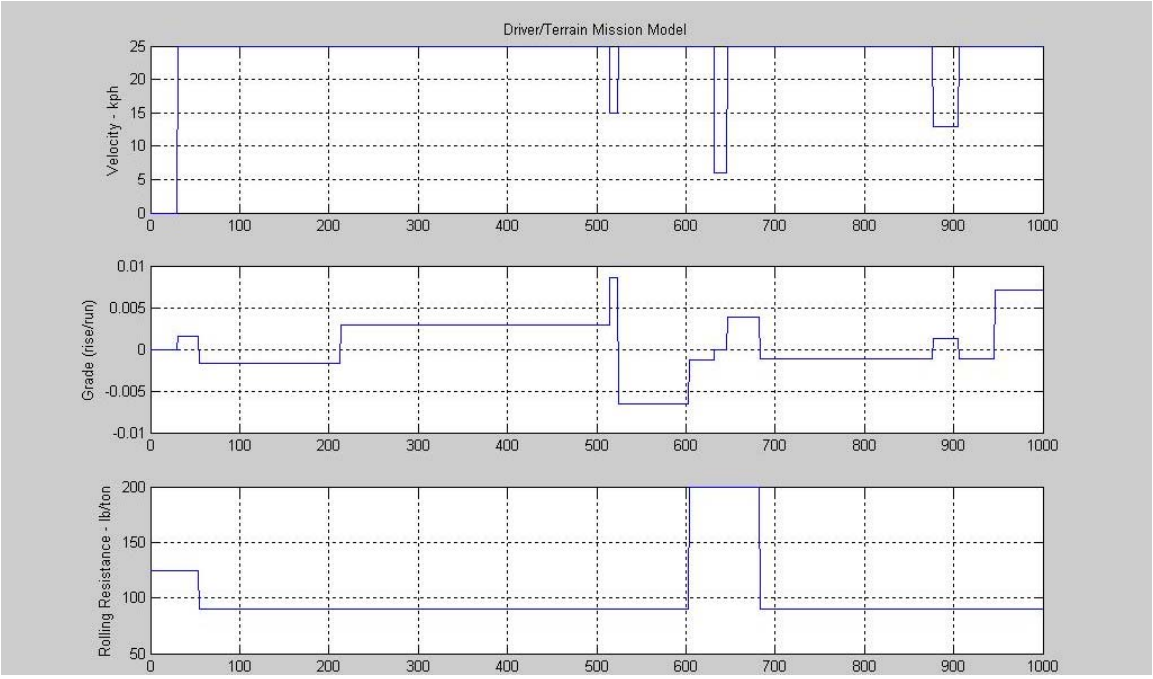

Figure II-6. Unit #83 environment profile for "deliberate attack" vignette

The power requirements for the unit's motion were easily achieved and remained below 600 kW for the time modeled. Figures II-7 to II-11 show the required engine power was below 600 kW in every vignette. The power requirement for movement sustained for extended periods of time in the simulation remained below 280 kW. Only a few power spikes occurred at times of sharp acceleration, only one of which approached 600 kW. This spike occurred during the Hasty Attack vignette during initial acceleration from 0 to 39 kph that occurred at 15 s as shown in figure II-8. The most significant spike of power regeneration occurred at about 60 s into the Hasty Attack vignette when the unit decelerated from 39 to 25 kph. This regeneration spike caused the bus power to peak at about -700 kW of power (or 700 kW of charging to the batteries). The power requirements for all vignettes are summarized in table II-5.

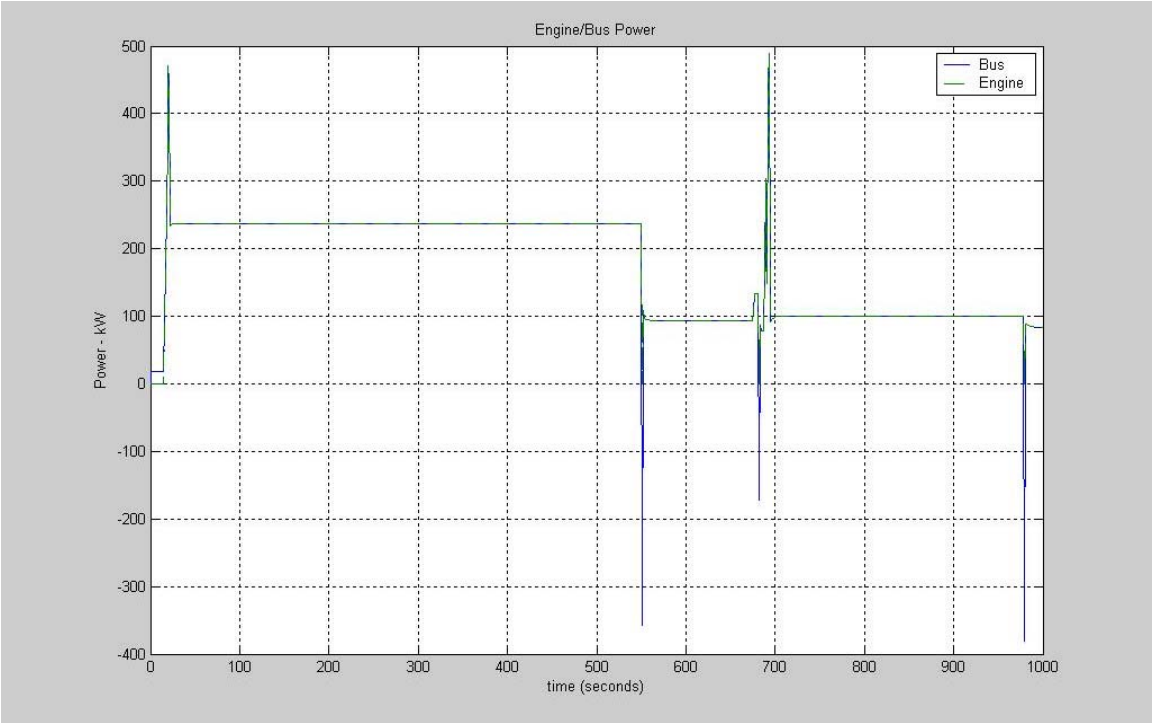

Figure II-7. Unit #83 power requirement profile for “Movement-To-Contact” vignette

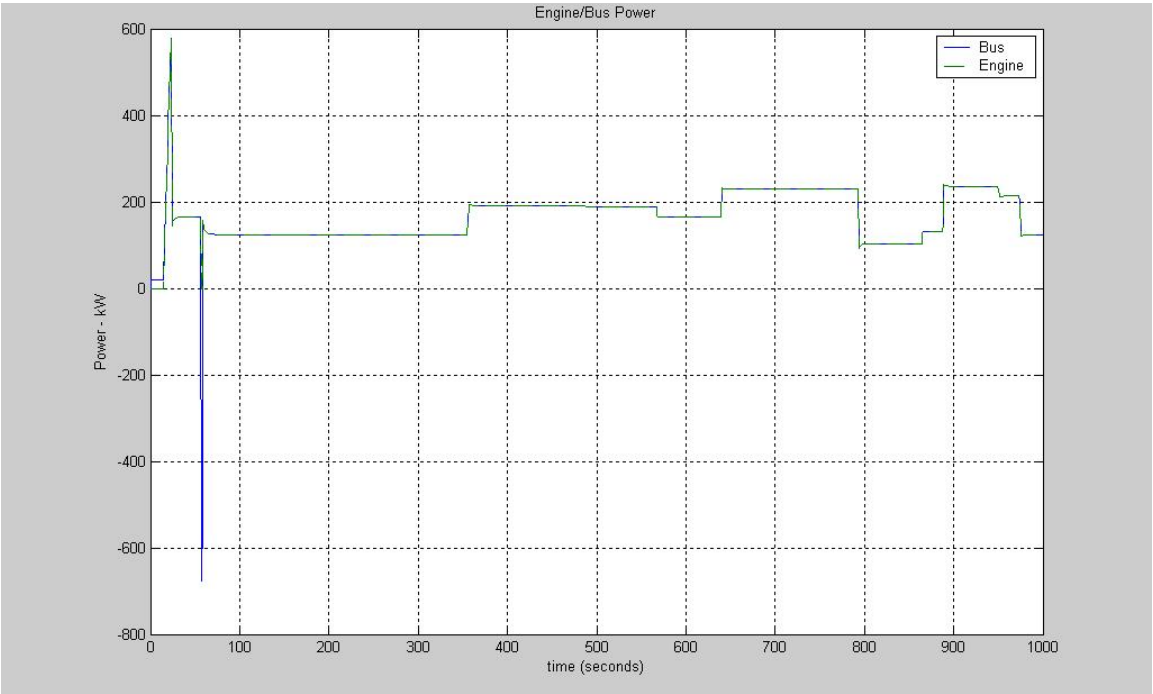

Figure II-8. Unit #83 power requirement profile for “Hasty Attack” vignette

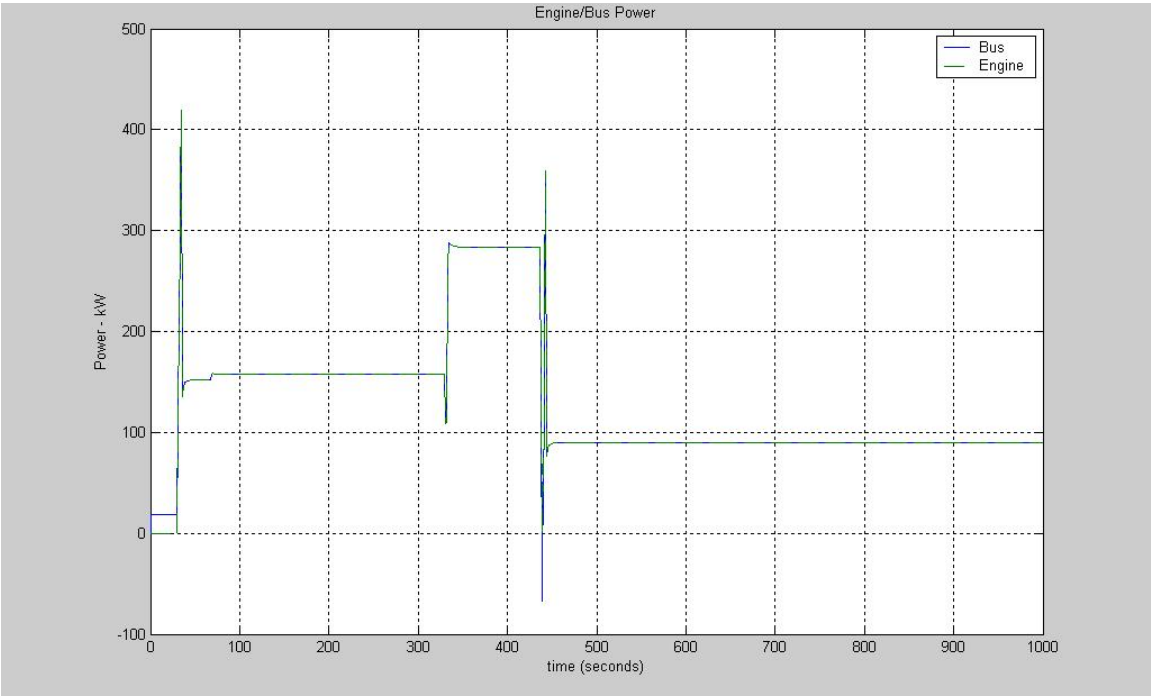

Figure II-9. Unit #83 power requirement profile for “Tactical Roadmarch” vignette

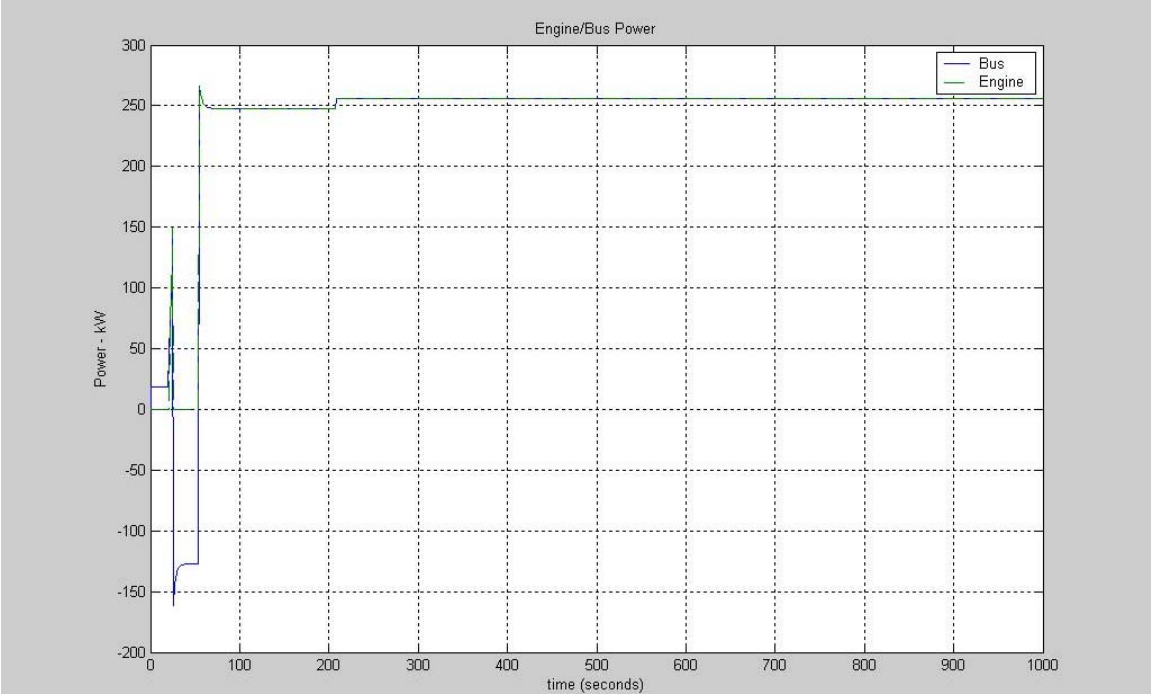

Figure II-10. Unit #83 power requirement profile for “Beach Exit Zone to ‘Deliberate Attack’ Attack

Position" vignette

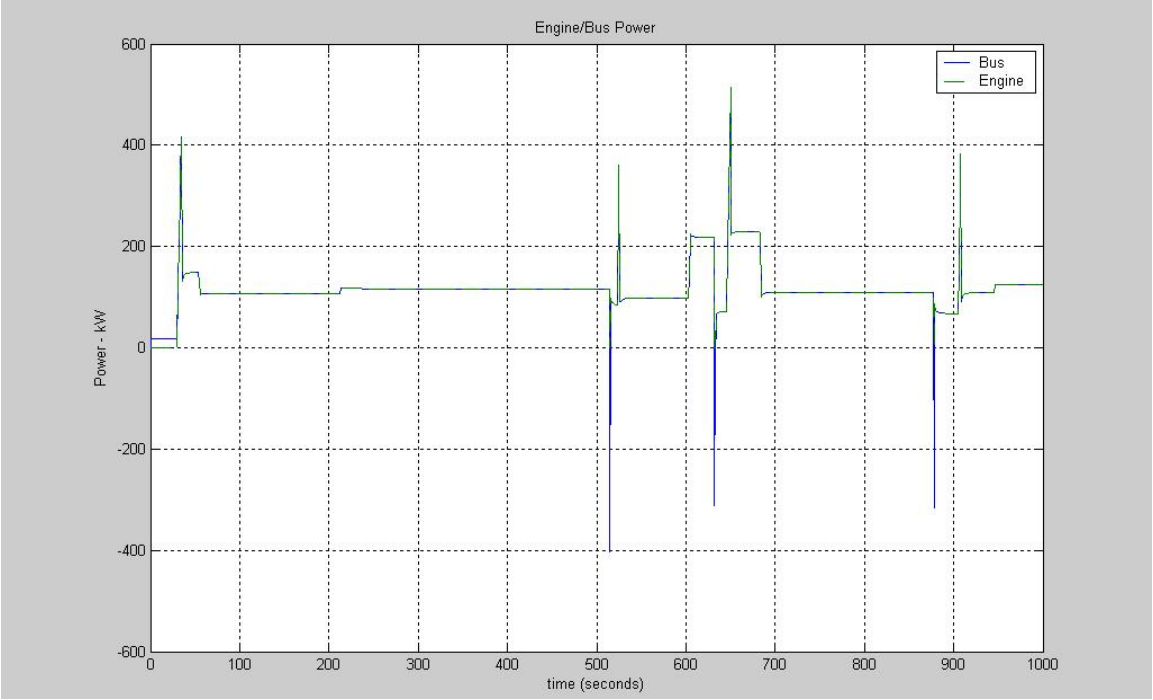

Figure II-11. Unit #83 power requirement profile for "Deliberate Attack" vignette

Table II-5. Summary of parameter ranges for all vignettes

	Range of Value in All Vignettes
Engine power (kW)	0 to 600
Bus power (kW)	-700 to 600 (negative=charging battery)
Unit Speed (kph)	0 to 39
Grade (rise/run)	-0.13 to 0.08
Rolling Resistance (lb/ton)	80 to 200

The results from the analysis on EM gun firing indicated high power requirements to successfully fire all shots during the battle. The five units each had different numbers of vignettes with engagements. Further, the number of shots taken per engagement varied significantly for each vehicle and for each vignette. Most engagements with gun firing required

bursts of several shots in short periods of time with little time for energy regeneration. However, some engagements were spaced far enough part in time for plenty of energy regeneration.

The power required for a unit to follow the JCATS firing profiles varied widely and included some peaks in power drawn. As a result, the power required to fire every shot was often much higher than the power to fire the majority of the shots taken throughout the entire battle. Therefore, the number of shots missed per vignette and in total was the principal measurement used gauge the power necessary for each Unit's mission. The number of missed shots with respect to time and vignette are shown in figures II-12 to II-31. The figures are grouped by Unit number and by the power setting. Table II-6 lists these figures relative to Unit number and the power setting.

Table II-6. List of figures by unit number and gun firing power requirements

Unit Number	500 kW Power	800 kW Power	1000 kW Power	1500 kW Power
Unit 83	Figure II-12	Figure II-13	Figure II-14	Figure II-15
Unit 7	Figure II-16	Figure II-17	Figure II-18	Figure II-19
Unit 88	Figure II-20	Figure II-21	Figure II-22	Figure II-23
Unit 504	Figure II-24	Figure II-25	Figure II-26	Figure II-27
Unit 793	Figure II-28	Figure II-29	Figure II-30	Figure II-31

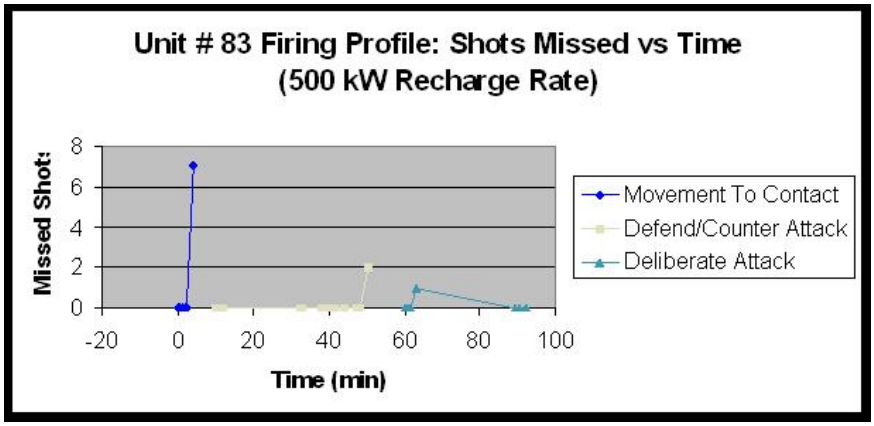

Figure II-12. EM gun shots missed for Unit 83 (500 kW power)

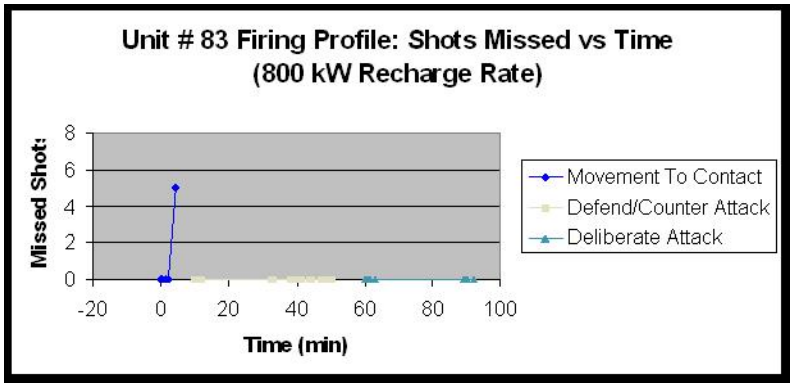

Figure II-13. EM gun shots missed for Unit 83 (800 kW power)

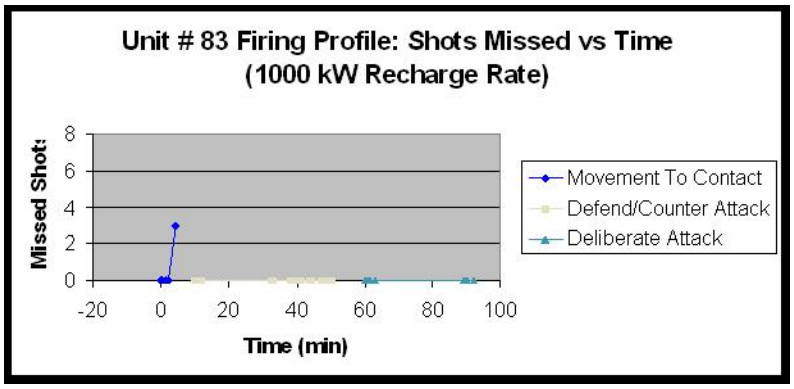

Figure II-14. EM gun shots missed for Unit 83 (1000 kW power)

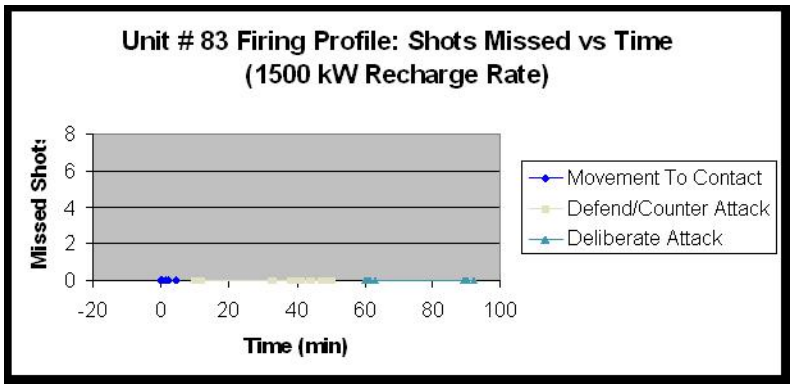

Figure II-15. EM gun shots missed for Unit 83 (1500 kW power)

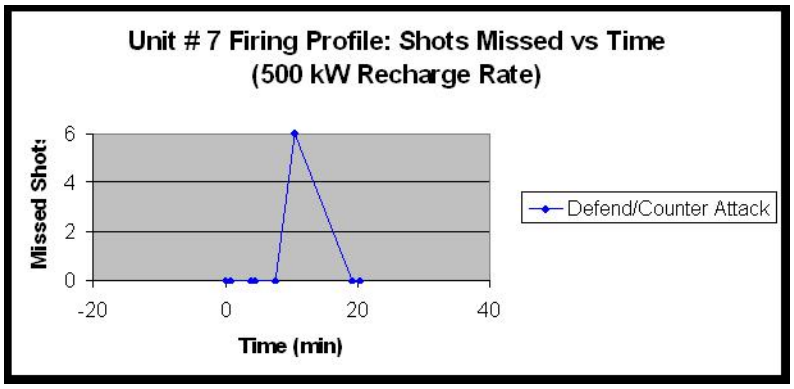

Figure II-16. EM gun shots missed for Unit 7 (500 kW power)

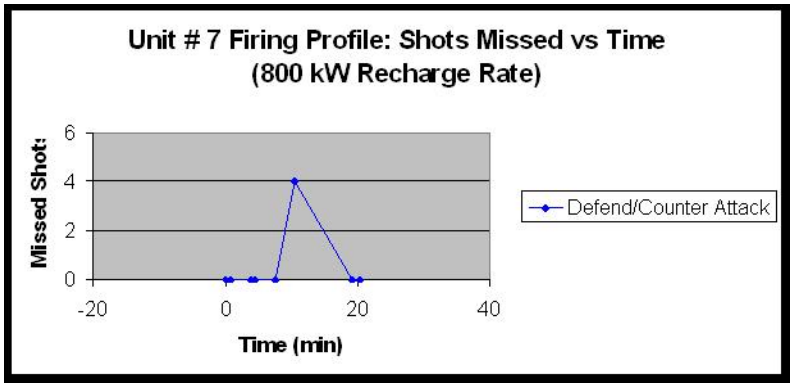

Figure II-17. EM gun shots missed for Unit 7 (800 kW power)

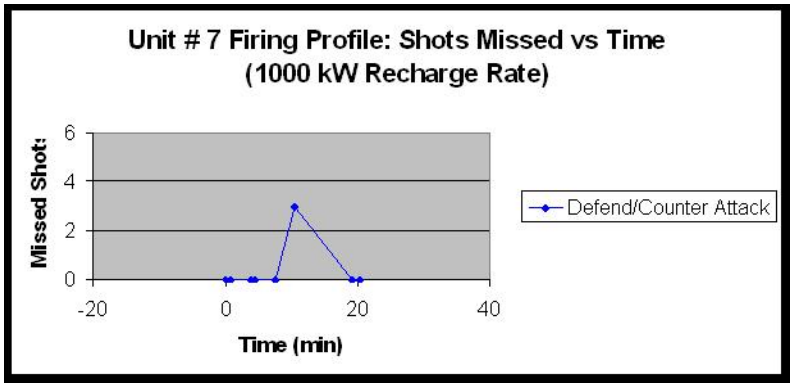

Figure II-18. EM gun shots missed for Unit 7 (1000 kW power)

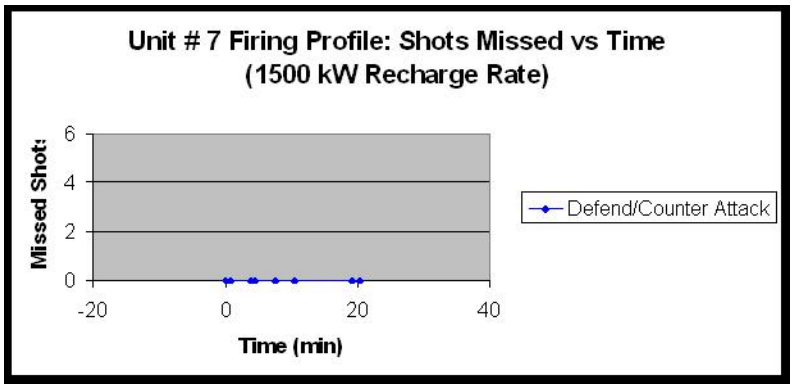

Figure II-19. EM gun shots missed for Unit 7 (1500 kW power)

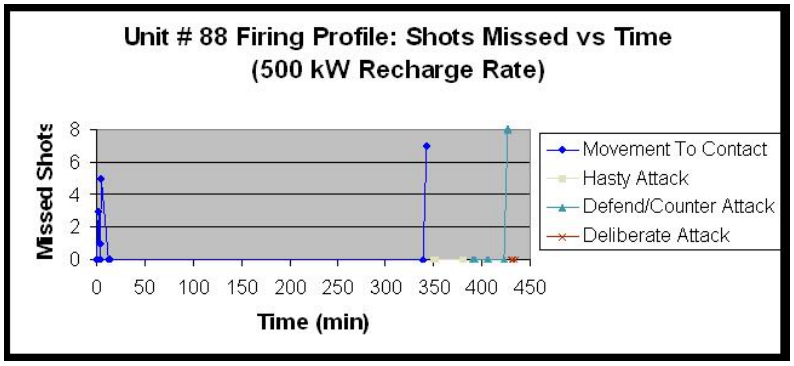

Figure II-20. EM gun shots missed for unit 85 (500 kW power)

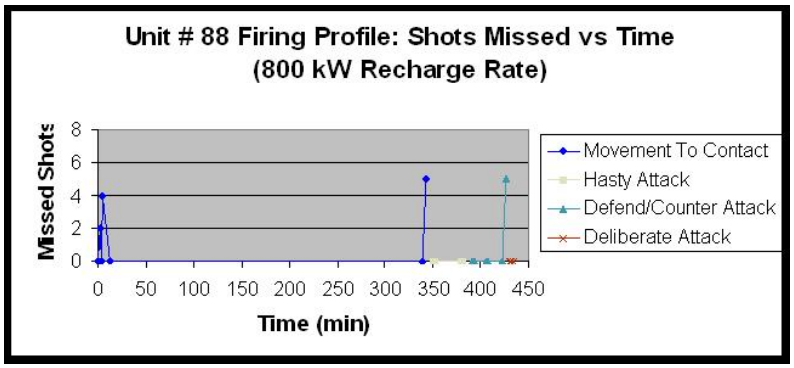

Figure II-21. EM gun shots missed for Unit 88 (800 kW power)

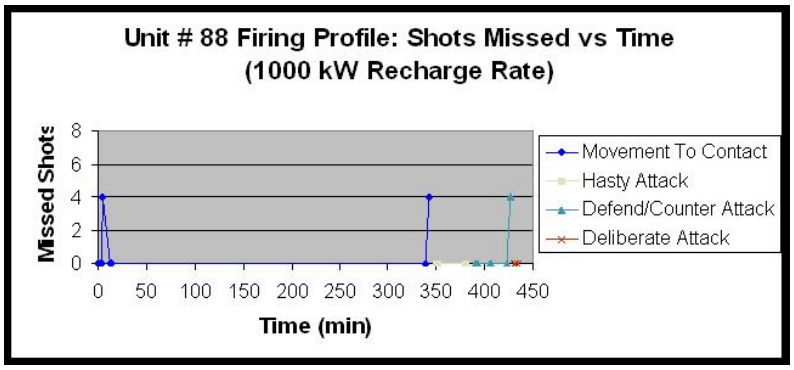

Figure II-22. EM gun shots missed for Unit 88 (1000 kW power)

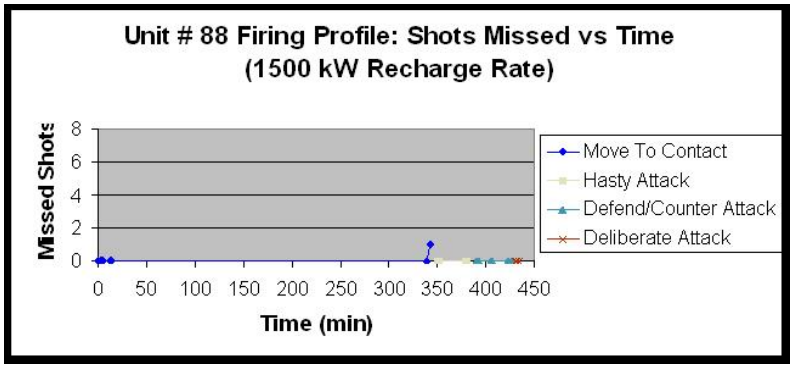

Figure II-23. EM gun shots missed for Unit 88 (1500 kW power)

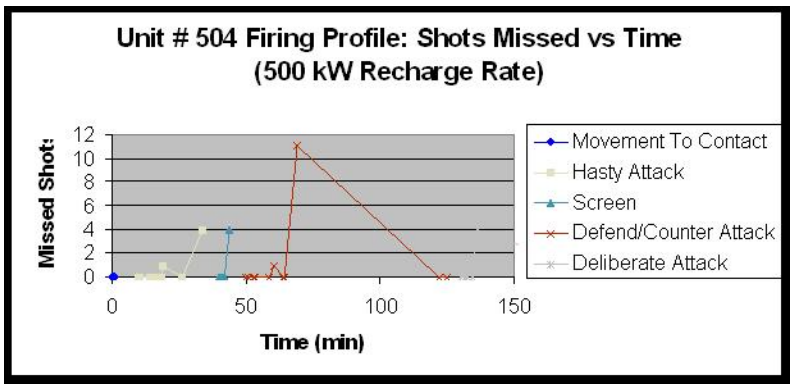

Figure II-24. EM gun shots missed for Unit 504 (500 kW power)

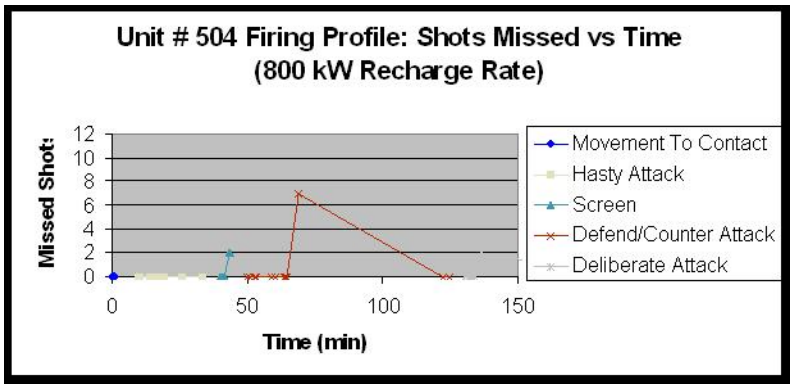

Figure II-25. EM gun shots missed for Unit 504 (800 kW power)

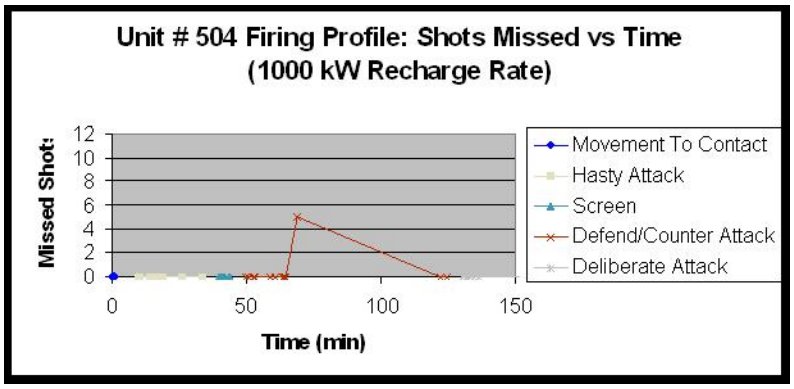

Figure II-26. EM gun shots missed for Unit 504 (1000 kW power)

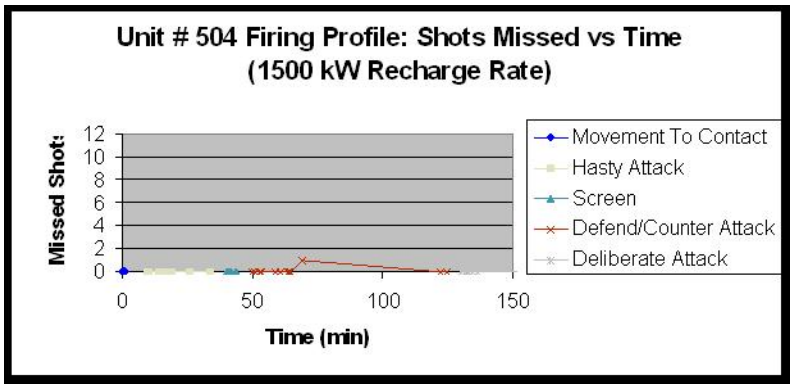

Figure II-27. EM gun shots missed for Unit 504 (1500 kW power)

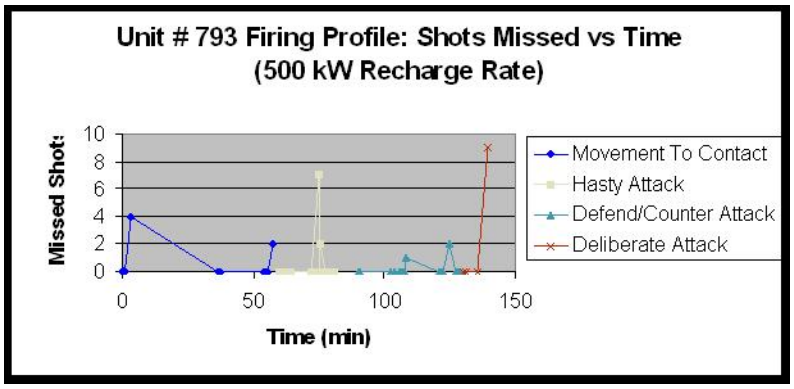

Figure II-28. EM gun shots missed for Unit 793 (500 kW power)

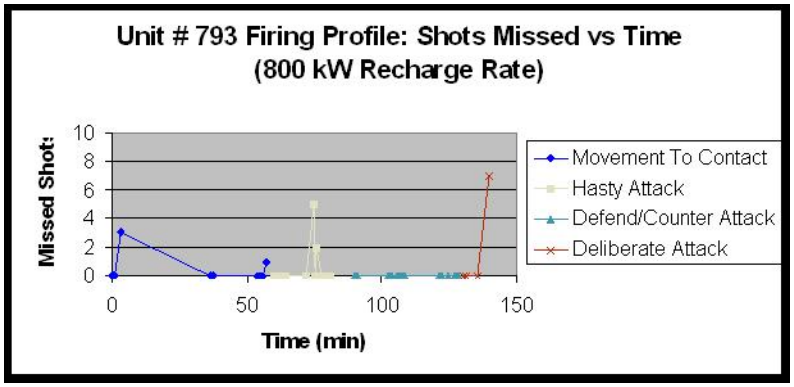

Figure II-29. EM gun shots missed for Unit 793 (800 kW power)

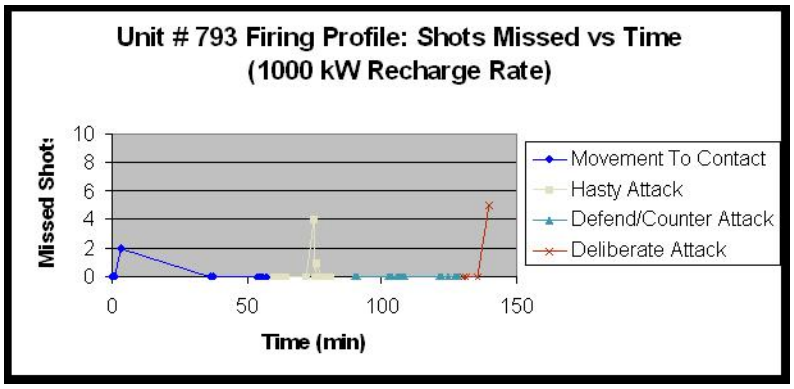

Figure II-30. EM gun shots missed for Unit 793 (1000 kW power)

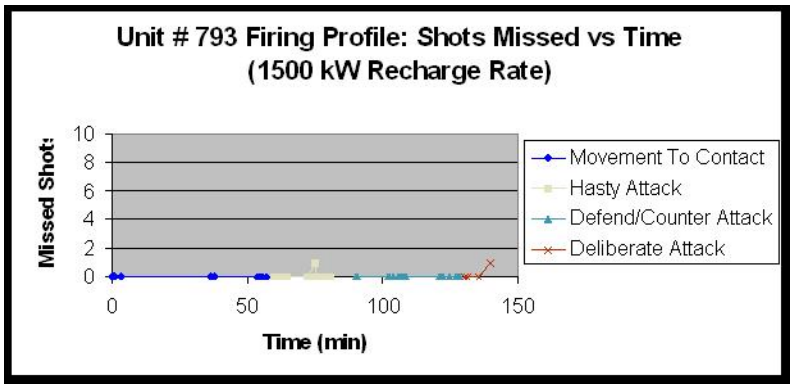

Figure II-31. EM gun shots missed for unit 793 (1500 kW power)

The different power levels implemented in the analyses each provided for different numbers of shots fired from each vehicle. Units 83, 7, 88, 504, and 793 each attempted to fire 55, 25, 78, 112, and 99 shots respectively during the battle. Table II-7 shows the number of shots missed and the number of times a group of consecutive shots (peaks in above figures) were missed relative to the available power. Increased available power resulted in fewer missed shots. A power setting of 1500 kW was nearly sufficient to provide enough power for every vehicle as seen in table II-7. With 1500 kW of power Units 83 and 7 missed zero shots, Units 88 and 504 missed one shot, and Unit 793 missed two shots.

Table II-7: Missed shots base on EM gun firing requirements

Unit Number	Total Number of Shots Taken	Total Number of Missed Shots	Number of Groups of Missed Shots
Unit 83			
500 kW	55	10	3
800 kW	55	5	1
1000 kW	55	3	1
1500 kW	55	0	0
Unit 7			
500 kW	25	6	1
800 kW	25	4	1
1000 kW	25	3	1
1500 kW	25	0	0
Unit 88			
500 kW	78	20	3
800 kW	78	14	3
1000 kW	78	12	3
1500 kW	78	1	1
Unit 504			
500 kW	113	21	5
800 kW	113	11	3
1000 kW	113	5	1
1500 kW	113	1	1
Unit 793			
500 kW	99	27	7
800 kW	99	18	5
1000 kW	99	12	3
1500 kW	99	2	2

Discussion, Conclusions and Recommendations

The power requirement for the hybrid-electric tank's movement was less than 600 kW based on the CHPSPerf model. The power requirement for mobility remained below 300 kW for most of the simulation except for the peaks due to rapid accelerations. Therefore, a vehicle with these prescribed abilities in power management could have sufficient mobility and have plenty of extra power for additional power loads. The model is currently being run for an extended simulation time to verify these results.

The power requirements for gun firing were more much more stringent. Approximately 1500 kW or more was required for each vehicle to fire every shot in every vignette of the battle. However, this high power requirement occurred only when significantly long and consecutive bursts of shots were taken, such as 10 shots in about 2 minutes. However, the power

requirements for firing the gun varied widely between engagements and vignettes so there was usually sufficient energy recharged to fire most of the shots. The existence of missed shots suggests the lethality of the vehicle may not be optimized for this battle, and some consideration should be made for the impact of this.

In summary, the vehicle has sufficient power for its mobility and has sufficient power for most of its firing requirements. A re-evaluation of the tactics and procedures to be implemented with these vehicles could help improve their lethality. However, the occasional nature of the long bursts of shots occurring on the battlefield, combined with the anticipated improvement in power technologies over the next dozen years indicate that we might satisfy the power requirement. The components in the vehicle should accommodate as much of the power load required in this study with the expectation that better components could replace them over time.

References

[II-1} Booz Allen, MEFFV Lethality Study: Status to Date, Interim Progress Review, Briefing to NSWC-CD and the MEFFV Project Office, 7 August 2003.

III. Vehicle Power Train

Introduction and Requirements

We performed a detailed study of the MEFFV system's mobility and weapon and defensive armaments power requirements. Results of the dynamic analyses, presented in Section II, were used in conjunction with the static analyses presented below to develop and verify the power system solution for the MEFFV. Based on the analyses we selected the series hybrid power system shown in figure III-1 for the MEFFV. A series hybrid solution is the obvious and logical choice for powering a system with high sustained non-mobility electrical power loads characteristic of EM gun equipped direct fire vehicles.

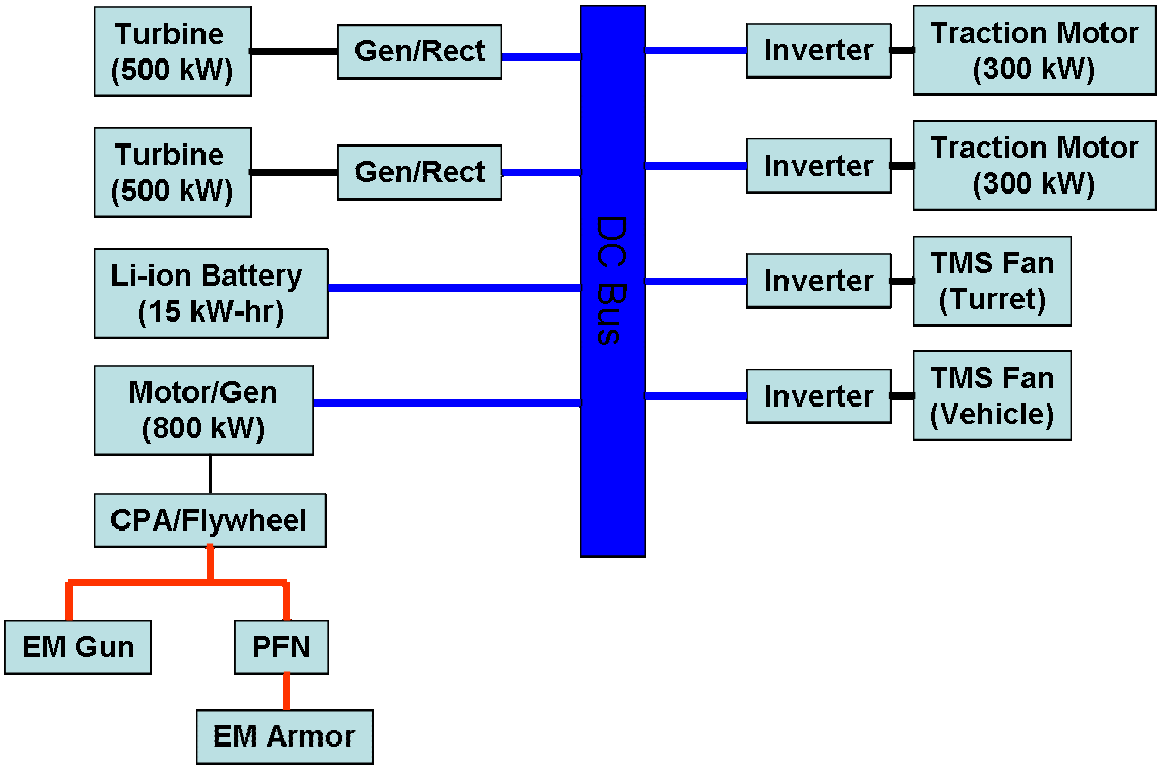

Figure III-1. Series hybrid power system for the MEFFV vehicle

The series hybrid power system envisioned for this application will provide power to multiple electric loads with diverse power requirements using multiple sources of on-board electric power. Intelligent and efficient integration of the power consuming and power producing components is accomplished through a re-configurable hierarchical control system that automatically selects the best component or combination of components for providing load power demands. This highly integrated and intelligent architecture makes possible high-power weapons systems operation, hypermobility, hill-climbing, and limited silent watch/mobility in a system weight class unachievable with conventional power architecture technologies.

The MEFFV power system departs from current hybrid combat vehicle practice out of necessity to meet the extreme demands of electric weapons and mobility systems within a 35-ton mass package. The major distinguishing features of the power system shown in [III-1] include an integrated multifunctional pulse power and pulse energy storage that supplies the energy to power both the EM gun system and the EM armor system. The multifunctional pulse power system allows us operate both the gun system and the EM armor solution from common pulse power components.

The twin turbine solution for the prime power producer is also a significant departure from the conventional prime power solution that uses high-speed diesel gensets as the power source. MEFFV's volumetric constraint is particularly difficult and places major restrictions on the selection of the engine for the platform. High-speed diesels are large bulky systems much larger and heavier than a turbine of comparable power output. Diesels tend to be less power dense than turbines of comparable power output. Compelling reasons for using diesel gensets in combat vehicle applications include the cost benefits of using a derivative of a mass produced item and part-load fuel consumption benefits of high compression ratio diesel cycles. Major issues with a diesel engine include the size and weight of the package and the heat rejection requirements for the system.

During the present study we examined both diesel and turbine solutions. For this application – volume limited, high sustained power - the twin turbine solution imposes smaller volume (a factor of 2) and thermal management burdens on the system. Our studies found that the turbine was the only power option capable of producing in excess of 1 MW within the allocated prime power volume envelope of MEFFV. The challenge for turbo-generator design,

and the focus of MEFFV power system technology development, should be turbine efficiency and, in particular, turbine efficiency during off-design, part-load operation of the vehicle.

Off-design performance issues associated with turbine power packs – response time and fuel consumption – can be partially addressed through careful control of the hybrid power system. For example, our control approach for MEFFV uses the energy storage system (in our case the battery pack) for instantaneous system response during both normal and high agility maneuvers. In this approach the turbogenerator responds to changes in the battery current draw by changing the engine power set point with a time constant chosen to minimize time spent in undesirable regions of the torque/speed band of the engine.

Additionally, a series hybrid design enables us to use two independent turbogenerators. During most of the operational life of the vehicle it will operate alternately off of one or the other of the turbines since each turbine can independently handle all of the vehicle's mobility loads. When the vehicle is in a combat situation, either as directed by the operator or by the operators selection of various systems on board the vehicle (i.e., activation of the radar system), the second turbine will be automatically brought on-line to provide power to the system bus sufficient to power the electric armaments on board the vehicle. This arrangement allows us to maintain good fuel consumption by operating the turbine at close to its full load at all times while having sufficient power to operate the EM gun at a sustained rate of fire of ~ 2 rounds/min. Also with this arrangement we have redundant power capabilities.

Supplementing turbine power during gun firing and transient maneuvers is a small (~ 10 kW-hr) Li-ion battery pack. It is used to relieve response time requirements on the turbine and to allow it to operate at nearer to full load conditions than would be possible if the system were to have a mechanical path between the engine and the drive motors.

Other options were examined for the energy storage system. Of particular interest in this regard is the use of the CPA flywheel as the load leveling and energy storage device for the system. Using the flywheel in the CPA as an alternative to the battery pack is a feasible option. As shown in table III-1 there is a small fuel consumption penalty (~ 5%) in using the flywheel but this must be weighed against the mass (200 kg) and volume (1 cubic meter) that is saved in removing the battery from the vehicle. Our rationale for using a battery pack as the primary load leveling device for the system is to maintain substantial mobility capabilities during gun firing

events. The energy storage device plays a key role in the system's mobility particularly during weapons firing events when most of the engine power is dedicated to recharging the CPA for weapons operations requiring the use of the mobility energy store to provide a substantial fraction of the mobility power. During gun firing operations the CPA is dedicated to supplying pulse energy to the weapons and armaments on-board the vehicle and cannot feasibly be used to supply mobility power to the vehicle.

Table III-1. Fuel consumption comparison between a Li-ion battery pack and the CPA flywheel for mobility load leveling on the MEFFV

Mission Segment	Single Turbine (500 kW) Fuel Consumption (kg)		Dual Turbines (1000 kW) Fuel Consumption (kg)	
	Battery	Flywheel	Battery	Flywheel
Deliberate Attack	56	59	61	66
Deliberate Attack to Attack Position	111	117	114	126
Hasty Attack	52	54	61	66
Movement to Contact	115	120	127	137
Tactical Road March	35	37	37	40

The band track sprocket drives are drive by individually controlled electric motors. Induction machines are used as the reference motor drive for the sizing exercise presented in this study. Our reason for using induction machines as opposed to permanent magnet machines is that in this size class the efficiency of the two classes of machines are roughly the same with the induction machine having an advantage in that it does not require a multi-speed gearbox in order to have the low speed torque for the hill climb while at the same time providing the power at road speed. The motors are driven by high-temperature oil cooled inverters mounted in a common box. Each sprocket drive motor is controlled to yield just the right amount of torque and speed for optimal *system* tractive effort, obstacle crossing, and skid-steer control. Anti-slip functions are built into the control system.

A high-voltage DC distribution system is used in the system for power distribution around the vehicle. For consistency with other vehicle's projected to be in the force during the 2020 timeframe the voltage level on the bus was taken to be on the order of 600 V. Most of the devices on the bus will operate directly from the high voltage bus most particularly the high

power components such as the flywheel motor/generator, the traction drives, turret drive and the turbogenerator.

A power management system controls the flow between power generation, storage, and users for maximum fuel economy, stealth, or other criteria. Power management is dynamically accomplished on a system basis in contrast to traditional subsystem optimization strategies. In this context, the mobility subsystem and mission module power users are part of an overall power management system.

Figure III-2 is a Work Breakdown Structure (WBS) for the MEFFV EM armor system, which defines the key subsystems and components shown in Appendix A. For the MEFFV application, we have considered separate turret and chassis protection systems, to eliminate the associated time delay involved in energizing the slip ring in a surprise attack. This system includes sensors to detect the impact of the threat on the module, discriminate the threat velocity and send a trigger to the output switch to energize the modules.

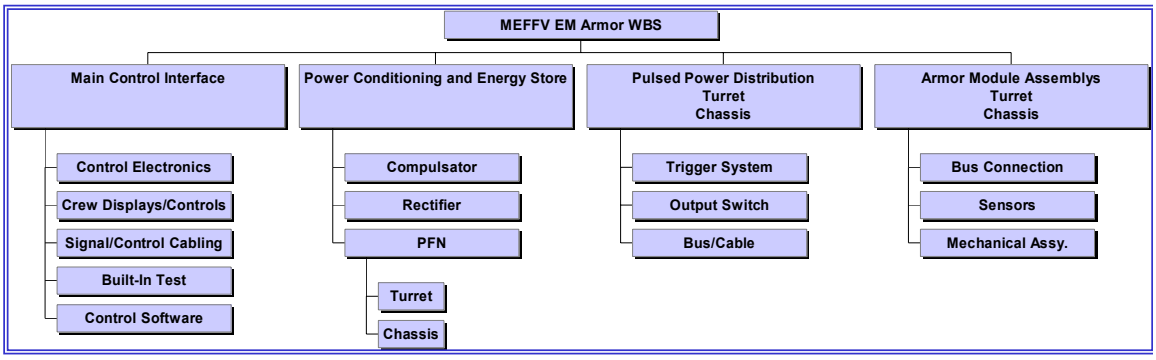

Figure III-2. EM armor system Work Breakdown Structure

The power conditioning and energy store system for the EM armor consists of a prime energy store, a voltage converter and a PFN. The prime energy store for the MEFFV is assumed to be the compulsators, whose design is discussed elsewhere. In order to dc charge the PFN, the voltage converter is a rectifier. The PFN is made up of a network of capacitors and inductors to store and condition the energy required for threat defeat.

The rectifier size and weight are determined by the engagement scenario and the energy stored in the PFNs. We have chosen an operating voltage of 16 kV, consistent with the compulsator output voltage.

The size (energy) of the PFN is determined by the threat. For both the chassis and turret, we must accommodate both top and side threats. To size the PFNs we utilized an EM armor design code developed by SAIC and PMC, Inc. This code models the threat warhead, computes the jet characteristics, the EM coupling to the jet and the resultant residual penetration for a given armor module and hull configuration. For the threat we have assumed a standard threat spectrum currently being considered by the Army for FCS top and side protection. The top threat consists of three warheads that we shall refer to as "Small", "Medium" and "Large". The side threats are unitary man-portable shaped charges. Identification of specific warheads is classified when associated with the defeat energy. Therefore, we will not identify the specific warheads in this report.

Besides the compulsators, the major internal weight and space claim associated with the EM armor system is due to the PFNs. The volume and weight of the PFNs depend largely on the energy density of the capacitors that make up the PFN, which is voltage dependent. State-of-art 16-kV biaxial oriented polypropylene (BOPP) dielectric capacitors manufactured by ICAR S.p.A. have a net energy density of 1.0 J/cc. Diamond-like-carbon film, currently under development by the U.S. Air Force could push this value to 2 to 4 J/cc net. (Here the term "net" includes the packaging efficiencies of a high voltage capacitor.) The energy density of the BOPP dielectric in the ICAR 1 J/cc capacitors is 2.15 J/cc. The energy density of DLC has been estimated at 7.7 to 9 j/cc. We have conservatively based our design on 100-μf, 16-kV, 2 J/cc units storing 12.8 kJ each.

There are two PFNs in the system – one in the turret and the other in the body of the vehicle. Total energy stored in each PFN at 16 kV charge is 205 kJ. Using two PFNs eliminates the need discharge through the turret slip ring. Although the slip ring could easily handle the required current (600-kA peak) when energized (under pressure), it would have to be continuously under pressure in order for top EM armor to be energized through the slip ring from a PFN in the chassis.

The PFNs are switched by laser triggered solid-state thyristor switches, of the type currently under development for TACOM by Opti-Switch Technology Corporation. We have separated the turret PFN into two modules, each with independent switching. This allows simultaneous engagement of two top threats. Engagement of a side threat on the turret requires the full energy of the top two modules. Engagement of a side threat on the chassis requires the full chassis PFN energy.

Pulsed power distribution is accomplished by Litz-wire based buses developed by SAIC under the sponsorship of TACOM. These buses have an inductance of 2.0 nH/ft, a resistance of 0.14 mΩ/ft and weigh 0.8 lb/ft.

The thermal management system for the vehicle was also sized during the study effort. One of the major advantages of a turbine engine for this application is the fact that it does not require large water or oil based thermal management systems. Air flow through the turbine is sufficient to cool both the turbine and the direct coupled high-speed generator. This is a major feature since the thermal control of the system during continuous mobility missions is reduced to removing the heat from the drive motors and the drive inverters which even at worst case conditions is only ~ 50 kW. For a diesel genset worst case prime power cooling loads exceed 1 MW which when added to the cooling load of the CPA and gun would make the TMS unacceptably large.

The major load on the TMS for the system the heat generated by the CPA and the gun during continuous firing events. At a firing rate of ~ 2 rounds/min the heat generated in the gun and the CPA and all the associated hardware is on the order of 600 kW split with ~ 200 kW being generated in the turret and the remaining 400 kW in the main body of the vehicle.

Removal of the generated energy is accomplished using two independent pressurized water circuits – one in the turret and the other in the main body of the vehicle. These circuits need only operate during the operation of the gun and/or CPA so that the power draw from the cooling fans (~ 50 kW during continuous gun operation) is minimal during the majority of the vehicle's operation. The thermal management system is sized to provide cooling to the system on a 49C day.

Methods Employed and Assumptions Used

The design of the power system for MEFFV was developed to meet the automotive performance of vehicles projected to be in the fleet during the 2015-2020 timeframe and to supply the power for the electric armaments on the vehicle. Table III-02 briefly lists some of the requirements used to size the power system, their origin and the impact, if any, on the power system. As is evident from the table, with an EM gun on board system power and energy storage requirements are driven by the need to supply power to the gun system.

Table III-2. Requirements to size the power system

Requirement	Power/Energy Impact	Comment
Continuous gun fire at 2 rds/min	1 MW	30 MJ recharge of the CPA
Top speed (90 kph)	480 kW	Motor gearing and maximum power
Cross Country Speed (50 kph)	470 kW	Motor capability/battery capability
60 Percent Slope (10 kph)	570 kW	Motor power capability/TMS sizing point
Acceleration to 30 kph (7 s)	570 kW	Motor torque at corner point capability

The mass and volume of the power system was estimated using scalings derived from existing component designs where available. The one major deviation from this approach to sizing the vehicle is the turbogenerator system where we made projections based on mildly aggressive technology development programs that for vehicular systems are not currently in place.

Technology Development Requirements

The MEFFV power system presented above is a conservative design with most of the technology for the electric machines and converters on the system bus either demonstrated or in the process of being demonstrated. The power system leverages work currently being performed under commercial and government funded hybrid electric power system programs. These programs are developing compact high-temperature liquid cooled inverters (CHPS, CTA and FCS) and compact high torque, high power traction motor drives (CHPS, FCS). Issues that are unique to the MEFFV program for the electrical components on the system power bus have more to do with scaling of the components from small vehicles (22-ton level for FCS Manned Ground Vehicle Platforms) up to the 35-ton level. Currents and torques will be higher for the MEFFV

than for the FCS vehicles but the basic technology is the same and, hence, is directly transferable from the FCS program to the MEFFV program.

Battery technology is being advanced in a number of government and private sector development programs. Technology efforts which aim at improving the power density of Li-ion batteries are currently being pursued by both the Army and the Air Force. The intent of this effort is to use the battery as the power source for high-power electric laser systems. Progress in this area is substantial with reported battery power densities approaching 10 to 12 kW/kg for pulse discharges on the order of milliseconds and approaching 5 kW/kg for long pulse discharges (on the order of seconds) [III-2]. Energy densities for these batteries are on the order of 75 W-hr/kg.

At the other end of the battery spectrum is work being performed in support of the FCS program in which Li-ion cell technology optimized for energy storage is being packaged into modules and battery packs suitable for integration into combat vehicle power systems. These batteries have energy storage capabilities at the cell level of 100 to 140 W-hr/kg with power densities between 0.5-1 kW/kg. The work under this program is more geared toward engineering battery packs for inclusion in combat power systems and includes developing vehicle integrated thermal management systems for batteries that use cooling air from the environmental control system, manufacturing technology for mass production of the cells and packs, and battery life-cycle studies and development to improve the end-of-life properties of the battery system.

The major uncertainty in the power system is the status of turbogenerator technology at the 500 kW – 1 MW class in the 2015-2020 timeframe. The most recent turbine development program for land systems was the 1.2 MW LV-100 Advanced Integrated Propulsion System (AIPS) power pack which was developed as an upgrade to the AGT1500 M1 engine. There are currently no major vehicular class turboshaft engines under development in 500 kW to 1MW class which is needed for a direct fire EM gun system such as the MEFFV. However, components such as high efficiency compressors and power turbines are being developed for aero applications that can be used to form the basis of a prime power source for a land vehicle.

The power plant we sized for the MEFFV uses a recuperated turbine cycle. As shown in figure III-3 the minimum fuel consumption for installed systems at the optimum pressure ratio can rival that of high-speed diesel cycles for turbine inlet temperatures (TIT) over ~ 1300°C. The

key to realizing the theoretical efficiency of the recuperated cycle is cycle temperature. Current generation turbines in the 500 kW class utilize metallic hot end (combustor, turbine, recuperator) components limiting the maximum cycle temperature to ~ 1000°C [III-3]. Ceramic hot end components are being developed for both aero engines and stationary powerplants that raise allowable temperature limits to on the order of 1300°C [III-4, III-5, III-6, III-7]. The technology being developed is directly applicable to moderate power turbine systems for vehicular application [III-8]. Using ceramic hot-end technology allows us to project specific fuel consumption in the range 0.36 lb/hp-hr for a cycle pressure ratio of 5.5 to 6.0. Also, using basic turbine component scaling relations we project turbine power densities approaching 2 kW/kg.

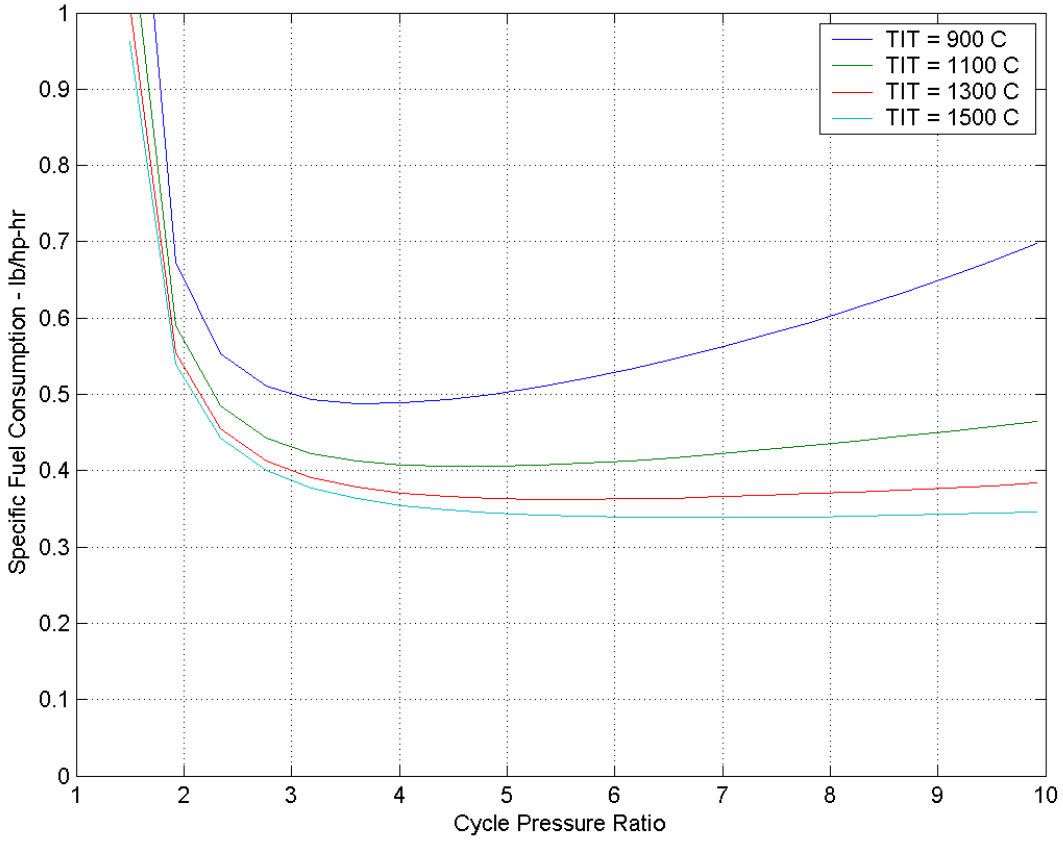

Figure III-3. Specific fuel consumption for a 500 kW recuperated cycle gas turbine -cycle calculation assumes compressor efficiency of 7%, turbine efficiency of 84%, and recuperator effectiveness of 85%

References

[III-1] MEFFV Lethality Study: Status to Date, Briefing to NSWC-CD and MEFFV Project Office, 7 August 2003.

[III-2] Matty, T. Private Communication

[III-3] Walsh, P.P. and Fletcher, P, *Gas Turbine Performance*, Blackwell Sciences, Ltd and ASME Press, 1998.

[III-4] Price, J.R, et. al, 1998, 'Ceramic Stationary Gas Turbine Development Program – Fifth Annual Summary', ASME 98-GT-181.

[III-5] Okuto, A., et. al., 1998, 'Development of a Low NOx Combustor for 300 kW-Class Ceramic Gas Turbine (CGT302)', ASME 98-GT-272.

[III-6] McDonald, C.F., 1996, 'The Exhaust Heat Recovery Exchanger – A Key Component for the Realization of High Efficiency in Very Small Gas Turbines'.

[III-7] Rodgers, C. and McDonald C.F., 1997, 'Automotive Turbogenerator Design Considerations and Technology Evolution', SAE-972673.

[III-8] Angelo, V.K. and Mauch, H.R., 1999, 'Advantages of the LV100 as a Power Producer in Hybrid Propulsion Systems for Future Fighting Vehicles', ASME 99-GT-416.

IV. Lethality Analysis

IAT will be submitting this section under separate cover.

V. Launch Package

IAT will be submitting this section under separate cover.

VI. Railgun

Introduction and requirements

The MEFFV application requires a tactically configured, fieldable electromagnetic launcher. Along with meeting the bore geometry and inductance specifications needed to deliver the projectile at the desired energy, the gun must also be lightweight, stiff, and provide for active cooling. The gun must be capable of containing the repulsive load seen by the rails during a shot. Enough rail preload needs to be developed such that no separation occurs as a result of the load. Structurally stiff guns, which minimize this deflection, have been seen to have lower bore wear, thus extending the life of the rails. A lightweight gun is desirable as well. As well as minimizing overall system weight, in a vehicle-mounted application a lighter gun is more maneuverable. Even with low gun weight, the barrel design should be such that it minimizes deflection along the barrel due to its weight. Finally, thought must be given to the manufacturability of the components. A view of the full gun assembly is shown in Figure VI-1.

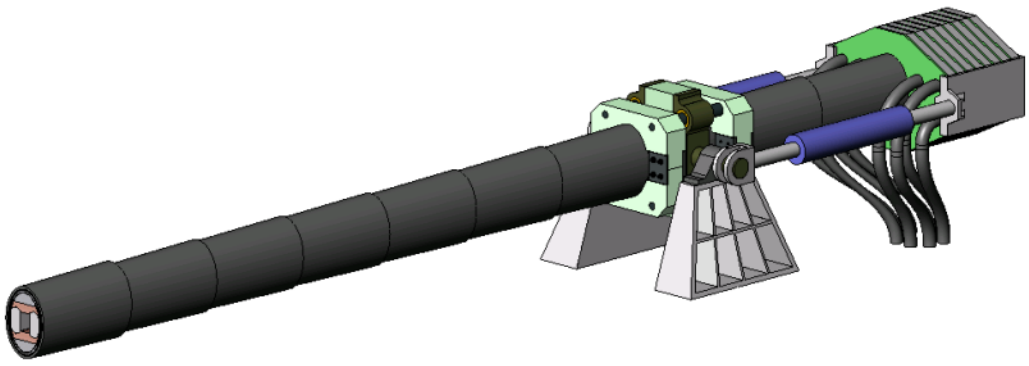

Figure VI-1. Full gun assembly

Methods Employed and Assumptions Used

The design proposed by UT-CEM is an evolution of previously proven designs. It consists of chromium copper rails with laminated ceramic sidewalls, preloaded by a composite over-wrap made up of multiple overlapping tapered bandings. The bandings will have an elliptical cross section. Between the rails and over-wrap will be a composite backing material to transfer the preload from the bandings to the rails. The breech of the gun will be made up of multiple, alternating polarity, bolted plates. At the muzzle end of the gun, a passive shunt will be installed. Cooling tubes will be placed between the rails and backing material. A cross sectional view of the barrel can be seen in figure VI-2.

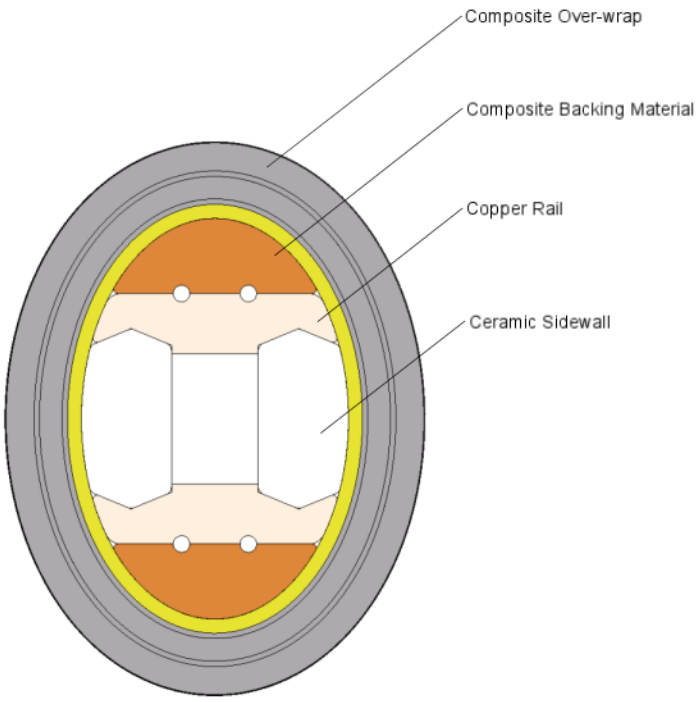

Figure VI-2. Railgun cross section

The barrel will be assembled by first bonding the rails to the sidewalls with adhesive film in an elevated temperature cure. The differing thermal expansions between the copper and ceramic will result in an axial preload being applied to the sidewalls. Once these components are bonded, the resulting assembly will be wrapped with a mica B-stage insulating tape. Cooling tubes and the backing material will be then put in place and the entire assembly will then have

the bandings installed. The each of the tapered bandings will be sequentially pressed on with interference and overlapping by fifty percent. The interference will provide the preload needed to keep the rails to sidewall interface in compression during the gunshot. The overlapping of the bandings will maintain axial strength in the barrel. The muzzle shunt will be installed on the front end of the gun, it's contact force also provided by the composite over-wrap. The breech plates will be sequentially assembled on the back of the gun, with a mechanical preload applied to provide the contact pressure to the rails.

The rails of the gun are to be made of chromium copper, giving both high strength and high conductivity. The rails will have slots milled into them transverse to the gun axis along their entire length. This will force the current to flow in the desired location, giving the optimal inductance gradient. This allows the rails to be shaped such that the sidewalls can be locked into place and still transfer the preload from the over-wrap. The slots will be backfilled with reinforced epoxy. Corners will be filleted to avoid any stress concentrations due to loading. Figure VI-3 shows a section of rail with the slots milled into it.

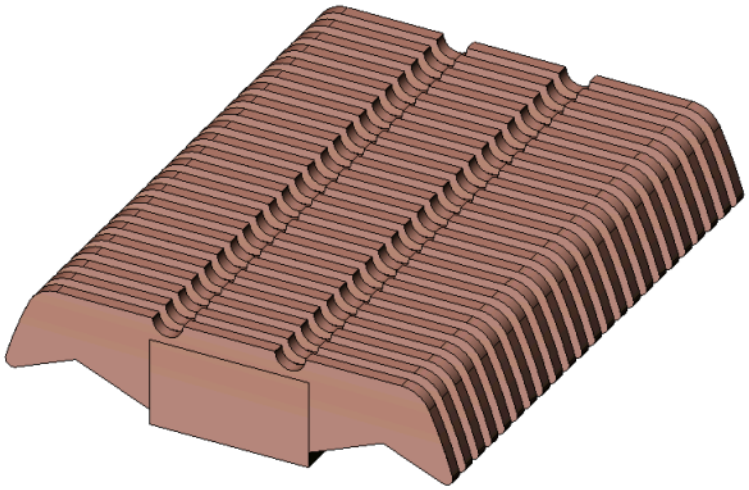

Figure VI-3. Gun rail with transverse slots

As in previous rail gun designs, the sidewalls will be made of a high modulus ceramic. It is imperative that the sidewalls remain in compression at all times. This will be achieved both by the preload applied by the composite bandings as well as the post cure axial compression developed during the rail bonding procedure. To achieve the length required for this gun

application, it may be necessary to build the sidewalls by laminating multiple pieces of ceramic. UT-CEM proposes laminating thin lengths, oriented in the rail-to-rail direction with staggered butt joints along the gun axis. The orientation of the ceramic pieces in the rail-to-rail direction is desired because that is the predominant loading direction. Once the entire sidewall is bonded together, the entire assembly can be ground to its final shape. If the butt joints along the bore surface are not sufficiently smooth, a wear resistant coating can be applied.

High strength carbon composite bandings will be installed to provide the required rail-to-rail preload. By using multiple press fit bandings, achieving this preload it eased compared to attempting to install one continuous over-wrap with the needed interference. Required press loads decrease with banding length, and manufacturing is simplified. Also, with shorter bandings, more flexibility is available in choosing a non axi-symmetric shape such as an elliptical cross section. The elliptical cross section allows the gun to be preloaded predominately in the rail-to-rail direction. Also, the increased moment area in an elliptical cross section will result in less barrel droop without a large mass increase. A section view of the gun barrel showing the assembled bandings with overlap and interference can be seen in figureVI-4. The bandings can be thought of having two distinct areas with different purposes. The exposed section of the banding is with its interference fit over the lower banding is present to provide preload to the rails. The carbon fibers in this section will be predominately wound in the hoop direction. The section of the banding underneath the adjacent banding should not have a high hoop modulus. This would only inhibit the outer bandings ability to provide preload. Instead this section will be wound at a much lower wind angle, decreasing its hoop strength, but adding axial strength. A transition region will be required between the two banding sections. This winding geometry can be achieved using a numerically controlled filament winding system.

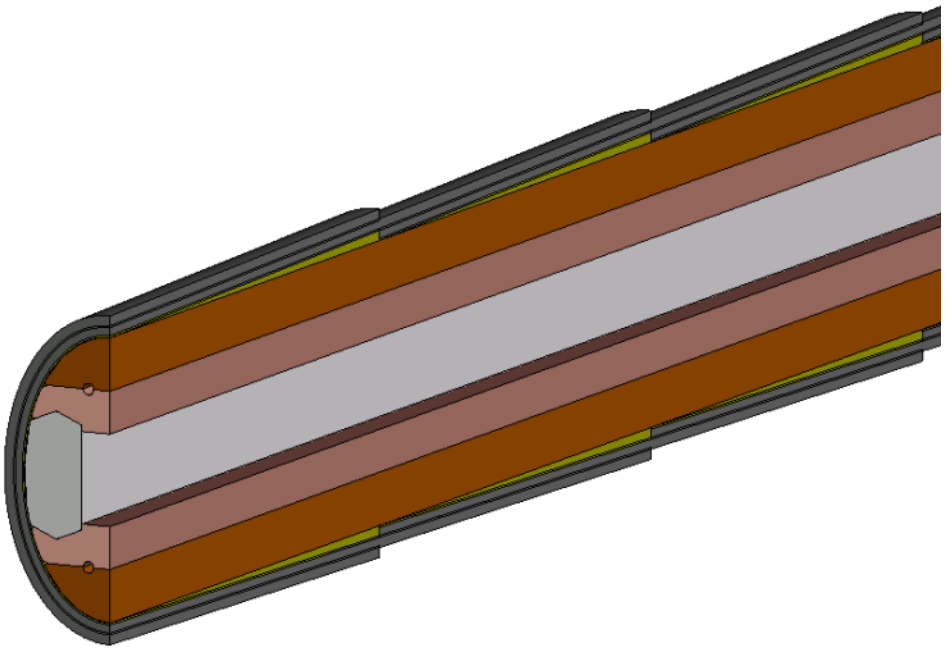

Figure VI-4. Barrel section view

The breech of the gun will consist of alternating aluminum and insulating plates in a bolted assembly. The laminated breech approach decreases the repulsion loads that must been contained. Coaxial cables will be fed through the front sides of the plates and have their connections made with alternating polarities on each subsequent plate. A mechanical preload mechanism will be used to provide the contacting force to the rails. An interface plate to the recoil mechanism will be installed on each side of the breech.

A passive muzzle shunt will be installed on the front end of the gun. The shunt will be an aluminum sleeve with slots milled into it creating a spiral current path along the gun connecting one rail to the other. The current path and length can be adjusted to need in this approach. The connection to the rails will be made using the preload provided by the composite over-wrap. An inner and outer insulating sleeve will be installed to isolate the shunt from the banding. The shunt with the outer banding and insulating sleeve removed can be seen in figure VI-5.

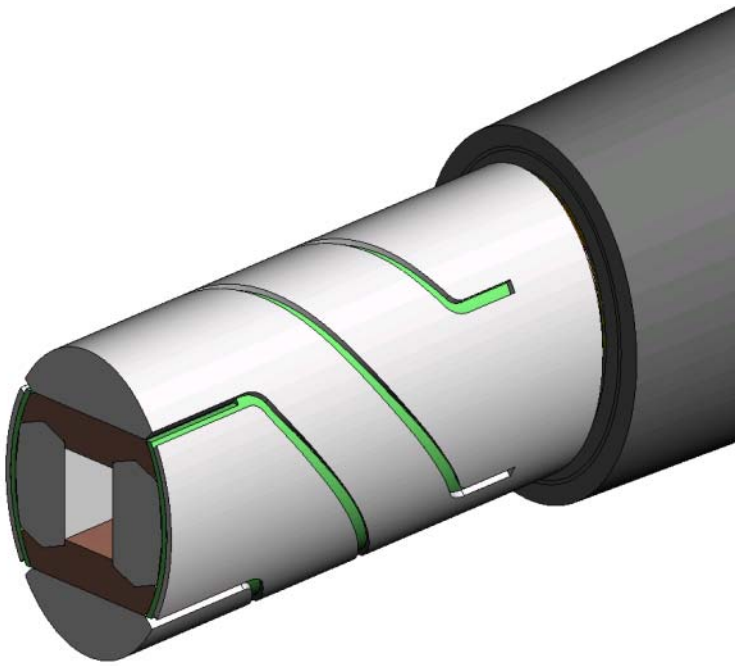

Figure VI-5.Passive muzzle shunt

Results of Analyses, Simulations, Trade Studies and Designs

The railgun inductance and resistance gradients were calculated using an in-house code based upon a paper by Lauer [VI-1]. The code functions by computing the current distribution of an infinitely long set of conductors, under the assumption that all the current flows on the surface of the conductors. Railgun L' and R' are derived from this current distribution. It is generally valid for any reasonable performing railgun with velocities over 1 km/s.

A two-dimensional finite element model was begun to determine the necessary banding properties and required interference to maintain adequate preload. This was a quarter-symmetry model that included the rails, sidewalls, and two composite bandings. Figure VI-6 shows the mesh created for this model. The repulsion load seen by the rails can be input and the required banding properties and interferences can be determined. They need to be set such that the rails and sidewalls remain in contact and in compression during the shot. To eliminate stress concentrations, added fidelity is needed in the model. In particular, details such a corner rounds need to be added, as well as the cooling passages. A similar geometry model can be used to investigate the cooling requirements of the gun. According to the machine simulation, to

maintain a two round per minute shot rate approximately 130 kW of heating will be developed due to rail losses. The cooling model can be used to determine the size, location, and number of cooling passages required as well as the needed flow rate. The temperature seen in the composite bandings will limit the allowable gun temperature.

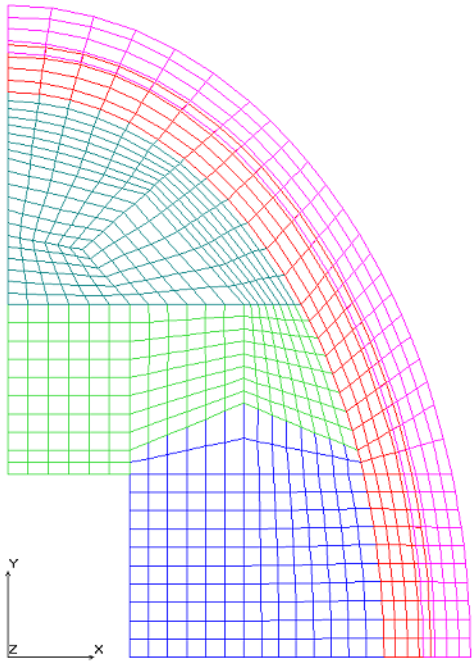

Figure VI-6. 2D FEA gun model

Technology Development Requirements

Development work will be required to construct the gun described above. In particular, some development work will be needed for the sidewalls, composite windings manufacturing, sequential banding assembly, and the muzzle shunt. While the use of ceramic sidewalls is not new to railguns, constructing one out of laminated ceramic sections is new. Trial assemblies would need to be built and tested to insure the structural integrity of the bonds, as well as investigating the possible need for a bore coating. Work will be needed to identify any possible difficulties in winding a non axi-symmetric composite banding with graded properties along its length. UT-CEM has experience winding complicated geometries, however any new variable requires some development. UT-CEM has created software tools that aid in not only

determining winding geometries, but also create models for use in analyses. These can be leveraged to expedite new development. UT-CEM has a large experience base in performing tapered banding press fits. However, this will be the first railgun constructed using multiple bandings as an over-wrap. UT-CEM has a plan for using a press that moves along the gun length to press the bandings, using the previous banding to react the load. This technique still needs to be proven effective. Finally, electromagnetic (EM) analysis of the muzzle shunt will be needed. It is expected that a detailed 3D EM model will have to be constructed to determine the geometry necessary to provide the proper characteristics. This same model should allow for investigating if there are any effects to the projectile as it passes through the shunt.

Discussion, conclusions and recommendations

UT-CEM is has proposed a lightweight and structurally stiff electromagnetic launcher solution. The design utilizes sequentially assembled composite bandings to provide a passive preload system. Encased in this composite over-wrap are high strength copper rails with ceramic sidewalls with excellent compressive strength and modulus properties, along with a composite backing material to transfer preload from the bandings. An elliptical cross section provides for added longitudinal stiffness required for a cantilevered gun at a reduced mass. The gun also uses a proven laminated plate breech design that reduces repulsive loads that must be contained. A passive muzzle shunt with adjustable characteristics is also proposed. Through the use of in house code and finite element analyses, the electrical, mechanical, and thermal performance of the gun can be predicted. Development will be required to some areas, particularly manufacturing processes. UT-CEM is confident in its experience with composites and testing that development will be successful.

References

[VI-1]. Leuer, J.A., “Electromagnetic Modeling of Complex Railgun Geometries”, IEEE Transactions on Magnetics, Vol. mag-22, No. 6, November 1986.

VII. Pulsed Alternator Design

Introduction and Requirements

Development of pulsed rotating machines for railgun applications has been funded largely by the Army and dates from the mid 1980's. Since the successful demonstration of the Iron Core Compulsator at the CEM there have been four new generations of light weight air-core machines designed. Three of these generations have been built and tested at the CEM. A comprehensive bibliography on pulsed alternator research at the CEM has been included at the end of this report section.

The latest generation concept represents what the CEM engineers believe to be the entry level machine that could be integrated into a main battle tank type chassis. If adequately funded, this prototype could be realized by 2010. Manufacture of the latest generation machine has not yet been funded, however there has been extensive engineering and analysis performed. As the solid model concept vehicle shows at the end of this report, a machine very similar to this will fit on an EMEFFV platform that weighs in the range of 35 tons.

The entire process for designing a prototype pulsed alternator (PA) for railgun applications has been evolving at the CEM over 15 years. Figure VII-1 shows the flow chart that is used to completely design a prototype PA for fabrication. For the purposes of this study, however, only the blocks indicated by heavier outlines were used. These blocks include the sizing algorithm, 1D nested ring analysis, finite filament analysis, and the coupled circuit/thermal simulation. The new CEM-UT sizing algorithm called the Advanced Pulsed Alternator Design System (APADS) was used for this effort.

APADS is a combination of MATLab scripts and FORTRAN source codes imported to the MATLab environment that together define an accurate solid model of the pulsed alternator best suited to drive the railgun load. The mission performance requirements needed to accomplish this task are presented in table VII-1. Output from APADS accurately defines all the PA critical design parameters and the resulting solid model contains basic dimensions and material properties consistent with all generator mechanical and winding geometries, and

composite banding materials. APADS also generates input files used by the performance simulation discussed in a following section.

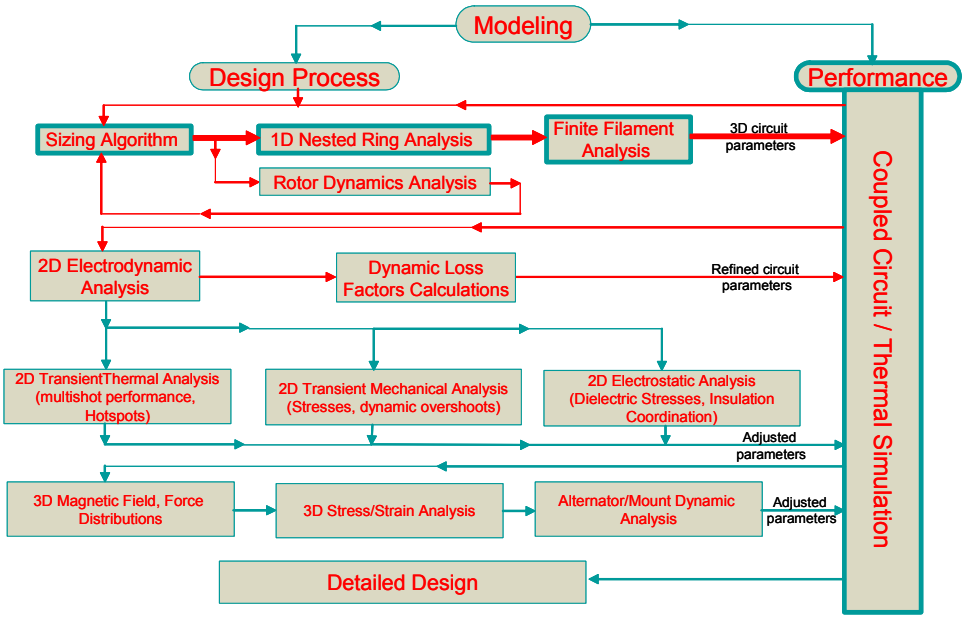

Figure VII-1. PA design methodology used at CEM

Table VII-1. Pulsed alternator performance requirements for EMEFFV concept

Parameter	Units	Value
ILP muzzle KE	MJ	9
Number of burst rounds stored		5
ILP exit velocity	m/s	2,500
Gun acceleration length	m	6
Gun rail L-prime	μH/m	0.61
Gun rail resistance gradient	μΩ/m	49.0
Design acceleration ratio		0.65
Design PPS net efficiency		0.35

Railgun power supply design requirements were derived from three sources. First, the battle simulations performed by Booz Allen as discussed in previous sections provided the number of burst rounds stored within the railgun pulsed power system (PPS). In addition to this the IAT also recommended a muzzle energy and velocity for the main weapon of the vehicle. Results of this and the integrated launch package (ILP) are reported in a separate classified document. A muzzle energy of 9 MJ at 2.5 km/s were settled on for the main EM gun. Using this information a railgun bore cross section was also recommended, and resulting predicted railgun parameters (L' and R') were quickly derived for that geometry. Consistent with ILP performance requirements, a railgun acceleration length was assumed (6 m), as were objectives for the current profile delivered by the PA (acceleration ratio) and assumed net PPS efficiency. As is typical with PA driven railgun systems, this efficiency is defined as;

$$Enet = \frac{E_{KE}}{E_{rotor}}$$

where E_{net} is the net system efficiency, E_{KE} is the ILP muzzle energy, and E_{rotor} is the net change in rotor energy during the entire shot interval. The requirements are shown in table VII-1.

Methodology and Analysis

The input file for APADS was built using the performance requirements defined by the launch package and lethality design. Besides the performance information used above, there are several other parameters required as input for APADS to correctly execute. These consider the topology of the alternator, operating peak frequency, current density levels, banding stress limits, and winding configurations used in the design. The input file used to generate the EMEFFV pulsed alternators design is shown in figure VII-2. The basic definitions of the inputs are inside the input file as shown.

```
*MEFFV_R0
* PA cooling config : 0=uncooled, 1=cooled using radiator layer, 2=FW integral cooling
* Cooling Config, Design Peak Current (A), Terminal Lugs per pole/polarity,
* est system efficiency, # shots stored inertially, accel ratio assumed
2,1.75e6,1,0.35,5,0.65
*Projo KE (J), Projo Vel (m/s), Gun Accel Length (m), L' (H/m), R' (ohm/m)
9e6,2500,6.0,0.61e-6,49e-06
*Poles, Electrical Frequency, Number of Phases, armature pole fraction, field pole fraction
4,750,4,0.5,0.8
*   Banding maximum allowable hoop stress, minimum banding thickness
390,0.25
*Field Coil Pole Packing Fraction (ins included), Outer ins thick (in), Inner ins thick (in),
*Field Coil Current Density, Armature material ( 1=Al, 2=Cu ), Arm Litz Insulation Thk (in)
0.77,0.08,0.04,3.375E+06,2,0.045
*Total Flux density (T) due to Outer FC, and Inner FC (small if none)
3.0,1e-12
*Peak Excitation Field Current, Charging Time for FC, Design FC delta-T per shot (C)
2.00E+05,0.025,30.
*Armature Temperature Rise              Armature Packing Fraction Compensating Packing Frac.
*AW packing fraction includes 45 mils radial outer and inner insulation
30,0.42,0.5
*electrical conductivities of the windings
*FW, CW, AW, Shell, Shield  (sigma pure cu=5.8e+07)
3.450e+07,3.450e+07,5.8e+07,5.65e+05,2.030e+07
*Thick of Comp. Winding (in),  Min B1 layer thickness, Radiator Layer Thickness, Bearing DN number
1e-12,2.559,0.375,1.75e06
*Starting L/D ratio, L/D Increment, Ending L/D ratio, Min Tip Speed, Max Tip Speed, Tip PSeed Inc
0.5,.01,0.51,700,800,5
end
```

Figure VII-2. APADS input file for EMEFFV design

The design of the air-core PA is based on the use of advanced graphite-epoxy composites. It is a four pole, four phase architecture with a rotating field winding, and features an integral flywheel for energy storage. APADS works by iteratively solving for particular pulsed alternator solutions matching all of the performance requirements in the input file and the geometrical constraints of the specific design topology desired. Using a maximum input electrical frequency, the solver finds rotor dimensions and winding combinations and geometries within multiple tip speed ranges. These windings are combined into a rotor structure (field winding) and armature winding structure using properties and experience gained over prototyping these machines at the CEM since the 1980's.

Once the structure to support the windings is designed, the code checks for appropriate energy storage in the rotor satisfying all input constraints and estimates the peak short circuit current capability of the design within acceptable thermal limits. The lowest mass machine solution with the largest peak current capability represents the design of choice in railgun applications for tactical armor applications. Once APADS has identified the optimal design solution, it then goes on to identify critical design features including the rotor banding designs based on user supplied material properties. The code then generates the input file for the railgun

and pulsed alternator which is used in the performance simulator. The PA self and mutual inductances then are computed using a 3D finite filament formulation.

Finally, APADS generates input files used in SOLIDWORKS to generate a 3D representation of the design output including accurate masses. The solid model is based upon an enhanced version of the latest generation PA concept generated by CEM for the Army 6.2 electric gun program. The solid model is intended to accurately represent the PA dimensions and mass, however, it is in no way a comprehensive representation of the machine. It is meant to be a true bulk representation of the PA for use in trade study analyses, and was well suited for use in this study. APADS generates a 14 page comprehensive text output file describing all facets of the PA design solution. The output resulting from the input file above from APADS is presented in Appendix B for reference. For quick reference here the major design aspects of the PA are presented in table VII-2. Figures VII-3 and VII-4 show the solid model generated by APADS and Solidworks. These are the same models used in the vehicle later in the report.

Table VII-2. EMEFFV PA design summary (per machine)

Design Parameter	**Value**	**Units**
PA outer diameter	1	m
PA total length	2	m
Rotor drum length	0.9	m
Flywheel length	0.13	m
Electrical frequency (full speed)	750	Hz
Design speed	22,500	rpm
Total energy storage @ design speed	130	MJ
Field Current	200	kA
Air-gap flux density	3	T
Peak voltage	9	kV
Minimum short circuit current	2	MA
Total mass (per machine, less drive motor)	1735	kg

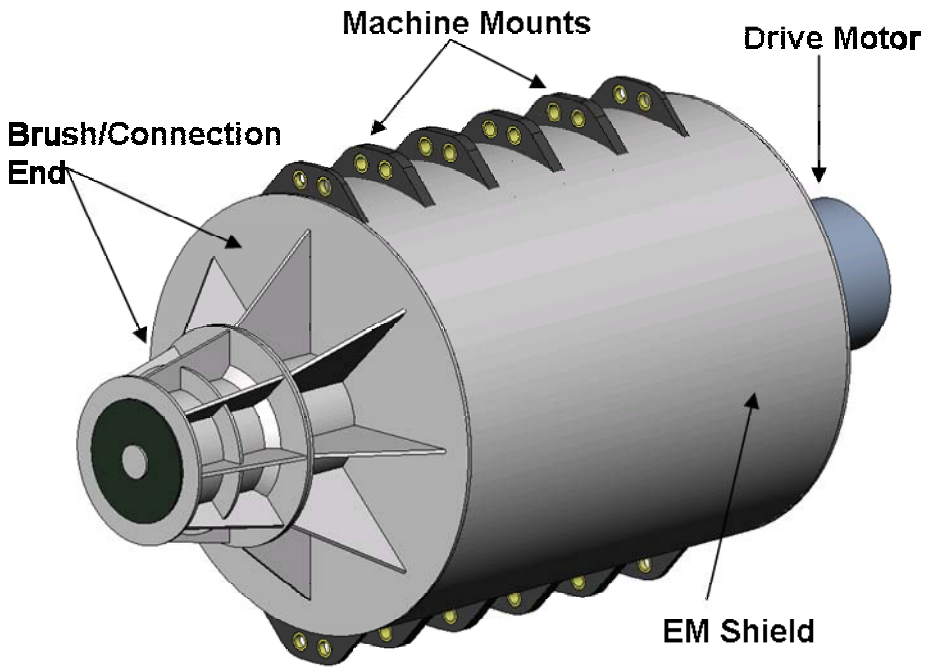

Figure VII-3. APADS generated solid model of pulsed alternator

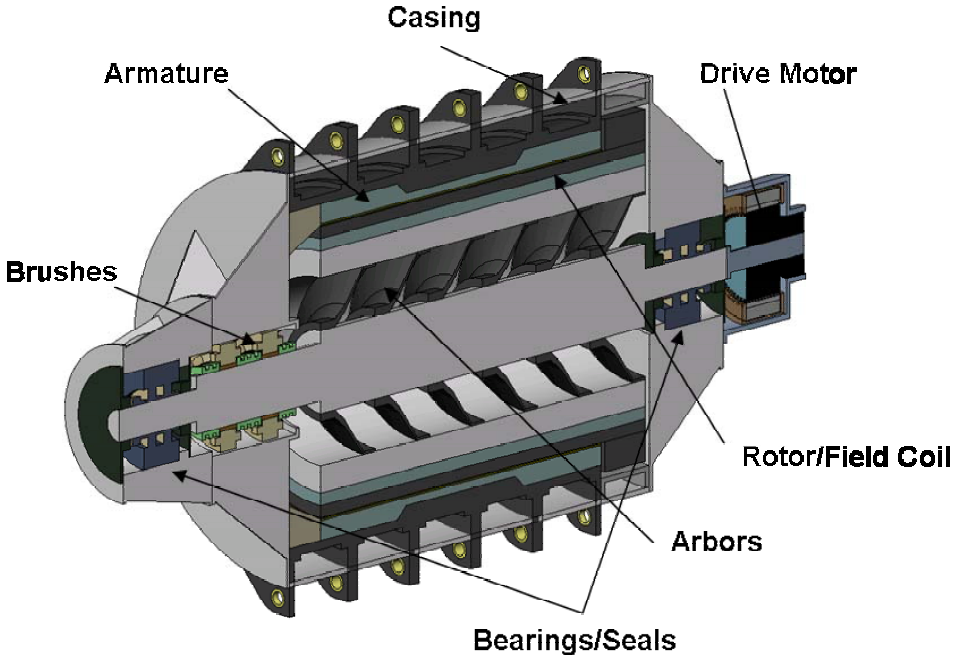

Figure VII-4. APADS generated solid model, sectioned view

As figure VII-1 shows, the entire PA design process is tied to a performance simulation of the PA-Railgun system. This simulation is essentially a detailed circuit analysis of the PPS. It was created in the Matlab-Simulink environment and this greatly facilitates modification of the model and/or the study of fault modes etc. The Simulink model includes detailed PA and railgun models that are written in FORTRAN and then compiled for use in Simulink. The PA model includes all winding impedances and respective couplings. The railgun model is based on models used at the CEM past since the late 1970's. The main block diagram used by Simulink is shown in figure VII-5.

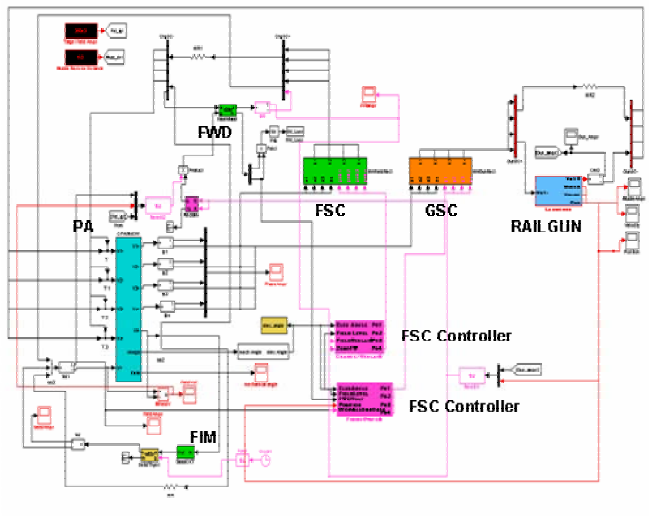

Figure VII-5. Simulink model used for performance PPS simulation

Figure VII-5 shows the complete layout of the PA-railgun simulation system. The following will better explain the acronyms used in the above figure along with how the PPS operates in general.

From the instant the gun is triggered to the time the generator is back to its pre-shot state (at reduced rotor speed) is less than a half of a second. A typical timeline for the PPS event cycle is presented in figure VII-6. For the PA, the time rate of fire is dependent on the brush seating and unseating time. A value of 200 ms is assumed in the time line below; quicker seating

times are certainly possible and are dependent on the detailed design of the PA brush system in general. In this case the ILP exits the railgun about 220 ms after the discharge is started.

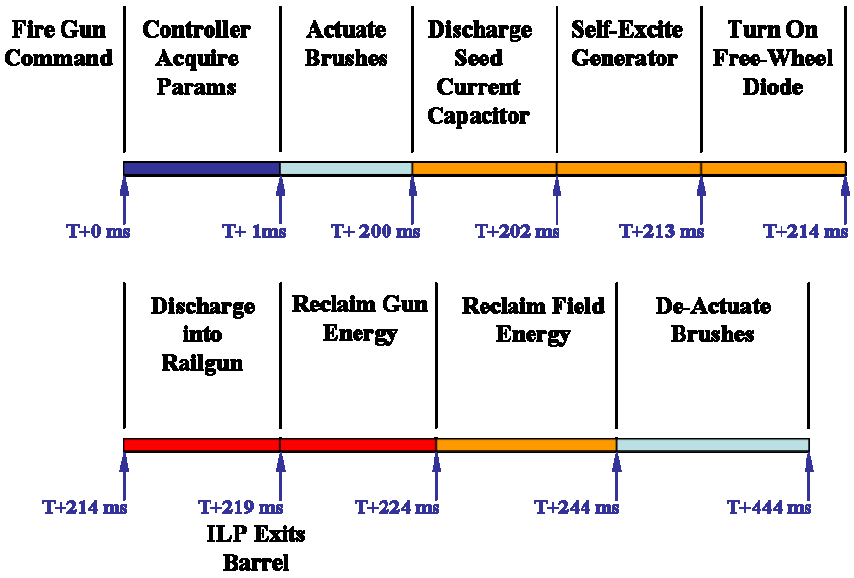

Figure VII-6. Main simulation block diagram from Simulink

It is assumed that the railgun is already loaded with the round of choice as selected by the user. Following the timeline above, the first action taken when commanded to fire is to acquire the current operating parameters of the PPS. The PPS Firing and Fault Control Module (FFCM) would do this. These parameters would include PPS auxiliary status, rotor speed and position feedback, winding temperatures, and what kind of round was loaded in the railgun. The FFCM would then command the brushes to actuate against the rotor shaft. After allowing some minimal time for the brushes to seat against the slip rings, the FFCM would discharge a seed current capacitor located within the Field Initiation Module (FIM). The FIM includes a 25kJ capacitor charged at no voltage greater than the normal operating voltage of the PA. It is believed that in a tactical system this capacitance may be borrowed from another on-board EM system such as might be included in the EM APS, or EM armor, etc.

After a very short dwell the FFCM then commands the Field Switch Converters (FSC) to begin gating. The self-excitation process has now begun. Harnessing flux to generate voltage from the FIM event, current is then fed back from the PA armature into the field winding using rotor kinetic energy. This is in effect a positive feed-back loop. The main PA field, under

control by the FFCM, is then boot strapped to its target value for the specific shot. When the field has reached its determined value, the Free Wheel Diode (FWD) is turned on, channeling the field into a known freewheel path for the main discharge sequence. The Gun Switch Converter (GSC) is then cycled by the FFCM tying the PA armatures to the railgun and propelling the ILP down the gun bore. As soon as the ILP has exited the railgun, the FFCM then begins reclaiming the magnetic energy remaining in the railgun by commanding the GSC to operate as a line commutated inverter. After this is accomplished, the FFCM does the same operation on the field winding by via appropriate gating of the FSC. When the current has been fully depleted, the brushes are then lifted off the rotor slip rings; the discharge cycle is now complete.

Results

Simulations were executed for each of the five 9 MJ rounds as demanded by the burst performance requirements derived by the data provided by BAH. Output plots from each of these simulations can be seen in Appendix C. In addition, as an example of the versatility of the PPS an additional shot was performed following the 5 round burst. This shot assumed an HE type round with a total 5 kg launch mass and 1,280 m/s exit velocity. This data too can be seen in the appendix. This bears out the fact that the PPS can deliver any ILP based upon the conservation of linear momentum of the tactical KE penetrator. This is shown graphically in figure VII-7, where the KE round (2.88 kg @ 2,500 m/s) is the baseline momentum for the PPS.

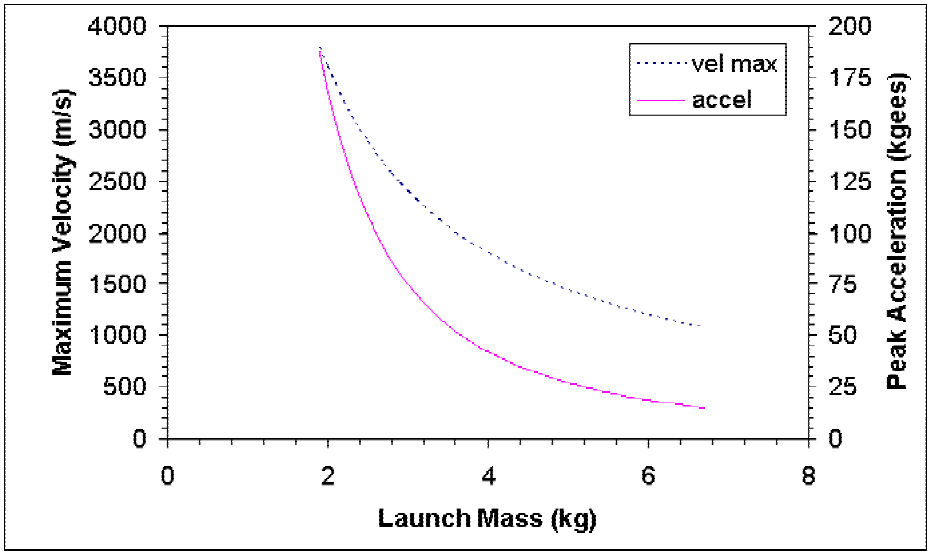

Figure VII-7. Constant momentum plots for determining payloads for EMEFFV railgun

Results from the six simulations were also compiled into a spreadsheet in order to summarize the entire PPS performance attributes and requirements. These results are presented below in table VII-3 for reference.

Table VII-3. PPS design summary

date notes		92503 MEFFV_R0 Shot 1	Shot2	Shot 3	Shot4	Shot 5	Shot6 HEP
Gun and ILP Data	**Units**						
Mass	**kg**	2.88	2.88	2.88	2.88	2.88	5
Velocity	**m/s**	2497	2562	2502	2556	2532	1280
Muzz Energy	**MJ**	9.0	9.5	9.0	9.4	9.2	4.1
Peak Gun Current	**MA**	2.69	2.9	2.82	2.92	2.89	2.06
Peak Projo Current	**MA**	2.68	2.89	2.81	2.9	2.88	2.04
Single Shot Action	**MA^2-sec**	23578	24192	23625	24135	23909	20984
Peak Accel	**kgees**	78.2	90.9	85.6	92	89.8	26.4
Acceleration Ratio	**%**	0.69	0.634	64.0	62.2	61.7	57.6
Barrel Length (total)	**m**	6	6	6	6	6	6
Distance to Muzzle Resistor	**m**	5.97	5.97	5.97	5.97	5.97	5.97
Lprime	**microH/m**	0.61	0.61	0.61	0.61	0.61	0.61
Rprime	**micOhm/m**	0.49	0.49	0.49	0.49	0.49	0.49
Muzzle Shunt L	**nano-H**	100.0	100	100	100	100	100
Muzzle Shunt R	**micro-Ohm**	100.0	100	100	100	100	100
Min Arm Volts/Trans Speed	**V/(m/s)**	40/1500	40/1500	40/1500	40/1500	40/1500	40/1500
Max Arm Volts/At Velocity	**V/(m/s)**	50/2500	50/2500	50/2500	50/2500	50/2500	50/2500
Arm Curr @ Exit	**kA**	528.0	583	316	315	294	0
CPA Data (Per Machine) (calculated at given speed)		**Shot 1**	**Shot2**	**Shot 3**	**Shot4**	**Shot 5**	**Shot6 HEP**
Poles, Phases		4, 4	4,4	4,4	4,4	4,4	4,4
Shots Stored (from top speed)	**Units**	5.22	4.46	3.74	3.10	2.18	3.09
Rotor Polar Moment	**kg-m^2**	36.40	36.40	34.6	34.6	34.6	34.6
Flywheel Polar Moment	**kg-m^2**	10.50	10.50	10.5	10.5	10.5	10.5
Rotor Energy	**MJ**	101.0	90.9	76.2	65.9	55.1	42.2
Flywheel Energy	**MJ**	29.1	26.2	23.1	20.0	16.7	12.8
Total Rotor Energy	**MJ**	130.2	117.1	99.3	85.9	71.8	55.1
Starting Rotor Speed	**rpm**	**22500**	**21336**	**20036**	**18638**	**17043**	**14921**
Ending Rotor Speed	**rpm**	21336	20036	18638	17043	14921	13663
Rotor Tip Speed	**m/s**	826	783	736	684	626	548
Flywheel Tip Speed	**m/s**	1000	948	890	828	757	663
Design for Banding Hoop Stress	**ksi**	390	390	390	390	390	390
Field Bridge Volts	**kV**	17	16.8	15.3	15.6	17.3	8.8
Avg Field Bridge Volts (Br to Shunt)	**kV**	2.87	2.84	2.51	2.68	3.18	
Gun Switch Volts	**kV**	16	15.4	13.3	13.9	13.9	7.4
Avg Gun Switch Volst (Br to Shunt)	**kV**	2.89	2.87	2.54	2.72	3.21	
Peak Arm Current	**MA**	1.26	1.34	1.26	1.355	1.362	0.951
Simulated Chrging Field Current	**kA**	195	195	195	205	260	150
Field Current at Trigger	**kA**	201	211	202	225	275	156
Field Action (Total per shot)	**MA^2-sec**	546.5	593.1	563.175	661.175	977.95	384.7
Avg. Armature Starting Temp	**C**	25	43	61.7	80.5	99.3	120.3
Avg. Armature Ending Temp	**C**	43	61.7	80.5	99.3	120.3	134.6
Armature Delta-Temp	**C**	18	18.7	18.8	18.8	21	14.3
Field Starting Temperature	**C**	25	39	54.5	69.2	86.4	111.9
Field Ending Temperature	**C**	39	54.5	69.2	86.4	111.9	121.9
Field Delta-Temp	**C**	14	15.5	14.7	17.2	25.5	10
Peak Power	**GW**	5.92	5.665	6.135	5.605	7.485	1.965
Average Power (Launch cycle)	**GW**	2.80	2.985	2.7595	2.9355	3.075	0.935
Average Discharge Torque	**MN-m**	1.24	1.4	1.382	1.605	1.905	0.635
outer armature radius	**m**	0.3736	0.3736	0.3736	0.3736	0.3736	0.3736
active length	**m**	0.3581	0.3581	0.3581	0.3581	0.3581	0.3581
avg arm shear stress	**psi**	1145.3	1293.1	1276.5	1482.4	1759.5	586.5
rotor diameter	**m**	0.7012	0.7012	0.7012	0.7012	0.7012	0.7012
rotor length (drum + flywheel)	**m**	1.05	1.05	1.05	1.05	1.05	1.05
generator diameter	**m**	1.08	1.08	1.08	1.08	1.08	1.08
generator length	**m**	2.10	2.10	2.10	2.10	2.10	2.10
Generator Mass ea.	**kg**	1643	1643	1643	1643	1643	1643
Flywheel Mass ea.	**kg**	92	92	92	92	92	92
FSC/GSC mass ea.	**kg**	625.6	625.6	625.6	625.6	625.6	625.6
FWD mass ea	**kg**	31	31	31	31	31	31
auxiliary mass ea. (1.5x for 2)	**kg**	150	150	150	150	150	150
Number gensets required		2	2	2	2	2	2
Total Mass	**kg**	4933.2	4933.2	4933.2	4933.2	4933.2	4933.2
Peak Brch Energy	**MJ**	18.5	18.5	19.1	18.2	19.3	9.49
Efficiency		0.36	0.36	0.34	0.34	0.28	0.23
net gun eff		0.65	0.66	0.64	0.67	0.65	0.55
rotor energy density (PA mass only)	**J/g**	79.2	71.3	60.4	52.3	43.7	33.5
PA Power Density	**MW/g**	1704	1817	1680	1787	1872	569

Table VII-4. Critical technology development areas for the pulsed alternators

Technology Area or Machine Subcomponent	**ROM Development Time (months)**
ROTOR	
Outer Banding	12-18
Structural Arbors	6-12
Cooling Arbor	12
Conductor Arbor	12
Field Winding Layer	12
STATOR	
Armature Conductors/Cooling	8
Outer Casing	12
Output Cables	6
Miscellaneous	
Drive Motor	12

Rotor Banding

The rotor banding maintians radial preload of the field winding throughout the operating speed range of the generator. The combination of a relatively massive field winding that has little built-in structural strength and the need to minimize the magnetic air-gap between the field winding and armature makes the rotor banding the highest stressed component within the generator. In addition, the operating temperature will approach 160°C. CEM has developed a low temperature (100°C) banding using T1000G which is already close to the strain requirements of the current design. Further development is required to demonstrate a system that can safely operate at temperatures approaching 160°C. Figure VII-8 shows a 3D representation of the rotor highlighting key technical development areas needed.

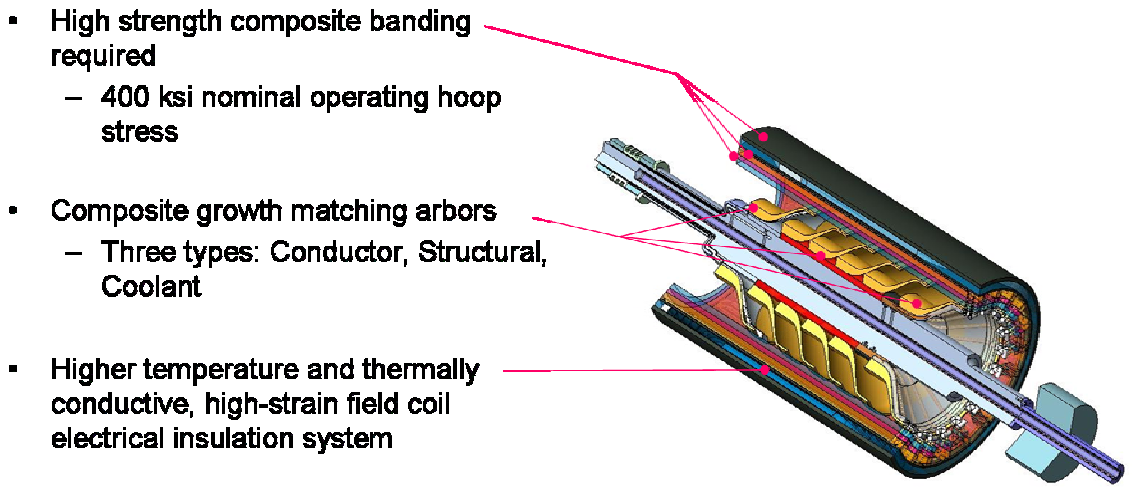

Figure VII-8. High performance PA rotor and development areas required

Rotor Arbors

The rotor arbors are responsible for tying the shaft to the main rotor body. Due to the extreme speeds of the rotor, there is no metal that can track the growth of the rotor body without failing. Therefore, the arbors are made from specially wound high strength pre-preg graphite fibers. There are three types of arbors used in the rotor. The first is the structural arbor. The structural arbors are responsible for the static and dynamic stability of the main rotor body and shaft. The conductor arbor contains conductors to couple the DC field winding to the shaft. The cooling arbor contains the cooling tubes that run from the shaft, through the field winding, and back. Both the conductor and cooling arbors have structural properties very closely resembling the structural arbors.

For several years now the CEM has been prototyping advanced composite arbor designs for high speed flywheel applications. Several prototypes have been made and successfully tested. The latest structural arbor version in support of the Army program was successfully tested in late 2003. Designs similar to these will be required for the prototype EMEFFV generator, but due to their critical nature they too will have to be specially designed and tested prior to use in the actual rotor. Neither the cooling or conductor arbor designs in the Army prototype have been developed to date. These too will require full development for EMEFFV PA's.

Field Winding

The EMEFFV PPS performance is based on high conductivity aluminum field winding turns that are potted in a high thermal conductivity, electrically non-conductive thermo-plastic. The Army program machine uses a lower conductivity (40% IACS) high strength material. To realize efficiency goals for the EMEFFV machine, the field winding needs to have conductivity approaching 60% IACS. This can only be realized by using a low strength, high purity alloy such as 1350. In operation, it is predicted that this material will experience some local yielding in the end-turn transition areas. This requires further engineering analysis and prototype development. In addition, the EMEFFV field winding has the cooling tubes integral with the field conductors; this too is a development item. Finally, the encapsulating thermo-plastic is also a development item. Some work in this area has already been accomplished in the Army program, but further development will be required for the EMEFFV tactical prototypes. This encapsulate must have good thermal properties, be a very good electrical dielectric, and have superior strength and strain characteristics.

Armature Windings

The stator armatures are comprised of heavily insulated copper litz wire that has cooling tubes transposed integrally within the conductor bundles. A prototype of this wire has been tested on the Army program, but further testing remains. The insulation and potting thermo-plastic also needs development. This would include life testing and detection of the onset of destructive corona formation within the conductor matrices. Figure VII-9 shows a stator design similar to the EMEFFV concept outlining the critical development items required.

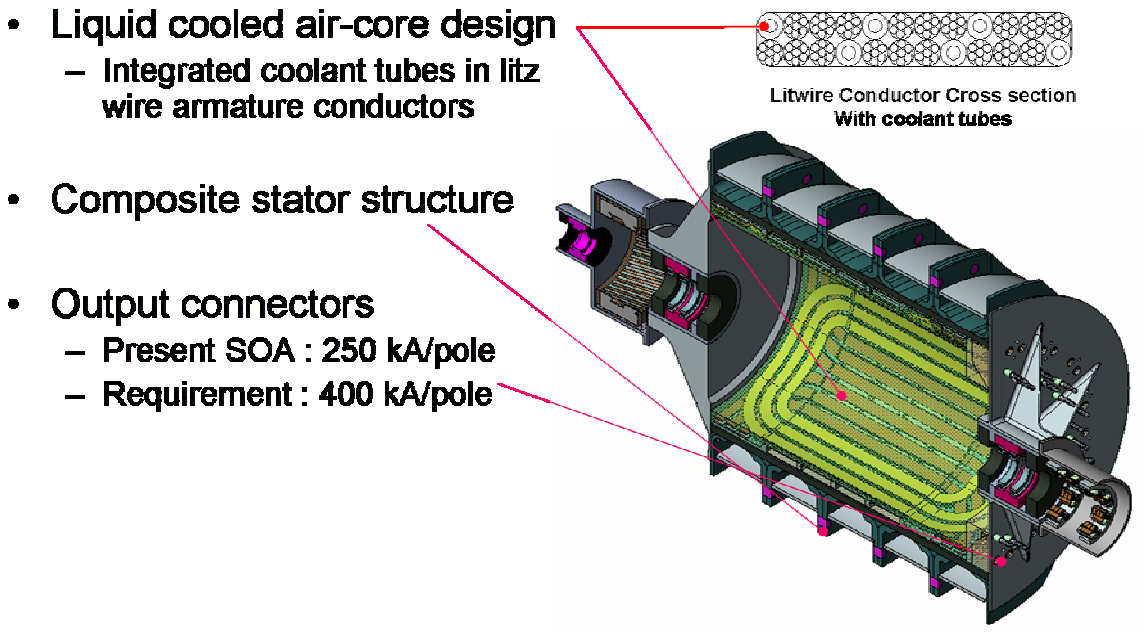

Figure VII-9. Advanced PA stator showing needed critical development areas

Armature Output Connectors

The four by four phase armature poles are connected in parallel, requiring an output terminal capable of carrying over 400 kA per the PA design requirement of 1.75 MA peak current. CEM has developed a connector and armature termination that is rated and tested at 250 kA. Further engineering analysis and prototyping is required, including potentially a new flexible bus cable.

Composite Stator

Another engineering development task is associated with the design and fabrication of the composite stator casing. This component must be low weight and high in strength in order to transmit discharge loads transmitted through it to ground by the armature windings. The SSFTP program has built and tested (1998) an initial prototype, however, that machine was far less powerful than the present concept for EMEFFV. In addition, the discharge torque has climbed to levels where it must be reacted at several points along the outside of the stator casing as shown in the above figures. The latest Army EMG program has invested in the development of the next generation stator casing; this development needs to continue.

Miscellaneous

The drive motor for the PA is a developmental item. Its high speed (22,500 rpm) and power density will require development of new structures and matching systems. The motor is envisioned as an induction machine that is straight forward except for its high speed. Extreme speed induction motors usually require the use of high strength alloys in the secondary (rotor) windings, including the rotor bars and end rings. This will most likely require some engineering development as it pertains to manufacturing the rotor.

Bibliography

The following list presents publications from UT-CEM in the field of pulsed alternators.

G.A. Wedeking, "Geometric Modeling and EM Analysis of Electrical Windings for Pulsed Alternators," 12th Electromagnetic Launch Technical Symposium, Snowbird, Utah, May 25-28, 2004. (CEM PR-353) pending

C.E. Penney, T.J. Hotz, and J.J. Hahne, "Sensor Developments for Compulsator-Driven Railgun Systems," Eleventh EML Technology Symposium, Saint-Louis, France, May 14-17, 2002 (CEM PR-299)

J.R. Kitzmiller, S.B. Pratap, and M.D. Driga, "An Application Guide for Compulsators," Eleventh EML Technology Symposium, Saint-Louis, France, May 14-17, 2002 (CEM PR-300)

H.P. Liu and J.J. Hahne, "High-Speed Compulsator Stator Thermal Management," Eleventh EML Technology Symposium, Saint-Louis, France, May 14-17, 2002 (CEM PR-303)

S.B. Pratap and M.D. Driga, "An Assessment of Losses in the Field Coil of the Compulsator Under Dynamic Conditions," Eleventh EML Technology Symposium, Saint-Louis, France, May 14-17, 2002 (CEM PR-308)

B.T. Murphy, J.R. Kitzmiller, R.C. Zowarka, J.J. Hahne, and W.A. Walls, "Rotordynamics Design and Test Results for a Model Scale Compulsator Rotor," IEEE Transactions on Magnetics, vol. 37 no. 1, January 2001 (CEM PR-273)

J.J. Hahne, J.R. Kitzmiller, and C.E. Penney, "Brush/Slip Ring Current Collector Performance and Anomalies During Compulsator Commissioning," IEEE Transactions on Magnetics, vol. 37 no. 1, January 2001 (CEM PR-274)

J.R. Kitzmiller, K.G. Cook, J.J. Hahne, T.J. Hotz, S.M. Manifold, J.A. Pappas, C.E. Penney, S.B. Pratap, B. Rech, R.F. Thelen, and W.A. Walls, "Predicted vs. Actual Performance of a Model Scale Compulsator System," IEEE Transactions on Magnetics, vol. 37 no. 1, January 2001 (CEM PR-276)

J.R. Kitzmiller, J.A. Pappas, S.B. Pratap, and M.D. Driga, "Single and Multiphase Compulsator System Architectures: A Practical Comparison," IEEE Transactions on Magnetics, vol. 37 no. 1, January 2001 (CEM PR-277

D. Eccleshall and S. B. Pratap, "Comparison of a Single Pulsed Alternator with Two or More in Parallel for Driving a Railgun," IEEE Transactions on Magnetics, vol. 37 no. 1, January 2001 (CEM PR-288)

R.C. Thompson, W.G. Brinkman, J.R. Kitzmiller, W.A. Walls, and J.H. Beno, "Viscoelasticity of Composite Structures for Compulsators," 9th EML Symposium, Edinburgh, Scotland, May 1998 (CEM PR-247)

S.B. Pratap and M.D. Driga, "Compensation in Pulsed Alternators," IEEE Transactions on Magnetics, Vol 35, No. 1, January 1999 (CEM PR-251)

K.G. Cook, B.T. Murphy, S.M. Manifold, T. Pak, M.D. Werst, J.R. Kitzmiller, W.A. Walls, A. Alexander, and K. Twigg, "Subscale Rotor Spin Testing for Compulsator Component Development," IEEE Transactions on Magnetics, Vol 35, No. 1, January 1999 (CEM PR-252)

B.T. Murphy, S.M. Manifold, and J.R. Kitzmiller, "Compulsator Rotordynamics and Suspension Design," IEEE Transactions on Magnetics, vol 33, no 1, Jan 1997. (CEM PR-207)

S.B. Pratap, J.P. Kajs, W.A. Walls, W.F. Weldon, and J.R. Kitzmiller, "A Study of Operating Modes for Compulsator Based EM Launcher Systems," IEEE Transactions on Magnetics, vol 33, no 1, Jan 1997. (CEM PR-212)

R.F. Thelen, "Field Excitation and Discharge Switching for Air-Core Compulsators," 10th IEEE Pulsed Power Conference, Albuquerque, NM, July 10-13, 1995 (CEM PN-223)

W.A. Walls, S.B. Pratap, J.P. Kajs, and J.R. Kitzmiller, "Topology Considerations for Lightweight Compulsator Electric Gun Power Supplies," 10th IEEE Pulsed Power Conference, Albuquerque, NM, July 10-13, 1995 (CEM PN-224)

S.B. Pratap, J.P. Kajs, W.A. Walls, W.F. Weldon, J.R. Kitzmiller, and S.K. Murthy, "Operating Modes for Compulsator Based Electromagnetic Launcher Systems," 10th IEEE Pulsed Power Conference, Albuquerque, NM. July 10-13, 1995 (CEM PN-226)

D.J. Wehrlen, R.A. Lee, and R.F. Thelen, "Power Electronics and Controls for Air Core Compulsator," IEEE Transactions on Magnetics, vol 31, no. 1, January 1995. (CEM PR-190)

R.L. Fuller, J.R. Kitzmiller, and R.F. Thelen, "Testing of an Air Core Compulsator Driven 0.60 Caliber Railgun System ," IEEE Transactions on Magnetics, vol 31, no. 1, January 1995. (CEM PR-197)

J.R. Kitzmiller, S.B. Pratap, T.A. Aanstoos, K.G. Cook, R.A. Kuenast, B.T. Murphy, and D.R. Perkins, "Optimization and Critical Design Issues of the Air Core Compulsator for the Cannon Caliber Electromagnetic Launcher System (CCEML)," IEEE Transactions on Magnetics, vol 31, no. 1, January 1995. (CEM PR-199)

S.K. Murthy and W.F. Weldon, "A Single Element Multiphase Compulsator Powered Railgun System," IEEE Transactions on Magnetics, vol 30, no 1, January 1994, pp 145-154 (CEM PR-200)

S.B. Pratap, J.R. Kitzmiller, T.A. Aanstoos, K.G. Cook, R.N. Headifen, R.A. Kuenast, R.A. Lee, H-P Liu, and D.J. Wehrlen, "Optimization and Design of the Air Core Compulsator for the Cannon Caliber Electromagnetic Launcher System (CCEML)," Ninth IEEE Pulsed Power Conference, Albuquerque, NM, June 21-23, 1993. (CEM PN-213)

S.B. Pratap, "Advanced Compulsator Technology," IEEE Transactions on Magnetics, Vol 29, No. 1, January 1993 (CEM PR-159)

S.M. Manifold, W.G. Brinkman, and E.G. Estes, "Fabrication of a Rotor for a Field Based, Self-Excited Compulsator Power Supply for a 9 MJ Railgun Demonstrator," IEEE Transactions on Magnetics, Vol 29, No. 1, January 1993 (CEM PR-161)

J.R. Kitzmiller, R.W. Faidley, R.N. Headifen, R.L. Fuller, and R.F. Thelen, "Manufacturing and Testing of an Air-Core Compulsator Driven 0.60 Caliber Railgun System," IEEE Transactions on Magnetics, Vol 29, No. 1, January 1993 (CEM PR-165)

J.D. Herbst, K.G. Cook, R.A. Kuenast, S.B. Pratap, R.C. Thompson, and H.D. Yun, "9 MJ Range Gun Compulsator Stator Design and Fabrication," IEEE Transactions on Magnetics, Vol 29, No. 1, January 1993 (CEM PR-166)

W.F. Weldon and S.B. Pratap, "Iron Core Compulsators for Railgun Power Supplies," IEEE Transactions on Magnetics, Vol 29, No. 1, January 1993 (CEM PR-167)

W.F. Weldon, "Homopolar Generator and Compulsator," Discovery, Research and Scholarship, The University of Texas at Austin, vol 13, no. 1, 1993, p 12-17. (CEM RO-80)

W.F. Weldon and C.W. Drummond, "Compulsators: Principles and Applications," Fifth International Conference on Electrical Machines and Drives, Savoy Place, London, UK, September 11 to 13, 1991. (CEM PR-146)

B. Rech and R.F. Thelen, "Turbine Drives for Compulsators," 6th EML Symposium, April 28-30, 1992, Austin, TX. (CEM PR-157)

A. W. Walls, S. B. Pratap, G. W. Brunson, K. G. Cook, J. D. Herbst, S. M. Manifold, B. M. Rech, R.F. Thelen, R. C. Thompson, and W. G. Brinkman, "A Field Based, Self-Excited Compulsator Power Supply for A 9 MJ Railgun Demonstrator," IEEE Transactions on Magnetics, Vol 27, No. 1, January 1991 (CEM PR-100)

S. B. Pratap, "Limitations on the Minimum Charging Time for the Field Coil of Air Core Compensated Pulsed Alternators," IEEE Transactions on Magnetics, Vol 27, No. 1, January 1991 (CEM PR-105)

J.R. Kitzmiller, R.N. Faidley, R.L. Fuller, R. Headifen, S.B. Pratap, M.L. Spann, and R.F. Thelen, "Final Design of an Air Core, Compulsator Driven 60 Caliber Railgun System," IEEE Transactions on Magnetics, Vol 27, No. 1, January 1991 (CEM PR-109)

D. E. Perkins, S. B. Pratap, M. L. Spann, R. F. Thelen, and M. D. Werst, "The CEM-UT Rapid-Fire Compulsator Railgun System-Recent Performance and Development Milestones," IEEE Transactions on Magnetics, Vol 27, No. 1, January 1991 (CEM PR-110)

S.B. Pratap, "Transient Eddy Current Distribution in the Shield of the Passively Compensated Compulsator Air Core Machines," IEEE Transactions on Magnetics, vol 27, no. 4, July 1991 (CEM PR-133)

W. A. Walls, M. L. Spann, S. B. Pratap, W. G. Brinkman, K. G. Cook, J. D. Herbst, S. M. Manifold, B. Rech, R. F. Thelen, and R. C. Thompson, "Design of a 20 GW, Self-Excited, Air-Core Compensated Pulsed Alternator Railgun Power Supply," 1990 International Conference on Electrical Machines. (CEM PR-126)

D. E. Perkins, S. B. Pratap, M. L. Spann, R. F. Thelen, and M. D. Werst, "The CEM-UT Rapid-Fire Compulsator Test Results and Performance Evaluation," Seventh IEEE Pulsed Power Conference, Monterey, CA, June 11-14, 1989. (CEM PN-150)

S. B. Pratap, M. L. Spann, W. A. Walls, and M. D. Driga, "Air Core Compensated Pulsed Alternators," Seventh IEEE Pulsed Power Conference, Monterey, CA, June 11-14, 1989. (CEM PN-151)

R. F. Thelen, "Pulse Discharge Control and Machine Protection for a Multi-Discharge Compulsator," IEEE Transactions on Magnetics, Vol. 25, No. 1, Jan 1989. (CEM PR-62)

W. A. Walls, M. L. Spann, S. B. Pratap, D. A. Bresie, W. G. Brinkman, J. R. Kitzmiller, J. D. Herbst, H. P. Liu, S. M. Manifold, and B. M. Rech, "Design of a Self-Excited, Air-Core Compulsator for a Skid-Mounted, Repetitive Fire 9 MJ Railgun System," IEEE Transactions on Magnetics, Vol. 25, No. 1, Jan 1989. (CEM PR-64)

M. D. Driga, S. B. Pratap, and W. F. Weldon, "Advanced Compulsator Design," IEEE Transactions on Magnetics, Vol. 25 No. 1, January 1989. (CEM PR-67)

S. B. Pratap, K. T. Hsieh, M. D. Driga, and W. F. Weldon, "Advanced Compulsator for Railguns," IEEE Transactions on Magnetics, Vol. 25, No. 1, January.1989. (CEM PR-68)

H. P. Liu, "Cooling for the Armature Windings in a Repetitively Fired Air-Core Compulsator," IEEE Transactions on Magnetics, Vol. 25, No. 1, January 1989. (CEM PR-70)

M. D. Werst, D. E. Perkins, S. B. Pratap, M. L. Spann, and R. F. Thelen, "Testing of a Rapid Fire Compensated Pulsed Alternator System," IEEE Transactions on Magnetics, Vol. 25, No. 1, January 1989. (CEM PR-71)

M. L. Spann, S. B. Pratap, M. D. Werst, W. A. Walls, and C. W. Fulcher, "Compulsator Research at The University of Texas at Austin--An Overview," IEEE Transactions on Magnetics, Vol. 25, No. 1, January 1989. (CEM PR-74)

S. B. Pratap, "Transient Eddy Current Distribution In the Shield of the Passively Compensated, Compensated Pulsed Alternator: Iron-Core Machines," Published in IEEE, July, 1990. (CEM PR-96)

M.D. Driga, S.B. Pratap, and W.F. Weldon, "Design of Compensated Pulsed Alternators With Current Waveform Flexibility," 6th IEEE Pulsed Power Conference, Arlington, VA, June 29-July 1, 1987. (CEM PN-110)

S.B. Pratap, S.M. Manifold, W.A. Walls, M.L. Spann, and W.F. Weldon, "9 MJ/Pulse Air Core Compulsator," 6th IEEE Pulsed Power Conference, Arlington, VA, June 29-July 1, 1987. (CEM PN-115)

M.L. Spann, S.B. Pratap, W.A. Walls, and J.D. Herbst, "The Conceptual Design of a Lightweight Compulsator-Driven Electromagnetic Accelerator," 6th IEEE Pulsed Power Conference, Arlington, VA, June 29-July 1, 1987. (CEM PN-117)

M. L. Spann, S. B. Pratap, W. G. Brinkman, D. E. Perkins, and R. F. Thelen, "A Rapid Fire, Compulsator-Driven Railgun System," IEEE Transactions on Magnetics, Vol. Mag-22, No. 6, pp 1753-1756, November 1986 (CEM PR-37)

S. B. Pratap, M. D. Driga, W. F. Weldon, and M. L. Spann, "Future Trends for Compulsators Driving Railguns," IEEE Transactions on Magnetics, Vol. Mag-22, No. 6, pp 1681-1683, November 1986 (CEM PR-38)

M. D. Werst, B. G. Brinkman, and M. L. Spann, "Fabrication of a Compensated Pulsed Alternator for a Rapid Fire Railgun System," IEEE Transactions on Magnetics, Vol. Mag-22, No. 6, pp 1812-1816, November 1986. (CEM PR-43)

S. B. Pratap, M. L. Spann, W. G. Brinkman, M. D. Werst, and M. R. Vaughn, "A Compulsator-Driven Rapid Fire Railgun System," presented at the fifth IEEE Pulsed Power Conference, Arlington, VA, June 10-12, 1985. (CEM PR-28)

S. B. Pratap, W. L. Bird, G. L. Godwin, and W. F. Weldon, "A Compulsator Driven, Rapid-Fire EM Gun," IEEE Transactions on Magnetics, Vol. Mag-20, No. 2, pp 211-214, March 1984 (CEM PR-16)

W.L. Bird , W.F. Weldon, B.M. Carder, and R.J. Foley, "The Compensated Pulsed Alternator Program: A Review," Third IEEE International Pulsed Power Conference, Albuquerque, NM, June 1-3, 1981. (CEM PN-71)

J.A. Parekh, W.L. Bird, A.C. Patel, and H.H. Woodson, "Space Harmonic Analysis of Magnetic Fields in a Compensated Pulsed Alternator or an Active Rotary Flux Compressor," Third IEEE International Pulsed Power Conference, Albuquerque, NM, June 1-3, 1981. (CEM PN-73)

W.L. Bird, W.F. Weldon, H.G. Rylander, H.H. Woodson, B.M. Carder, , and , "The Compensated Pulsed Alternator: Preliminary Test Results," Eighth Symposium on Engineering Problems of Fusion Research, San Francisco, CA, November 13-16, 1979. (CEM PN-58)

B.M. Carder, B.T. Merritt, W.L. Gagnon, W.L. Bird, W.F. Weldon, and R.C. Zowarka, Jr., "Driving Parallel Flashlamps with a Compensated Pulsed Alternator," Fourteenth Pulse Power Modulator Symposium, Orlando, FL, June 3-5, 1980 (CEM PN-64)

W.F. Weldon, M.D. Driga, W.L. Bird, K.M. Tolk, H.H. Woodson, and H.G. Rylander, "Compulsator--A High Power Compensated Pulsed Alternator," Second International Conference on Energy Storage, Compression, and Switching, Venice, Italy, December 5-8, 1978. (CEM PN-46)

W.L. Bird, D.J.T. Mayhall, W.F. Weldon, H.G. Rylander, and H.H. Woodson, "Applying a Compensated Pulsed Alternator to a Flashlamp Load for NOVA-Part II,," Second IEEE International Pulsed Power Conference, Lubbock, TX, June 12-14, 1979. (CEM PN-49)

M. Brennan, W.L. Bird, J.H. Gully, M.L. Spann, K.M. Tolk, W.F. Weldon, H.G. Rylander, and H.H. Woodson, "The Mechanical Design of a Compensated Pulsed Alternator Prototype," Second IEEE International Pulsed Power Conference, Lubbock, TX, June 12-14, 1979. (CEM PN-50)

J.H. Gully, W.L. Bird, T.M. Bullion, H.G. Rylander, W.F. Weldon, and H.H. Woodson, "Design of the Armature Windings of a Compensated Pulsed Alternator Engineering Prototype," Second IEEE International Pulsed Power Conference, Lubbock, TX, June 12-14, 1979. (CEM PN-52)

M.A. Pichot, W.L. Bird, M. Brennan, M.D. Driga, J.H. Gully, H.G. Rylander, K.M. Tolk, W.F. Weldon, and H.H. Woodson, "The Design, Assembly, and Testing of a Desk Model Compensated Pulsed Alternator," Second IEEE International Pulsed Power Conference, Lubbock, TX, June 12-14, 1979. (CEM PN-53)

W.F. Weldon, W.L. Bird, M.D. Driga, K.M. Tolk, H.G. Rylander, and H.H. Woodson, "Fundamental Limitations and Design Considerations for Compensated Pulsed Alternators," Second IEEE International Pulsed Power Conference, Lubbock, TX, June 12-14, 1979. (CEM PN-55)

H-P Liu, C.S. Hearn, M.D. Werst, J.J. Hahne, and D. Bogard, "Splits of Windage Losses in Integrated Transient Rotor and Stator Thermal Analysis of a High Speed Compulsator During Multiple Discharges," 12th Electromagnetic Launch Technical Symposium, Snowbird, Utah, May 25-28, 2004. (CEM PR-358)

J. R. Kitzmiller, R. W. Faidley, R. L. Fuller, R.N. Headifen, S. B. Pratap, M. L. Spann, and R. F. Thelen, "Design of a 600 MW Pulsed Air-Core Compulsator," 1990 International Conference on Electrical Machines. (CEM PR-125)

Advanced Conceptual Design Development of a Multigigawatt Pulsed Flywheel Alternator (CHPS II). : J.H. Beno and T.A. Aanstoos (CEM RF-194)

Design and Optimization of Compulsator Power Supplies for AAN Concepts : S.B. Pratap and W.A. Walls : Interim Report to Dr. Ian McNab, IAT, UT-Austin (CEM RF-185)

Development of Compulsator Rotor Technology, Rotor 2A. : K.G. Cook, T.T. Pak, and S.M. Manifold : submitted to Ian McNab, IAT (CEM RF-169)

Development of Compulsator Rotor Technology Series 2B Rotor. : K.G. Cook, T.T. Pak, B.T. Murphy, S.M. Manifold, J.R. Kitzmiller, and W. A. Walls (CEM RF-174)

Development of Compulsator Rotor Technology. : K.G. Cook, S.M. Manifold, B.T. Murphy, J.R. Kitzmiller, W.A. Walls, and M.D. Werst : Annual Technical Report for the Period of October 1996 to December 1996, presented to Ian McNab, IAT (CEM RF-163)

Stand Alone Repetitive Fire Compulsator Driven 9 MJ EM Gun System : J.D. Herbst, W.A. Walls, and R.F. Thelen (CEM RF-150)

Compensated Pulsed Alternators. : W.A. Walls : IAT Seminar, December 1995 (CEM RO-112)

Focused Technology Program: Validation of the Full-Scale Compulsator Design. : W.A. Walls, S.M. Manifold, S.B. Pratap, and J.R. Kitzmiller (CEM RO-105)

Topology Considerations for Lightweight Compulsator Electric Gun Power Supplies. : W.A. Walls, S.B. Pratap, J.P. Kajs, and J.R. Kitzmiller : Distribution limited to government only (CEM RO-107)

Compulsator Power Supply Development for Electrothermal Launchers. : S.K. Murthy : White paper presented to General Dynamics (CEM RO-90)

Characterization of a Rectified, Polyphase Alternator as a Pulsed Power Supply for an Electromagnetic Aircraft Launch System. : T.A. Aanstoos, J.S. Hsu, R.C. Zowarka, S.B. Pratap, and J.H. Gully : Final report to General Atomics, Purchase Order M233501, presented to General Atomics, ATTN: Ms S. McKelvey, Receiving Dept, 3483 Dunhill St., San Diego, CA 92121 (CEM RF-126)

Research and Development of a Compensated Pulsed Alternator for a Rapid Fire Electromagnetic Gun. : D.E. Perkins, M.L. Spann, R.F. Thelen, M.D. Werst, W.G. Brinkman, and S.B. Pratap : Final Report covering the reporting period of July 12, 1983 to

December 12, 1988. Presented to U.S. Army AMCCOM, under contract No. DAAK10-83-C-0126, December 1990. (CEM RF-88)

Compulsator Driven Electrothermal-Gun System. : S.B. Pratap and J. H. Gully : White paper presented to Commander Craig Dampier, Naval Sea System Command, Department of the Navy, April 1991. (CEM RO-72)

Advanced Compulsator Technology for Electric Gun Applications. : J.H. Gully and W.A. Walls : White paper presented to Ms. Libby Hildi, Electric Armaments Program Office, Picatinny Arsenal, NJ, June 1991. (CEM RO-74)

Research and Development of a 10 MJ Compensated Pulsed Alternator. : W.F. Weldon, H.H. Woodson, J.H. Gully, M.L. Spann, W.G. Brinkman, and S. M. Solomon : Final Report covering the reporting period of November 1985 to July 1987 : presented to U.S. Army ARDEC under contract No. DAAA21-85-C-0211, July 1990. (CEM RF-87)

Parametric Design and Cost Analysis of a Compensated Pulsed Alternator for a Portable, Small Caliber, EM Launch System. : W.F. Weldon, J.H. Gully, and S.B. Pratap : Final report presented to Martin Marietta Energy Systems, Inc., Oak Ridge, TN under contract No. DE-AC05-840R21400. (CEM RF-66)

Conceptual Design of a Torque Compensated Compulsator. : S. B. Pratap : Submitted to GA Technologies, Contract No. SC074107, June, 1986. (CEM RF-57)

Research and Development of a Compensated Pulsed Alternator for a Rapid Fire Electromagnetic Gun. : M. L. Spann, S. B. Pratap, W. F. Weldon, H. G. Rylander, H. H. Woodson, J. H. Gully, and M. V. Vaughn : Interim Report, U. S. Army, Armament R & D Command Contract No. DAAK-10-83-C-0126, July 12, 1983 to April 15, 1984. (CEM RF-45)

Continued Development of Compensated Pulsed Alternators and Rotary Flux Compressors for Pulse Power Generation: Task G -- Cost Model and Manufacturing Plan. : C. A. Morgan, H. G. Rylander, H. H. Woodson, W. F. Weldon, and W. L. Bird : Task G, Lawrence Livermore National Laboratory, Subcontract No. 8030909, December 1982. (CEM RF-35)

Continued Development of Compensated Pulsed Alternators and Rotary Flux Compressors for Pulse Power Generation: Task H -- Voltage Distributions in the Windings of Rotary Flux Compressors. : S. B. Pratap, H. G. Rylander, H. H. Woodson, and W. F. Weldon : Task H, Lawrence Livermore National Laboratory, Subcontract No. 8030909, December 1982. (CEM RF-36)

Continued Development of Compensated Pulsed Alternators and Rotary Flux Compressors for Pulsed Power Generation: Task F.4 -- Electrical Discharge Tests of a 20-cm-Diameter Active Rotary Flux Compressor :

W. L. Bird : Task F.4, Lawrence Livermore National Laboratory, Subcontract No. 8030909, March 1982. (CEM RF-28)

Continued Development of Compensated Pulsed Alternators and Rotary Flux Compressors for Pulsed Power Generation: Task F.2 -- CPA/ARFC Capacitor-Driver Parameter Study. : W. L. Bird, H. G. Rylander, H. H. Woodson, and W. F. Weldon : Task F.2, Lawrence Livermore National Laboratory, Subcontract No. 8030909, March 1982; Naval Surface Weapons Center Report No. F10-81-0386-A003, Task C.1. (CEM RF-29)

Continued Development of Compensated Pulsed Alternators and Rotary Flux Compressors for Pulsed Power Generation: Task F.3 -- ARFC Electromagnetics -- Magnetic Saturation and Voltage Distribution in Air-Gap Windings. : W. L. Bird, D. R. Brown, S. B. Pratap, and W.F. Weldon : Task F.3, Lawrence Livermore National Laboratory, Subcontract No. 8030909, March 1982; Naval Surface Weapons Center Report No. F10-81-0386-A004-1, Task C.2. (CEM RF-30)

Continued Development of Compensated Pulsed Alternators and Rotary Flux Compressors for Pulsed Power Generation: Task F.5 -- Electromagnetic Shear Strength Tests and Dielectric Strength Tests Using A Rewound ARFC. : W. L. Bird, H. G. Rylander, H. H. Woodson, and W. F. Weldon : Task F. 5, Lawrence Livermore National Laboratory, Subcontract No. 8030909, March 1982; Naval Surface Weapons Center Report No. F10-81-0386-A004-2, Task C.3. (CEM RF-31)

Preliminary Design of a Compensated Pulsed Alternator or Brushless Rotary Flux Compressor for the Camelot Pulsed Power System. : W. F. Weldon : Harry Diamond Laboratories,

DELHD-PO-B and Naval Surface Weapons Center Contact No. N60921-C-80-C-A033, December 1980. (CEM RF-21)

The Continued Testing and Evaluation of the Engineering Prototype Compulsator and the Evaluation of Advanced Compulsator Concepts, 1980. : W. L. Bird : Lawrence Livermore National Laboratory, Subcontract No. 8030909, March 1981. (CEM RF-25)

The Design and Fabrication of a Second-Generation Compensated Pulsed Alternator. : K. M. Tolk : Naval Surface Weapons Center Contract No. N60921-78-C-A249 Conceptual Design Phase, May 1980. (CEM RF-15)

Detailed Design, Fabrication, and Testing of an Engineering Prototype Compensated Pulsed Alternator. : W. L. Bird and H. H. Woodson : Lawrence Livermore Laboratory Purchase Order No. 3325309, March 1980. (CEM RF-16)

A Study of the Engineering Limitations to Pulse Discharge Time for a Compensated Pulsed Alternator. : K. M. Tolk, W. L. Bird, and M. D. Driga : Los Alamos Scientific Laboratories Purchase Order No. N68-0899H-1, May 1979. (CEM RF-12)

VIII. Power Electronics

Introduction and Requirements

The power converters on a rail gun pulsed power supply control the flow of power between the alternators and the field coil and alternators and the rail gun. Figure VIII-1 is a generalized and simplified circuit diagram of a rail gun system. Field coil-related components are shown in blue and rail gun-related components in green.

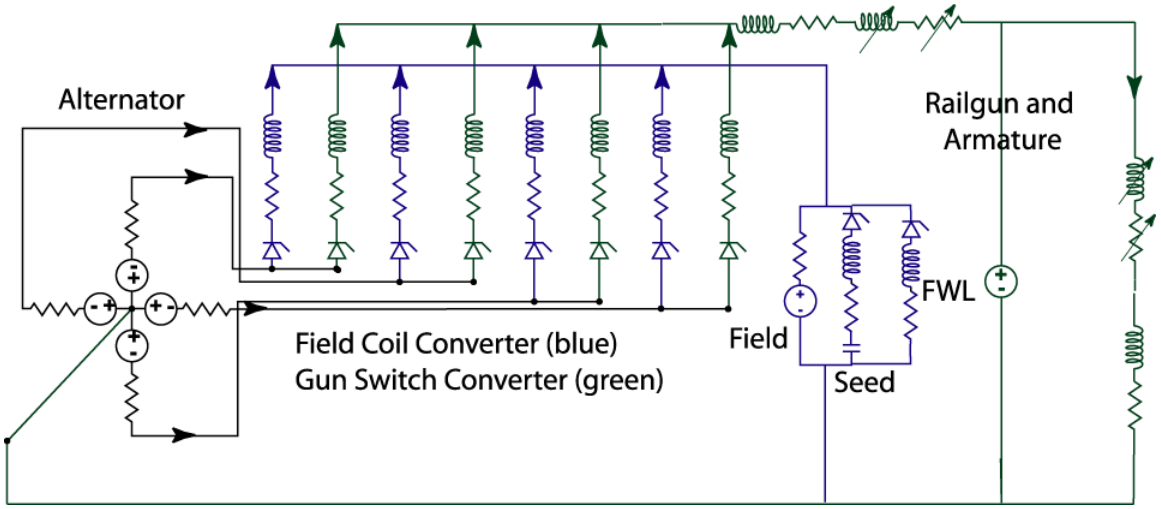

Figure VIII-1. Generalized rail gun and pulsed power supply schematic

The field components consist of the field coil itself, a seed circuit, the field coil converter (FCC) and a freewheel leg (FWL). The rail gun components consist of the gun and armature, the DC bus, and the gun switch converter (GSC). Both the GSC and FCC are bi-directional line-commutated converters that allow power flow in either direction. That is, both converters can operate as controlled rectifiers and inverters.

Operation of the system can be described as consisting of four operations: field charge, gun discharge, gun energy reclaim, and field energy reclaim. Once the pulsed alternator (PA) rotor is at the desired operating speed, the first operation starts with the discharge of the capacitor in the seed circuit into the field coil. When current is flowing in the field coil, a voltage is induced on the armature windings of the alternator. The field coil converter is then turned on at a firing

angle, thereby feeding armature current back into the field coil. These four operations are manifest in the current traces shown in figure VIII-2.

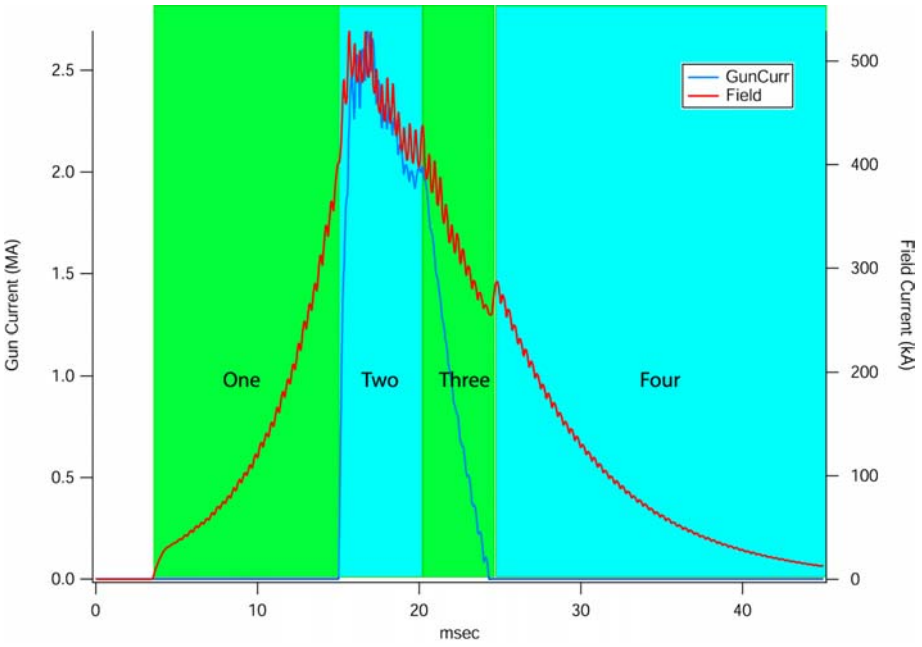

Figure VIII-2. The four phases of a pulsed power supply are evident in the response of the field and armature currents.

As can be seen in figure VIII-2, the current in the field coil continues to rise as armature current feedback is provided and the armature voltage increases. During this phase of operation (and during gun discharge), the rotor slows as energy is transferred according to Faraday's law from the kinetic energy of the rotor to the magnetic energy stored in the field.

When the voltage on the armature is high enough due to the FC ampere-turns to drive the rail gun, the freewheel circuit is turned on. The freewheel circuit isolates the field coil converter from the field circuit during the gun shot. Previous trade studies performed in the Army's 6.2 Electric Gun Program have shown that isolating the FC during the gun shot reduces the size of the FCC because the FC is subjected to a very high amount of electrical action (I^2t) due to the armature reaction. Armature reaction is the response of the field coil to the very large magnetic field that is produced by the armature during the multi-million ampere gun discharge. As a result of the discharge current, extreme currents are induced in the field coil. The Army trade studies showed that use of a separate isolation circuit, one not subjected to the switching transients of

charge and inversion, resulted in a smaller overall FC and FWL converter than a FC that is designed to handle both the switching transients and armature reaction.

Inspection of figure VIII-1 reveals that both the FCC and GSC are half wave (HW) converters. Once again, the trades performed for the Army based on the entire design of the PPS show that, for this application, half wave converters consume significantly less volume and mass that full bridge, or full wave (FW) circuits. In addition, the half-wave converter topology has advantages in controls and fault handling. Because there are fewer switching actions per cycle, the demands on controller bandwidth and capacity are reduced. In addition, because the current return is through the neutral connection rather than an armature winding, fault currents are carried through approximately one-half the silicon as in a FW circuit and the consequences of a large current fault are proportionally reduced.

These advantages come with costs. An HW converter applies approximately one-half the voltage from a given alternator. As a result, the charge cycle is longer and is less efficient and the alternator must be designed to overcome the voltage limitation. However, the mass and volume penalties to the alternator for increased voltage generation are significantly less than the penalties associated with FW converters.

Both the GSC and FCC handle extremely large peak power at voltage on the order of 15 kV. The extreme operating conditions drive the designer toward switching devices that can handle high current and voltage. While lower-power devices can be used, the mass, volume, and reliability penalties associated with packaging large numbers of small devices quickly become apparent.

Therefore, the device most often chosen is a symmetrical thyristor, or SCR. Even large thyristors cannot handle the entire discharge power. As a result, the SCRs are arranged in appropriate series- and parallel-connected arrangements.

The thyristors control the power flow, must share and withstand voltage, turn on under relatively extreme rates of current rise, and turn off when current flow through them reverses. In addition, because the devices are arranged in series-parallel arrays, the SCRs must share current and voltage well; no single device can handle the thermal or voltage loads impressed by the alternator.

Tables VIII-1 through VIII-5 show the electrical requirements of the power converters for a five-shot burst as derived from the mGun rail gun performance simulator. The requirements are boiled down to worst-case shot and worst-case phase loads. These worst-case loads are then applied as requirements to each pole phase module in the system so that any section of the power converter can handle the worst part of a discharge. Fault analyses and design are beyond the scope of this project.

Table VIII-1. Shot 1 converter design requirements

GSC

Phase	1	2	3	4	
Ipk (A)	2.46E+06	2.52E+06	2.33E+06	2.32E+06	
Action (A^2s)	5.07E+09	5.77E+09	5.92E+09	4.54E+09	
di/dt on (A/s)	8.78E+09	9.23E+09	9.23E+09	8.64E+09	
Vfwd (V)	12.1E+3	12.2E+3	11.1E+3	11.9E+3	
Vrev (V)	15.6E+3	14.7E+3	13.1E+3	14.3E+3	
min tq (s)	153.0E-6	175.0E-6	109.0E-6	119.0E-6	

FCC

Phase	1	2	3	4	FWL
Ipk (A)	309.3E+3	336.5E+3	359.6E+3	400.3E+3	529.0E+3
Action (A^2s)	1.21E+08	1.27E+08	1.27E+08	2.03E+08	1.54E+09
di/dt on (A/s)	3.24E+09	4.76E+09	3.10E+09	3.60E+09	3.49E+09
Vfwd (V)	12.8E+3	12.8E+3	12.2E+3	12.0E+3	5.2E+3
Vrev (V)	15.9E+3	17.1E+3	13.5E+3	14.7E+3	8.1E+3
min tq (s)	279.0E-6	291.0E-6	281.0E-6	268.0E-6	368.0E-6

Worst case phase	**GSC**	**FCC**	**FWL**
Ipk (A)	1.3E+6	200.1E+3	264.5E+3
Action (A^2s)	1.5E+9	50.7E+6	384.0E+6
di/dt on (A/s)	4.6E+9	2.4E+9	1.7E+9
Vfwd (V)	12.2E+3	12.8E+3	5.2E+3
Vrev (V)	15.6E+3	17.1E+3	8.1E+3
min tq (s)	109.0E-6	268.0E-6	368.0E-6

Worst case pole	**GSC**	**FCC**	**FWL**
Ipk (A)	314.7E+3	50.0E+3	66.1E+3
Action (A^2s)	92.6E+6	3.2E+6	24.0E+6
di/dt on (A/s)	1.2E+9	594.9E+6	435.8E+6

Table VIII-2. Shot 2 converter design requirements

GSC					
Phase	1	2	3	4	
Ipk (A)	2.64E+06	2.68E+06	2.46E+06	2.41E+06	
Action (A^2s)	5.02E+09	6.23E+09	5.44E+09	4.91E+09	
di/dt on (A/s)	8.88E+09	8.92E+09	8.47E+09	8.52E+09	
Vfwd (V)	11.4E+3	11.4E+3	12.0E+3	10.8E+3	
Vrev (V)	15.4E+3	14.5E+3	13.0E+3	14.2E+3	
min tq (s)	200.0E-6	207.0E-6	202.0E-6	194.0E-6	
FCC					
Phase	1	2	3	4	FWL
Ipk (A)	420.8E+3	323.6E+3	346.0E+3	371.5E+3	561.4E+3
Action (A^2s)	2.09E+08	1.34E+08	1.32E+08	1.83E+08	1.63E+09
di/dt on (A/s)	3.45E+09	3.07E+09	2.97E+09	3.41E+09	3.76E+09
Vfwd (V)	12.7E+3	13.1E+3	11.6E+3	11.6E+3	5.0E+3
Vrev (V)	14.5E+3	15.6E+3	16.8E+3	13.4E+3	8.7E+3
min tq (s)	301.0E-6	311.0E-6	300.0E-6	292.0E-6	404.0E-6
Worst case phase	**GSC**	**FCC**	**FWL**		
Ipk (A)	1.3E+6	210.4E+3	280.7E+3		
Action (A^2s)	1.6E+9	52.2E+6	408.4E+6		
di/dt on (A/s)	4.5E+9	1.7E+9	1.9E+9		
Vfwd (V)	12.0E+3	13.1E+3	5.0E+3		
Vrev (V)	15.4E+3	16.8E+3	8.7E+3		
min tq (s)	194.0E-6	292.0E-6	404.0E-6		
Worst case pole	**GSC**	**FCC**	**FWL**		
Ipk (A)	334.6E+3	52.6E+3	70.2E+3		
Action (A^2s)	97.4E+6	3.3E+6	25.5E+6		
di/dt on (A/s)	1.1E+9	431.2E+6	470.3E+6		

Table VIII-3. Shot 3 converter design requirements

GSC					
Phase	1	2	3	4	
Ipk (A)	2.51E+06	2.47E+06	2.52E+06	2.42E+06	
Action (A^2s)	5.84E+09	6.07E+09	5.37E+09	4.48E+09	
di/dt on (A/s)	7.32E+09	8.03E+09	8.09E+09	7.56E+09	
Vfwd (V)	9.4E+3	11.4E+3	10.2E+3	9.3E+3	
Vrev (V)	13.3E+3	13.1E+3	10.8E+3	12.2E+3	
min tq (s)	186.0E-6	201.0E-6	197.0E-6	244.0E-6	
FCC					
Phase	1	2	3	4	FWL
Ipk (A)	314.0E+3	341.4E+3	363.4E+3	403.1E+3	542.8E+3
Action (A^2s)	1.19E+08	1.72E+08	1.52E+08	1.89E+08	1.54E+09
di/dt on (A/s)	2.40E+09	3.17E+09	2.79E+09	2.90E+09	8.89E+04
Vfwd (V)	9.0E+3	10.8E+3	10.8E+3	10.3E+3	4.7E+3
Vrev (V)	14.3E+3	15.3E+3	12.2E+3	13.2E+3	7.2E+3
min tq (s)	326.0E-6	340.0E-6	331.0E-6	321.0E-6	423.0E-6
Worst case phase	**GSC**	**FCC**	**FWL**		
Ipk (A)	1.3E+6	201.6E+3	271.4E+3		
Action (A^2s)	1.5E+9	47.3E+6	385.3E+6		
di/dt on (A/s)	4.0E+9	1.6E+9	44.5E+3		
Vfwd (V)	11.4E+3	10.8E+3	4.7E+3		
Vrev (V)	13.3E+3	15.3E+3	7.2E+3		
min tq (s)	186.0E-6	321.0E-6	423.0E-6		
Worst case pole	**GSC**	**FCC**	**FWL**		
Ipk (A)	315.0E+3	50.4E+3	67.9E+3		
Action (A^2s)	94.9E+6	3.0E+6	24.1E+6		
di/dt on (A/s)	1.0E+9	395.8E+6	11.1E+3		

Table VIII-4. Shot 4 converter design requirements

GSC					
Phase	1	2	3	4	
Ipk (A)	2.71E+06	2.65E+06	2.39E+06	2.56E+06	
Action (A^2s)	4.87E+09	5.54E+09	5.55E+09	5.69E+09	
di/dt on (A/s)	7.74E+09	7.52E+09	7.67E+09	7.61E+09	
Vfwd (V)	10.5E+3	10.6E+3	9.6E+3	8.9E+3	
Vrev (V)	13.9E+3	12.9E+3	12.0E+3	13.0E+3	
min tq (s)	256.0E-6	287.0E-6	246.0E-6	227.0E-6	
FCC					
Phase	1	2	3	4	FWL
Ipk (A)	449.2E+3	350.3E+3	372.7E+3	399.7E+3	581.1E+3
Action (A^2s)	2.60E+08	1.62E+08	1.62E+08	2.25E+08	1.73E+09
di/dt on (A/s)	3.10E+09	2.61E+09	2.71E+09	2.96E+09	8.79E+04
Vfwd (V)	11.0E+3	11.3E+3	10.2E+3	10.4E+3	4.3E+3
Vrev (V)	13.5E+3	14.5E+3	15.6E+3	12.6E+3	8.0E+3
min tq (s)	349.0E-6	368.0E-6	348.0E-6	341.0E-6	466.0E-6
Worst case phase	**GSC**	**FCC**	**FWL**		
Ipk (A)	1.4E+6	224.6E+3	290.6E+3		
Action (A^2s)	1.4E+9	65.0E+6	433.3E+6		
di/dt on (A/s)	3.9E+9	1.6E+9	44.0E+3		
Vfwd (V)	10.6E+3	11.3E+3	4.3E+3		
Vrev (V)	13.9E+3	15.6E+3	8.0E+3		
min tq (s)	227.0E-6	341.0E-6	466.0E-6		
Worst case pole	**GSC**	**FCC**	**FWL**		
Ipk (A)	339.0E+3	56.1E+3	72.6E+3		
Action (A^2s)	88.9E+6	4.1E+6	27.1E+6		
di/dt on (A/s)	967.4E+6	387.9E+6	11.0E+3		

Table VIII-5. Shot 5 converter design requirements

GSC					
Phase	1	2	3	4	
Ipk (A)	2.50E+06	2.72E+06	2.65E+06	2.50E+06	
Action (A^2s)	5.66E+09	7.44E+09	5.77E+09	4.82E+09	
di/dt on (A/s)	7.36E+09	9.05E+09	8.62E+09	7.55E+09	
Vfwd (V)	10.2E+3	11.8E+3	10.7E+3	9.9E+3	
Vrev (V)	13.9E+3	13.4E+3	12.4E+3	12.9E+3	
min tq (s)	204.0E-6	303.0E-6	308.0E-6	289.0E-6	
FCC					
Phase	1	2	3	4	FWL
Ipk (A)	433.5E+3	469.0E+3	497.7E+3	548.6E+3	692.4E+3
Action (A^2s)	2.78E+08	2.95E+08	2.95E+08	4.76E+08	2.39E+09
di/dt on (A/s)	7.28E+09	3.13E+09	3.33E+09	3.41E+09	9.73E+04
Vfwd (V)	11.4E+3	12.1E+3	11.7E+3	11.0E+3	4.7E+3
Vrev (V)	16.2E+3	17.3E+3	14.1E+3	15.2E+3	8.1E+3
min tq (s)	400.0E-6	422.0E-6	411.0E-6	385.0E-6	522.0E-6
Worst case phase	**GSC**	**FCC**	**FWL**		
Ipk (A)	1.4E+6	274.3E+3	346.2E+3		
Action (A^2s)	1.9E+9	119.0E+6	598.5E+6		
di/dt on (A/s)	4.5E+9	3.6E+9	48.6E+3		
Vfwd (V)	11.8E+3	12.1E+3	4.7E+3		
Vrev (V)	13.9E+3	17.3E+3	8.1E+3		
min tq (s)	204.0E-6	385.0E-6	522.0E-6		
Worst case pole	**GSC**	**FCC**	**FWL**		
Ipk (A)	340.5E+3	68.6E+3	86.5E+3		
Action (A^2s)	116.3E+6	7.4E+6	37.4E+6		
di/dt on (A/s)	1.1E+9	909.8E+6	12.2E+3		

In addition to being able to handle the electrical stresses, the devices must be packaged efficiently and be able to reject heat at rates fast enough to keep their electrical junctions below about 120°C. As the temperature rises beyond this point, the ability of the junction to recover and withstand voltage is degraded.

Figure VIII-3 shows a diagram of a thyristor packaged using Silicon Power Corporation's Light Silicon Sandwich Technology. This type of reduced-package SCR was pioneered by CEM and SPCO and was refined into a working device by SPCO under subcontract to CEM during the Army Focused Technology Program. One of the advantages of this package stems from its

reduced mechanical packaging. Functions, such as press load distribution and thermal expansion compensation, are removed from the package and must now be built into the clamp package. As a result, the mass and volume associated with this hardware can now be integrated into the clamp at reduced mass and volume per device.

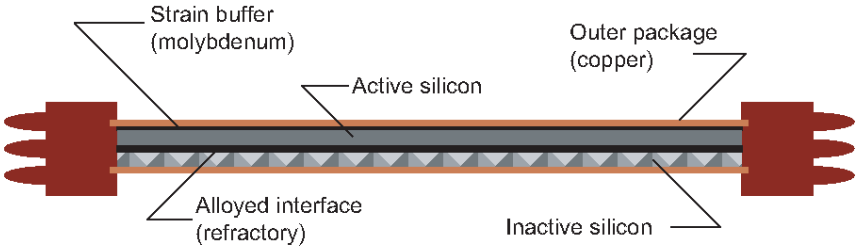

Figure VIII-3. Outline view of SPCO LSS package

Another significant advantage of the advanced packaging technique is that it allows the thermal-management hardware to be thermally and physically close to the silicon junction. This reduces the thermal time constant of the system and allows rapid burst-fire rates that are not limited by converter temperature rise.

Figure VIII-4 shows a schematic of a series of packaged devices sandwiched between aluminum pole pieces. These pole pieces carry current into the devices and absorb the thermal energy produced by the losses at the device junction. Because the high thermal capacity and low thermal conductivity pole pieces can be located so close to the junction, thermal equilibrium can be reached within 50 to 100 ms. As a result, rate of burst fire is limited elsewhere in the rail gun system.

The size of the pole pieces is determined by the five-shot burst requirement of the system. The thermal inertia of the posts is more than adequate to absorb all of the energy adiabatically from the burst (see analysis later in this section). The heat load from the two-shot-per-minute requirement will be handled by using standard coolant flow heat pucks. The pole pieces will be manufactured with coolant passages adequate to remove the steady-state heat generated by the continuous shot rate. Power losses and thermal management requirements for the converters were passed on to the vehicle systems designers. Detailed transient thermal and heat transfer

analysis for the converter were beyond the scope of this trade study. However, the cooling methods to be used are industry-standard and well understood.

Figure VIII-4. LSS devices with thermal-management pole pieces

Methods Employed and Assumptions Used

Electrical Design and Trades

The converter trade study was focused on determining the best combination of device characteristics and near-term packaging technology that could be reasonably forecast while satisfying the basic performance requirements and minimizing mass and volume. This was accomplished by using and extending existing design tools that allowed the team to examine several converter point designs based on four different devices and two overall converter packaging approaches. The devices, all thyristors, ranged from currently available state of the art to a conceptual new SiC SCR. They included an off the shelf 125 mm device, an interim (but not yet demonstrated) high voltage 125 mm device, a near-term 150 mm high voltage device, and a composite silicon carbide device based on current crystal manufacturing capability but requiring significant development. The converter package concepts include a dense, closely coupled topography and a dense topography where the GSC can be moved away from the alternators while the FCC remained within close proximity. As the point designs were carried toward conceptual design, interim comparisons were made and approaches eliminated until the two converter packaging approaches and two device choices remained.

The basic converter electrical design was accomplished using CEM's existing system performance simulation and an upgraded version of the power converter trade study comparison algorithm. The algorithm was modified to accommodate more device comparisons and to satisfy a design constraint that was placed on the converters for the first time in this study.

The alternator topography chosen is a four-phase radial field arrangement. Each phase is made up of four armature poles. A typical four-pole, four phase armature winding is illustrated in figure VIII-5. There are four separately–terminated armature windings per pole to which converter modules can be connected. The new constraint was to require that the converter design be accomplished at the worst-pole level rather than the worst-phase level. This means that the number of parallel devices is determined by the action or rate-of current rise from the worst case pole. The net result, because the devices are discrete devices, is that the overall design contains a few more devices and is therefore more conservative from a thermal and current sharing perspective.

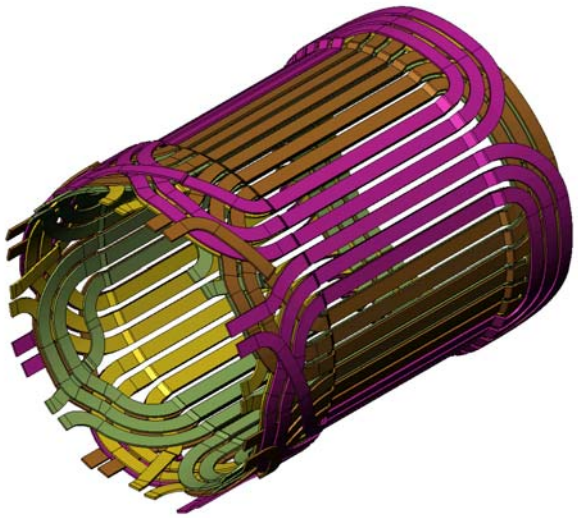

Figure VIII-5. Four phase, four pole winding

The parallel arrangement of the devices is determined by the greater requirement of the rate of current rise or virtual junction temperature rise, both with an applied factor-of safety of two. Conventional design techniques using peak or average currents are not adequate for pulsed duty machines. In any event, those data sheet ratings are based on assumptions about continuous heat removal and are actually derived from a virtual junction temperature calculation.

Previous work at CEM has shown that for the first-pass design, a device's maximum $\int I^2 dt$ rating (either explicit or based upon the peak non-cyclical surge current rating) provides a means to obtain a reliable estimate of junction temperature without making detailed device thermal analyses. As long as the critical rate of current rise rating is not exceeded, then the junction temperature will not exceed the manufacturer's rating as long as the maximum action per device is not exceeded. Therefore, the number of parallel devices per pole is the greater of

$$n_{parallel} = \sqrt{1.4 \frac{\int_0^{t_{discharge}} i_{pole}^2 \, dt}{\int_0^{8.3e-3} i_{TSM}^2 \, dt}} \qquad \text{(VIII-1)}$$

or

$$n_{parallel} = 2 \frac{\frac{di_{pole,maximum}}{dt}}{\frac{di_{critical,device}}{dt}} \qquad \text{(VIII-2)}$$

where

$t_{discharge}$ is the total time that the device is subjected to current

i_{pole} is the worst-case current from a pole

i_{TSM} is the maximum surge current capability of the device

$di/dt_{pole,\ maximum}$ is the worst case current rise at turn on

$di/dt_{\ device,\ critical}$ is the critical rate of current rise for the device.

The number of parallel devices is based on the worst-case phase and on the greater of the peak maximum forward or reverse impressed voltage divided by the device rating and using a factor of safety of two.

Device characteristics used in the trade study algorithm are based on scaling from the off-the-shelf SPCO SPT411A thyristor for the silicon devices. This device is shown in figure VIII-6. The silicon carbide device is based data from conduction and recovery testing of 6 mm devices at the University of Texas Institute for Applied Technology. A conceptual drawing of the silicon

carbide device is shown in figure VIII-7. The resulting device characteristics are shown in table VIII-6. The scaling methods and derivation or forecast of device characteristics are detailed in Appendix D.

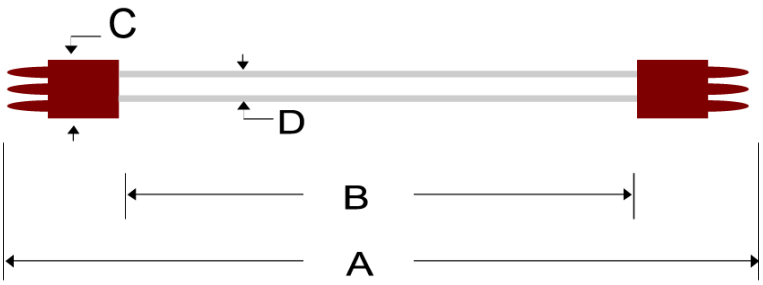

Figure VIII-6. Outline drawing used for determination of device characteristics and packaging design - dimensions are referenced to table VIII-6

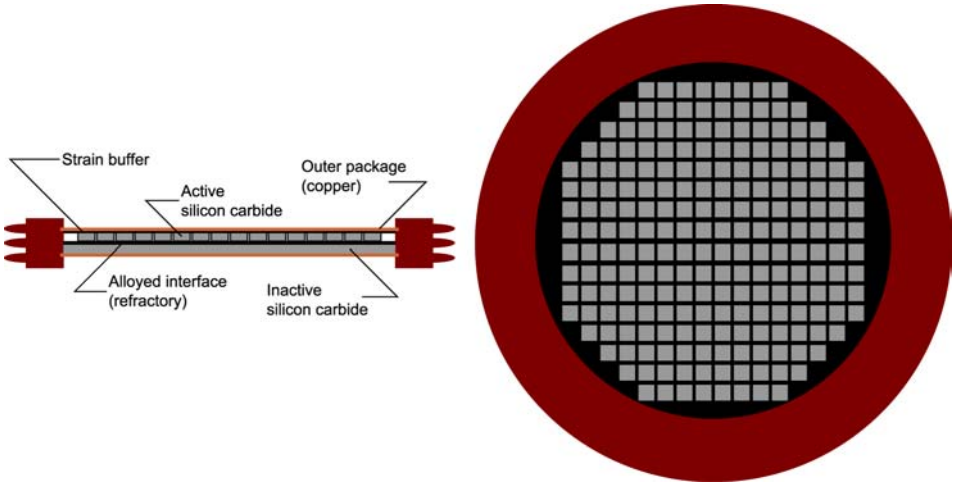

Figure VIII-7. Conceptual silicon carbide device - concept developed by researchers at the Institute for Advanced Technology and the Center for Electromechanics

Table VIII-6. Characteristics of devices used in trade study

Device Type	**SPCO 411**	**5 in. HV**	**6 in adv**	**5 in SiC**		Dimension Reference
Diameter	125.0E-3	125.0E-3	150.0E-3	125.0E-3	m	
Ipk (1.0 ms)	220.0E+3	145.0E+3	210.0E+3		A	
Action	25.0E+6	15.7E+6	27.4E+6	90.0E+6	A^2s	
di/dt crit	20.0E+9	20.0E+9	20.0E+9	34.5E+9	A/s	
Vdrm/rrm	5.0E+3	9.0E+3	11.0E+3	11.0E+3	V	
tq	400.0E-6	100.0E-6	100.0E-6	100.0E-6	s	
Pole dia	106.4E-3	106.4E-3	128.0E-3	106.4E-3	m	B
Pole thickness	4.6E-3	7.5E-3	8.4E-3	4.6E-3	m	D
Pole height	7.8E-3	6.3E-3	5.9E-3	7.8E-3	m	D-C/2
OD	162.7E-3	162.7E-3	184.0E-3	162.7E-3	m	A
Overall Thick	20.1E-3	20.1E-3	20.1E-3	20.1E-3	m	C
Dev mass	479.0E-3	6.81E-01	989.0E-3	479.0E-3	kg	
External Post thick	8.9E-3	7.3E-3	6.9E-3	8.9E-3	m	

The detailed results of the design and trade study are shown in tables VIII-7 through VIII-11. Shot #1 is reflected in table VIII-7, shot #2 in table VIII-8, and so on. The tables include all of the preliminary design data for the GSC, FWC and FWL including input and resultant factors-of-safety (FOS), numbers of parallel and series devices per phase pole, resultant nominal stresses (based on perfect sharing), and a summary of the converter design if that particular analysis was accepted in the trade as the design requirements.

Table VIII-7. Shot 1 power converter trades design data

Gun Switch Converter

Device Type: SPCO 411

	Input FOS	No. Devices	Nom Stress	Nom FOS	Converter Design Summary	
Ipk (A)	na	na	104.9E+3	na	No. parallel devices per pole	3
Action (A^2s)	1.4	3	10.3E+6	2.4	No. series devices	7
di/dt on (A/s)	2	1	384.5E+6	52.0	Total devices per phase	84
Vfwd (V)	2	5	1.7E+3	2.9	Total devices per aternator	336
Vrev (V)	2	7	2.2E+3	2.2	Total devices per PPS	672
tq	na	na	na	Below threshhold		

Device Type: 5in HV

	Input FOS	No. Devices	Nom stress	Nom FOS	Converter Design Summary	
Ipk (A)	na	na	104.9E+3	na	No. parallel devices per pole	3
Action (A^2s)	1.4	3	10.3E+6	1.5	No. series devices	4
di/dt on (A/s)	2	1	384.5E+6	52.0	Total devices per phase	48
Vfwd (V)	2	3	3.1E+3	2.9	Total devices per alternator	192
Vrev (V)	2	4	3.9E+3	2.3	Total devices per PPS	384
tq	na	na	na	Above threshold		

Device Type: 6in Adv

	Input FOS	No. Devices	Nom stress	Nom FOS	Converter Design Summary	
Ipk (A)	na	na	104.9E+3	na	No. parallel devices per pole	3
Action (A^2s)	1.4	3	10.3E+6	2.7	No. series devices	3
di/dt on (A/s)	2	1	384.5E+6	52.0	Total devices per phase	36
Vfwd (V)	2	3	4.1E+3	2.7	Total devices per alternator	144
Vrev (V)	2	3	5.2E+3	2.1	Total devices per PPS	288
tq	na	na	na	Above threshold		

Device Type: 5in SiC

	Input FOS	No. Devices	Nom stress	Nom FOS	Converter Design Summary	
Ipk (A)	na	na	157.4E+3	na	No. parallel devices per pole	2
Action (A^2s)	1.4	2	23.1E+6	3.8	No. series devices	3
di/dt on (A/s)	2	1	576.7E+6	59.8	Total devices per phase	24
Vfwd (V)	2	3	4.1E+3	2.7	Total devices per alternator	96
Vrev (V)	2	3	5.2E+3	2.1	Total devices per PPS	192
tq	na	na	na			

Field Coil Converter

Device Type: SPCO 411

	Input FOS	No. Devices	Nom stress	Nom FOS	Converter Design Summary	
Ipk (A)	na	na	50.0E+3	na	No. parallel devices per pole	1
Action (A^2s)	1.4	1	3.2E+6	7.9	No. series devices	7
di/dt on (A/s)	2	1	594.9E+6	33.6	Total devices per phase	28
Vfwd (V)	2	6	1.8E+3	2.7	Total devices per alternator	112
Vrev (V)	2	7	2.4E+3	2.0	Total devices per PPS	224
tq	na	na	na	Above threshold		

Device Type: 5in HV

	Input FOS	No. Devices	Nom stress	Nom FOS	Converter Design Summary	

Ipk (A)	na	na	50.0E+3	na	No. parallel devices per pole	1
Action (A^2s)	1.4	1	3.2E+6	5.0	No. series devices	4
di/dt on (A/s)	2	1	594.9E+6	33.6	Total devices per phase	16
Vfwd (V)	2	3	3.2E+3	2.8	Total devices per alternator	64
Vrev (V)	2	4	4.3E+3	2.1	Total devices per PPS	128
tq	na	na	na	Above threshold		

Device Type: 6in Adv

	Input FOS	No. Devices	Nom stress	Nom FOS	Converter Design Summary	
Ipk (A)	na	na	50.0E+3	na	No. parallel devices per pole	1
Action (A^2s)	1.4	1	3.2E+6	8.6	No. series devices	3
di/dt on (A/s)	2	1	594.9E+6	33.6	Total devices per phase	12
Vfwd (V)	1.8	3	4.3E+3	2.6	Total devices per alternator	48
Vrev (V)	1.8	3	5.7E+3	1.9	Total devices per PPS	96
tq	na	na	na	Above threshold		

Device Type: 5in SiC

	Input FOS	No. Devices	Nom stress	Nom FOS	Converter Design Summary	
Ipk (A)	na	na	50.0E+3	na	No. parallel devices per pole	1
Action (A^2s)	1.4	1	3.2E+6	27.8	No. series devices	3
di/dt on (A/s)	2	1	594.9E+6	58.0	Total devices per phase	12
Vfwd (V)	1.8	3	4.3E+3	2.6	Total devices per alternator	48
Vrev (V)	1.8	3	5.7E+3	1.9	Total devices per PPS	96
tq	na	na	na	Above threshold		

Free Wheel Leg

Device Type: SPCO 411

	Input FOS	No. Devices	Nom stress	Nom FOS	Converter Design Summary	
Ipk (A)	na	na	52.9E+3	na	No. parallel devices	5
Action (A^2s)	1.4	5	15.4E+6	1.6	No. series devices	4
di/dt on (A/s)	2	1	348.6E+6	57.4	Total devices per phase	na
Vfwd (V)	2	3	1.3E+3	3.8	Total devices per alternator	20
Vrev (V)	2	4	2.0E+3	2.5	Total devices per PPS	40
tq	na	na	na	Above threshold		

Device Type: 5in HV

	Input FOS	No. Devices	Nom stress	Nom FOS	Converter Design Summary	
Ipk (A)	na	na	44.1E+3	na	No. parallel devices	6
Action (A^2s)	1.4	6	10.7E+6	1.5	No. series devices	2
di/dt on (A/s)	2	1	290.5E+6	68.8	Total devices per phase	na
Vfwd (V)	2	2	2.6E+3	3.5	Total devices per alternator	12
Vrev (V)	2	2	4.0E+3	2.2	Total devices per PPS	24
tq	na	na	na	Above threshold		

Device Type: 6in Adv

	Input FOS	No. Devices	Nom stress	Nom FOS	Converter Design Summary	
Ipk (A)	na	na	52.9E+3	na	No. parallel devices	5
Action (A^2s)	1.4	5	15.4E+6	1.8	No. series devices	2
di/dt on (A/s)	2	1	348.6E+6	57.4	Total devices per phase	na
Vfwd (V)	2	1	2.6E+3	4.2	Total devices per alternator	10
Vrev (V)	2	2	4.0E+3	2.7	Total devices per PPS	20
tq	na	na	na	Above threshold		

Device Type: 5in SiC						
	Input FOS	**No. Devices**	**Nom stress**	**Nom FOS**	**Converter Design Summary**	
Ipk (A)	na	na	88.2E+3	na	No. parallel devices	3
Action (A^2s)	1.4	3	42.7E+6	2.1	No. series devices	2
di/dt on (A/s)	2	1	581.0E+6	59.3	Total devices per phase	na
Vfwd (V)	2	1	2.6E+3	4.2	Total devices per alternator	6
Vrev (V)	2	2	4.0E+3	2.7	Total devices per PPS	12
tq	na	na	na	Above threshold		

Table VIII-8. Shot 2 power converter trades design data

Gun Switch Converter

Device Type: SPCO 411						
	Input FOS	**No. Devices**	**Nom Stress**	**Nom FOS**	**Converter Design Summary**	
Ipk (A)	na	na	111.5E+3	na	No. parallel devices per pole	3
Action (A^2s)	1.4	3	10.8E+6	2.3	No. series devices	7
di/dt on (A/s)	2	1	371.8E+6	53.8	Total devices per phase	84
Vfwd (V)	2	5	1.7E+3	2.9	Total devices per alternator	336
Vrev (V)	2	7	2.2E+3	2.3	Total devices per PPS	672
tq	na	na	na	Below threshhold		
Device Type: 5in HV						
	Input FOS	**No. Devices**	**Nom stress**	**Nom FOS**	**Converter Design Summary**	
Ipk (A)	na	na	111.5E+3	na	No. parallel devices per pole	3
Action (A^2s)	1.4	3	10.8E+6	1.5	No. series devices	4
di/dt on (A/s)	2	1	371.8E+6	53.8	Total devices per phase	48
Vfwd (V)	2	3	3.0E+3	3.0	Total devices per alternator	192
Vrev (V)	2	4	3.9E+3	2.3	Total devices per PPS	384
tq	na	na	na	Above threshold		
Device Type: 6in Adv						
	Input FOS	**No. Devices**	**Nom stress**	**Nom FOS**	**Converter Design Summary**	
Ipk (A)	na	na	111.5E+3	na	No. parallel devices per pole	3
Action (A^2s)	1.4	3	10.8E+6	2.5	No. series devices	3
di/dt on (A/s)	2	1	371.8E+6	53.8	Total devices per phase	36
Vfwd (V)	2	3	4.0E+3	2.8	Total devices per alternator	144
Vrev (V)	2	3	5.1E+3	2.1	Total devices per PPS	288
tq	na	na	na	Above threshold		
Device Type: 5in SiC						
	Input FOS	**No. Devices**	**Nom stress**	**Nom FOS**	**Converter Design Summary**	
Ipk (A)	na	na	167.3E+3	na	No. parallel devices per pole	2
Action (A^2s)	1.4	2	24.3E+6	3.6	No. series devices	3
di/dt on (A/s)	2	1	557.7E+6	61.8	Total devices per phase	24
Vfwd (V)	2	3	4.0E+3	2.8	Total devices per alternator	96
Vrev (V)	2	3	5.1E+3	2.1	Total devices per PPS	192
tq	na	na	na	Above threshold		

Field Coil Converter

Device Type: SPCO 411						
	Input FOS	**No. Devices**	**Nom stress**	**Nom FOS**	**Converter Design Summary**	
Ipk (A)	na	na	52.6E+3	na	No. parallel devices per pole	1
Action (A^2s)	1.4	1	3.3E+6	7.7	No. series devices	7
di/dt on (A/s)	2	1	431.2E+6	46.4	Total devices per phase	28
Vfwd (V)	2	6	1.9E+3	2.7	Total devices per alternator	112
Vrev (V)	2	7	2.4E+3	2.1	Total devices per PPS	224
tq	na	na	na	Above threshold		
Device Type: 5in HV						
	Input FOS	**No. Devices**	**Nom stress**	**Nom FOS**	**Converter Design Summary**	

Ipk (A)	na	na	52.6E+3	na	No. parallel devices per pole	1
Action (A^2s)	1.4	1	3.3E+6	4.8	No. series devices	4
di/dt on (A/s)	2	1	431.2E+6	46.4	Total devices per phase	16
Vfwd (V)	2	3	3.3E+3	2.7	Total devices per alternator	64
Vrev (V)	2	4	4.2E+3	2.1	Total devices per PPS	128
tq	na	na	na	Above threshold		

Device Type: 6in Adv

	Input FOS	No. Devices	Nom stress	Nom FOS	Converter Design Summary	
Ipk (A)	na	na	52.6E+3	na	No. parallel devices per pole	1
Action (A^2s)	1.4	1	3.3E+6	8.4	No. series devices	3
di/dt on (A/s)	2	1	431.2E+6	46.4	Total devices per phase	12
Vfwd (V)	1.8	3	4.4E+3	2.5	Total devices per alternator	48
Vrev (V)	1.8	3	5.6E+3	2.0	Total devices per PPS	96
tq	na	na	na	Above threshold		

Device Type: 5in SiC

	Input FOS	No. Devices	Nom stress	Nom FOS	Converter Design Summary	
Ipk (A)	na	na	52.6E+3	na	No. parallel devices per pole	1
Action (A^2s)	1.4	1	3.3E+6	27.0	No. series devices	3
di/dt on (A/s)	2	1	431.2E+6	80.0	Total devices per phase	12
Vfwd (V)	1.8	3	4.4E+3	2.5	Total devices per alternator	48
Vrev (V)	1.8	3	5.6E+3	2.0	Total devices per PPS	96
tq	na	na	na	Above threshold		

Free Wheel Leg

Device Type: SPCO 411

	Input FOS	No. Devices	Nom stress	Nom FOS	Converter Design Summary	
Ipk (A)	na	na	56.1E+3	na	No. parallel devices	5
Action (A^2s)	1.4	5	16.3E+6	1.5	No. series devices	4
di/dt on (A/s)	2	1	376.2E+6	53.2	Total devices per phase	na
Vfwd (V)	2	2	1.2E+3	4.0	Total devices per alternator	20
Vrev (V)	2	4	2.2E+3	2.3	Total devices per PPS	40
tq	na	na	na	Above threshold		

Device Type: 5in HV

	Input FOS	No. Devices	Nom stress	Nom FOS	Converter Design Summary	
Ipk (A)	na	na	40.1E+3	na	No. parallel devices	7
Action (A^2s)	1.4	7	8.3E+6	1.9	No. series devices	2
di/dt on (A/s)	2	1	268.7E+6	74.4	Total devices per phase	na
Vfwd (V)	2	2	2.5E+3	3.6	Total devices per alternator	14
Vrev (V)	2	2	4.3E+3	2.1	Total devices per PPS	28
tq	na	na	na	Above threshold		

Device Type: 6in Adv

	Input FOS	No. Devices	Nom stress	Nom FOS	Converter Design Summary	
Ipk (A)	na	na	56.1E+3	na	No. parallel devices	5
Action (A^2s)	1.4	5	16.3E+6	1.7	No. series devices	2
di/dt on (A/s)	2	1	376.2E+6	53.2	Total devices per phase	na
Vfwd (V)	2	1	2.5E+3	4.4	Total devices per alternator	10
Vrev (V)	2	2	4.3E+3	2.5	Total devices per PPS	20
tq	na	na	na	Above threshold		

Device Type: 5in SiC						
	Input FOS	**No. Devices**	**Nom stress**	**Nom FOS**	**Converter Design Summary**	
Ipk (A)	na	na	93.6E+3	na	No. parallel devices	3
Action (A^2s)	1.4	3	45.4E+6	1.9	No. series devices	2
di/dt on (A/s)	2	1	627.0E+6	55.0	Total devices per phase	na
Vfwd (V)	2	1	2.5E+3	4.4	Total devices per alternator	6
Vrev (V)	2	2	4.3E+3	2.5	Total devices per PPS	12
tq	na	na	na	Above threshold		

Table VIII-9. Shot 3 power converter trades design data

Gun Switch Converter

Device Type: SPCO 411

	Input FOS	No. Devices	Nom Stress	Nom FOS	Converter Design Summary	
Ipk (A)	na	na	105.0E+3	na	No. parallel devices per pole	3
Action (A^2s)	1.4	3	10.5E+6	2.4	No. series devices	6
di/dt on (A/s)	2	1	337.2E+6	59.3	Total devices per phase	72
Vfwd (V)	2	5	1.9E+3	2.6	Total devices per alternator	288
Vrev (V)	2	6	2.2E+3	2.3	Total devices per PPS	576
tq	na	na	na	Below threshhold		

Device Type: 5in HV

	Input FOS	No. Devices	Nom stress	Nom FOS	Converter Design Summary	
Ipk (A)	na	na	105.0E+3	na	No. parallel devices per pole	3
Action (A^2s)	1.4	3	10.5E+6	1.5	No. series devices	3
di/dt on (A/s)	2	1	337.2E+6	59.3	Total devices per phase	36
Vfwd (V)	2	3	3.8E+3	2.4	Total devices per alternator	144
Vrev (V)	2	3	4.4E+3	2.0	Total devices per PPS	288
tq	na	na	na	Above threshold		

Device Type: 6in Adv

	Input FOS	No. Devices	Nom stress	Nom FOS	Converter Design Summary	
Ipk (A)	na	na	105.0E+3	na	No. parallel devices per pole	3
Action (A^2s)	1.4	3	10.5E+6	2.6	No. series devices	3
di/dt on (A/s)	2	1	337.2E+6	59.3	Total devices per phase	36
Vfwd (V)	2	3	3.8E+3	2.9	Total devices per alternator	144
Vrev (V)	2	3	4.4E+3	2.5	Total devices per PPS	288
tq	na	na	na	Above threshold		

Device Type: 5in SiC

	Input FOS	No. Devices	Nom stress	Nom FOS	Converter Design Summary	
Ipk (A)	na	na	157.5E+3	na	No. parallel devices per pole	2
Action (A^2s)	1.4	2	23.7E+6	3.7	No. series devices	3
di/dt on (A/s)	2	1	505.7E+6	68.2	Total devices per phase	24
Vfwd (V)	2	3	3.8E+3	2.9	Total devices per alternator	96
Vrev (V)	2	3	4.4E+3	2.5	Total devices per PPS	192
tq	na	na	na	Above threshold		

Field Coil Converter

Device Type: SPCO 411

	Input FOS	No. Devices	Nom stress	Nom FOS	Converter Design Summary	
Ipk (A)	na	na	50.4E+3	na	No. parallel devices per pole	1
Action (A^2s)	1.4	1	3.0E+6	8.5	No. series devices	7
di/dt on (A/s)	2	1	395.8E+6	50.5	Total devices per phase	28
Vfwd (V)	2	5	1.5E+3	3.2	Total devices per alternator	112
Vrev (V)	2	7	2.2E+3	2.3	Total devices per PPS	224
tq	na	na	na	Above threshold		

Device Type: 5in HV

	Input FOS	No. Devices	Nom stress	Nom FOS

Ipk (A)	na	na	50.4E+3	na	No. parallel devices per pole	1
Action (A^2s)	1.4	1	3.0E+6	5.3	No. series devices	4
di/dt on (A/s)	2	1	395.8E+6	50.5	Total devices per phase	16
Vfwd (V)	1.8	3	2.7E+3	3.3	Total devices per alternator	64
Vrev (V)	1.8	4	3.8E+3	2.4	Total devices per PPS	128
tq	na	na	na	Above threshold		

Device Type: 6in Adv

	Input FOS	No. Devices	Nom stress	Nom FOS	Converter Design Summary	
Ipk (A)	na	na	50.4E+3	na	No. parallel devices per pole	1
Action (A^2s)	1.4	1	3.0E+6	9.3	No. series devices	3
di/dt on (A/s)	2	1	395.8E+6	50.5	Total devices per phase	12
Vfwd (V)	1.8	2	3.6E+3	3.0	Total devices per alternator	48
Vrev (V)	1.8	3	5.1E+3	2.2	Total devices per PPS	96
tq	na	na	na	Above threshold		

Device Type: 5in SiC

	Input FOS	No. Devices	Nom stress	Nom FOS	Converter Design Summary	
Ipk (A)	na	na	50.4E+3	na	No. parallel devices per pole	1
Action (A^2s)	1.4	1	3.0E+6	29.8	No. series devices	3
di/dt on (A/s)	2	1	395.8E+6	87.1	Total devices per phase	12
Vfwd (V)	1.8	2	3.6E+3	3.0	Total devices per alternator	48
Vrev (V)	1.8	3	5.1E+3	2.2	Total devices per PPS	96
tq	na	na	na	Above threshold		

Free Wheel Leg

Device Type: SPCO 411

	Input FOS	No. Devices	Nom stress	Nom FOS	Converter Design Summary	
Ipk (A)	na	na	54.3E+3	na	No. parallel devices	5
Action (A^2s)	1.4	5	15.4E+6	1.6	No. series devices	3
di/dt on (A/s)	2	1	8.9E+3	2.2E+6	Total devices per phase	na
Vfwd (V)	2	2	1.6E+3	3.2	Total devices per alternator	15
Vrev (V)	2	3	2.4E+3	2.1	Total devices per PPS	30
tq	na	na	na	Above threshold		

Device Type: 5in HV

	Input FOS	No. Devices	Nom stress	Nom FOS	Converter Design Summary	
Ipk (A)	na	na	45.2E+3	na	No. parallel devices	6
Action (A^2s)	1.4	6	10.7E+6	1.5	No. series devices	2
di/dt on (A/s)	2	1	7.4E+3	2.7E+6	Total devices per phase	na
Vfwd (V)	2	2	2.3E+3	3.9	Total devices per alternator	12
Vrev (V)	2	2	3.6E+3	2.5	Total devices per PPS	24
tq	na	na	na	Above threshold		

Device Type: 6in Adv

	Input FOS	No. Devices	Nom stress	Nom FOS	Converter Design Summary	
Ipk (A)	na	na	54.3E+3	na	No. parallel devices	5
Action (A^2s)	1.4	5	15.4E+6	1.8	No. series devices	2
di/dt on (A/s)	2	1	8.9E+3	2.2E+6	Total devices per phase	na
Vfwd (V)	2	1	2.3E+3	4.7	Total devices per alternator	10
Vrev (V)	2	2	3.6E+3	3.1	Total devices per PPS	20
tq	na	na	na	Above threshold		

Device Type: 5in SiC						
	Input FOS	**No. Devices**	**Nom stress**	**Nom FOS**	**Converter Design Summary**	
Ipk (A)	na	na	90.5E+3	na	No. parallel devices	3
Action (A^2s)	1.4	3	42.8E+6	2.1	No. series devices	2
di/dt on (A/s)	2	1	14.8E+3	2.3E+6	Total devices per phase	na
Vfwd (V)	2	1	2.3E+3	4.7	Total devices per alternator	6
Vrev (V)	2	2	3.6E+3	3.1	Total devices per PPS	12
tq	na	na	na	Above threshold		

Table VIII-10. Shot 4 power converter trades design data

Gun Switch Converter

Device Type: SPCO 411

	Input FOS	No. Devices	Nom Stress	Nom FOS	Converter Design Summary	
Ipk (A)	na	na	113.0E+3	na	No. parallel devices per pole	3
Action (A^2s)	1.4	3	9.9E+6	2.5	No. series devices	6
di/dt on (A/s)	2	1	322.5E+6	62.0	Total devices per phase	72
Vfwd (V)	2	5	1.8E+3	2.8	Total devices per alternator	288
Vrev (V)	2	6	2.3E+3	2.2	Total devices per PPS	576
tq	na	na	na	Below threshhold		

Device Type: 5in HV

	Input FOS	No. Devices	Nom stress	Nom FOS	Converter Design Summary	
Ipk (A)	na	na	113.0E+3	na	No. parallel devices per pole	3
Action (A^2s)	1.4	3	9.9E+6	1.6	No. series devices	4
di/dt on (A/s)	2	1	322.5E+6	62.0	Total devices per phase	48
Vfwd (V)	2	3	2.6E+3	3.4	Total devices per alternator	192
Vrev (V)	2	4	3.5E+3	2.6	Total devices per PPS	384
tq	na	na	na	Above threshold		

Device Type: 6in Adv

	Input FOS	No. Devices	Nom stress	Nom FOS	Converter Design Summary	
Ipk (A)	na	na	113.0E+3	na	No. parallel devices per pole	3
Action (A^2s)	1.4	3	9.9E+6	2.8	No. series devices	3
di/dt on (A/s)	2	1	322.5E+6	62.0	Total devices per phase	36
Vfwd (V)	2	2	3.5E+3	3.1	Total devices per alternator	144
Vrev (V)	2	3	4.6E+3	2.4	Total devices per PPS	288
tq	na	na	na	Above threshold		

Device Type: 5in SiC

	Input FOS	No. Devices	Nom stress	Nom FOS	Converter Design Summary	
Ipk (A)	na	na	169.5E+3	na	No. parallel devices per pole	2
Action (A^2s)	1.4	2	22.2E+6	4.0	No. series devices	3
di/dt on (A/s)	2	1	483.7E+6	71.3	Total devices per phase	24
Vfwd (V)	2	2	3.5E+3	3.1	Total devices per alternator	96
Vrev (V)	2	3	4.6E+3	2.4	Total devices per PPS	192
tq	na	na	na	Above threshold		

Field Coil Converter

Device Type: SPCO 411

	Input FOS	No. Devices	Nom stress	Nom FOS	Converter Design Summary	
Ipk (A)	na	na	56.1E+3	na	No. parallel devices per pole	1
Action (A^2s)	1.4	1	4.1E+6	6.2	No. series devices	7
di/dt on (A/s)	2	1	387.9E+6	51.6	Total devices per phase	28
Vfwd (V)	2	5	1.6E+3	3.1	Total devices per alternator	112
Vrev (V)	2	7	2.2E+3	2.2	Total devices per PPS	224
tq	na	na	na	Above threshold		

Device Type: 5in HV

	Input FOS	No. Devices	Nom stress	Nom FOS	Converter Design Summary

Ipk (A)	na	na	56.1E+3	na	No. parallel devices per pole	1
Action (A^2s)	1.4	1	4.1E+6	3.9	No. series devices	4
di/dt on (A/s)	2	1	387.9E+6	51.6	Total devices per phase	16
Vfwd (V)	2	3	2.8E+3	3.2	Total devices per alternator	64
Vrev (V)	2	4	3.9E+3	2.3	Total devices per PPS	128
tq	na	na	na	Above threshold		

Device Type: 6in Adv

	Input FOS	No. Devices	Nom stress	Nom FOS	Converter Design Summary	
Ipk (A)	na	na	56.1E+3	na	No. parallel devices per pole	1
Action (A^2s)	1.4	1	4.1E+6	6.7	No. series devices	3
di/dt on (A/s)	2	1	387.9E+6	51.6	Total devices per phase	12
Vfwd (V)	1.8	2	3.8E+3	2.9	Total devices per alternator	48
Vrev (V)	1.8	3	5.2E+3	2.1	Total devices per PPS	96
tq	na	na	na	Above threshold		

Device Type: 5in SiC

	Input FOS	No. Devices	Nom stress	Nom FOS	Converter Design Summary	
Ipk (A)	na	na	56.1E+3	na	No. parallel devices per pole	1
Action (A^2s)	1.4	1	4.1E+6	21.7	No. series devices	3
di/dt on (A/s)	2	1	387.9E+6	88.9	Total devices per phase	12
Vfwd (V)	1.8	2	3.8E+3	2.9	Total devices per alternator	48
Vrev (V)	1.8	3	5.2E+3	2.1	Total devices per PPS	96
tq	na	na	na	Above threshold		

Free Wheel Leg

Device Type: SPCO 411

	Input FOS	No. Devices	Nom stress	Nom FOS	Converter Design Summary	
Ipk (A)	na	na	58.1E+3	na	No. parallel devices	5
Action (A^2s)	1.4	5	17.3E+6	1.4	No. series devices	4
di/dt on (A/s)	2	1	8.8E+3	2275054.0	Total devices per phase	na
Vfwd (V)	2	2	1.1E+3	4.6	Total devices per alternator	20
Vrev (V)	2	4	2.0E+3	2.5	Total devices per PPS	40
tq	na	na	na	Above threshold		

Device Type: 5in HV

	Input FOS	No. Devices	Nom stress	Nom FOS	Converter Design Summary	
Ipk (A)	na	na	41.5E+3	na	No. parallel devices	7
Action (A^2s)	1.4	7	8.8E+6	1.8	No. series devices	2
di/dt on (A/s)	2	1	6.3E+3	3185075.6	Total devices per phase	na
Vfwd (V)	2	1	2.2E+3	4.2	Total devices per alternator	14
Vrev (V)	2	2	4.0E+3	2.2	Total devices per PPS	28
tq	na	na	na	Above threshold		

Device Type: 6in Adv

	Input FOS	No. Devices	Nom stress	Nom FOS	Converter Design Summary	
Ipk (A)	na	na	58.1E+3	na	No. parallel devices	5
Action (A^2s)	1.4	5	17.3E+6	1.6	No. series devices	2
di/dt on (A/s)	2	1	8.8E+3	2275054.0	Total devices per phase	na
Vfwd (V)	2	1	2.2E+3	5.1	Total devices per alternator	10
Vrev (V)	2	2	4.0E+3	2.7	Total devices per PPS	20
tq	na	na	na	Above threshold		

Device Type: 5in SiC						
	Input FOS	**No. Devices**	**Nom stress**	**Nom FOS**	**Converter Design Summary**	
Ipk (A)	na	na	96.9E+3	na	No. parallel devices	3
Action (A^2s)	1.4	3	48.1E+6	1.8	No. series devices	2
di/dt on (A/s)	2	1	14.7E+3	2353111.1	Total devices per phase	na
Vfwd (V)	2	1	2.2E+3	5.1	Total devices per alternator	6
Vrev (V)	2	2	4.0E+3	2.7	Total devices per PPS	12
tq	na	na	na	Above threshold		

Table VIII-11. Shot 5 power converter trades design data

Gun Switch Converter

Device Type: SPCO 411

	Input FOS	No. Devices	Nom Stress	Nom FOS	Converter Design Summary	
Ipk (A)	na	na	113.5E+3	na	No. parallel devices per pole	3
Action (A^2s)	1.4	3	12.9E+6	1.9	No. series devices	6
di/dt on (A/s)	2	1	377.3E+6	53.0	Total devices per phase	72
Vfwd (V)	2	5	2.0E+3	2.5	Total devices per alternator	288
Vrev (V)	2	6	2.3E+3	2.2	Total devices per PPS	576
tq	na	na	na	Below threshhold		

Device Type: 5in HV

	Input FOS	No. Devices	Nom stress	Nom FOS	Converter Design Summary	
Ipk (A)	na	na	85.1E+3	na	No. parallel devices per pole	4
Action (A^2s)	1.4	4	7.3E+6	2.2	No. series devices	4
di/dt on (A/s)	2	1	283.0E+6	70.7	Total devices per phase	64
Vfwd (V)	2	3	2.9E+3	3.1	Total devices per alternator	256
Vrev (V)	2	4	3.5E+3	2.6	Total devices per PPS	512
tq	na	na	na	Above threshold		

Device Type: 6in Adv

	Input FOS	No. Devices	Nom stress	Nom FOS	Converter Design Summary	
Ipk (A)	na	na	113.5E+3	na	No. parallel devices per pole	3
Action (A^2s)	1.4	3	12.9E+6	2.1	No. series devices	3
di/dt on (A/s)	2	1	377.3E+6	53.0	Total devices per phase	36
Vfwd (V)	2	3	3.9E+3	2.8	Total devices per alternator	144
Vrev (V)	2	3	4.6E+3	2.4	Total devices per PPS	288
tq	na	na	na	Above threshold		

Device Type: 5in SiC

	Input FOS	No. Devices	Nom stress	Nom FOS	Converter Design Summary	
Ipk (A)	na	na	170.3E+3	na	No. parallel devices per pole	2
Action (A^2s)	1.4	2	29.1E+6	3.0	No. series devices	3
di/dt on (A/s)	2	1	565.9E+6	60.9	Total devices per phase	24
Vfwd (V)	2	3	3.9E+3	2.8	Total devices per alternator	96
Vrev (V)	2	3	4.6E+3	2.4	Total devices per PPS	192
tq	na	na	na	Above threshold		

Field Coil Converter

Device Type: SPCO 411

	Input FOS	No. Devices	Nom stress	Nom FOS	Converter Design Summary	
Ipk (A)	na	na	68.6E+3	na	No. parallel devices per pole	1
Action (A^2s)	1.4	1	7.4E+6	3.4	No. series devices	7
di/dt on (A/s)	2	1	909.8E+6	22.0	Total devices per phase	28
Vfwd (V)	2	5	1.7E+3	2.9	Total devices per alternator	112
Vrev (V)	2	7	2.5E+3	2.0	Total devices per PPS	224
tq	na	na	na	Above threshold		

Device Type: 5in HV

	Input FOS	No. Devices	Nom stress	Nom FOS	Converter Design Summary

Ipk (A)	na	na	68.6E+3	na	No. parallel devices per pole	1
Action (A^2s)	1.4	1	7.4E+6	2.1	No. series devices	4
di/dt on (A/s)	2	1	909.8E+6	22.0	Total devices per phase	16
Vfwd (V)	2	3	3.0E+3	3.0	Total devices per alternator	64
Vrev (V)	2	4	4.3E+3	2.1	Total devices per PPS	128
tq	na	na	na	Above threshold		

Device Type: 6in Adv

	Input FOS	No. Devices	Nom stress	Nom FOS	Converter Design Summary	
Ipk (A)	na	na	68.6E+3	na	No. parallel devices per pole	1
Action (A^2s)	1.4	1	7.4E+6	3.7	No. series devices	3
di/dt on (A/s)	2	1	909.8E+6	22.0	Total devices per phase	12
Vfwd (V)	1.8	2	4.0E+3	2.7	Total devices per alternator	48
Vrev (V)	1.8	3	5.8E+3	1.9	Total devices per PPS	96
tq	na	na	na	Above threshold		

Device Type: 5in SiC

	Input FOS	No. Devices	Nom stress	Nom FOS	Converter Design Summary	
Ipk (A)	na	na	68.6E+3	na	No. parallel devices per pole	1
Action (A^2s)	1.4	1	7.4E+6	11.8	No. series devices	3
di/dt on (A/s)	2	1	909.8E+6	37.9	Total devices per phase	12
Vfwd (V)	1.8	2	4.0E+3	2.7	Total devices per alternator	48
Vrev (V)	1.8	3	5.8E+3	1.9	Total devices per PPS	96
tq	na	na	na	Above threshold		

Free Wheel Leg

Device Type: SPCO 411

	Input FOS	No. Devices	Nom stress	Nom FOS	Converter Design Summary	
Ipk (A)	na	na	57.7E+3	na	No. parallel devices	6
Action (A^2s)	1.4	6	16.6E+6	1.5	No. series devices	4
di/dt on (A/s)	2	1	8.1E+3	2.5E+6	Total devices per phase	na
Vfwd (V)	2	2	1.2E+3	4.3	Total devices per alternator	24
Vrev (V)	2	4	2.0E+3	2.5	Total devices per PPS	48
tq	na	na	na	Above threshold		

Device Type: 5in HV

	Input FOS	No. Devices	Nom stress	Nom FOS	Converter Design Summary	
Ipk (A)	na	na	43.3E+3	na	No. parallel devices	8
Action (A^2s)	1.4	8	9.4E+6	1.7	No. series devices	2
di/dt on (A/s)	2	1	6.1E+3	3.3E+6	Total devices per phase	na
Vfwd (V)	2	2	2.3E+3	3.9	Total devices per alternator	16
Vrev (V)	2	2	4.1E+3	2.2	Total devices per PPS	32
tq	na	na	na	Above threshold		

Device Type: 6in Adv

	Input FOS	No. Devices	Nom stress	Nom FOS	Converter Design Summary	
Ipk (A)	na	na	57.7E+3	na	No. parallel devices	6
Action (A^2s)	1.4	6	16.6E+6	1.6	No. series devices	2
di/dt on (A/s)	2	1	8.1E+3	2.5E+6	Total devices per phase	na
Vfwd (V)	2	1	2.3E+3	4.7	Total devices per alternator	12
Vrev (V)	2	2	4.1E+3	2.7	Total devices per PPS	24
tq	na	na	na	Above threshold		

Device Type: 5in SiC						
	Input FOS	**No. Devices**	**Nom stress**	**Nom FOS**	**Converter Design Summary**	
Ipk (A)	na	na	86.5E+3	na	No. parallel devices	4
Action (A^2s)	1.4	4	37.4E+6	2.4	No. series devices	2
di/dt on (A/s)	2	1	12.2E+3	2.8E+6	Total devices per phase	na
Vfwd (V)	2	1	2.3E+3	4.7	Total devices per alternator	8
Vrev (V)	2	2	4.1E+3	2.7	Total devices per PPS	16
tq	na	na	na	Above threshold		

Device Triggering and Protection

A positive voltage differential and a gate pulse are required for an SCR to conduct. The gate pulse is typically generated by a capacitive discharge across the SCR gate and cathode. The gate pulse requirements are highly specific to the characteristics and assembly of the SCR, and as such are difficult to predict for conceptual devices. However, just as the 411A SCR was used to scale the mass and volume of the advanced SCRs for the pulsed alternator converters, a similar technique was used to help estimate gate circuit physical characteristics.

While CEM has not built a gate circuit and tested the 411A SCR, the pulsed power converter team has extensive experience with the SPCO 402B SCR both in the lab and with a compensated pulsed alternator. The dimensions of the gate circuit enclosure built for the 402B SCR and previously tested by CEM are 15.2 cm x 40.6 cm x 50.8 cm. This represented a gate volume of 5200 cm^3 per SCR. The gate requirements of the 411A SCR represent a 10x reduction in gate current compared to the 402B. As a result, the design team has applied the same 10x reduction in gate circuit volume. The dimensions of the trigger volume modeled in the tank assembly are 15.2 cm x 15.2 cm x 25.4 cm for a module of 12 devices, or 500 cm^3 per SCR. The geometry selected is equal in cross-section and roughly one half the length of an SCR module which is advantageous for packaging.

The trigger volume allowance is believed to be conservative for several reasons. First, the baseline 402B gate circuit was a first generation design made to be easy to assemble, test, and maintain. As such, it could be made smaller with a second design iteration and more aggressive packaging. Second, the trigger allowance for the advanced device is based on that of an off-the shelf SCR (411A). It is possible that device advances would lead to further reductions in gate requirements. Finally, there are several novel gating approaches that could further reduce the

gate circuit. These novel ideas include optical triggering and gating using energy stored in the equalization circuit capacitors. While CEM believes the above assumptions lead to a conservative approach, the uncertainty in the requirements of the advanced device specifically due to its gate design and physical dimensions warrants this approach.

Pulsed power SCRs typically require RC equalization networks for static and dynamic voltage sharing due to the large variation in critical device parameters for prototype SCRs and the multiple series and parallel SCR arrangements required for pulsed alternator systems. The issues inherent to dynamic voltage sharing are shown graphically in figure VIII-8. Because each device stores a slightly different amount of charge in its junction, the times required for each junction to clear, or recover, is different. As a result, one device will always turn off more quickly than the others. Without dynamic sharing protection circuits to provide an alternate current path during the time difference, the fastest device would have all of the impressed voltage across it and would fail.

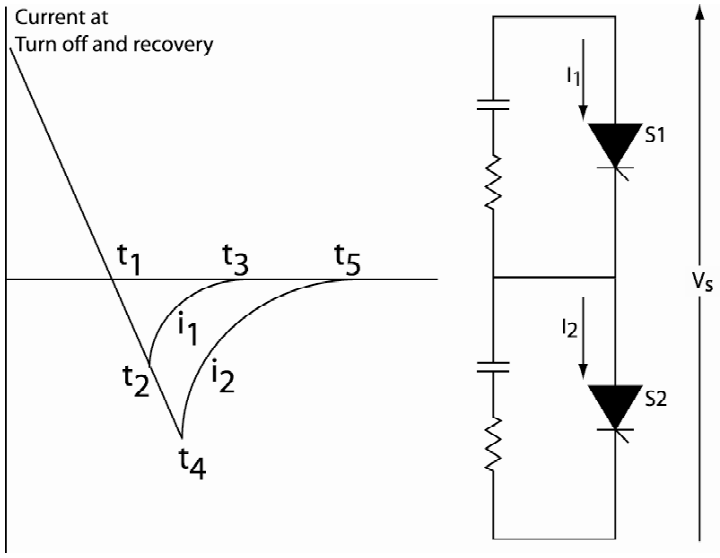

Figure VIII-8. Recovery characteristics of two devices connected in parallel and protection circuit showing the alternate current path

To facilitate static voltage sharing, grading resistors are connected across each SCR. The grading resistors are typically much smaller than the dynamic equalization circuit and, as a result, were not included in the gate circuit mass and volume estimate. The dynamic equalization circuit includes a series capacitor and resistor connected across each SCR and helps reduce

variations in the reverse voltage spike between series SCRs that can occur when the converter leg turns off.

As mentioned above, the dynamic equalization (snubber) circuit dwarfs in mass and volume the grading resistors. Further, because the snubber capacitor dwarfs the snubber resistor, the capacitor is the primary unit for estimating equalization circuit mass and volume. Each 402B SCR in the converter required a 4.6 cm diameter capacitor that was 18.4 cm long and weighed 0.5 kg. Similar to the estimates used for the gate circuit, there is a good deal of uncertainty in the snubber requirements for an advanced device, but since the need for snubbers is a result of critical parameter variation within a lot of SCRs, there is no reason to believe the snubber requirements will decrease significantly in future devices made with similar manufacturing techniques. However, advances in capacitor design could proportionally reduce snubber mass and volume. For all of these reasons, a per-device mass of 0.4 kg was chosen for the converter design. The placeholder volume for the snubbers, like the gate circuits was estimated to be roughly equal to one half of a converter module and would be contain 12 independent static and dynamic equalization circuits with appropriate insulation.

Mechanical Design and Trades

When designing pulsed power systems it is critical that bus work impedance be low to maximize system performance and efficiency. This implies that the major system components- CPA, converters, and rail gun, be as closely coupled as possible. Closely coupled pulsed power systems generally have the added benefit of being lighter due to shorter bus runs. This approach ultimately leads to converter modules that are mounted at the alternator endplate and arrayed in a circle pattern around the brush box. This virtually eliminates the need for any AC bus work and the converter modules are conveniently located for connection to the field coil at the brush box.

The performance increase usually comes at the expense of access that can make assembly, maintenance, and repair of the converters or alternator more involved. In the best case, maintenance work can be cramped and difficult. In the worst case, simple maintenance of the CPA might require the disassembly and removal of converter modules. The non-thrust end of the pulsed alternator must accommodate several connections that impact the design of bus work and packaging of the converter. These connections, shown in figure VIII-9, include armature winding

terminations, field coil brush connections, stator and field coil coolant connections, bearing lube oil, brush purge gas, and diagnostics.

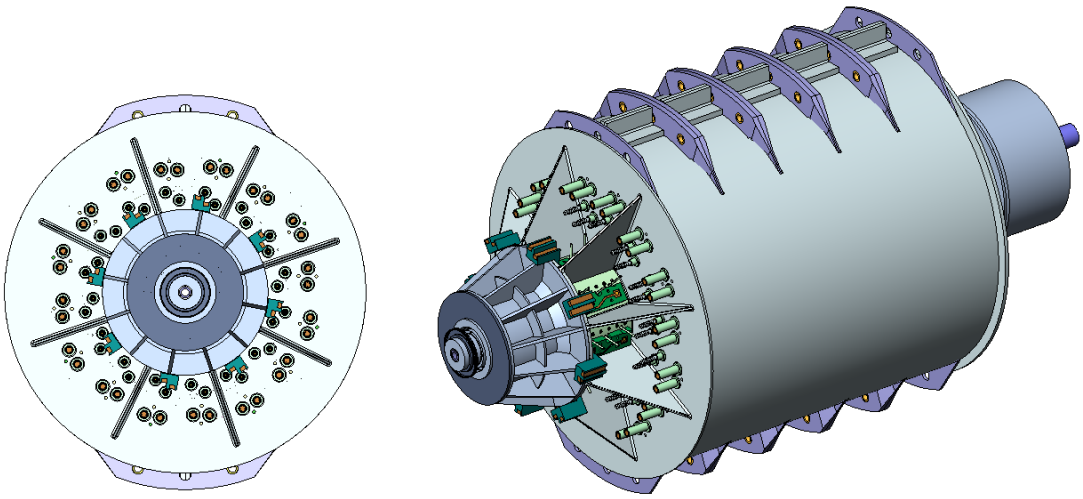

Figure VIII-9. Connection end of a pulsed alternator showing the connections through the endplates to the armature poles and through the brush box to the field coil and the coolant connections through the endplates

As discussed previously, the alternator's armature winding consists of a four-phase, four-pole winding. The armature windings therefore include a total of 16 terminated pairs (phase and neutral) for connection to the FCC and GSC. The baseline concept is for these armature terminations to protrude axially from insulated thru holes in the endplates. Other options for terminating the stator windings were considered including radial taps thru the stator outer diameter, just inboard of the endplates. However, space constraints within the tank make endplate axial penetrations the preferred approach.

There are eight pairs of conductors (field coil positive and neutral) that penetrate radially through the brush box and are distributed uniformly around its circumference. The FW leg is connected in parallel across the field coil, as is the field initiation module (FIM), which provides seed current to the field coil for a discharge. In addition to the electrical connections, the brush box requires occasional access for maintenance. Rotor dynamic considerations have led to a rotor design with bearings outboard of the brushes. As a result, access to the brushes for maintenance or repair must be radial, which can interfere with tightly packaged switch modules.

Masses were estimated for the GSC, FCC, and FW leg based on both the 150 mm advanced device and the 125 mm SiC device (summarized in table VIII-12). Converters based on an off-the-shelf device or a near-term device would lead to a converter with more devices (as shown in Table VIII-7), a larger footprint within the tank and, as a result, lead to less optimized bussing and greater overall converter mass. However, mass considerations were not a primary concern when developing packaging concepts. The reason for this is that the design team assumed, for a converter based on a given device, the same number of devices will be required regardless of how the devices themselves are arranged. The SCR mass represents a significant portion of the total converter mass as does the pole piece mass which is directly proportional to the number of SCRs. Further, the design team believes that the optimal number of devices within a single clamped module is approximately twelve devices.

Table VIII-12. Per CPA mass summary for converters based on 150 mm advanced SCR and 125 mm SiC SCR

		Qty	Mass (kg)	Total
150 mm advanced SCR	GSC/FCC	16	53.15	850.4
	FW Leg	1	51.80	51.8
		150 mm converter Total		902.2
125 mm advanced SCR	GSC/FCC	16	33.94	543.0
	FW Leg	1	31.31	31.3
		125 mm converter Total		574.3

CEM has experience building a module with twelve devices. If less devices are clamped within a module, more clamps are required overall in the converter leading to increased converter mass. If more SCRs are clamped within a single clamp, the assembly difficulty and risk is increased due to the increasing number of components and corresponding machining tolerance buildup. Even if these difficulties are overcome, a module with significantly more devices than twelve will eventually lead to a mechanically unstable module aspect ratio. A detailed bill of materials and mass estimate for converters based on a 150 mm advanced and 125 mm SiC SCR is shown in tables VIII-13 and VIII-14.

Table VIII-13. Module bill of materials and mass estimate for converter modules based on the 150 mm advanced device

Component description	Material	Mass (kg)	Qty	Ext
SCRs	150 mm	0.99	12	11.86
Gate circuit	various	1.00	12	11.97
Snubber	various	0.50	12	5.99
Plate, Clamp	titanium	2.77	2	5.53
Platen, Clamp	titanium	1.22	2	2.44
Platen Insulator, Clamp	G10	0.32	4	1.29
Guide Pin, Clamp	6061	0.08	1	0.08
Belleville	titanium	0.91	1	0.91
Guide, Belleville	6061	0.08	1	0.08
Clamp Hardware	various	0.68	2	1.36
Double Pole Piece, Conductor	6061	0.91	1	0.91
Single Pole Piece, Conductor	6061	0.73	6	4.35
Snubber Pole Piece, Conductor	6061	0.72	8	5.74
Insulator, Banding	G10	0.03	4	0.13
Banding	composite	0.26	2	0.52
Combined GSC/FCC Module Total				**53.15**

Component description	Material	Mass (kg)	Qty	Ext
SCRs	150 mm	0.99	12	11.86
Gate circuit	various	1.00	12	11.97
Snubber	various	0.50	12	5.99
Plate, Clamp	titanium	2.77	2	5.53
Platen, Clamp	titanium	1.22	2	2.44
Platen Insulator, Clamp	G10	0.32	2	0.64
Guide Pin, Clamp	6061	0.08	1	0.08
Belleville	titanium	0.91	1	0.91
Guide, Belleville	6061	0.08	1	0.08
Clamp Hardware	various	0.68	2	1.36
Double Pole Piece, Conductor	6061	0.91	5	4.54
Single Pole Piece, Conductor	6061	0.73	2	1.45
Snubber Pole Piece, Conductor	6061	0.72	6	4.31
Insulator, Banding	G10	0.03	4	0.13
Banding	Composite	0.26	2	0.52
FWL Module Total				**51.80**

Table VIII-14. Module bill of materials and mass estimate for converter modules based on the 125 mm SiC device

Component description	Material	Mass (kg)	Qty	Ext
SCRs	125 mm	0.51	9	4.61
Gate circuit	various	1.00	9	8.98
Snubber	various	0.50	9	4.49
Plate, Clamp	titanium	2.13	2	4.26
Platen, Clamp	titanium	0.91	2	1.81
Platen Insulator, Clamp	G10	0.32	3	0.97
Guide Pin, Clamp	6061	0.08	1	0.08
Belleville	titanium	0.68	1	0.68
Guide, Belleville	6061	0.08	1	0.08
Clamp Hardware	various	0.45	2	0.91
Double Pole Piece, Conductor	6061	0.77	1	0.77
Single Pole Piece, Conductor	6061	0.68	4	2.72
Snubber Pole Piece, Conductor	6061	0.49	6	2.94
Insulator, Banding	G10	0.03	4	0.13
Banding	Composite	0.26	2	0.52
Combined GSC/FCC 125 mm SiC SCR		**Module Total**		**33.94**

Component description	Material	Mass (kg)	Qty	Ext
SCRs	125 mm	0.51	8	4.10
Gate circuit	various	1.00	8	7.98
Snubber	various	0.50	8	3.99
Plate, Clamp	titanium	2.13	2	4.26
Platen, Clamp	titanium	0.91	2	1.81
Platen Insulator, Clamp	G10	0.32	2	0.64
Guide Pin, Clamp	6061	0.08	1	0.08
Belleville	titanium	0.68	1	0.68
Guide, Belleville	6061	0.08	1	0.08
Clamp Hardware	various	0.45	2	0.91
Double Pole Piece, Conductor	6061	0.77	1	0.77
Single Pole Piece, Conductor	6061	0.68	5	3.40
Snubber Pole Piece, Conductor	6061	0.49	4	1.96
Insulator, Banding	G10	0.03	4	0.13
Banding	Composite	0.26	2	0.52
FWL Module Total				**31.31**

The competing desires of the design team to closely couple the converter to the alternator while maintaining room for making connections and providing space for maintenance led the design team to develop two packaging concepts. The first concept, shown mechanically in figure VIII-10, shows the converter modules packaged in a radial pattern around the brush box that closely couples the converter to the CPA. The electrical arrangement is shown in figure VIII-11.

The centerpiece of this concept is a combined GSC/FCC module which uses a novel arrangement of SCRs to include both the GSC and FCC required for one pole phase of the alternator within a single clamp. The size of each of the sixteen modules positions them at a diameter larger than that of the pulsed alternator. This creates interference with neighboring modules when packaged next to the second CPA in the tank. To avoid interference, the modules for each alternator must be offset axially.

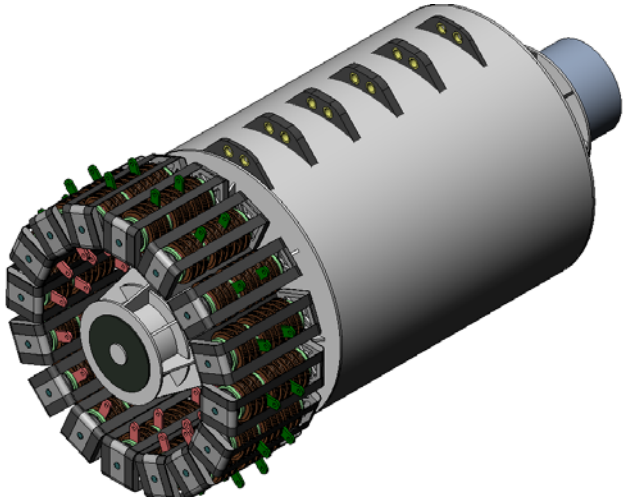

Figure VIII-10. Closely coupled converter packaging concept showing converter modules rigidly mounted to the CPA endplates and arrayed around the brush box

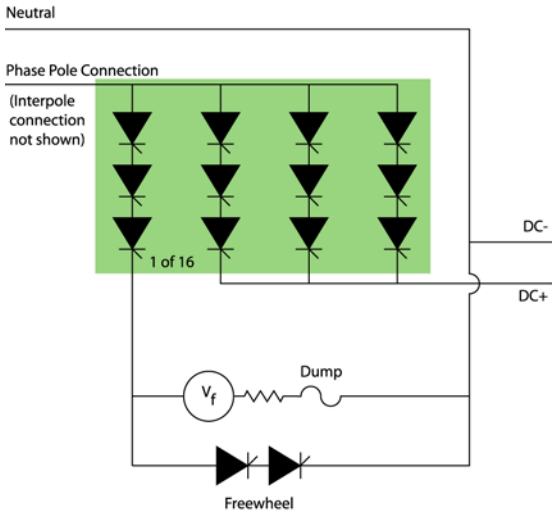

Figure VIII-11. Electrical arrangement for packaging concept #1

The combined GSC/FCC module, shown in figure VIII-12, used in the closely coupled packaging concept clamps both the FCC and GSC for one pole phase of the machine within a single clamp. The clamp plates and the platens used to distribute the clamp load uniformly across the diameter of the SCRs are titanium. The clamp plates are nominally 2.5 cm thick but have material removed where possible to decrease mass. Off-the-shelf 125 mm SCRs typically require a clamp load of 12,000 kg. The design team assumed the required preload for the 125 mm SiC device was identical. For mass estimates with the 150 mm advanced SCR the required preload was considered to be proportional to its cross-sectional area. The preload in this module design is provided by a loading bolt threaded into the top clamp plate which bears against the clamp platen. The clamp load is reacted by two composite bandings. Load variations within an SCR stack can lead to the mechanical failure of the silicon within the thin pack SCRs. A belleville washer, included between the lower clamp plate and clamp plate, accommodates thermal expansion within the converter module caused by resistive heating in the devices and pole pieces. The conceptual Belleville is titanium and would be calibrated so that its deflection indicates when the SCR stack is at the required load.

The two composite bandings used to react the clamp load are 3.8 cm wide by 2.5 mm thick. Composites provide a much lighter means of supporting the clamp load than through bolts. They should also distribute the load more uniformly across the clamp plates than thru bolts and eliminate the stress concentrations caused by thru holes. Composite bandings have the added benefit of reducing the footprint of the module because the bandings can be positioned much closer to the devices than a 2 cm bolt. The bandings will be insulated to prevent a tracking path for voltage breakdowns as will the clamp platens from neighboring SCR stacks.

The uppermost SCR stack in the combined GSC/FCC module is the FCC required for one pole phase of an alternator with 125 mm SiC device. It is connected on the one side to the field DC positive conductor (shown in red) and on the other side to the AC armature phase conductor (shown in green). The phase conductor also brings current into the first of two parallel legs required for the GSC. Each parallel path in the GSC converter is connected on its DC side thru two conductors (shown in blue) to the positive gun bus.

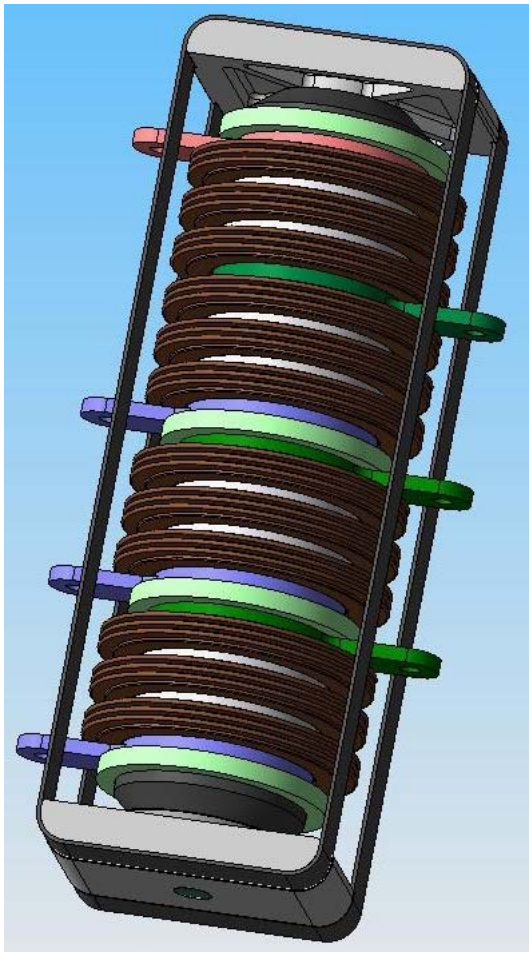

Figure VIII-12. Combined GSC and FCC module for converter packaging concept #1

All the series stacks in the combined GSC/FCC module require three devices for voltage hold--off as enumerated in the converter electrical design section above. Each SCR requires an actively--cooled aluminum pole piece on either side. As previously mentioned, preliminary thermal analysis shows that the pole pieces are adequate for the five shot burst requirement. A transient analysis will eventually be required to verify that the heat absorbed by the actively cooled pole pieces can be removed quickly enough between shots to keep the SCR junction temperatures below their limit.

The most convenient bussing arrangement for this packaging concept is for the FCC and GSC of the two alternators to be connected in common on the DC side of the converters. That is,

the GSC modules for each machine would be connected in common via flexible hexapolar cable on the DC side of the rail gun. The flexible cable must be designed to withstand the repulsion load of between the alternating polarity conductor strands. This cable is a development item since previous versions of this hexapolar cable cannot withstand the current required for this application. The FCC for each alternator would be connected on the DC negative side of the field coils, which operate in parallel. A thorough synchronization analysis for operation of the two alternators in this circuit is required before the bussing details can be finalized, but is beyond the scope of this project. There are potential fault modes that make this bussing scheme less desirable than connecting the two alternators on the AC side of the converters. This does not necessarily eliminate either of the packaging concepts, but would necessitate the use of jumpers between identical pole phases of the two alternators in the closely coupled packaging concept.

The second packaging concept (mechanical arrangement shown in figure VIII-13, electrical arrangement in figure VIII-14), separates the FCC (red) and the GSC (blue) into discreet modules. The FW leg module and four FCC modules, shown in figure VIII-15, for each CPA remain closely coupled to the pulsed alternators, but in this concept the GSC for each CPA has been packaged separately and moved directly below the turret. This substantially lengthens the AC portion of the bus that connects to the GSC but leads to greatly improved maintenance access and similar significant length reductions in the DC bus to the rail gun. The AC connections to the GSC would likely be made via flexible hexapolar cable. At this time the design team envisions GSC converter modules that combine the parallel paths required for identical pole phases of both CPAs. That is, the top half of the GSC module, shown in figure VIII-16, would represent the GSC for one pole phase of CPA number one, while the bottom half of the module would represent the GSC for the same pole phase of CPA number two.

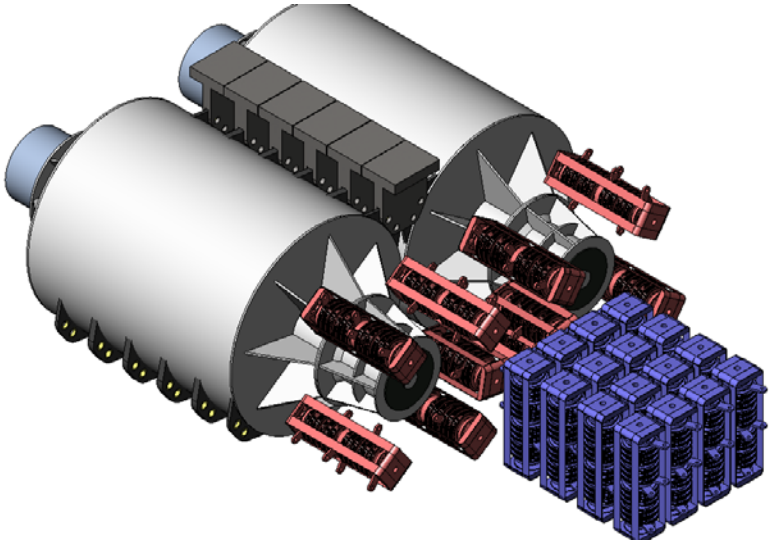

Figure VIII-13. Converter packaging concept #2 with separate GSC and FCC converter modules

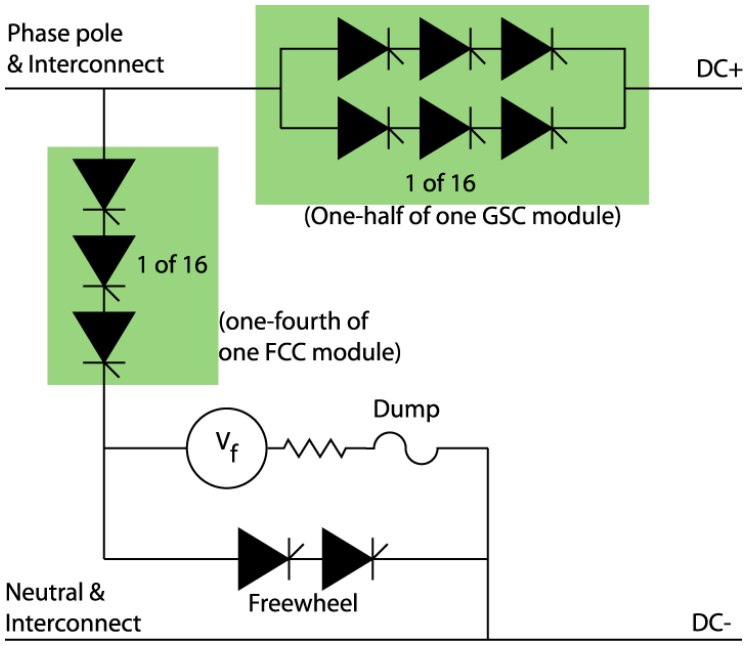

Figure VIII-14. Electrical arrangement for packaging concept #2

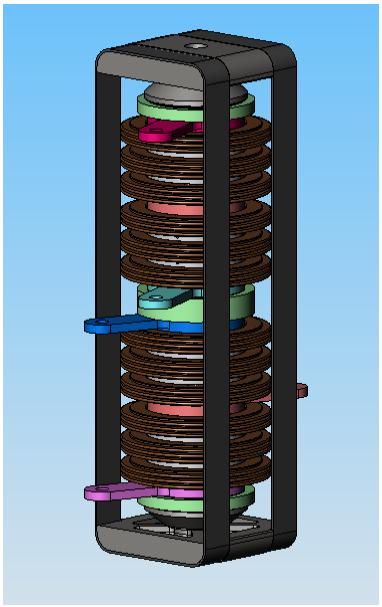

Figure VIII-15. FCC module for converter packaging concept #2

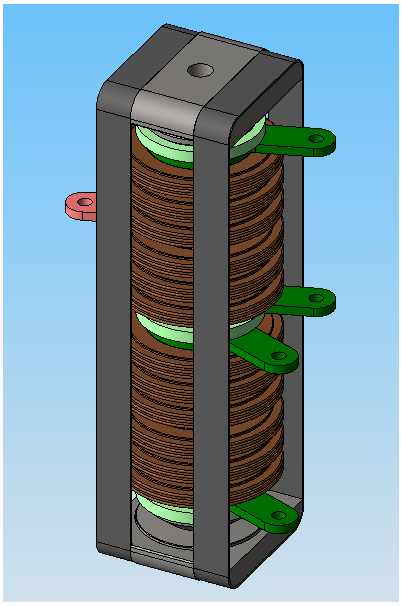

Figure VIII-16. GSC module for converter packaging concept #2

The FCC module for packaging concept #2, shown in figure VIII-15, includes the single series stack required for each of four pole phases of the FCC. That is, the top three devices correspond to pole 1, phase1 of the FCC. The second three devices correspond to pole 1 phase 2 of the FCC, and so on. As such, four like modules are required per CPA. The module's clamp

plate and preload mechanism are identical to the combined GSC/FCC module for packaging concept #1, as is the banding except in length. The stacks each require three series SCRs and are connected to the field DC bus via two conductors (shown at the rear of the module in red). By alternating the orientation of the center two series stacks, the each half of the module can connected to the DC bus by a single conductor which reduces the number of conductors and insulators within the module. A 2.5 cm thick G-10 insulator separates the top and bottom half of the modules. Each of the four series stacks are connected to their corresponding pole phase by one of four identical conductors (shown multi-colored at the front of the module). This conductor configuration leads to a convenient bussing arrangement with the pole phase conductors arrayed outward for connection to the armature terminations in the endplates and the field DC conductors arrayed inward for connection to the field coil at the brush box.

As mentioned above, the top half of the GSC modules for this packaging concept, shown in figure VIII-16, contains the two parallel legs required for the GSC with the 125 mm SiC device. These legs are connected on the DC side to the gun bus thru two conductors (shown in green) and to the armature pole phase thru a single conductor (shown in red). The two parallel paths conduct in opposite directions so an extra conductor and insulator is not needed between the top two stacks. Each parallel path requires three SCRs to withstand the predicted GSC voltages. The bottom half of the module, contains the identical GSC pole phase for the second pulsed alternator. The top and bottom halves are shown insulated from one another, but this may not be necessary once the aforementioned synchronization analysis is completed.

The FW leg requires four parallel paths of two series devices for conduction during the gun discharge. It should be noted that the freewheel leg for both packaging concepts utilizes a single identical module for each CPA, shown in Figure VIII-17 for the 125 mm SiC SCR. Once again the clamp plates and preload mechanism are identical to the other modules and the composite bandings are the same except in length. Connections are made thru the three conductors (shown in red) to the field DC positive bus and two conductors (shown in yellow) to the field DC negative bus.

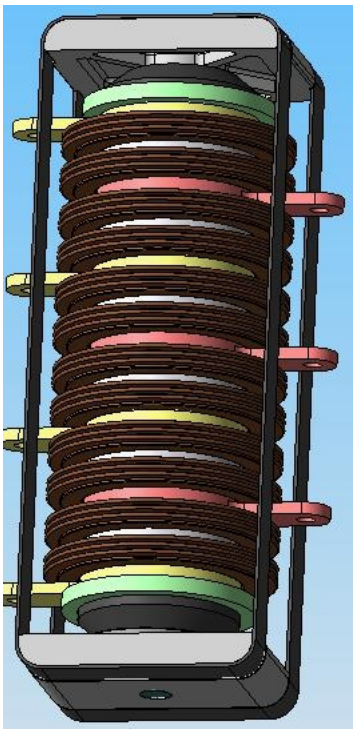

Figure VIII-17. FW leg module for both converter packaging concepts

Thermal Analysis and Design

The most stressing heat loads in the power converters are due to the burst shot performance requirement. Between shots in a burst, little or no heat can be removed from the system and the heat must be absorbed in the thermal inertia of the system without undue temperature rise.

The thermal analysis of the converter was done based on the steady-state temperature rise of the primary heat transfer devices within the converters and was performed on a per-device, worst case pole, worst case shot basis. That is, the losses from the highest current device in the highest current shot were imposed as the heat load on each device.

The detailed analysis is shown in Appendix E and is summarized here. The per-shot power loss in each device was calculated based on the on-state voltage for an SPT411. This estimate is considered valid for each of the two baseline devices. The 6 in. advanced thyristor is estimated to be able to withstand the same surge action as the 411. This implies that the on-state voltage characteristics for the two devices are the same. The actual on-state characteristic of the projected SiC device was assumed, in the absence of better information, to be the same or less

than the 411. In any event, the SiC device will be thinner than the silicon device for the same voltage hold-off (and therefore likely have a lower IR drop) and the permissible operating temperature will be significantly higher, so this assumption is acceptable.

The on-state voltage drop of the SPT411 was taken from data sheet curves

$$v(i)= 168x10^{-6}i(t)-0.7 \text{ V} \quad \text{(VIII-3)}$$

The energy loss was computed from the current in a device

$$E_{loss} = \int_0^{ton} i_{dev} v(i) dt \quad \text{(VIII-4)}$$

and the steady-state temperature rise in the device-heat sink (pole piece) system was assumed to be adiabatic

$$\Delta T_{shot} = \frac{E_{loss}}{mc_p} \quad \text{(VIII-5)}$$

where m and c_p are the mass and the specific heat of the heat sink.

The worst-case per-shot temperature rises of the GSC, FCC and FWL devices is 2.6 C, 1.6 C, and 3.9 C, respectively. Therefore, the worst case burst temperature rise is about 20 C.

Results of Trade Studies and Technology Development Requirements

Trades

The electrical design trades are summarized in table VIII-15. The trades resulted in a determination of the number of devices required and the series-parallel configurations needed for the four device types. This information was used as the basis for the mechanical and thermal analyses and trades. However, an initial configuration determination was made based on the numbers of devices required. To the first order, converter mass and volume are proportional to the device count. Therefore, the 411 and 5 in. high-voltage devices were eliminated from further consideration prior to performing the next-level trades.

The packaging trades boiled down to two primary concepts, one where all of the devices are located close to the alternators and the GSC and FCC modules are co-located, and one where the GSC and FCC modules are packaged separately. While the closely coupled packaging concept is

very attractive from a performance and efficiency perspective, the design team felt that the discreet converter packages in the second concept are more realistic considering the variety of connections and access required for operation of the pulsed power system. In addition, the second packaging concept makes connection on the AC side for synchronous operation of the two pulsed alternators much easier to accommodate. It should be emphasized that both packaging schemes fit within the volume of the tanks and the preliminary design of such a converter package could be used to more closely analyze and select a leading candidate.

Table VIII-15. Summary of electrical design trades

	Worst-case phase - GSC					Worst-case phase - FCC					Worst-case phase - FWL				
Shot	I^2t	di/dt_{or}	I_{pk}	$V_{fwd/rev}$	t_q	I^2t	di/dt_{or}	I_{pk}	$V_{fwd/rev}$	t_q	I^2t	di/dt_{or}	I_{pk}	$V_{fwd/rev}$	t_q
		A/s	A	V	s	A^2-s	A/s	A	V	s	A^2-s	A/s	A	V	s
1	5E+9	6E+9	3E+6	)E+3	)9E-6	IE+6	4E+9	)0E+3	'E+3	)8E-6		7E+9	)4E+3	E+3	)8E-6
2	6E+9	5E+9	3E+6	)E+3	)4E-6	)E+6	7E+9		'E+3	)2E-6	)8.E+6	9E+9	)1E+3	E+3	)4E-6
	5E+9	0E+9	3E+6	)E+3	)6E-6	'E+6	6E+9		)E+3	)1E-6	)5.E+6	IE+3	'1E+3	E+3	)3E-6
4	4E+9	9E+9	4E+6	IE+3	)7E-6	)E+6	6E+9	)5E+3	)E+3	I1E-6	)3.E+6	IE+3	)1E+3	E+3	)6E-6
5	9E+9	5E+9	4E+6	IE+3	)4E-6	I9E+6		'4E+3	'E+3	)5E-6	)9.E+6	)E+3	I6E+3	E+3	)2E-6
worst	E+9	E+9	E+6	)E+3	)9E-6	I9E+6	E+9	'4E+3	'E+3		)9E+6	E+9	I6E+3	E+3	)8E-6

	Per-pole configuration - GSC				Per-pole configuration - FCC				Configuration - FWL			
		5in HV	6in adv	5in SiC	411B	5in HV	6in adv	5in SiC	411B	5in HV	6in adv	5in SiC
Shot 1												
Parallel	3	3	3	2	1	1	1	1	5	6	5	3
Series	7	4	3	3	7	4	3	3	4	2	2	2
Shot 2												
Parallel	3		3	2	1	1	1	1		7	5	3
Series	7	4	3	3	7	4	3	3	4	2	2	2
Shot 3												
Parallel	3	3	3	2	1		1	1	5	6	5	3
Series	6	3	3	3	7	4	3	3	3	2	2	2
Shot 4												
Parallel	3	3	3	2	1	1	1	1	5	7	5	3
Series	6	4	3	3	7	4	3	3	4	2	2	
Shot 5												
Parallel	3	4	3	2	1		1	1	6	8	6	4
Series	6	4	3	3	7	4		3	4	2	2	2
Worst case (this row accounts for the combined worst cases of all the shots)												
Parallel	3	4	3	2	1	1	1	1	6	8	6	4
Series	7	4	3	3	7	4	3	3	4	2	2	
Total (per phase)	84	64	36	24	28	16	12	12	na	na	na	na
Total (per alt)	336	256	144	96	112	64	48	48	24	16	12	8

Technology Development

Silicon Devices

The most critical technology development activities for the power converters relate to the discrete switching devices. The near-term baseline device is the 150 mm, 11 kV thyristor. While 150 mm and 11 kV or greater thyristors have been demonstrated (and can be purchased off-the-shelf), these two characteristics have not been demonstrated in the same device. In addition, this device must be demonstrated with the a charge-sweeping time, t_q, of 100 μs or less and losses as low or lower than existing 5 kV devices. Development of a device with this combination of characteristics will be key to achieving the mass and volume estimates outlined in this report. The technical complexities and risks inherent in this development argue that an interim device development be undertaken to show short-term progress toward the 150 mm goal and this interim goal is perhaps best represented by the 125 mm high-voltage device.

Silicon Power corporation has proposed a device concept that would meet the MEFFV goals. The device is an extension of the SPT411 LSS package, but modified for higher voltage and reduced losses. This would be accomplished by using an asymmetric thyristor as the turn-on device and a diode wafer would replace the inactive silicon used in the 411. The concept is illustrated in figure VIII-18.

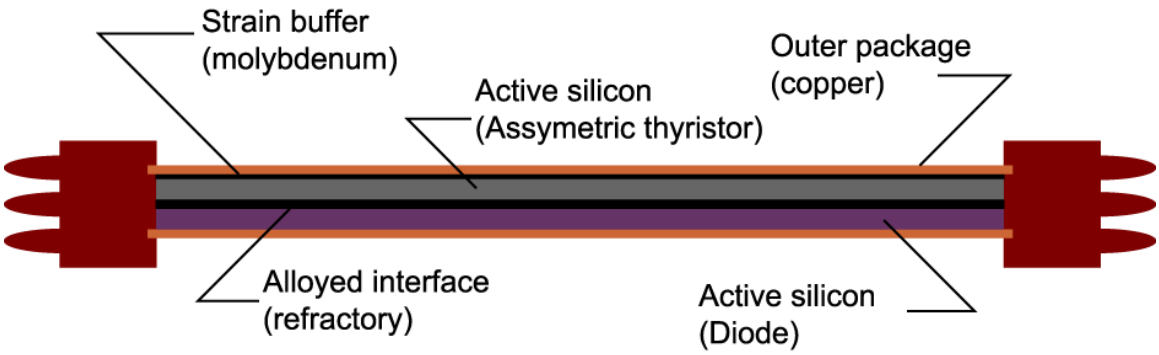

Figure VIII-18. All-active silicon LSS device

Diodes have inherently shorter t_q times than thyristors., However, it is unlikely that the use of a two-layer device in the turn-off role will, by itself, achieve a tq under 100 us. t_q can be reduced

by using a device that can be counter pulsed. The concept, termed "gate-assisted turn-off" was also developed by SPCO. This concept is illustrated in figures VIII-19 and VIII-20. Charge sweeping is accelerated by introducing a reverse current through the junction at turn-off. In addition to being able to significantly reduce t_q, the method can also be accomplished with a minimum of additional circuitry, packaging, or trigger energy.

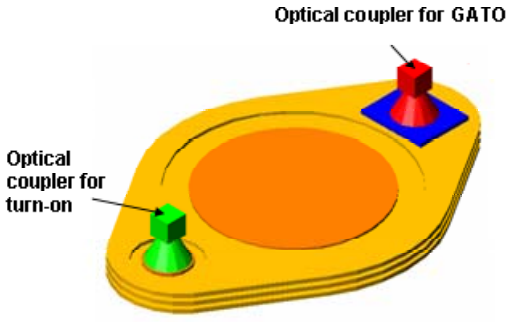

Figure VIII-19. GATO device outline (courtesy of Silicon Power Corporation)

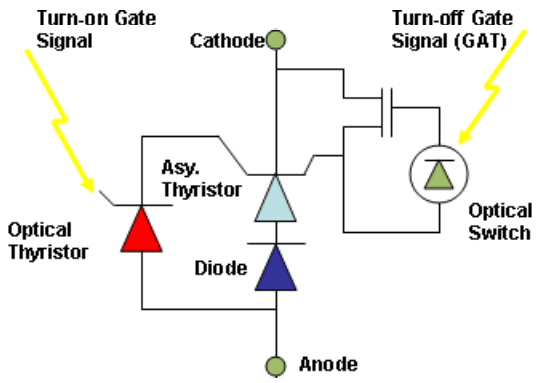

Figure VIII-20. Operation of a GATO device (Courtesy of Silicon Power Corporation)

Silicon Carbide Devices

Silicon carbide switch devices hold enormous potential for use in electric guns. Because the devices can withstand higher temperature operation (300° C) and have greater thermal

conductivity, they will have a much higher action capability and be more readily cooled. As a result, fewer parallel devices will be required.

In addition, SiC has a much higher voltage standoff cabability than silicon. Therefore, higher voltage wafers can be manufactured with smaller thickness. Reduced thickness translates into lower losses, and fewer devices in series. The higher carrier velocity of SiC will mean devices that can turn off more quickly and have a reduced protection requirement.

SiC devices demonstrated include diodes, thyristors and MOSFETs. However, SiC crystal manufacturing difficulties have limited the size and types of devices that have been made so far to about 6 mm by 6 mm. The highest voltage wafer is about 12 kV.

The scaling and performance characteristic forecast for the SiC device takes these limitations into account. Even though the device forecast is realizable with current SiC wafer manufacturing technology, a number of development items remain, including

- Development of device edge treatment and passivation
- High-temperature device package, connections, clamp
- Bonding techniques or determination of clamping requirements
- Demonstration of near simultaneous triggering and turn off within a single package
- In-package gate structure, connections and wiring

Module Developments

The modules and bussing required for the converters in this conceptual design require several development items beyond development of the SCRs themselves. The first would be a reliable and small trigger assembly for repetitive operation of the modules. This effort could include exploration of novel triggering concepts (such as snubber triggering) for further reduction of gate circuit mass and volume. Another development item that would help reduce the overall converter footprint is reduced-size high-voltage capacitors for the equalization circuits. The snubber circuits for a module of twelve devices can often be equal to or greater than half the size of the SCR module itself.

The composite bandings for the modules are not highly stressed nor expected to be difficult to design or build. However, they will require development to prove they can be reliably wound and cured. Prototypes and coupons must also be tested to ensure the winding process yields the expected results. The banding preload mechanism must also be developed. While the preload bolt concept is not revolutionary, the tooling and assembly process must be developed so the correct torque can be achieved and the module assembled reliably without transmitting torque to the SCRs themselves which would lead to mechanical failures.

Actively cooled pole pieces will also require development to determine the preferred method of fabrication. Two concepts include milling of passages and diffusion bonding of two mating parts or drilling a series of blind holes and using mechanical lee plugs to create a labyrinth. Either concept must prove reliable to build and capable of cooling the SCRs adequately.

No multi-shot, cooled module has ever been built and tested for a rail gun power converter. Many of the development items above could be resolved relatively inexpensively by building and operating a proof-of-principle cooled, multishot converter module and associated controls and protection

Finally, the bussing of the converters will likely require the development of a flexible cable for connection of the converters to the CPA or rail gun that can handle in excess of 300 kA. Previous experience with a flexible hexapolar cable at CEM has been limited to lower current levels. As a result, a new concept must be designed, built, and tested to determine if it can handle the electrical, mechanical, and thermal loads generated by the pulsed power system. The design must include the main body of the cable, the termination designs on either end of the cables, and the transition region between the terminations and main body.

IX: Vehicle Development and Solid Modeling

Development of the vehicle began with a meeting at the CEM with members of the SAIC FCS development team on October 29, 2003. During this meeting critical aspects of the FCS vehicle was shown to the CEM MEFFV design team and this was extremely useful in getting the effort launched, as well as identifying the critical components needed to develop the solid model. Naturally, in the remaining two months of the program a fully developed detail model of the vehicle was not possible. However, the MEFFV design team felt it was extremely important to develop a valid concept that demonstrated that the EMG technology could in fact be incorporated into a 35 Ton class tracked vehicle chassis.

As previously mentioned, one goal of the vehicle development initial meeting was to identify the major components that were to be specifically identified for vehicle integration. These are list in table IX-1.

Table IX-1. Vehicle solid model minimum components list

COMPONENT	COMMENTS
Vehicular Major Systems	
Prime Mover : LV-50-2	2 turbines, each with 500 kW alternator
Rectifiers	Rectifiers for the alternators
EM Armor	EM armor and power supplies, outlines only
Tracks and Suspension	
Track motors	1 per side, outline only
Motor drives	For 2 track motors and 2 pulsed alternators
Crew compartment	Bare, firewall separating turret, hatches and sights over crew
NBC System	Outline only
ECS	Outline only
Heat exchangers	For all required systems
Turret	Retractable M240 robotic machine gun, main gun magazine store, rough concept autoloader, main gun cooling pack, pop-up gun sight, APS (no specific details)
EMG Major Systems	
Pulsed alternators	2, based on solid model design code
FSC	Field charging switches
GSC	Main gun switches
Main Bus	Concept, clamp ring allowing turret to rotate
FIM	Field seed current assumed tapped from APS or EM armor power supplies
Railgun breech/recoil mounts	Concept design based upon existing models
Auxiliaries	Specific pulsed alternator lube, vacuum, etc

The decision to use 2 turbines was driven by a combination of mobility and recharge time of the pulsed alternators for firing the main gun. In addition the use of 2 prime movers added redundancy to the vehicle. For normal mobility situations, only one prime mover would be used. Whenever the vehicle was in a hot zone, both prime movers would be operating and the main gun alternators ready to fire.

The vehicle was developed using SolidWorks tm. All of the components outside of the EM gun hardware came via direct support of SAIC. The target weight for the vehicle was 35 tons. It was quickly realized that this would require the use of titanium armor in both the main chassis and turret. Additional armor was to be gained through the use of field integrated EM armor appliqués. These too were modeled in the final vehicle concept. The final concept, including a full application of EM armor came in at 42 tons. Without the EM tiles, the tank weighs in at 39 tons. Table IX-2 presents a comprehensive list of components, volumes, and masses represented in the vehicle solid model.

Figures IX-1 to IX-11 presents a series of solid models of the vehicle. The first presents plane views of the vehicle and outline its dimensions and hull/turret armor thicknesses used. The remaining views are solid models and are sequenced so that the reader can see subcomponent additions as the vehicle solid model is fully developed.

Table IX-2: Solid model contents and weight estimates

Description	Mass (kg)	Mass (lbs)
EMEFFV Vehicle w/ EM tiles	38,120	84,040
EMEFFV Vehicle w/o EM tiles	35,170	77,375
- Hull	27150	59,860
- Body	16,170	35,650
- Track Assemblies	2,770	6,110
- Pulsed Alternators	3,290	7,250
- PPS Auxiliaries	600	1,320
- Vacuum Pumps	136	300
- Oil Pallet Assembly	135	298
- PPS Mounts	329	725
- Switching	905	2000
- Gun Switch Converter	360	794
- Field Coil Converters	182	401
- Snubbers	327	721
- Free Wheel Leg	36	79
- Vehicle Auxiliaries	392	864
- Heat Exchangers	72	159
- Fans	120	265
- Battery Modules	200	441
- Turbines	569	1,250
- Track Motors	480	1,060
- Motor Converter/Inverter	50	110
- EM Armor	1922	4,240
- Main Bus	21	46
- Capacitor Bank	221	487
- Tiles	1680	3,700
- Turret	10,970	24,180
- Body	6,190	13,650
- EM Gun Assembly	3,150	6,940
- EM Gun	2,030	4,480
- Mount	854	1,880
- Loader Assembly	266	586
- Turret Auxiliaries	158	348
- Heat Exchanger	38	84
- Fans	120	265
- OSCW Gun Assembly	33	73
- EM Armor	1,440	3,170
- Turret Bus	16	35
- Capacitor Bank	150	331
- Tiles	1270	2,800

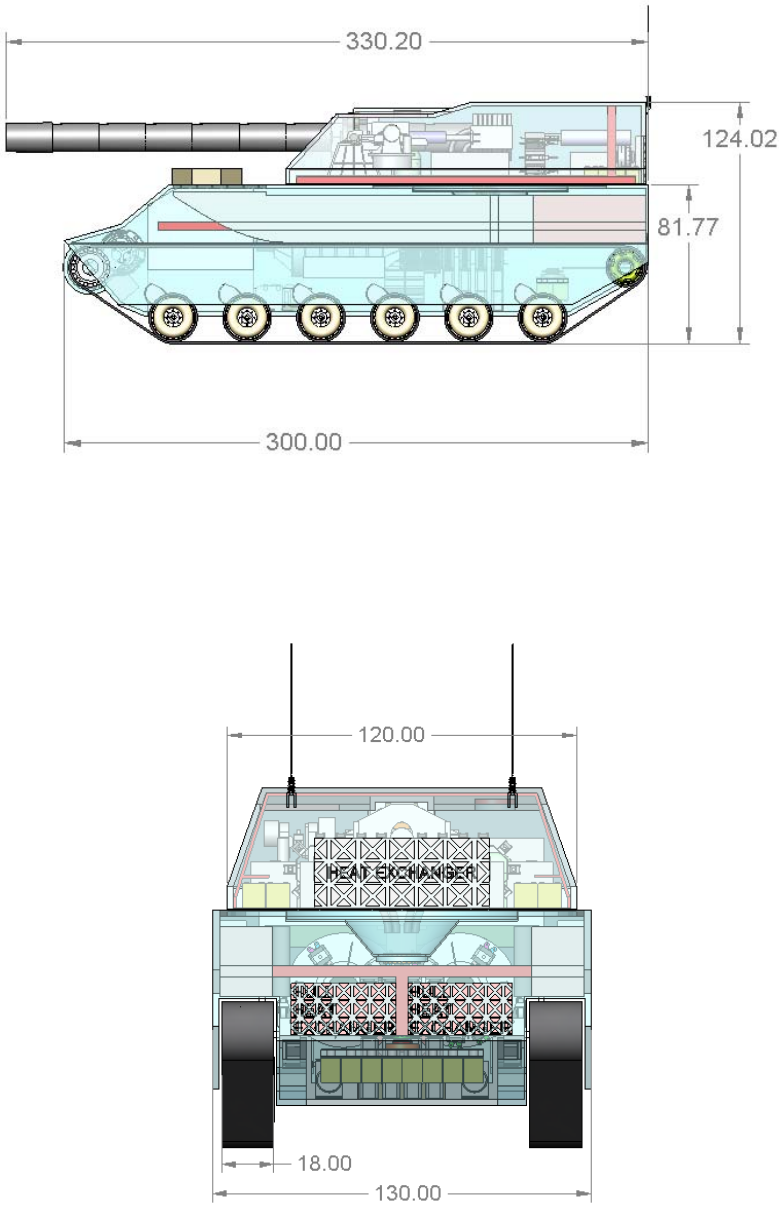

Figure IX-1. Vehicle views, showing overall dimension (in.)

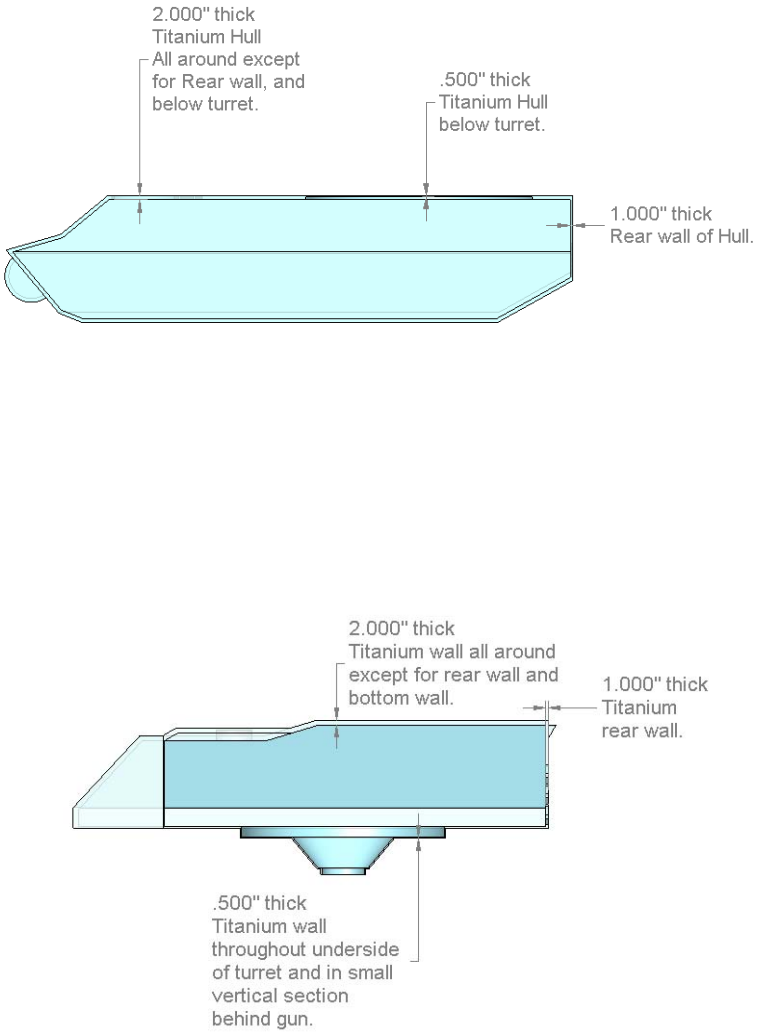

Figure IX-2. Hull and turret side views showing titanium armor thickness used

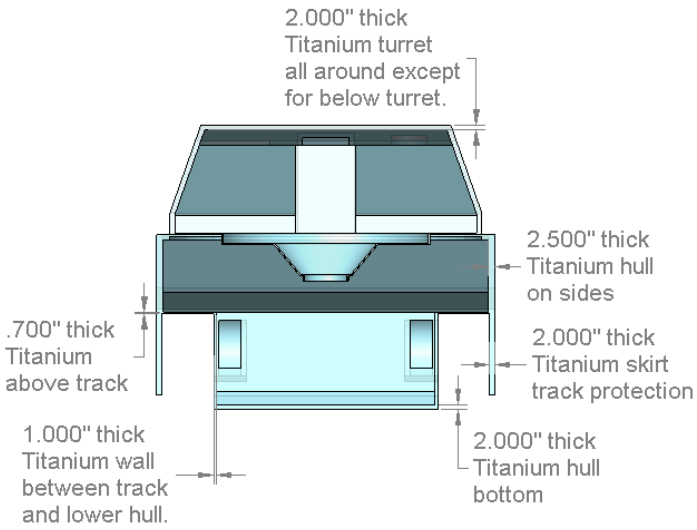

Figure IX-3. Vehicle hull and turret end view showing titanium armor thickness

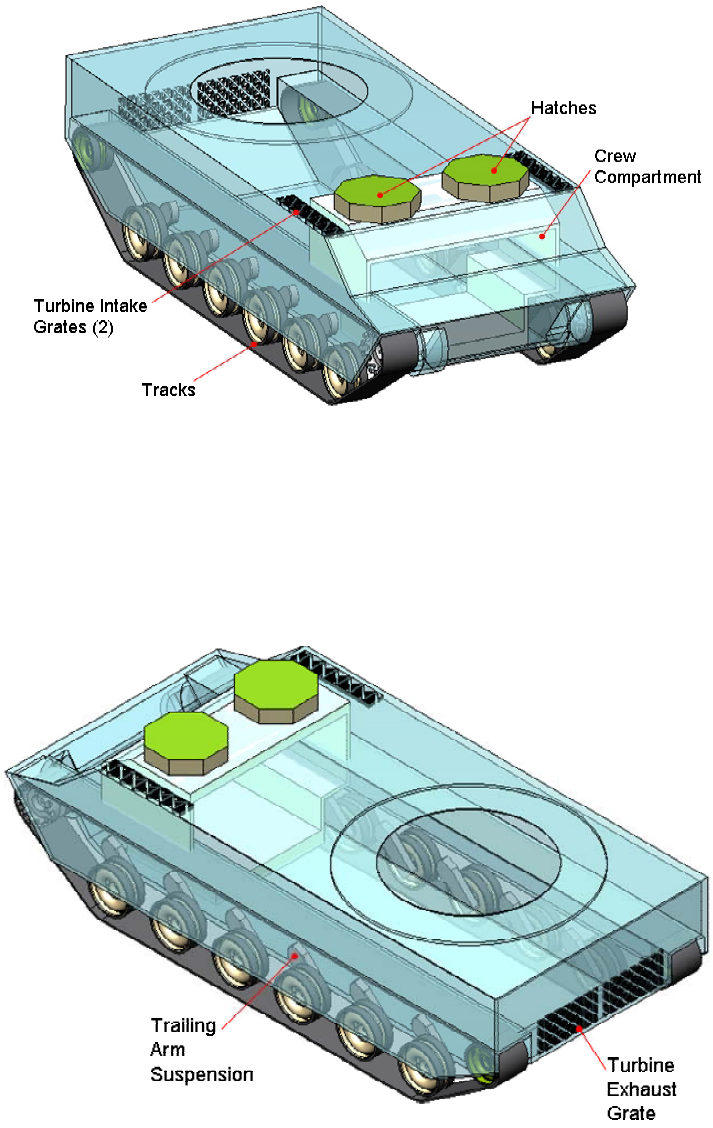

Figure IX-4. Vehicle model set 1

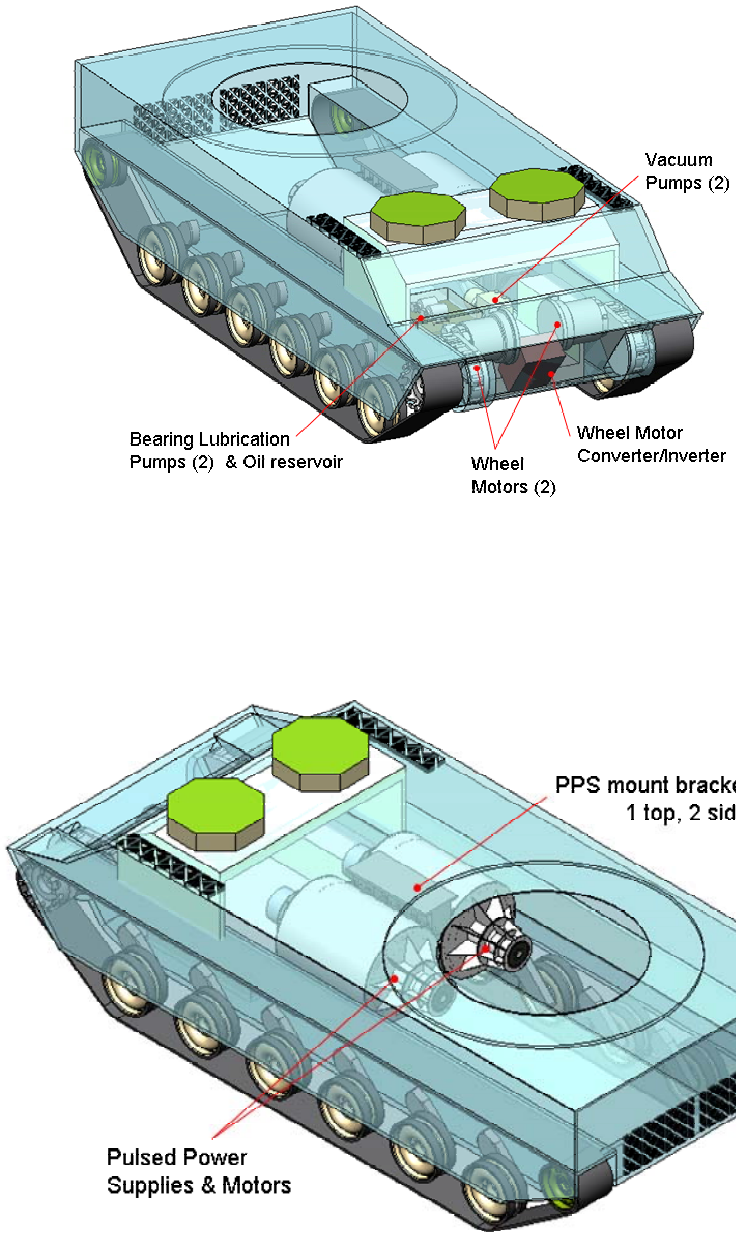

Figure IX-5. Vehicle model set 2

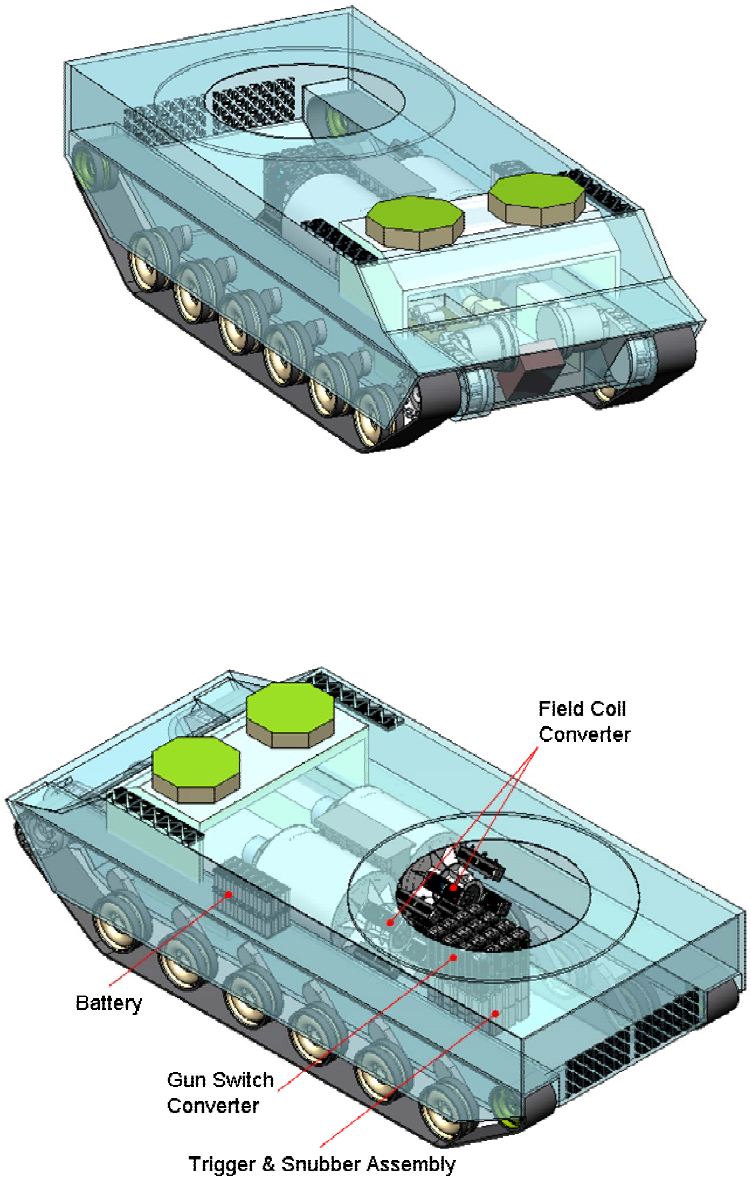

Figure IX-6. Vehicle model set 3

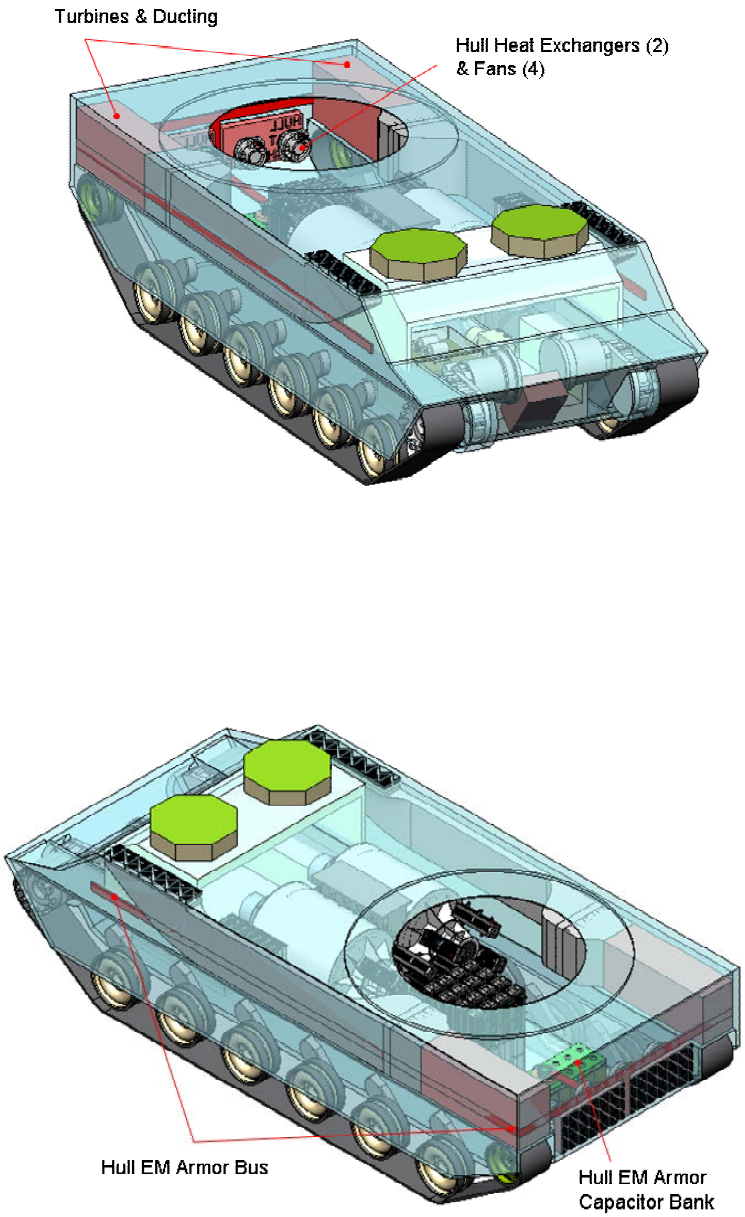

Figure IX-7. Vehicle model set 4

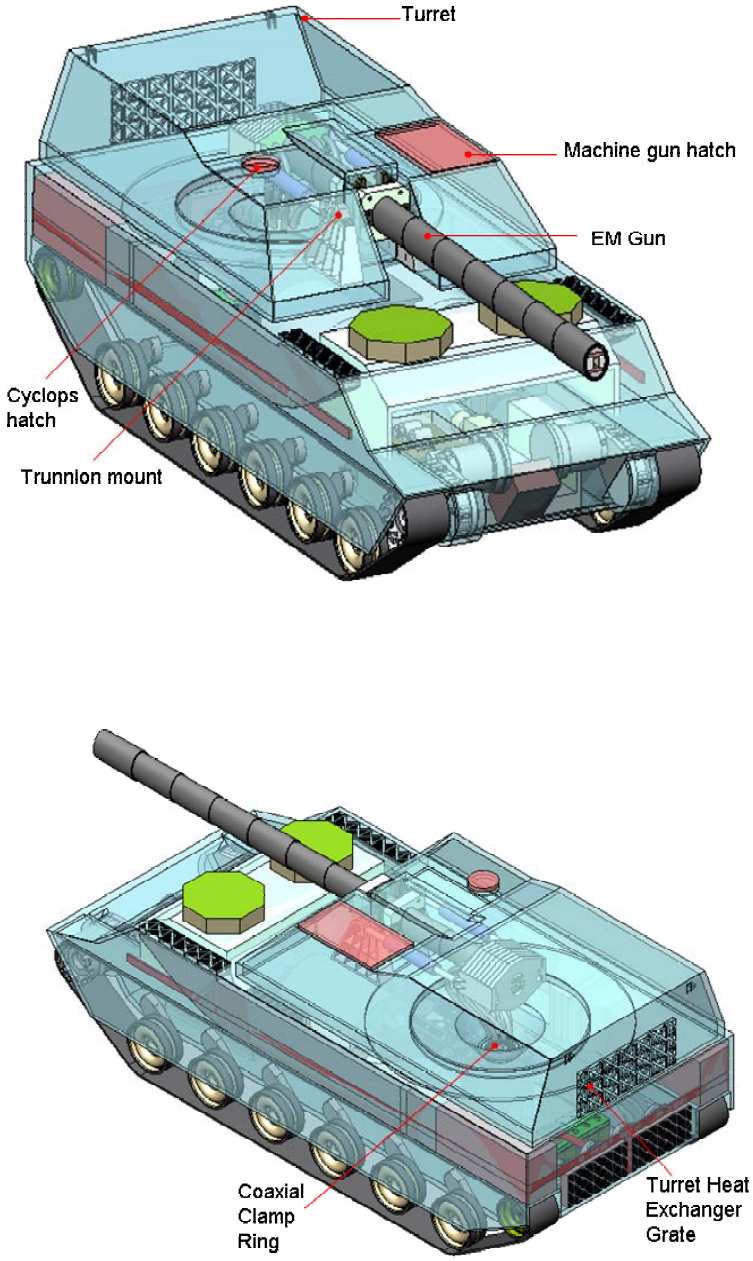

Figure IX-8. Vehicle model set 5

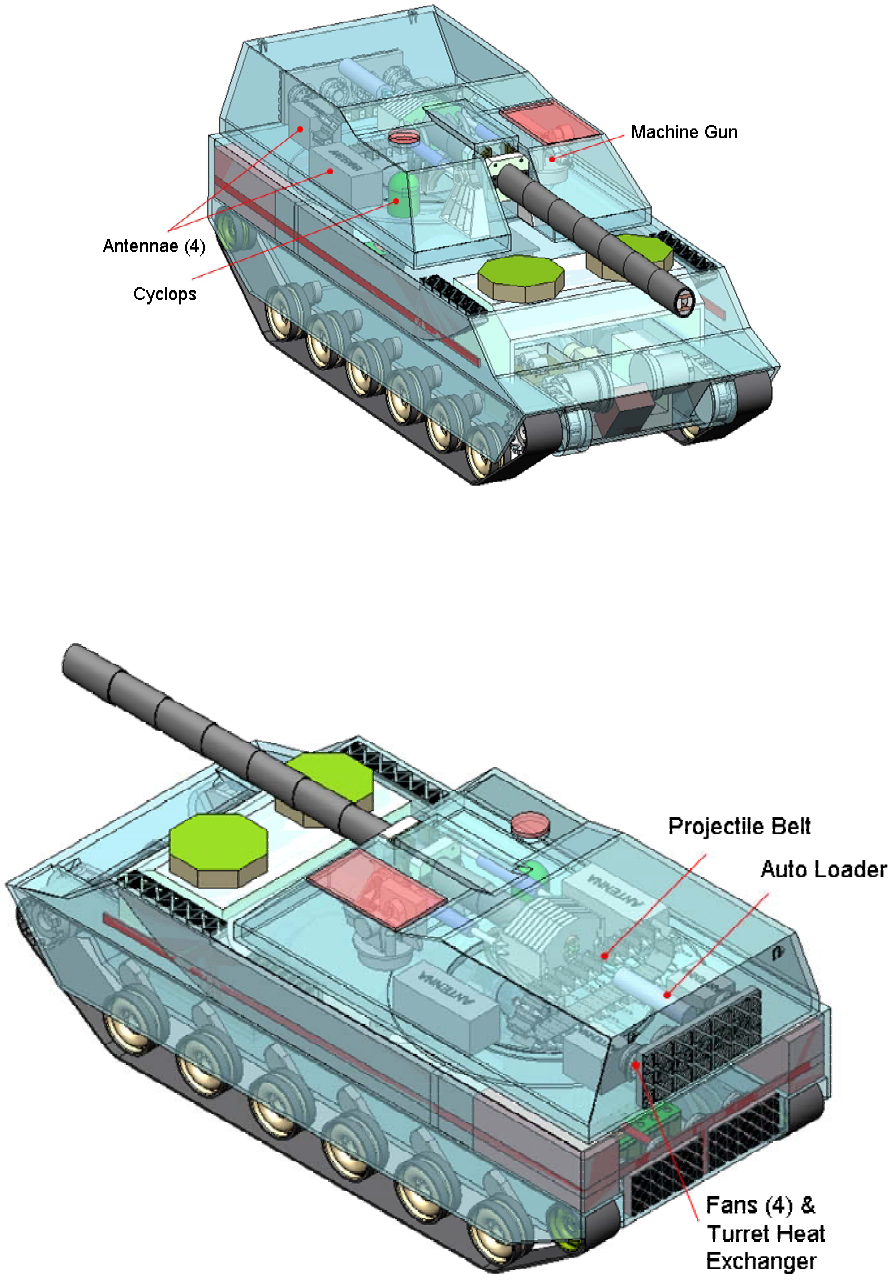

Figure IX-9. Vehicle model set 6

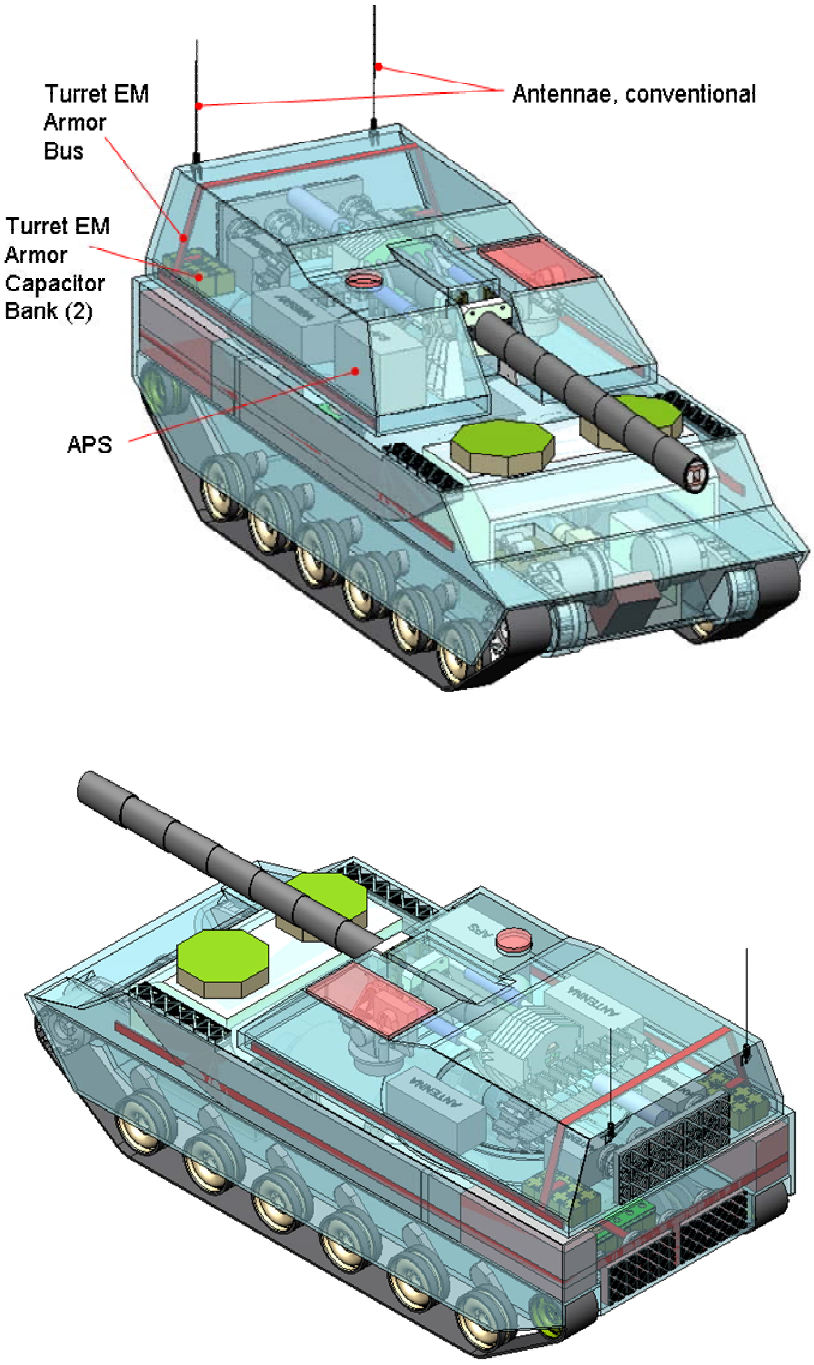

Figure IX-10. Vehicle model set 7

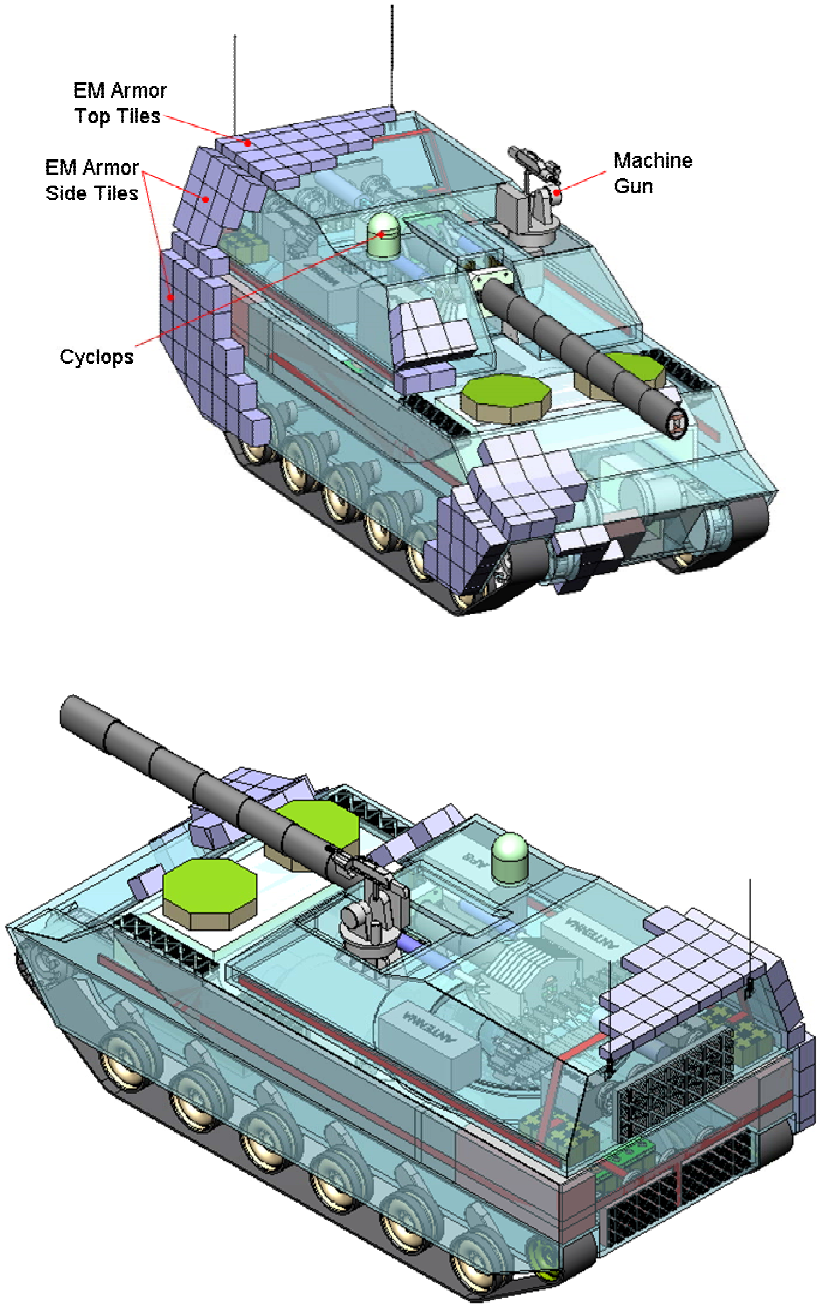

Figure IX-11. Vehicle model set 8

X. Conclusions and Recommendations

This study has produced the first truly viable railgun power supply to be integrated into a tactical weapons platform. There are no other concepts on the board that contain the level of design engineering as the present Marine Corp. EMEFFV concept. The PA designed in this study is an advanced prototype that is two generations ahead of what the CEM has demonstrated. The design is based heavily on lessons learned with self-excited air-core pulsed alternators and as such the CEM believes it can be prototyped. There are no fundamental physical limits to accomplishing this goal.

However, this is a very high performance rotating machine possessing many totally unique features. Therefore, as discussed above, there are many areas which the CEM would advise further development in before integrating with a full scale prototype. The U.S. Army is continuing development of some (but not all) of these areas presently under the 6.2 EGP research program. More funding in this area would further reduce risk and enhance probability of early success for the technology.

Finally, there is still room for technology growth. The composite material developments assumed in the design can be realized in the near term. There may be further gains to be had in the area of composite strength limits as that materials research area is being continued. An increase in composite matrix strain levels can reduce the size of the generator and this effect can be readily implemented within the design tool APADS.

Appendix A: Conceptual Design Of An Electromagnetic Armor System For The MEFFV

Electromagnetic (EM) armor provides protection against high velocity penetrating threats, specifically RPG and HEAT threats. It works in conjunction with conventional ballistic armor to provide an overall lightweight solution to vehicle protection against a range of conventional and asymmetric threats. At SAIC, work is presently under way to develop the component technology and engineer EM armor systems for legacy systems and the U.S. Army's Future Combat System. The conceptual design presented here for the USMC MEFFV is based on twenty year's effort by SAIC and the U.S. Army to bring EM armor systems to the battlefield.

The principles of EM armor are well known and demonstrated. Figure A-1 illustrates the basic principles.

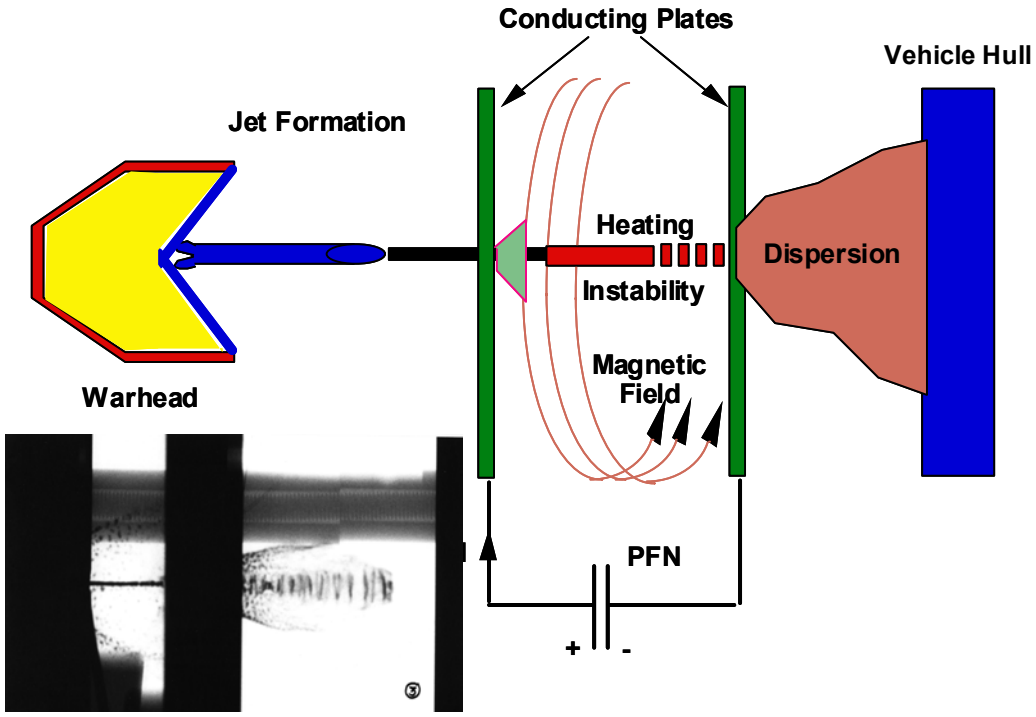

Figure A-1. Principle of operation of EM armor.

The armor system consists of an electrical pulse-forming network (PFN) capable of providing a high voltage, high current discharge to electrodes, which are either integrated or form an external appliqué attached to the vehicle hull. (The PFN and associated control systems may either be integrated into the vehicle, or may be integrated into the armor modules themselves.) When penetrated by a shaped charge jet, a conducting path through the jet completes the electrical circuit, allowing a current to flow through the jet. A combination of ohmic heating, magnetic compressional heating, shock heating and magnetohydrodynamic (MHD) instabilities causes the jet to heat and break up. An expansion region behind the second electrode plate allows the jet to disperse without penetrating the vehicle hull. In practice, there is some penetration caused by elements of the jet that are not totally dispersed, but the typical reduction in penetration is 80 – 90%. The inset in figure A-1 is a flash radiograph of a dispersed jet.

Figure A-2 is a Work Breakdown Structure (WBS) for the MEFFV EM armor system, which defines the key subsystems and components. For the MEFFV application, we have considered separate turret and chassis protection systems, to eliminate the associated time delay involved in energizing the slip ring in a surprise attack. This system includes sensors to detect the impact of the threat on the module, discriminate the threat velocity and send a trigger to the output switch to energize the modules.

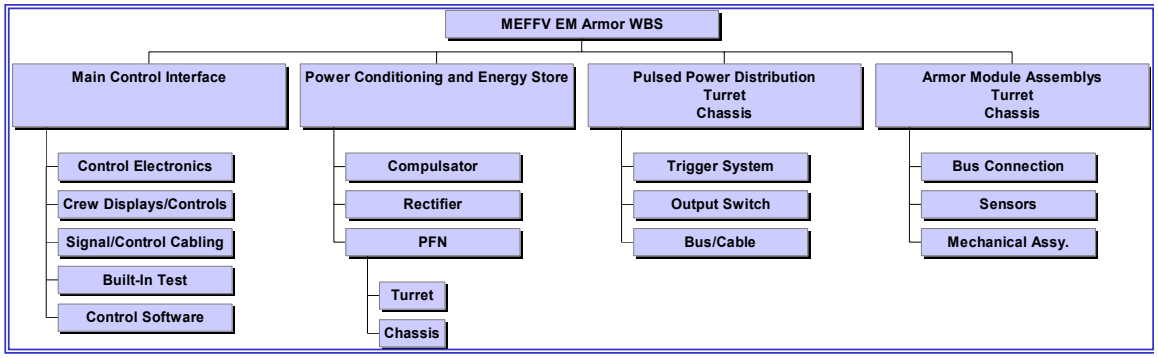

Figure A-2. EM armor system Work Breakdown Structure

Power Conditioning and Energy Store

The power conditioning and energy store system consists of a prime energy store, a voltage converter and a PFN. The prime energy store for the MEFFV is assumed to be the compulsators, whose design is discussed elsewhere. In order to dc charge the PFN, the voltage converter is a rectifier. The PFN is made up of a network of capacitors and inductors to store and condition the energy required for threat defeat.

Rectifier

The rectifier size and weight are determined by the engagement scenario and the energy stored in the PFNs. We have chosen an operating voltage of 16 kV, consistent with the compulsator output voltage. Since the MEFFV time dependent engagement scenario, i.e., number of RPG or HEAT round hits per minute is unspecified, the rectifier power-level is at present undetermined.

PFN

The size (energy) of the PFN is determined by the threat. For both the chassis and turret, we must accommodate both top and side threats. To size the PFNs we utilized an EM armor design code developed by SAIC and PMC, Inc. This code models the threat warhead, computes the jet characteristics, the EM coupling to the jet and the resultant residual penetration for a given armor module and hull configuration. For the threat we have assumed a standard threat spectrum currently being considered by the Army for FCS top and side protection. The top threat consists of three warheads that we shall refer to as "Small", "Medium" and "Large". The side threats are unitary man-portable shaped charges. Identification of specific warheads is classified when associated with the defeat energy. Therefore, we will not identify the specific warheads in this report.

Besides the compulsators, the major internal weight and space claim associated with the EM armor system is due to the PFNs. The volume and weight of the PFNs depend largely on the energy density of the capacitors that make up the PFN, which is voltage dependent. State-of-art 16-kV biaxial oriented polypropylene (BOPP) dielectric capacitors manufactured by ICAR S.p.A. have a net energy density of 1.0 J/cc. Diamond-like-carbon film, currently under development by the U.S. Air Force could push this value to 2 to 4 J/cc net. (Here the term "net"

includes the packaging efficiencies of a high voltage capacitor.) The energy density of the BOPP dielectric in the ICAR 1 J/cc capacitors is 2.15 J/cc. The energy density of DLC has been estimated at 7.7 to 9 j/cc. We have conservatively based our design on 100-µf, 16-kV, 2 J/cc units storing 12.8 kJ each.

Figure A-3 shows the placement of the PFNs and associated bus work in the MEFFV. Separate systems for the turret and main chassis are shown. Total energy stored in each PFN at 16 kV charge is 205 kJ. This arrangement eliminates the need to pass current through the turret slip ring. Although the slip ring could easily handle the required current (600-kA peak) when energized (under pressure), it would have to be continuously under pressure in order for top EM armor to be energized through the slip ring from a PFN in the chassis.

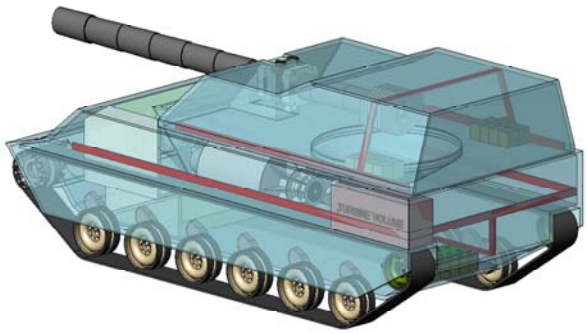

Figure A-3. Integration of EM armor system

The PFNs are switched by laser triggered solid-state thyristor switches, of the type currently under development for TACOM by Opti-Switch Technology Corporation. We have separated the turret PFN into two modules, each with independent switching. This allows simultaneous engagement of two top threats. Engagement of a side threat on the turret requires the full energy of the top two modules. Engagement of a side threat on the chassis requires the full chassis PFN energy.

Pulsed Power Distribution

Pulsed power distribution is accomplished by Litz-wire based buses developed by SAIC under the sponsorship of TACOM. These buses have an inductance of 2.0 nh/ft, a resistance of 0.14 mΩ/ft and weigh 0.8 lb/ft.

Armor Module Assemblies

The basic module construction for top protection consists of two 2024-T3 aluminum electrodes separated by a non-conducting foam, backed by a foam drift region and a third aluminum backing plate, all integrated into a weatherproof case with associated hull attachment hardware. Also integrated into each module is a break-screen sensor that is used to detect the jet tip, discriminate velocity, and provide a trigger signal to the output switch of the PFN. The titanium vehicle hull provides the required residual ballistic protection. The weight of the basic module, not including attachment hardware and weather protection is 11.4 lb/sq.ft., and the thickness of the top protection modules is 4.5 inches (not including the 2 in-thick Ti hull). The basic module construction for side protection is the same as the top, except that the inter-electrode gap and expansion regions are thicker, resulting in an overall module thickness of 8.7 inches and a weight of 12.1 lb/sq.ft. Both the top and side modules can be attached as appliqué, but details of the attachment hardware have not been developed.

System Performance

Figure A-4 left shows the calculated performance of the top armor system against the "large" top threat, and figure A-4 right shows that of the side system against the largest of the side threats. For the top threat, we assumed a 2-inch thick Ti hull, and for the side threat, a 1.5-inch thick Ti skirt or 2-inch Ti hull. The expansion of individual jet segments is shown in a time resolved snapshot, and the final residual penetrations in the hull (and skirt) are shown. Details of these calculations are classified (U.S. Army Research Laboratory SCG for Reactive Armor Technologies, 21 Feb. 2002) since they specify the threat and the EM parameters (current, pulse length, energy) required to defeat a specified threat.

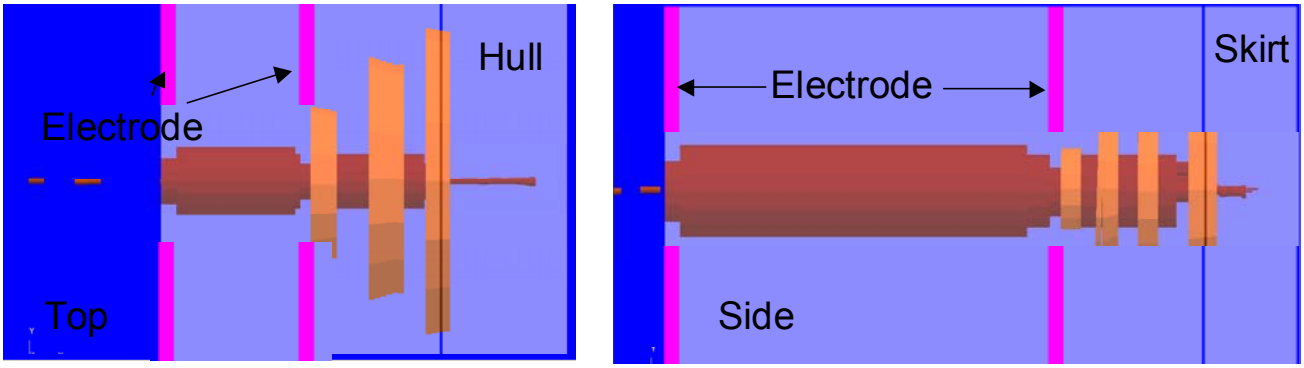

Figure A-4. Calculated performance of the MEFFV EM armor against top (left) and side (right) threats.

System Weights and Volumes

Table 1 gives estimated EM armor system weights and volumes for the turret and chassis. Since shot rates are not known it was not possible to estimate the weight of the required rectifier. The area of the chassis and turrets was taken from the CAD model of the MEFFV, and module areal density for both top and side protection was taken to be 12.6 lb/sq. ft. to allow for some attachment hardware. Due to the requirement to have separate PFNs for the turret and chassis, total power system weight for the vehicle is 1,067 lb. If power could be delivered through the slip ring to the turret, this weight could be reduced to ~ 550 lb. Even with separate power systems for the turret and chassis, the overall weight (power system plus armor modules) added to the vehicle by the EM system is ~ 15 lb/sq. ft.

APPENDIX B: Output File From APADS

MEFFV_r0.txt 01-Oct-2003 15:50:41
ldratio = 0.5 vtip01 = 775

Design of a Multiphase Pulsed Alternator With Optional Quadrature Axis Compensation
---

Design Requirements Summarized

Muzzle KE (J) = 9e+006 ILP Mass = 2.88(kg) and Velocity = 2.5e+003(m/s)
Number of Shots Stored = 5
Target Acceleration Ratio = 0.65
Target PPS Net Efficiency = 0.35
Gun Acceleration Length = 6
Gun Lprime (H) = 6.1000e-007 Rprime (ohm) = 4.9000e-005
Calculated Launch Time (s) = 0.00492
Peak Current Required for Gun (A) = 2.81e+006
Number of Parallel PAs Required for Mission = 2
Estimated Alternator Voltage Required (V) = 7672
Estimated Energy Storage Required for Alternator (J) = 1.28e+008
Machine Configuration 2 : Cooling Integrated With FW Conductor, Optional CW and Single FW Layer
B1 Layer is Composite, Arbors Must Be Used

Generator Radii (m) (in)
---

remo =	0.538221	21.1898
rem =	0.525984	20.708
rmo =	0.424384	16.708
rao =	0.373584	14.708
rai =	0.35813	14.0996
rb3o =	0.351145	13.8246
rfwo =	0.321935	12.6746
rb1o =	0.291203	11.4647
rb1i =	0.226204	8.90569
rshaft =	0.0996495	3.92321
rshftbrng =	0.0388889	1.53106

Rotor Lengths (m) (in)

Active Length =	0.35813	14.0996
Impedance Length =	0.498768	19.6365
Total Length =	0.92068	36.2472

Flywheel Dimensions (m) (in)
Layer No. Outer Radius

7	0.424413	16.7092

```
  6      0.408295       16.0746
  5      0.389245       15.3246
  4      0.370195       14.5746
  3      0.351145       13.8246
  2      0.321935       12.6746
  1      0.291203       11.4647
1 IR      0.226204                    8.90569
Flywheel Length =   0.1294 (m)       5.09 (in)

Armature Conductor Dimensions (m)
------------------------------

Phase # 1   Thickness = 0.00772688      Width = 0.0468791      Conductors/pole = 6
Phase # 2   Thickness = 0.00772688      Width = 0.0468791      Conductors/pole = 6
Phase # 3   Thickness = 0.00772688      Width = 0.0468791      Conductors/pole = 6
Phase # 4   Thickness = 0.00772688      Width = 0.0468791      Conductors/pole = 6

Estimated Banding Hoop Stresses (psi)
-------------------------------------

Hoop stress Stator Case = 139873
Hoop stress B3          = 389528
Compressive discharge pressure = 7936.75   (psi)

Phase 1 armature average shear stress = 2271.14
Phase 2 armature average shear stress = 2271.14
Phase 3 armature average shear stress = 2177.2
Phase 4 armature average shear stress = 2177.2

Rotor Polar Moments of Inertia (kg-m^2)
---------------------------------------

M.I. B3       = 10.3761
M.I. FW-Outer = 13.7427
M.I. B1       = 10.6205
M.I. Arbors   = 0.724283
M.I. Shaft    = 0.903163
Total Moment  = 36.3668

Kinetic energy stored in the rotor (MJ) = 1.009479e+008


Flywheel Polar Moments of Inertia (kg-m^2)
------------------------------------------

 Layer  7    = 1.52095
 Layer  6    = 1.57966
 Layer  5    = 1.364
 Layer  4    = 1.16891
 Layer  3    = 1.45785
 Layer  2    = 1.93086
 Layer  1    = 1.4922
Total Flywheel Moment  = 10.5144

Kinetic energy stored in the Flywheel (MJ) = 2.918626e+007
```

Total Kinetic Energy Stored in Rotor (MJ) = 1.301341e+008

Ampturns per pole in the field coil = 3.076780e+006

Generated Phase Voltages

	Blv voltage	Circuit Voltage
Phase # 1	Voltage = 5858.94	Voltage = 8844.09
Phase # 2	Voltage = 5858.94	Voltage = 8844.09
Phase # 3	Voltage = 5858.94	Voltage = 8478.27
Phase # 4	Voltage = 5858.94	Voltage = 8478.27

Designed Action Values (A^2-s)
---

phase # 1 Action = 1.475410e+009
phase # 2 Action = 1.475410e+009
phase # 3 Action = 1.475410e+009
phase # 4 Action = 1.475410e+009

Other Machine Parameters
---

rotor speed (rpm) = 22500
tip speed of rotor (m/s) = 827.366
electrical frequency (Hz) = 750
number of poles = 4
peak design amperes (A) = 1.75e+006
max short circuit amps = 2.0437e+006
armature packing fraction = 0.42
armature deltemp (C) = 30
B-field at armature (T) = 3
max excitation current (A)= 200000
max field J (A/m^2) = 3.375e+008
field W. packing frac = 0.77
field W. deltemp (C) = 11.3253
rotor kinetic energy (J) = 1.30134e+008
estimated efficiency = 0.00498796
muzzle energy (J) = 9e+006
armature losses (J) = 2.03324e+006
field W. losses (J) = 2.10955e+006

Circuit Parameters (x1.2 for arm W self inductance)

Inductance - row # 1 : 1.721925e-006 1.069594e-022 -1.674527e-006 -3.076057e-022
Inductance - row # 2 : 1.069594e-022 1.721925e-006 1.025352e-022 -1.674527e-006
Inductance - row # 3 : -1.674527e-006 1.025352e-022 1.722433e-006 1.069588e-022
Inductance - row # 4 : -3.076057e-022 -1.674527e-006 1.069588e-022 1.722433e-006
Phase Displacement = 90
Resistance - Phase = 1 0.00017289
Resistance - Phase = 2 0.00017289
Resistance - Phase = 3 0.000171632
Resistance - Phase = 4 0.000171632

Mutual A & F1 1 = 9.38387e-006
Mutual A & F1 2 = 9.38387e-006
Mutual A & F1 3 = 8.99573e-006
Mutual A & F1 4 = 8.99573e-006

Mutual A 1 & MagShield = 6.84129e-007
Mutual A 2 & MagShield = 6.84129e-007
Mutual A 3 & MagShield = 7.13644e-007
Mutual A 4 & MagShield = 7.13644e-007

Mutual F1 & Magshield = 4.41025e-006
Resistance of Magshield = 0.000301241
inductance of Magshield = 1.44796e-006

Electrical Parameters of the Field Winding

No. of turns per pole 1 = 16
Conductor x-section area (m^2) = 6.771325e-004
Field coil kerf width (in) = -0.0176875
Inductance of the outer coil (H) = 1.095778e-004
Resistance of the outer coil(ohm) = 3.747812e-003
Eff. inductance of field coil (H) = 1.095778e-004
Eff. resistance of field coil(ohm)= 3.747812e-003
Desired time to charge (s) = 2.500000e-002
Actual time to charge (s) = 6.313045e-003
Initial seed current (amps) = 2.500000e+004
Alpha derived from input (1/s) = 83.1777
Alpha derived from design (1/s) = 329.388
Dissipated energy (chrg&recl) (J) = 1.592438e+006
Peak energy in field coil (J) = 2.191556e+006

Mass Schedule (kg)

Environmental Shield = 102.0
Stator Outer Casing = 230.8
Armature Backing Ring = 136.0
Armature Winding = 147.4
B3 Banding = 91.4
Field Coil 1 = 145.9
B1 Banding = 156.2
Arbor Mass Total = 28.1
Shaft = 70.7
Stator End Plates = 390.0
Brush Box = 18.2
Bearings and Seals = 33.7
Flywheel Rotor Mass = 92.4
Total Rotor Mass = 514.0
Total Alternator Mass = 1642.7

****

TEMPST Input File Generated by CPA Design Code for * EGP8r5_1.txt 01-Oct-2003 15:50:41

Inner Pressure = 0 , Outer Pressure = 0
Friction Coefficient = 0.05 , Rotor Length = 36.2472
Rotational Speed = 2356.19

********** MATERIAL DEFINITIONS **********

ring name material er et nurt nutr cter ctet
rho temp ir or wgt energy

1 BAND 1 IM745/45 1.470e+006 7.750e+006 0.0300 0.1582 +2.00e-005 +1.80e-007 1.500e-004 +0.0
8.9057 11.4647 343.7 29.4
2 FIELD COIL FCOIL AXIAL 8.377e+006 3.410e+005 0.2550 0.0104 +1.40e-005 +1.80e-005 2.400e-004 +0.0
11.4647 12.6746 308.1 36.6
3 BAND 3 T1000G/70FV 1.330e+006 2.713e+007 0.0170 0.3468 +2.61e-005 +1.78e-007 1.500e-004 +0.0
12.6746 13.8246 200.9 28.7

Total Weight (lb) (kg) = 852.8 386.8
Rotor Polar Moment of Inertia (kg-m^2) = 34.1
Rotor Energy Stored (MJ) = 9.47e+001
Rotor Tip Speed (m/s) = 827.4

summary of interface condition at 2356.19 rad/sec ***

interface no. interference interface pressure first ring last ring assembly pressure press load
axial stress
1 5.0000e-003 5.2576e+002 1
2 1.4630e+001 1 -21
2 6.7500e-002 1.8723e+004 1
3 5.4234e+003 389 -7734

Output For Layer : BAND 1

radius rad stress hoop stress rad disp spin disp hoop
strain

8.9057	-4.36557e-011	9.69542e+004	1.11412e-001	1.44065e-001	1.25102e-002
9.4175	1.31139e+003	9.12935e+004	1.10684e-001	1.43317e-001	1.17530e-002
9.9293	1.80317e+003	8.63925e+004	1.10321e-001	1.43430e-001	1.11106e-002
10.4411	1.60373e+003	8.19418e+004	1.10053e-001	1.44069e-001	1.05404e-002
10.9529	8.05098e+002	7.77168e+004	1.09655e-001	1.44954e-001	1.00115e-002
11.4647	-5.25764e+002	7.35513e+004	1.08929e-001	1.45850e-001	9.50122e-003

Output For Layer : FIELD COIL

radius rad stress hoop stress rad disp spin disp hoop
strain

11.4647	-5.25764e+002	3.38318e+003	1.13929e-001	1.45850e-001	9.93734e-003
11.7067	-4.14300e+003	3.27291e+003	1.13837e-001	1.45919e-001	9.72408e-003
11.9487	-7.76884e+003	3.16253e+003	1.13641e-001	1.45882e-001	9.51077e-003
12.1906	-1.14059e+004	3.05202e+003	1.13341e-001	1.45738e-001	9.29739e-003
12.4326	-1.50565e+004	2.94133e+003	1.12937e-001	1.45488e-001	9.08392e-003
12.6746	-1.87228e+004	2.83044e+003	1.12428e-001	1.45129e-001	8.87033e-003

Output For Layer : BAND 3

radius	rad stress	hoop stress	rad disp	spin disp	hoop strain
12.6121	-1.87228e+004	3.70007e+005	1.75026e-001	1.45129e-001	1.38776e-002
12.8546	-1.40739e+004	3.55850e+005	1.70920e-001	1.42085e-001	1.32964e-002
13.0971	-9.93493e+003	3.43842e+005	1.67654e-001	1.39654e-001	1.28009e-002
13.3396	-6.24367e+003	3.33688e+005	1.65136e-001	1.37761e-001	1.23794e-002
13.5821	-2.94708e+003	3.25133e+005	1.63283e-001	1.36339e-001	1.20219e-002
13.8246	2.54659e-011	3.17961e+005	1.62023e-001	1.35328e-001	1.17199e-002

summary of interface condition at 0 speed ***

interface no.	interference	interface pressure	first ring	last ring	assembly pressure	press load	axial stress
1		5.0000e-003	5.8931e+003		1		
2	1.4630e+001	1	-21				
2		6.7500e-002	5.4234e+003		1		
3	5.4234e+003	389	-7734				

Output For Layer : BAND 1

radius	rad stress	hoop stress	rad disp	spin disp	hoop strain
8.9057	-9.09495e-013	-2.84156e+004	-3.26530e-002	0.00000e+000	-3.66653e-003
9.4175	-1.50565e+003	-2.70928e+004	-3.26327e-002	0.00000e+000	-3.46512e-003
9.9293	-2.80181e+003	-2.62857e+004	-3.31094e-002	0.00000e+000	-3.33452e-003
10.4411	-3.94139e+003	-2.58714e+004	-3.40151e-002	0.00000e+000	-3.25781e-003
10.9529	-4.96251e+003	-2.57614e+004	-3.52987e-002	0.00000e+000	-3.22277e-003
11.4647	-5.89309e+003	-2.58904e+004	-3.69212e-002	0.00000e+000	-3.22042e-003

Output For Layer : FIELD COIL

radius	rad stress	hoop stress	rad disp	spin disp	hoop strain
11.4647	-5.89309e+003	-1.01062e+003	-3.19212e-002	0.00000e+000	-2.78430e-003
11.7067	-5.79200e+003	-9.94645e+002	-3.20826e-002	0.00000e+000	-2.74054e-003
11.9487	-5.69469e+003	-9.79236e+002	-3.22412e-002	0.00000e+000	-2.69831e-003
12.1906	-5.60094e+003	-9.64362e+002	-3.23972e-002	0.00000e+000	-2.65754e-003
12.4326	-5.51056e+003	-9.49994e+002	-3.25506e-002	0.00000e+000	-2.61816e-003
12.6746	-5.42336e+003	-9.36105e+002	-3.27016e-002	0.00000e+000	-2.58009e-003

Output For Layer : BAND 3

radius	rad stress	hoop stress	rad disp	spin disp	hoop strain
12.6121	-5.42336e+003	6.24293e+004	2.98962e-002	0.00000e+000	2.37044e-003
12.8546	-4.17276e+003	5.94086e+004	2.88343e-002	0.00000e+000	2.24311e-003
13.0971	-3.01907e+003	5.69533e+004	2.79998e-002	0.00000e+000	2.13786e-003
13.3396	-1.94731e+003	5.49994e+004	2.73748e-002	0.00000e+000	2.05215e-003
13.5821	-9.44643e+002	5.34927e+004	2.69441e-002	0.00000e+000	1.98379e-003

13.8246 8.18545e-012 5.23870e+004 2.66948e-002 0.00000e+000 1.93096e-003
TEMPST Input File Generated by CPA Design Code for the FLYWHEEL of* EGP8r5_1.txt 01-Oct-2003 15:50:41

Inner Pressure = 0 , Outer Pressure = 0
Friction Coefficient = 0.05 , Rotor Length = 36.2472
Rotational Speed = 2356.19

********** MATERIAL DEFINITIONS **********

ring	name	material	er	et	nurt	nutr	cter	ctet	rho	temp	ir	or	wgt	energy
1	BAND 1	IM745/45	1.470e+006	7.750e+006	0.0300	0.1582	+2.00e-005	+1.80e-007	1.500e-004	+0.0	8.9057	11.4647	343.7	29.4
2	FIELD COIL	FCOIL AXIAL	8.377e+006	3.410e+005	0.2550	0.0104	+1.40e-005	+1.80e-005	2.400e-004	+0.0	11.4647	12.6746	308.1	36.6
3	BAND 3	T1000G/70FV	1.330e+006	2.713e+007	0.0170	0.3468	+2.61e-005	+1.78e-007	1.500e-004	+0.0	12.6746	13.8246	200.9	28.7
4	FLYBAND #	4T1000G/70FV	1.330e+006	2.713e+007	0.0170	0.3468	+2.61e-005	+1.78e-007	1.500e-004	+0.0	13.8246	14.5746	140.4	23.0
5	FLYBAND #	5T1000G/70FV	1.330e+006	2.713e+007	0.0170	0.3468	+2.61e-005	+1.78e-007	1.500e-004	+0.0	14.5746	15.3246	147.9	26.9
6	FLYBAND #	6T1000G/70FV	1.330e+006	2.713e+007	0.0170	0.3468	+2.61e-005	+1.78e-007	1.500e-004	+0.0	15.3246	16.0746	155.3	31.1
7	FLYBAND #	7T1000G/70FV	1.330e+006	2.713e+007	0.0170	0.3468	+2.61e-005	+1.78e-007	1.500e-004	+0.0	16.0746	16.7092	137.2	30.0

Total Weight (lb) (kg) = 1433.6 650.3
Rotor Polar Moment of Inertia (kg-m^2) = 74.1
Rotor Energy Stored (MJ) = 2.06e+002
Rotor Tip Speed (m/s) = 1000.0

summary of interface condition at 2356.19 rad/sec ***

interface no.	interference	interface pressure	first ring	last ring	assembly pressure	press load	axial stress
1		5.0000e-003	5.4198e+002		1		
2	1.4630e+001		1	-21			
2		4.0500e-002	1.8738e+004		1		
3	3.2213e+003		232	-4704			
3		5.0000e-003	5.3802e+003		1		
4	3.6781e+002		29	-865			
4		5.0000e-003	2.0024e+003		1		
5	3.5286e+002		29	-831			
5		6.0000e-003	5.3370e+002		1		
6	3.9798e+002		35	-937			
6		3.2000e-002	5.7066e+002		1		
7	1.7946e+003		164	-4817			

Output For Layer : BAND 1

radius	rad stress	hoop stress	rad disp	spin disp	hoop strain

8.9057	-4.36557e-011	9.68760e+004	1.11322e-001	1.35282e-001	1.25001e-002
9.4175	1.30724e+003	9.12190e+004	1.10594e-001	1.34540e-001	1.17435e-002
9.9293	1.79546e+003	8.63202e+004	1.10230e-001	1.34524e-001	1.11014e-002
10.4411	1.59288e+003	8.18706e+004	1.09960e-001	1.34919e-001	1.05314e-002
10.9529	7.91442e+002	7.76459e+004	1.09558e-001	1.35460e-001	1.00027e-002
11.4647	-5.41980e+002	7.34801e+004	1.08827e-001	1.35919e-001	9.49236e-003

Output For Layer : FIELD COIL

radius	rad stress	hoop stress	rad disp	spin disp	hoop strain
11.4647	-5.41980e+002	3.37999e+003	1.13827e-001	1.35919e-001	9.92848e-003
11.7067	-4.15895e+003	3.26977e+003	1.13735e-001	1.35945e-001	9.71537e-003
11.9487	-7.78452e+003	3.15944e+003	1.13539e-001	1.35866e-001	9.50220e-003
12.1906	-1.14213e+004	3.04898e+003	1.13238e-001	1.35680e-001	9.28895e-003
12.4326	-1.50716e+004	2.93834e+003	1.12834e-001	1.35388e-001	9.07561e-003
12.6746	-1.87378e+004	2.82749e+003	1.12324e-001	1.34990e-001	8.86214e-003

Output For Layer : BAND 3

radius	rad stress	hoop stress	rad disp	spin disp	hoop strain
12.6391	-1.87378e+004	3.11019e+005	1.47922e-001	1.34990e-001	1.17035e-002
12.8762	-1.52836e+004	2.98051e+005	1.43974e-001	1.31778e-001	1.11814e-002
13.1133	-1.22656e+004	2.86713e+005	1.40639e-001	1.29083e-001	1.07249e-002
13.3504	-9.63547e+003	2.76767e+005	1.37838e-001	1.26834e-001	1.03247e-002
13.5875	-7.35201e+003	2.68009e+005	1.35504e-001	1.24972e-001	9.97268e-003
13.8246	-5.38019e+003	2.60264e+005	1.33573e-001	1.23440e-001	9.66198e-003

Output For Layer : FLYBAND # 4

radius	rad stress	hoop stress	rad disp	spin disp	hoop strain
13.8246	-5.38019e+003	2.38108e+005	1.22283e-001	1.23440e-001	8.84531e-003
13.9746	-4.51655e+003	2.33871e+005	1.21273e-001	1.22618e-001	8.67813e-003
14.1246	-3.75194e+003	2.29888e+005	1.20363e-001	1.21898e-001	8.52155e-003
14.2746	-3.08113e+003	2.26130e+005	1.19542e-001	1.21267e-001	8.37444e-003
14.4246	-2.49939e+003	2.22570e+005	1.18798e-001	1.20716e-001	8.23578e-003
14.5746	-2.00243e+003	2.19183e+005	1.18121e-001	1.20235e-001	8.10460e-003

Output For Layer : FLYBAND # 5

radius	rad stress	hoop stress	rad disp	spin disp	hoop strain
14.5746	-2.00243e+003	2.21949e+005	1.19607e-001	1.20235e-001	8.20654e-003
14.7246	-1.55837e+003	2.18688e+005	1.18985e-001	1.19814e-001	8.08067e-003
14.8746	-1.19253e+003	2.15563e+005	1.18414e-001	1.19444e-001	7.96082e-003
15.0246	-9.01702e+002	2.12555e+005	1.17886e-001	1.19118e-001	7.84621e-003
15.1746	-6.82965e+002	2.09644e+005	1.17393e-001	1.18826e-001	7.73613e-003
15.3246	-5.33696e+002	2.06815e+005	1.16926e-001	1.18561e-001	7.62992e-003

Output For Layer : FLYBAND # 6

radius	rad stress	hoop stress	rad disp	spin disp	hoop strain
15.3236	-5.33696e+002	2.10820e+005	1.19180e-001	1.18561e-001	7.77754e-003
15.4738	-4.12516e+002	2.08016e+005	1.18725e-001	1.18316e-001	7.67265e-003
15.6240	-3.57538e+002	2.05271e+005	1.18286e-001	1.18083e-001	7.57076e-003
15.7742	-3.66745e+002	2.02569e+005	1.17854e-001	1.17855e-001	7.47130e-003
15.9244	-4.38325e+002	1.99898e+005	1.17423e-001	1.17626e-001	7.37375e-003
16.0746	-5.70659e+002	1.97244e+005	1.16985e-001	1.17389e-001	7.27762e-003

Output For Layer : FLYBAND # 7

radius	rad stress	hoop stress	rad disp	spin disp	hoop strain
16.0476	-5.70659e+002	2.43794e+005	1.44323e-001	1.17389e-001	8.99344e-003
16.1799	-3.51559e+002	2.41111e+005	1.43868e-001	1.17169e-001	8.89174e-003
16.3122	-1.86430e+002	2.38493e+005	1.43436e-001	1.16934e-001	8.79314e-003
16.4446	-7.37216e+001	2.35930e+005	1.43022e-001	1.16680e-001	8.69723e-003
16.5769	-1.20116e+001	2.33412e+005	1.42621e-001	1.16403e-001	8.60363e-003
16.7092	8.41283e-012	2.30930e+005	1.42228e-001	1.16099e-001	8.51199e-003

summary of interface condition at 0 speed ***

interface no.	interference	interface pressure	first ring	last ring	assembly pressure	press load	axial stress
1		5.0000e-003	4.3242e+003		1		
2	1.4630e+001	1	-21				
2		4.0500e-002	3.9759e+003		1		
3	3.2213e+003	232	-4704				
3		5.0000e-003	1.7152e+003		1		
4	3.6781e+002	29	-865				
4		5.0000e-003	1.8184e+003		1		
5	3.5286e+002	29	-831				
5		6.0000e-003	1.8606e+003		1		
6	3.9798e+002	35	-937				
6		3.2000e-002	1.7946e+003		1		
7	1.7946e+003	164	-4817				

Output For Layer : BAND 1

radius	rad stress	hoop stress	rad disp	spin disp	hoop strain
8.9057	-9.09495e-013	-2.08507e+004	-2.39600e-002	0.00000e+000	-2.69041e-003
9.4175	-1.10481e+003	-1.98801e+004	-2.39451e-002	0.00000e+000	-2.54262e-003
9.9293	-2.05590e+003	-1.92878e+004	-2.42949e-002	0.00000e+000	-2.44679e-003
10.4411	-2.89210e+003	-1.89838e+004	-2.49595e-002	0.00000e+000	-2.39050e-003
10.9529	-3.64137e+003	-1.89031e+004	-2.59013e-002	0.00000e+000	-2.36479e-003
11.4647	-4.32421e+003	-1.89977e+004	-2.70919e-002	0.00000e+000	-2.36307e-003

Output For Layer : FIELD COIL

radius	rad stress	hoop stress	rad disp	spin disp	hoop strain
11.4647	-4.32421e+003	-7.01976e+002	-2.20919e-002	0.00000e+000	-1.92695e-003
11.7067	-4.24922e+003	-6.91072e+002	-2.22106e-002	0.00000e+000	-1.89726e-003
11.9487	-4.17706e+003	-6.80550e+002	-2.23272e-002	0.00000e+000	-1.86860e-003
12.1906	-4.10755e+003	-6.70388e+002	-2.24419e-002	0.00000e+000	-1.84091e-003
12.4326	-4.04056e+003	-6.60568e+002	-2.25547e-002	0.00000e+000	-1.81415e-003
12.6746	-3.97594e+003	-6.51072e+002	-2.26656e-002	0.00000e+000	-1.78827e-003

Output For Layer : BAND 3

radius	rad stress	hoop stress	rad disp	spin disp	hoop strain
12.6391	-3.97594e+003	2.63803e+004	1.29321e-002	0.00000e+000	1.02319e-003
12.8762	-3.43465e+003	2.45045e+004	1.21954e-002	0.00000e+000	9.47126e-004
13.1133	-2.94448e+003	2.28865e+004	1.15557e-002	0.00000e+000	8.81222e-004
13.3504	-2.49840e+003	2.14954e+004	1.10040e-002	0.00000e+000	8.24244e-004
13.5875	-2.09037e+003	2.03046e+004	1.05322e-002	0.00000e+000	7.75139e-004
13.8246	-1.71521e+003	1.92916e+004	1.01335e-002	0.00000e+000	7.33003e-004

Output For Layer : FLYBAND # 4

radius	rad stress	hoop stress	rad disp	spin disp	hoop strain
13.8246	-1.71521e+003	-2.86470e+003	-1.15667e-003	0.00000e+000	-8.36679e-005
13.9746	-1.72941e+003	-3.21099e+003	-1.34506e-003	0.00000e+000	-9.62506e-005
14.1246	-1.74697e+003	-3.55338e+003	-1.53458e-003	0.00000e+000	-1.08646e-004
14.2746	-1.76774e+003	-3.89267e+003	-1.72561e-003	0.00000e+000	-1.20887e-004
14.4246	-1.79159e+003	-4.22964e+003	-1.91851e-003	0.00000e+000	-1.33003e-004
14.5746	-1.81841e+003	-4.56500e+003	-2.11362e-003	0.00000e+000	-1.45021e-004

Output For Layer : FLYBAND # 5

radius	rad stress	hoop stress	rad disp	spin disp	hoop strain
14.5746	-1.81841e+003	-1.79932e+003	-6.27865e-004	0.00000e+000	-4.30794e-005
14.7246	-1.82005e+003	-2.15896e+003	-8.29211e-004	0.00000e+000	-5.63146e-005
14.8746	-1.82525e+003	-2.51206e+003	-1.03026e-003	0.00000e+000	-6.92631e-005
15.0246	-1.83385e+003	-2.85951e+003	-1.23142e-003	0.00000e+000	-8.19603e-005
15.1746	-1.84568e+003	-3.20216e+003	-1.43307e-003	0.00000e+000	-9.44388e-005
15.3246	-1.86062e+003	-3.54077e+003	-1.63558e-003	0.00000e+000	-1.06729e-004

Output For Layer : FLYBAND # 6

radius	rad stress	hoop stress	rad disp	spin disp	hoop strain
15.3236	-1.86062e+003	4.50438e+002	6.18848e-004	0.00000e+000	4.03853e-005
15.4738	-1.84000e+003	7.97654e+001	4.09419e-004	0.00000e+000	2.64589e-005
15.6240	-1.82328e+003	-2.80122e+002	2.02798e-004	0.00000e+000	1.29799e-005
15.7742	-1.81026e+003	-6.30271e+002	-1.46487e-006	0.00000e+000	-9.28651e-008
15.9244	-1.80075e+003	-9.71650e+002	-2.03793e-004	0.00000e+000	-1.27976e-005

16.0746 -1.79456e+003 -1.30516e+003 -4.04589e-004 0.00000e+000 -2.51695e-005

Output For Layer : FLYBAND # 7

radius rad stress hoop stress rad disp spin disp hoop strain

16.0476	-1.79456e+003	4.49116e+004	2.69336e-002	0.00000e+000	1.67836e-003
16.1799	-1.41525e+003	4.42767e+004	2.66987e-002	0.00000e+000	1.65011e-003
16.3122	-1.04694e+003	4.37140e+004	2.65019e-002	0.00000e+000	1.62466e-003
16.4446	-6.88802e+002	4.32200e+004	2.63421e-002	0.00000e+000	1.60187e-003
16.5769	-3.40067e+002	4.27913e+004	2.62183e-002	0.00000e+000	1.58162e-003
16.7092	-1.90994e-011	4.24251e+004	2.61294e-002	0.00000e+000	1.56377e-003

****

Machine Radii Recap Following TEMPST Results

** AT REST **

Layer # Inner Rad Outer Rad Hoop Stress Hoop Strain

BAND 1 8.8730 11.4278 -2.8416e+004 -3.6665e-003
FIELD COIL 11.4328 12.6419 -1.0106e+003 -2.7843e-003
BAND 3 12.7045 13.8513 +6.2429e+004 +2.3704e-003

** AT SPEED **

Layer # Inner Rad Outer Rad Hoop Stress Hoop Strain

BAND 1 9.0171 11.5736 +9.6954e+004 +1.2510e-002
FIELD COIL 11.5786 12.7870 +3.3832e+003 +9.9373e-003
BAND 3 12.8496 13.9866 +3.7001e+005 +1.3878e-002

****

Impedance Output Summary
Coil Self-Inductances and Resistance

Coil	Parameter	Space Harmonics	Finite Filament
Arm11	Inductance(H)	+1.7219e-006	+2.3329e-006
Arm12	Inductance(H)	+1.0696e-022	+0.0000e+000
Arm13	Inductance(H)	-1.6745e-006	-2.1978e-006
Arm14	Inductance(H)	-3.0761e-022	+0.0000e+000
Arm21	Inductance(H)	+1.0696e-022	+0.0000e+000
Arm22	Inductance(H)	+1.7219e-006	+2.3329e-006
Arm23	Inductance(H)	+1.0254e-022	+0.0000e+000
Arm24	Inductance(H)	-1.6745e-006	-2.1978e-006
Arm31	Inductance(H)	-1.6745e-006	-2.1978e-006
Arm32	Inductance(H)	+1.0254e-022	+0.0000e+000
Arm33	Inductance(H)	+1.7224e-006	+2.3341e-006
Arm34	Inductance(H)	+1.0696e-022	+0.0000e+000

Arm41	Inductance(H)	-3.0761e-022	+0.0000e+000
Arm42	Inductance(H)	-1.6745e-006	-2.1978e-006
Arm43	Inductance(H)	+1.0696e-022	+0.0000e+000
Arm44	Inductance(H)	+1.7224e-006	+2.3341e-006
Arm1	Resistance(Ohm)	+1.7289e-004	+2.1686e-004
Arm2	Resistance(Ohm)	+1.7289e-004	+2.1686e-004
Arm3	Resistance(Ohm)	+1.7163e-004	+2.1279e-004
Arm4	Resistance(Ohm)	+1.7163e-004	+2.1279e-004
Field	Inductance(H)	+1.5493e-004	+1.5493e-004
Field	Resistance(Ohm)	+3.7478e-003	+3.1133e-003
Shield	Inductance(H)	+1.4480e-006	+2.3679e-006
Shield	Resistance(Ohm)	+3.0124e-004	+3.8563e-004

Coil to Coil Mutual Inductances

Coil Pairs	Parameter	Space Harmonics	Finite Filament	
**********				
AW-FW 1 1	Inductance(H)	9.3839e-006	1.2731e-005	-1.2609e-008
AW-FW 2 1	Inductance(H)	9.3839e-006	1.2731e-005	-1.2609e-008
AW-FW 3 1	Inductance(H)	8.9957e-006	1.1933e-005	-1.4819e-008
AW-FW 4 1	Inductance(H)	8.9957e-006	1.1933e-005	-1.4819e-008
AW-Shld 1	Inductance(H)	6.8413e-007	8.6812e-007	
AW-Shld 2	Inductance(H)	6.8413e-007	8.6812e-007	
AW-Shld 3	Inductance(H)	7.1364e-007	9.2591e-007	
AW-Shld 4	Inductance(H)	7.1364e-007	9.2591e-007	
FW-Shld	Inductance(H)	4.4103e-006	5.0850e-006	-6.6680e-009

Max Current Prediction from PARAACT = 2.0437e+006 amps
Max Current Prediction from FF3D = 1.9789e+006 amps

APPENDIX C: Railgun PPS Simulations Results

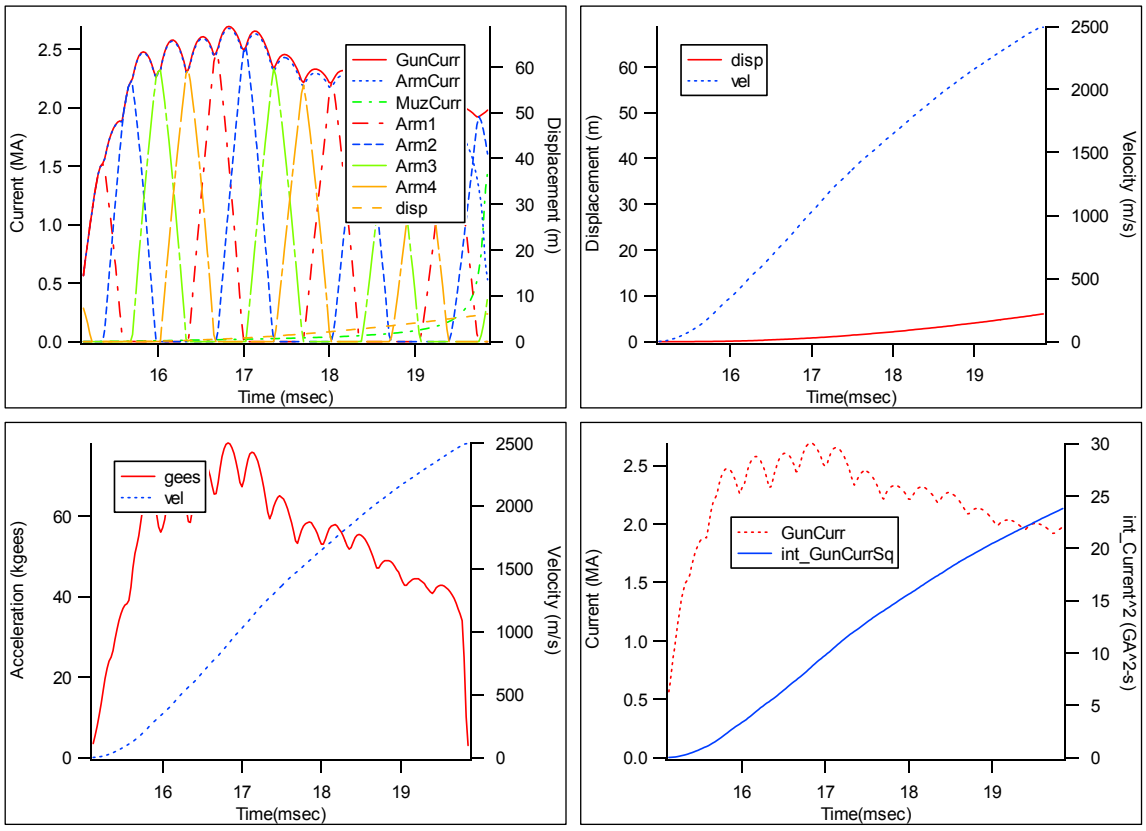

Figure C-1. Gun Performance Data Shot 1

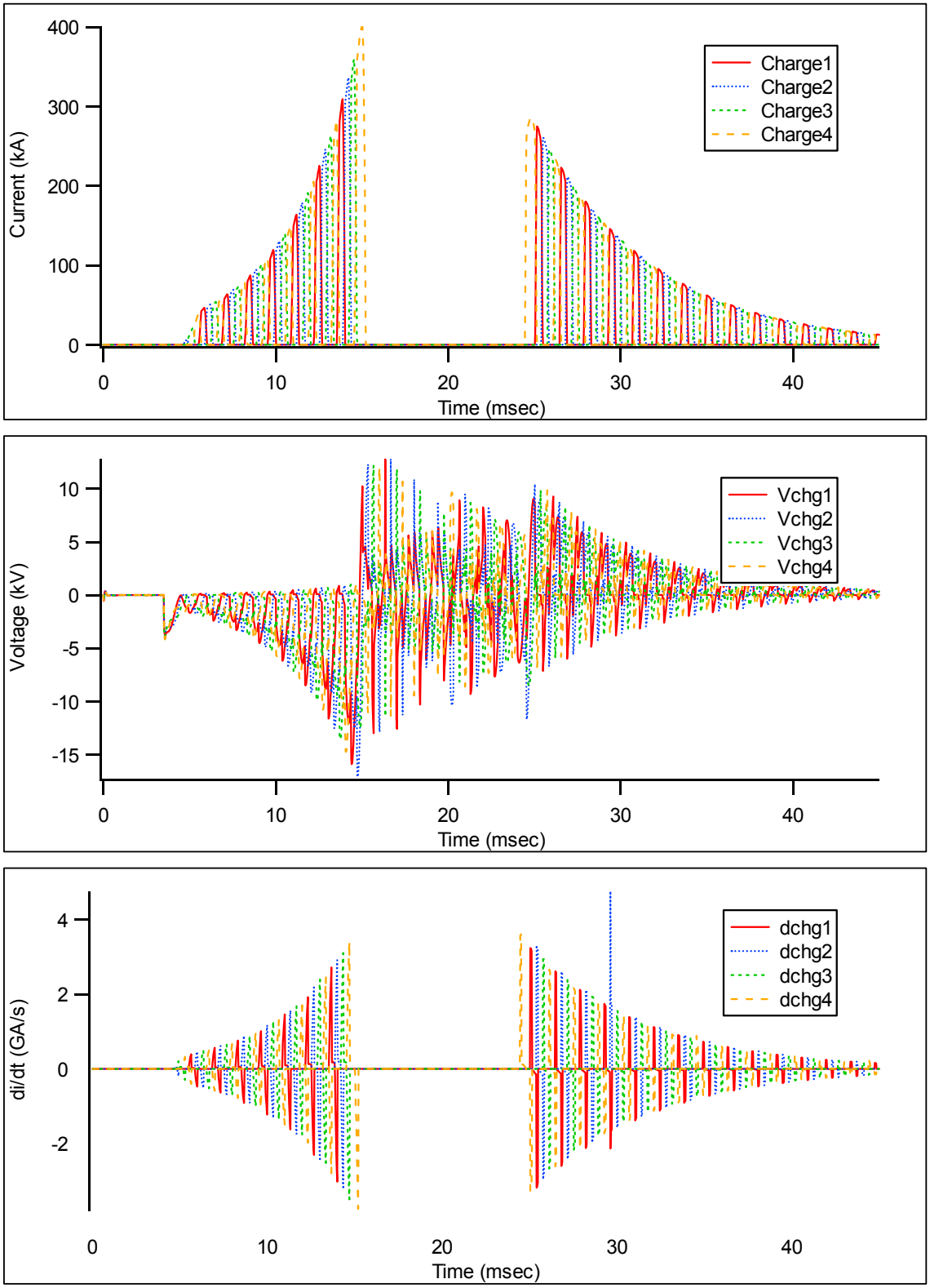

Figure C-2. Field Coil Converter Data Shot 1

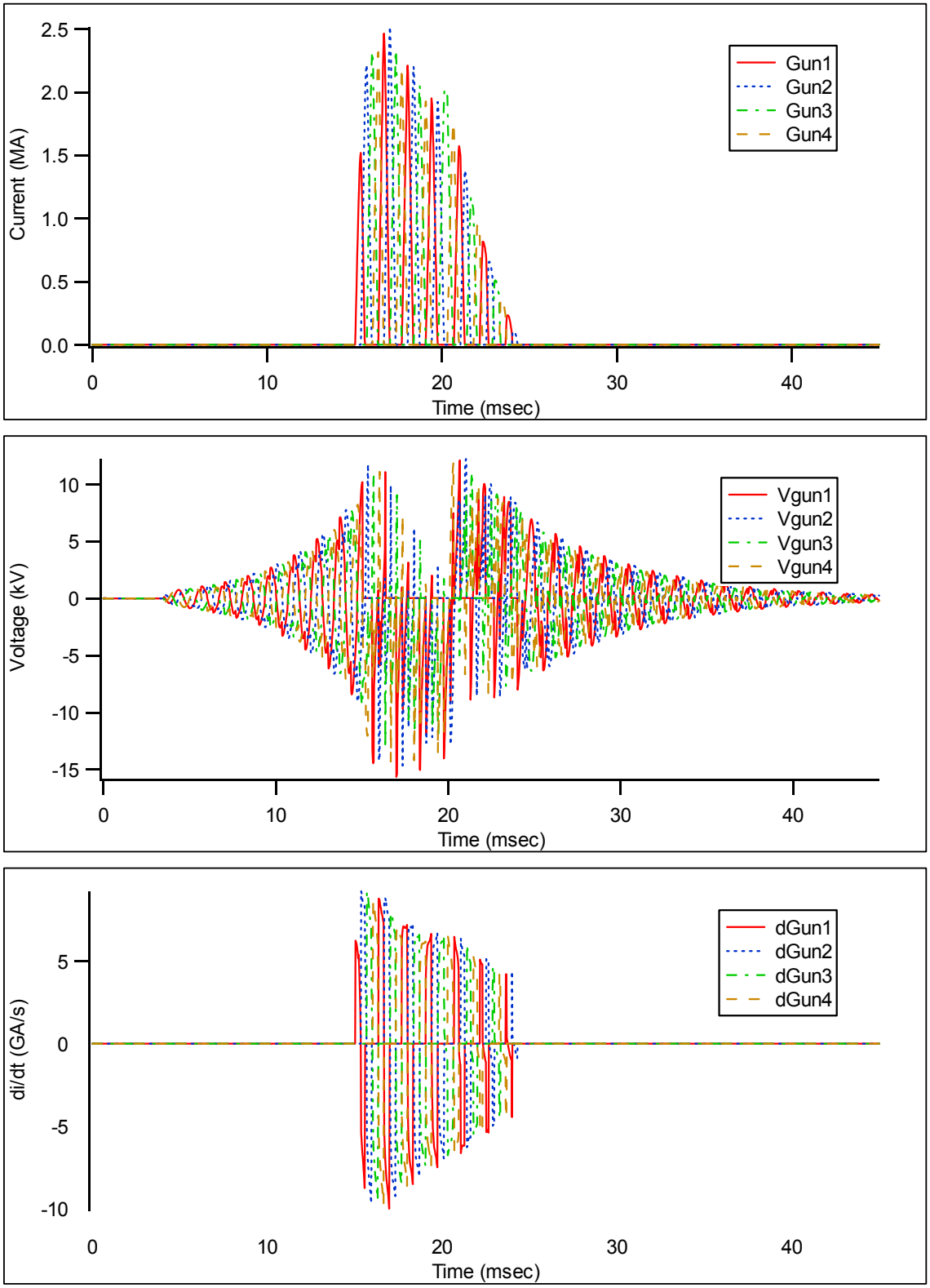

Figure C-3. Gun Switch Converter Data Shot 1

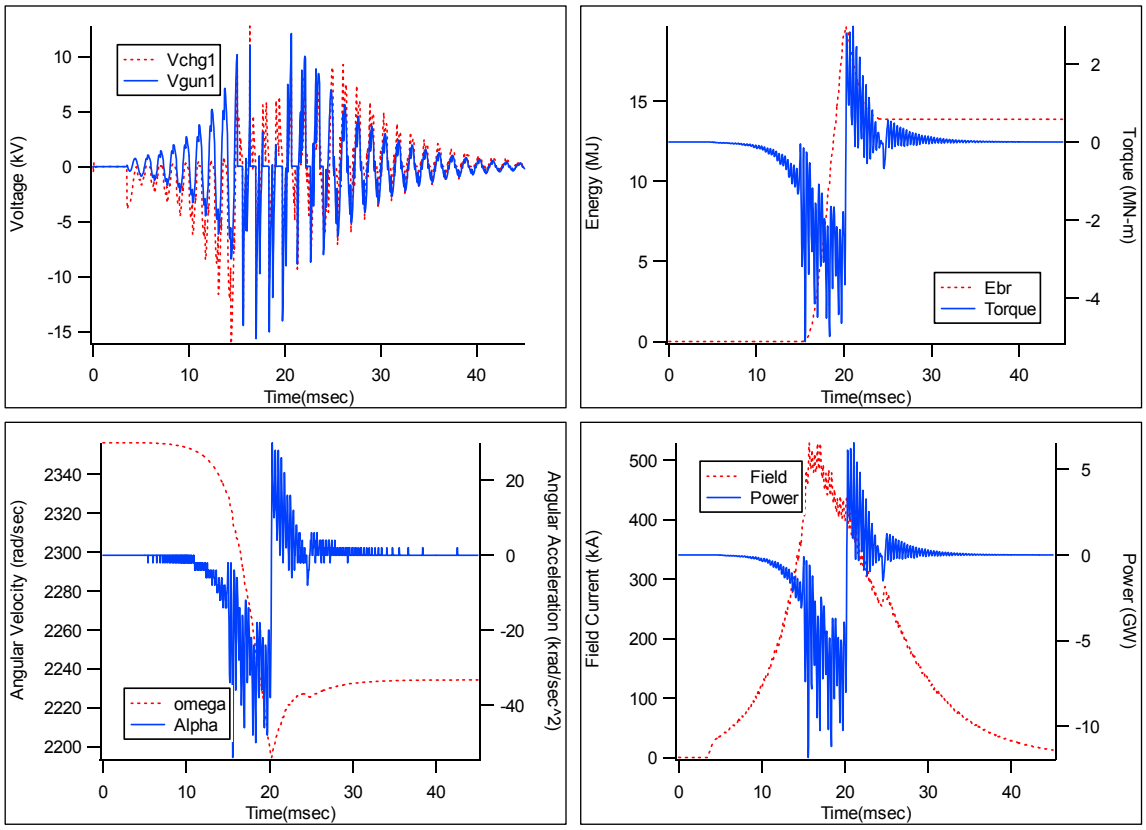

Figure C-4. Miscellaneous Data Shot 1

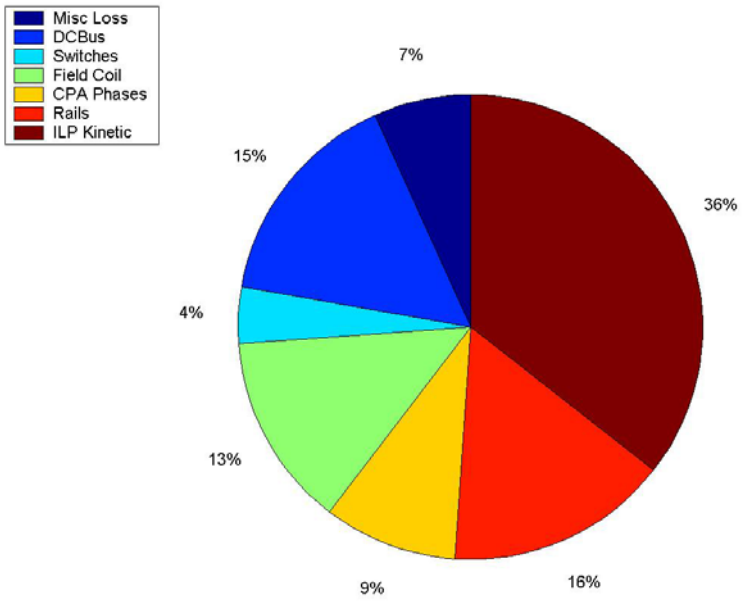

Figure C-5. PPS System Energy Balance and Efficiency (shot 1, 26.2 MJ used)

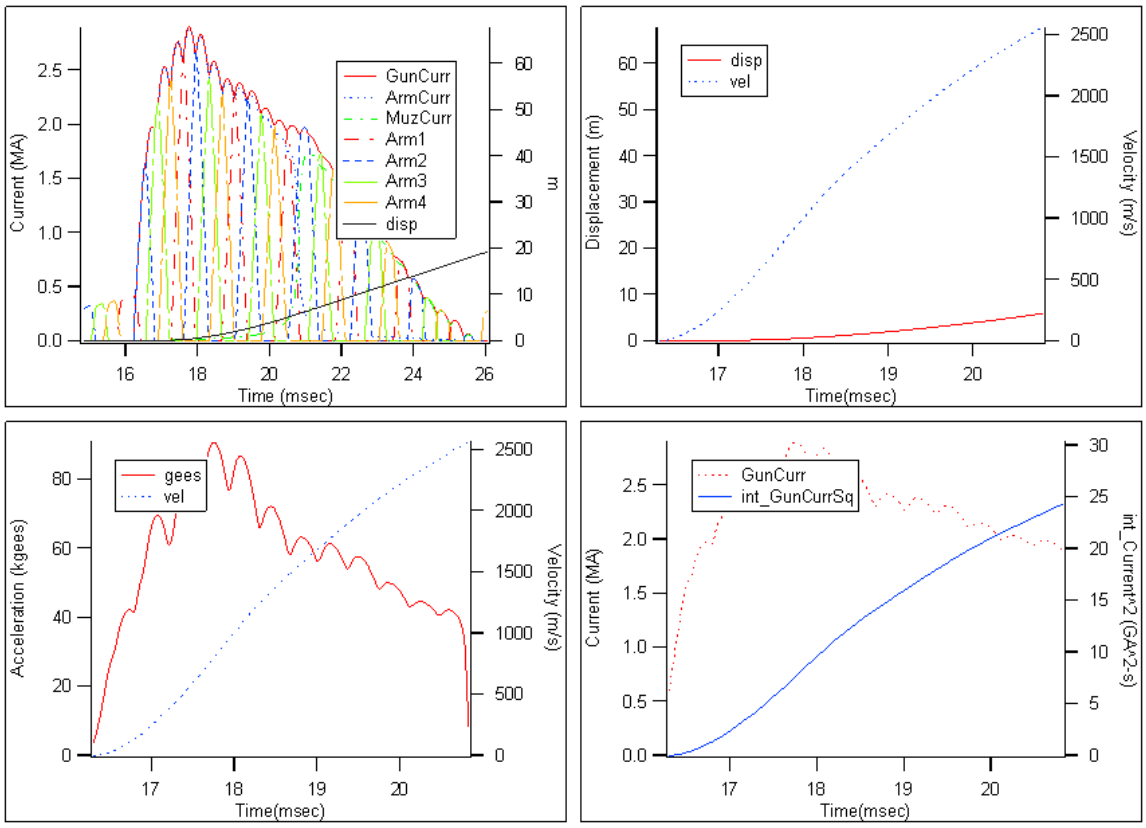

Figure C-6. Gun Performance Data Shot 2

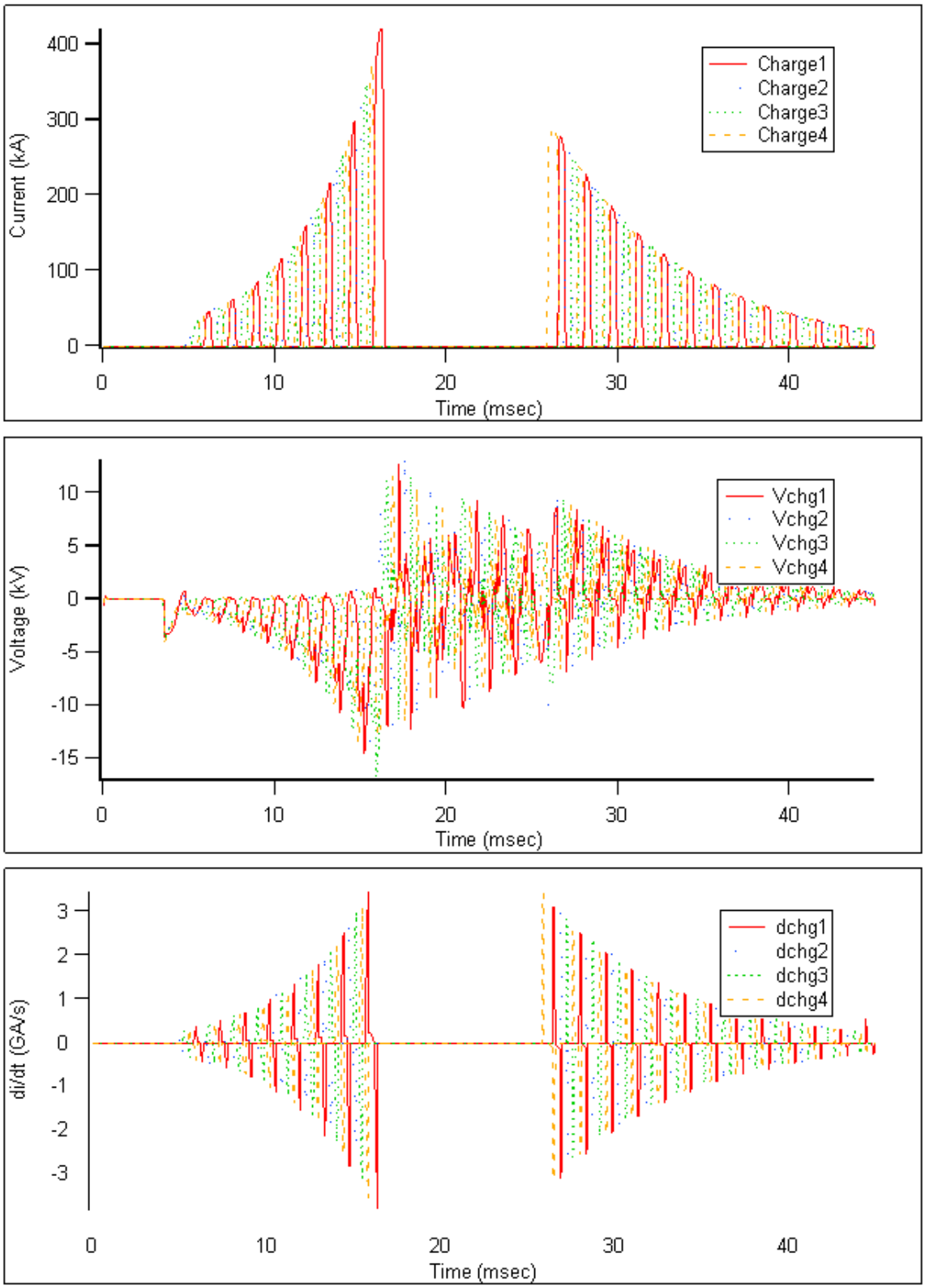

Figure C-7. Field Coil Converter Data Shot 2

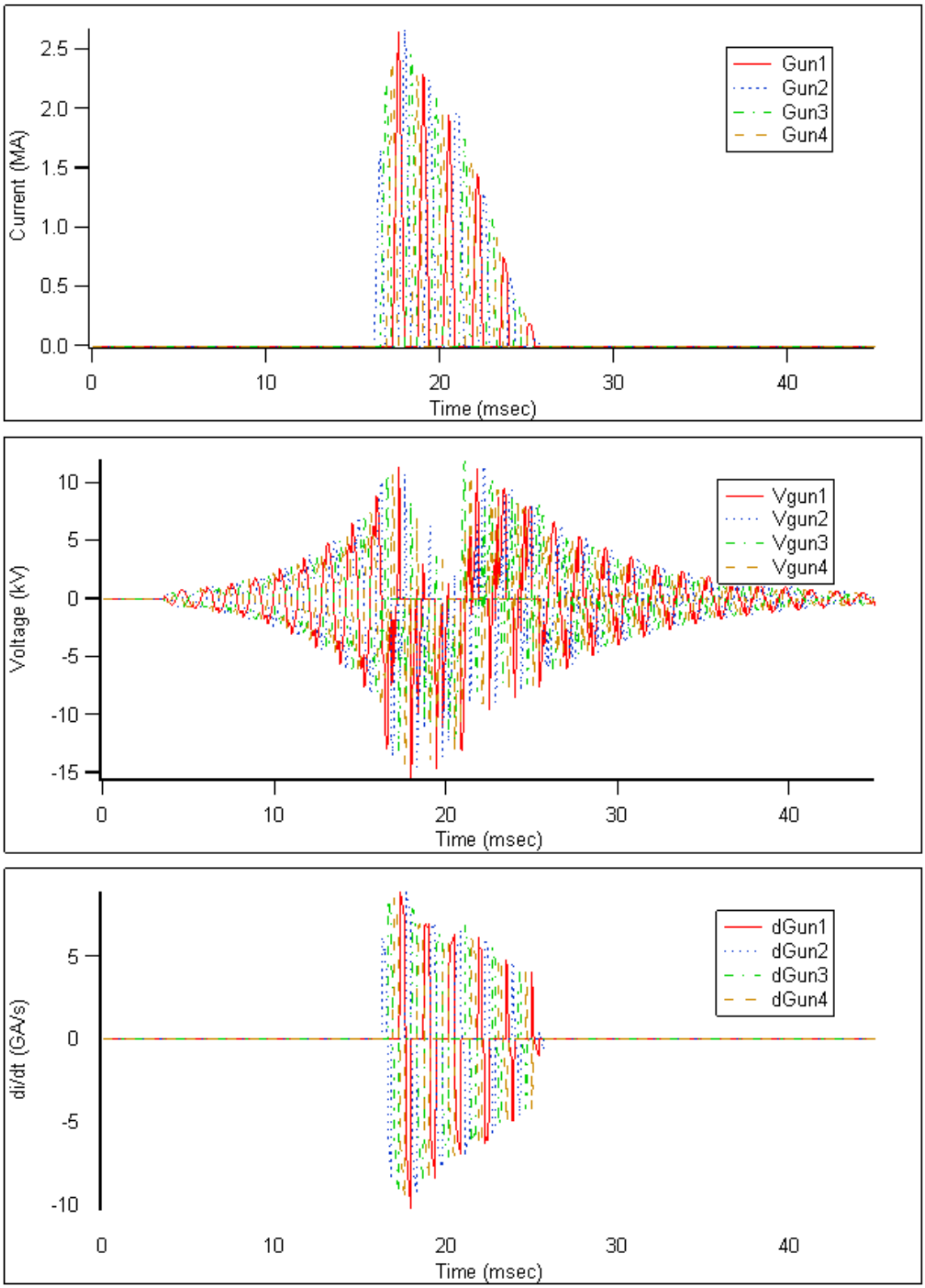

Figure C-8. Gun Switch Converter Data Shot 2

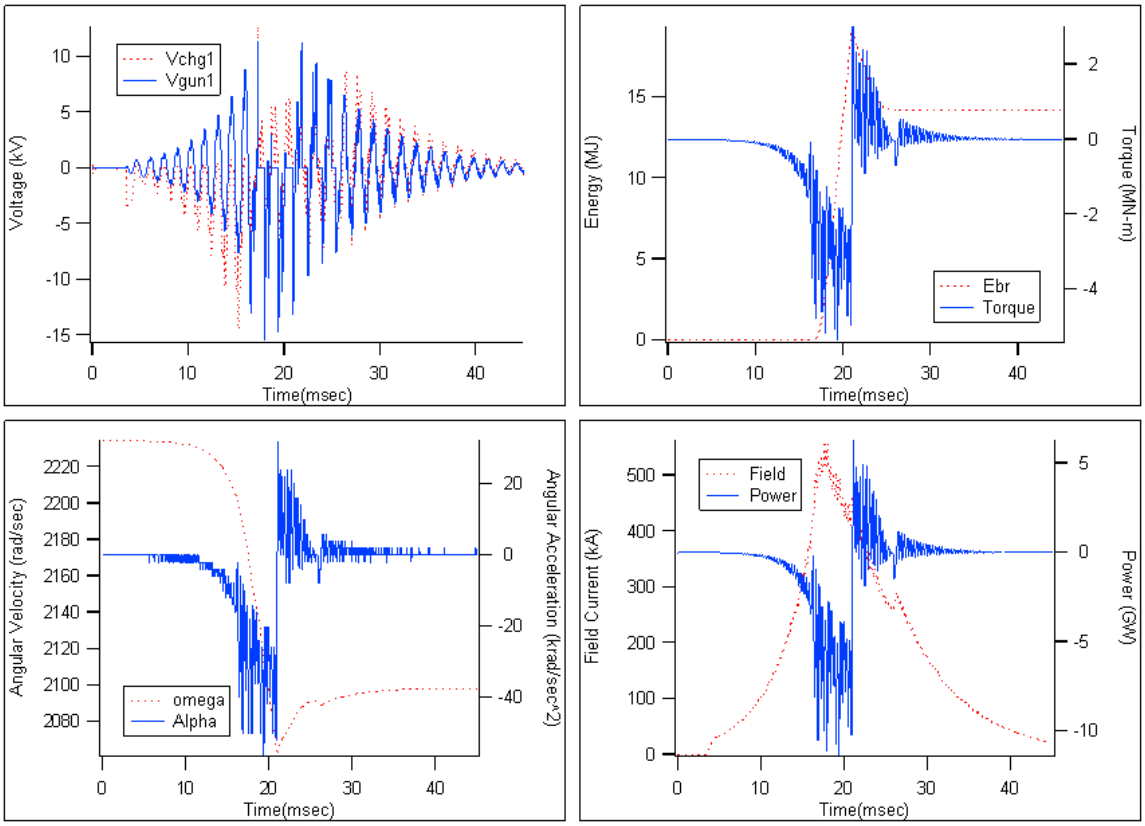

Figure C-9. Miscellaneous Data Shot 2

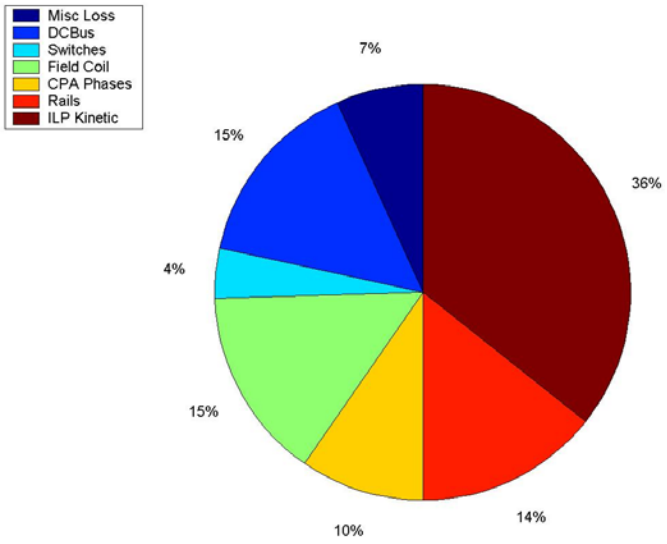

Figure C-10. PPS System Energy Balance and Efficiency (shot 2, 27.7 MJ used)

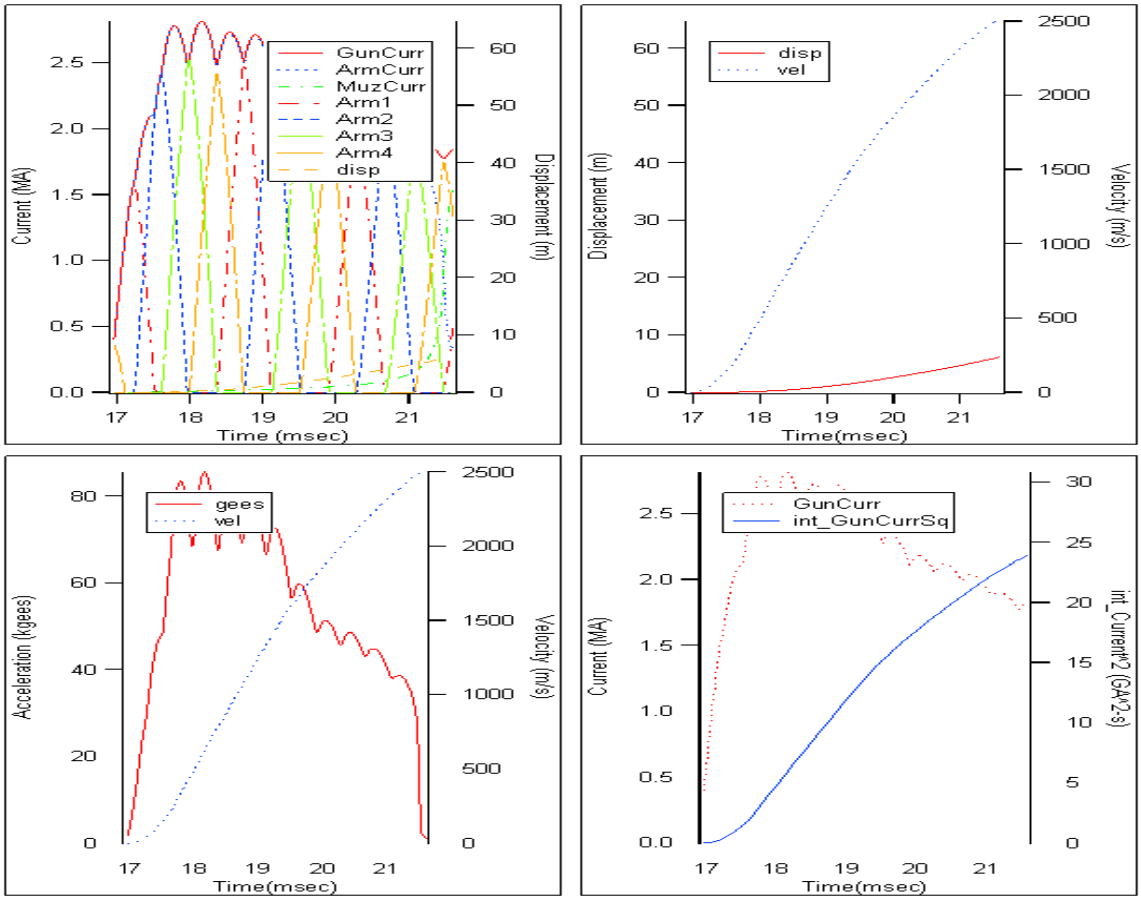

Figure C-11. Gun Performance Data Shot 3

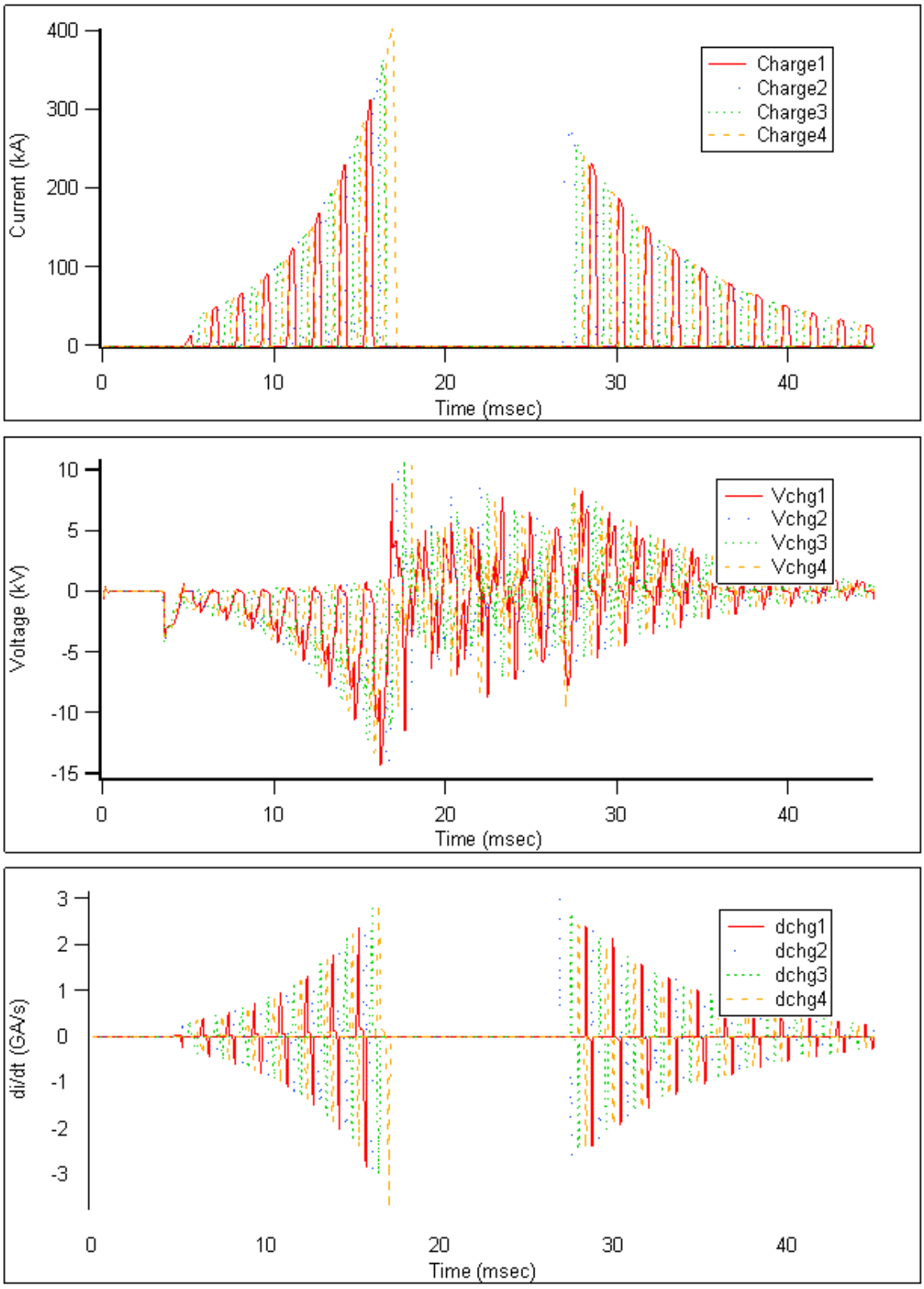

Figure C-12. Field Coil Converter Data Shot 3

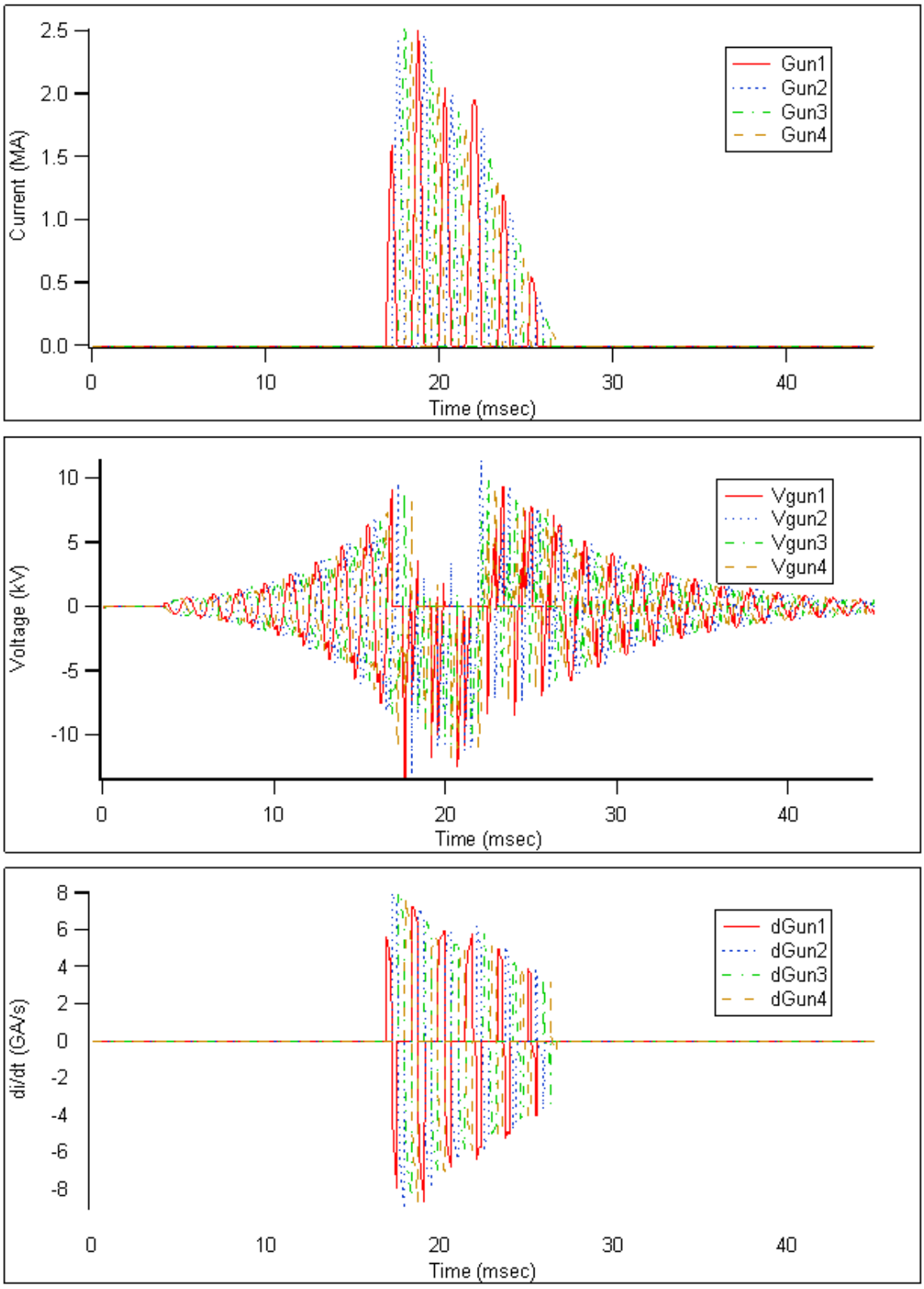

Figure C-13. Gun Switch Converter Data Shot 3

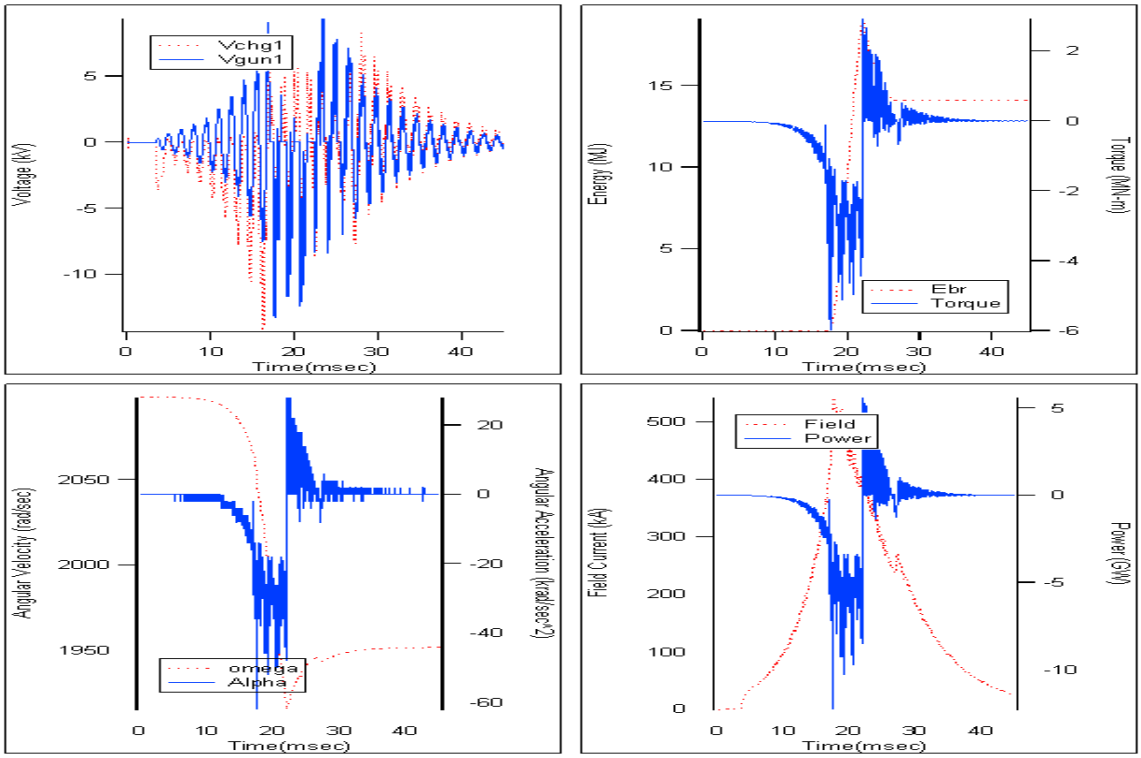

Figure C-14. Miscellaneous Data Shot 3

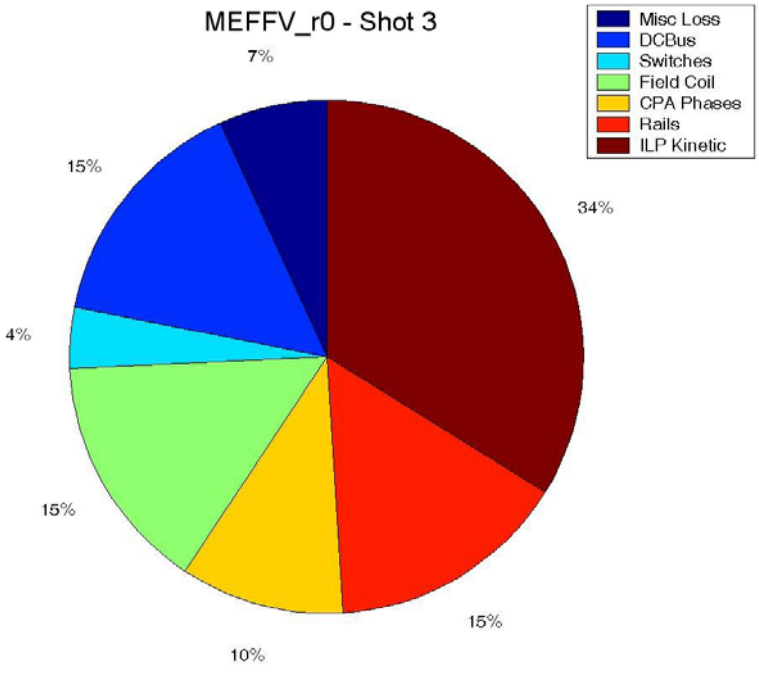

Figure C-15. PPS System Energy Balance and Efficiency (shot 3, 27.8 MJ used)

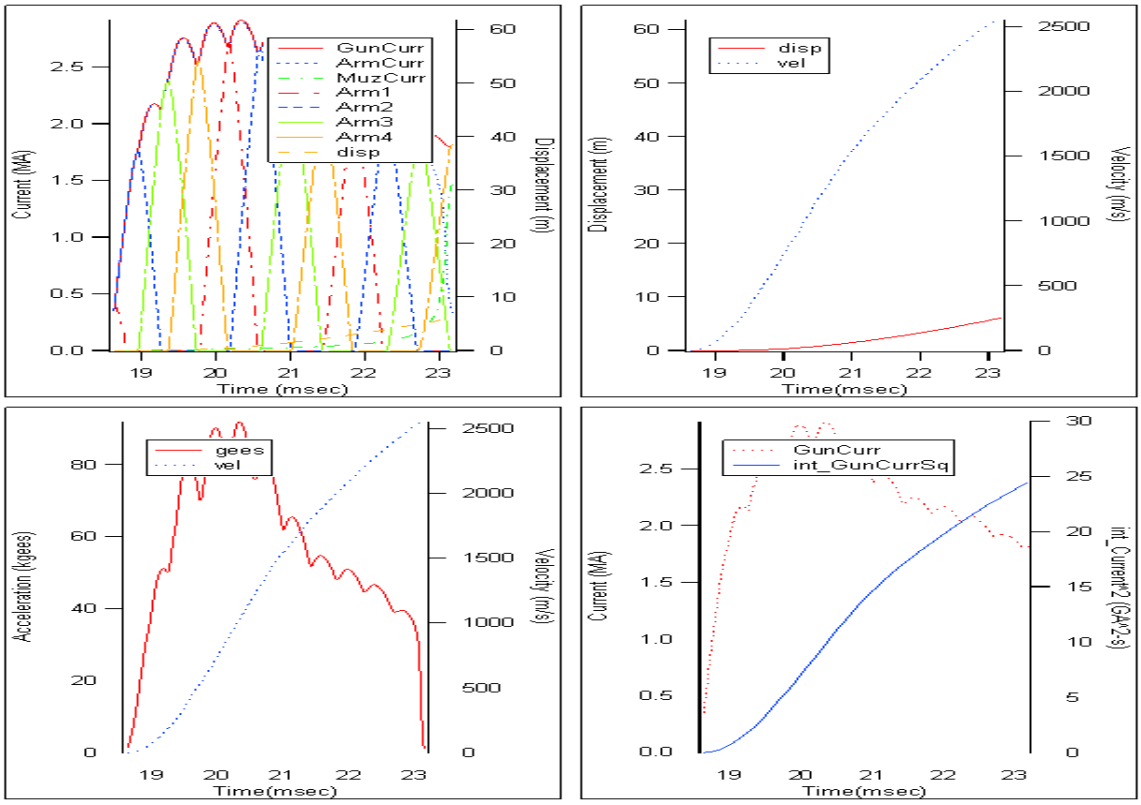

Figure C-16. Gun Performance Data Shot 4

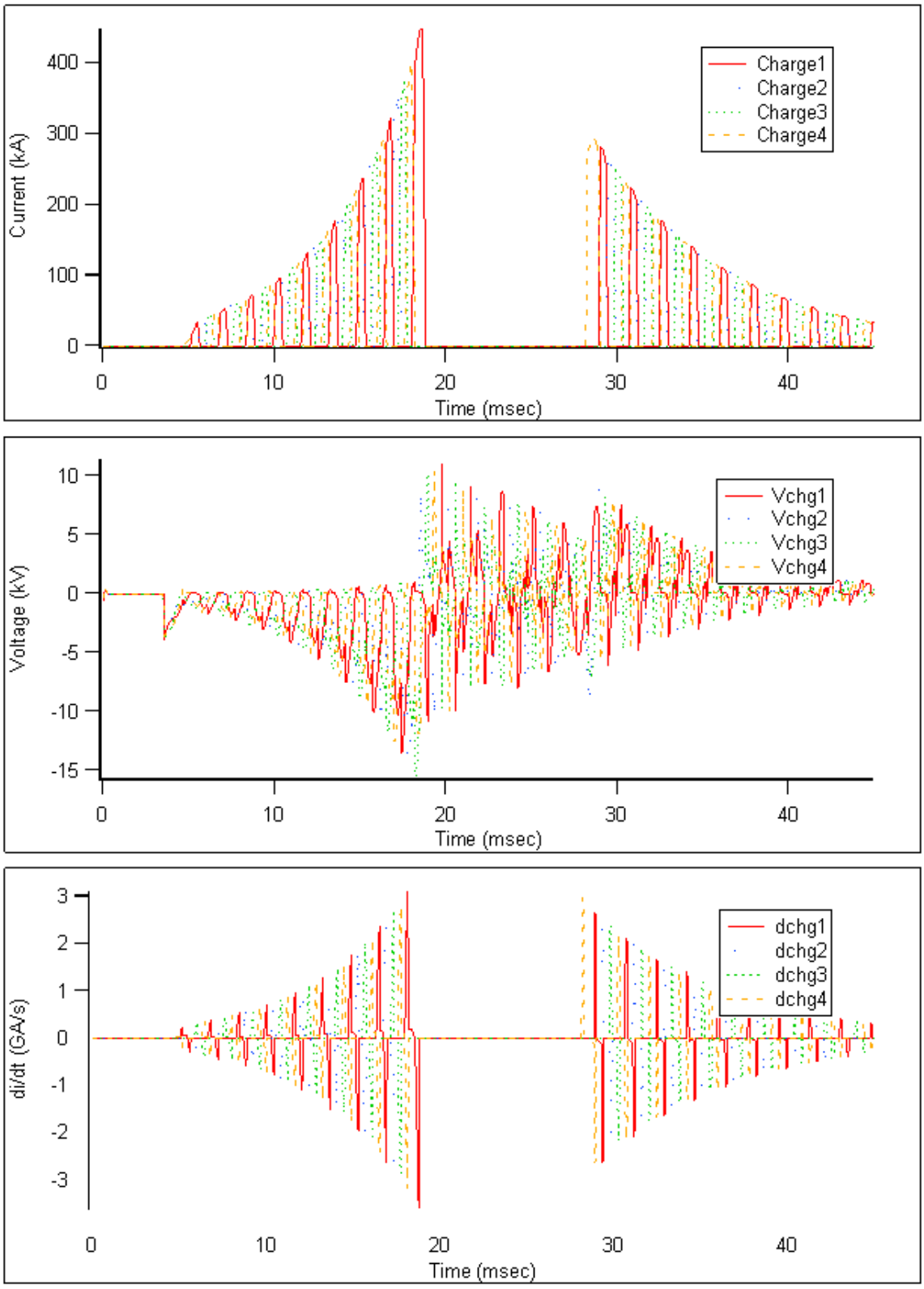

Figure C-17. Field Coil Converter Data Shot 4

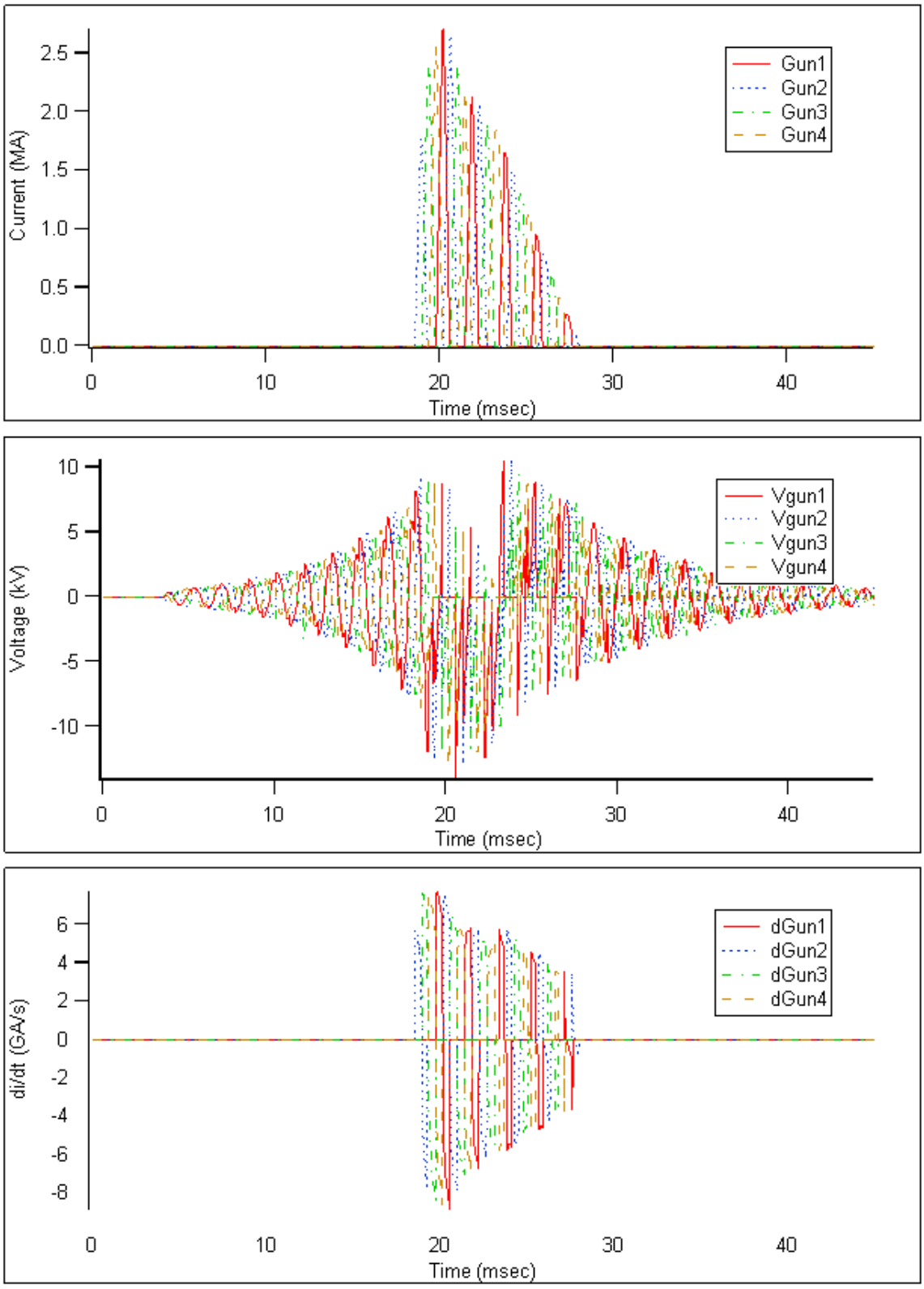

Figure C-18. Gun Switch Converter Data Shot 4

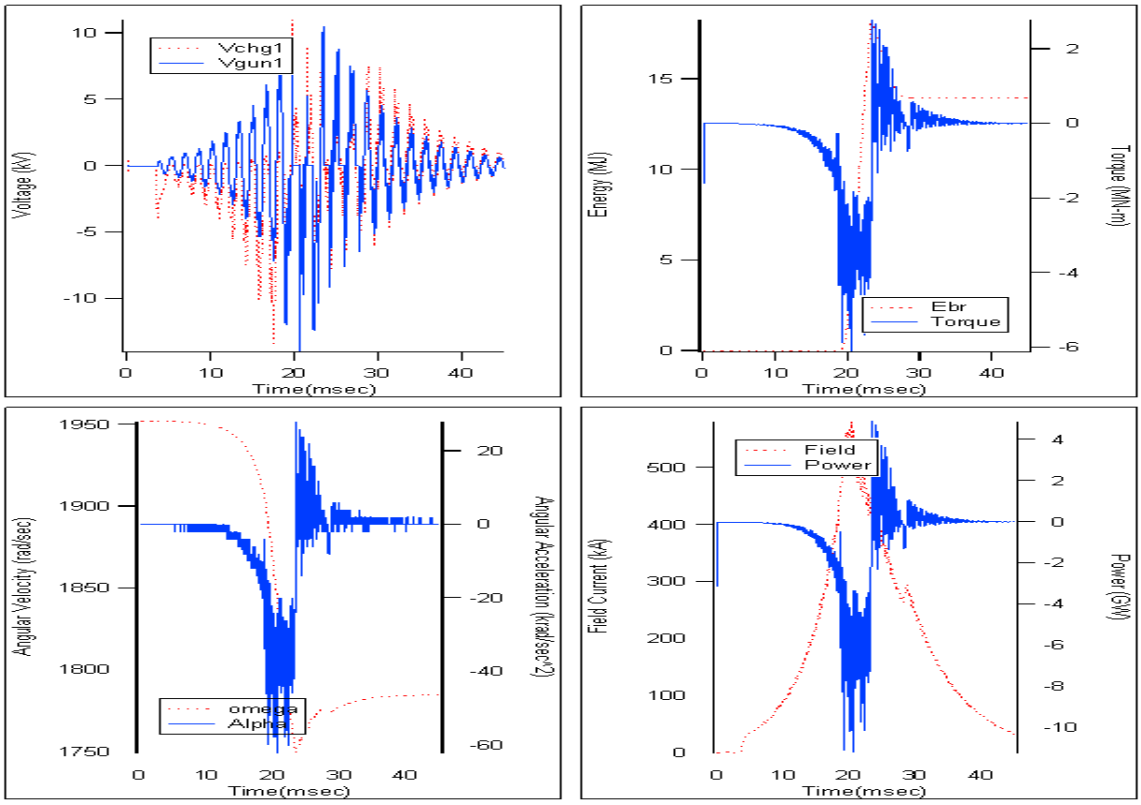

Figure C-19. Miscellaneous Data Shot 4

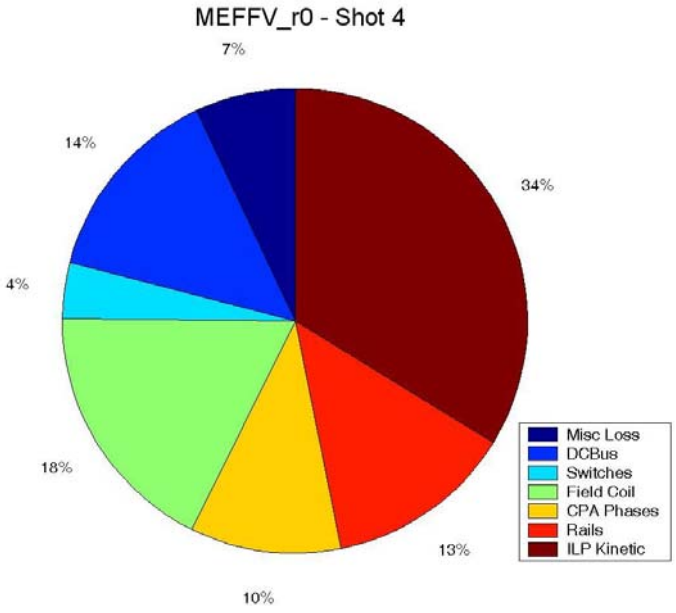

Figure C-20. PPS System Energy Balance and Efficiency (shot 4, 29.3 MJ used)

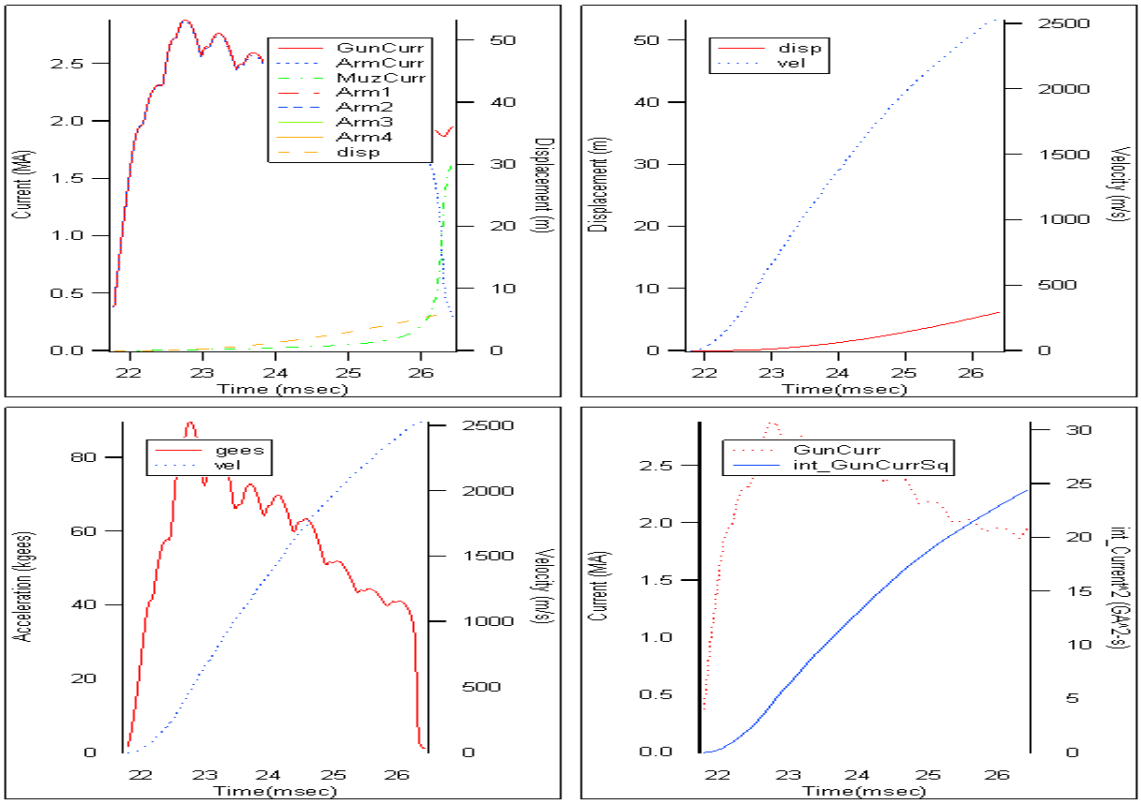

Figure C-21. Gun Performance Data Shot 5

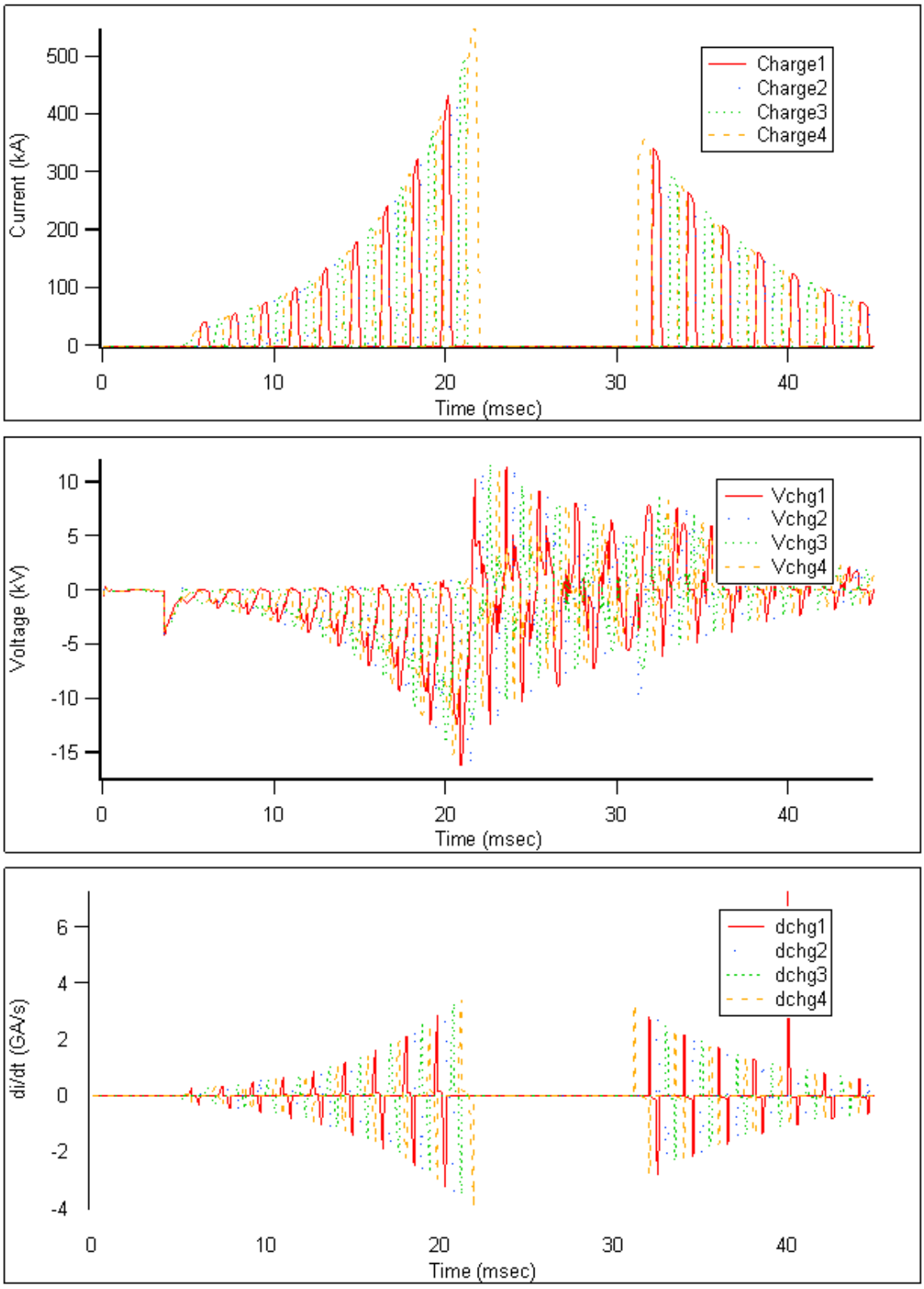

Figure C-22. Field Coil Converter Data Shot 5

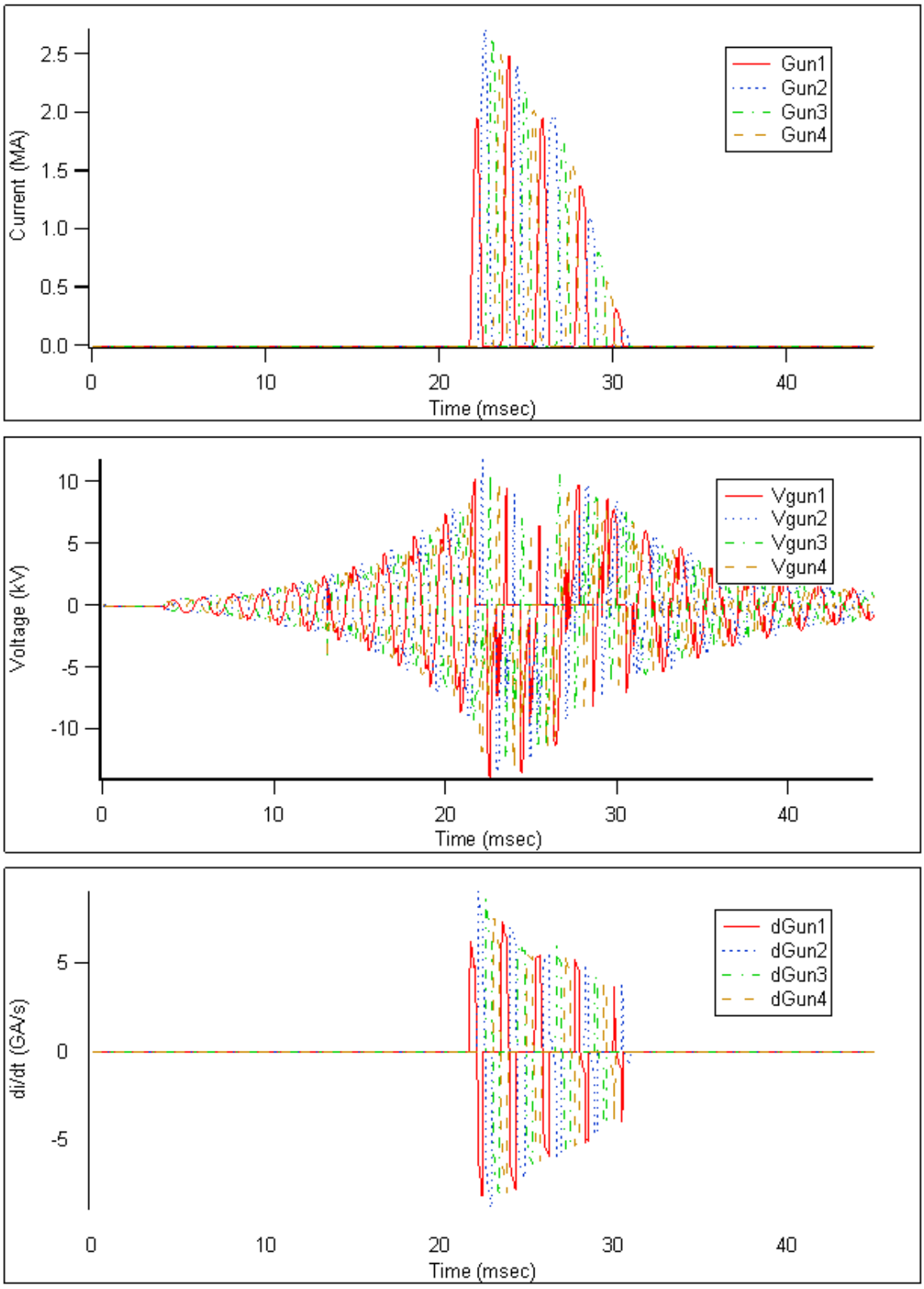

Figure C-23. Gun Switch Converter Data Shot 5

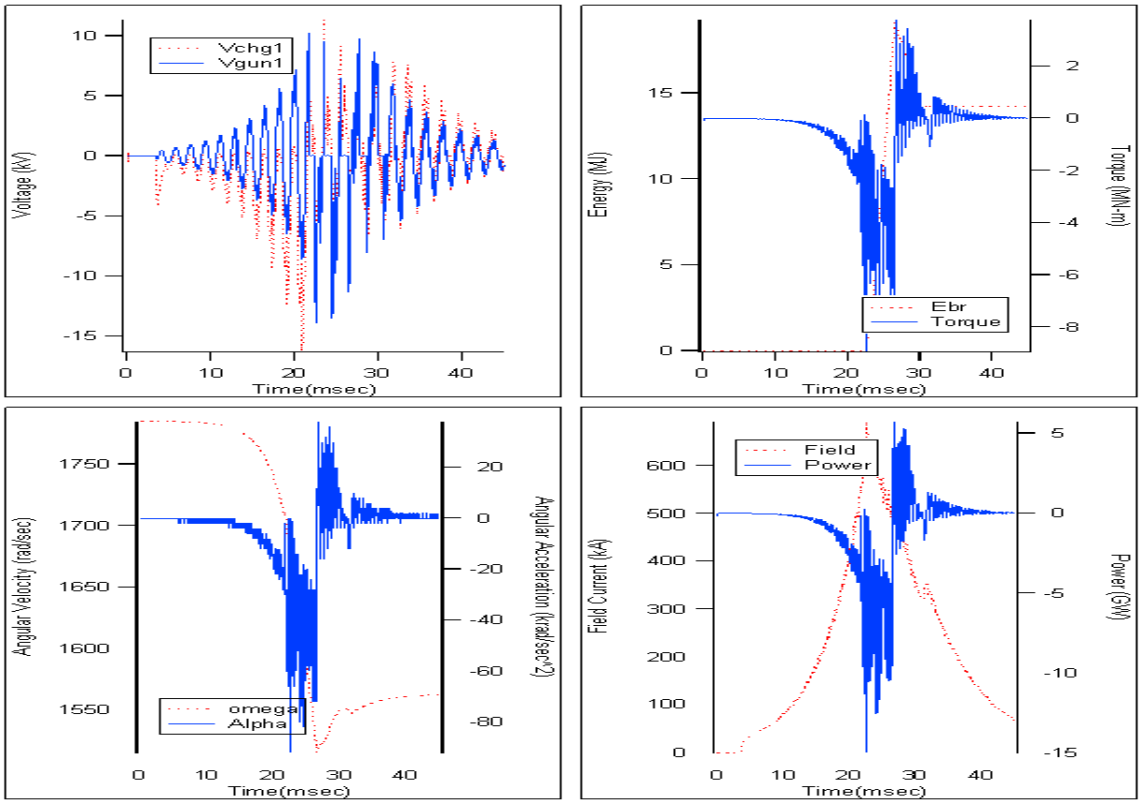

Figure C-24. Miscellaneous Data Shot 5

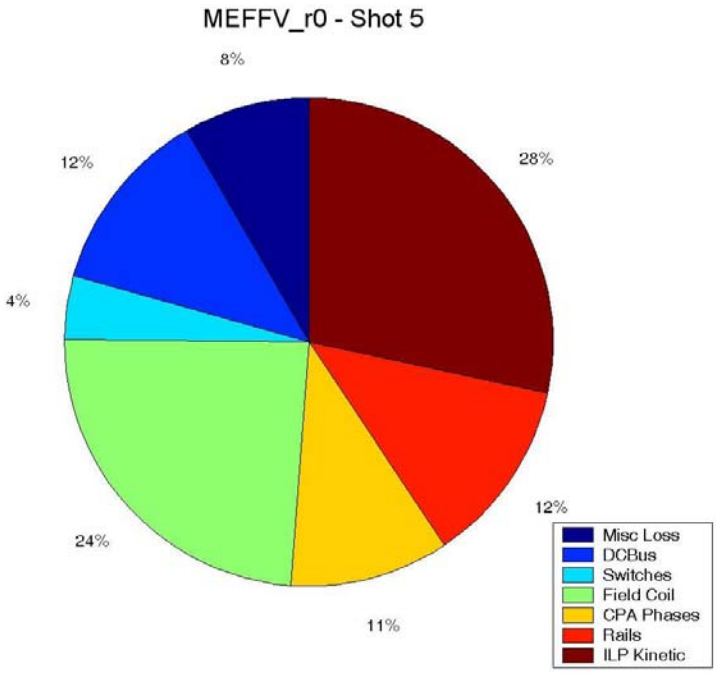

Figure C-25. PPS System Energy Balance and Efficiency (shot 5, 34.9 MJ used)

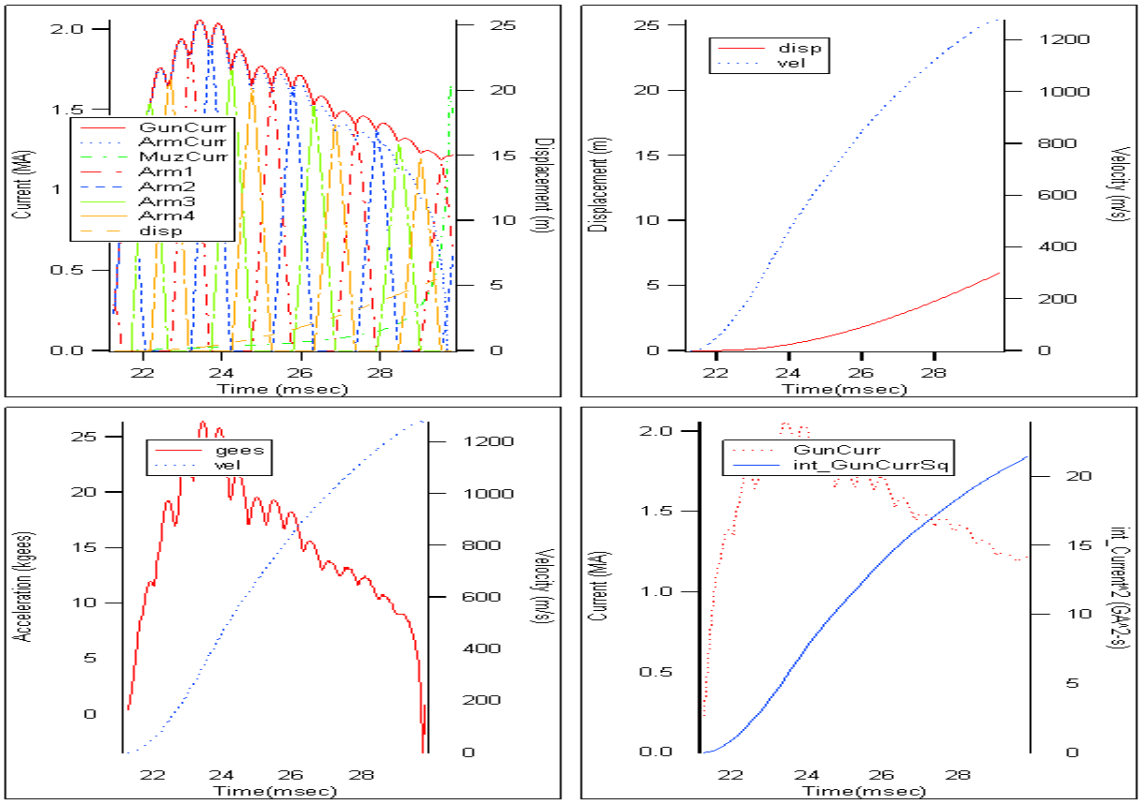

Figure C-26. Gun Performance Data Shot 6 (HE round)

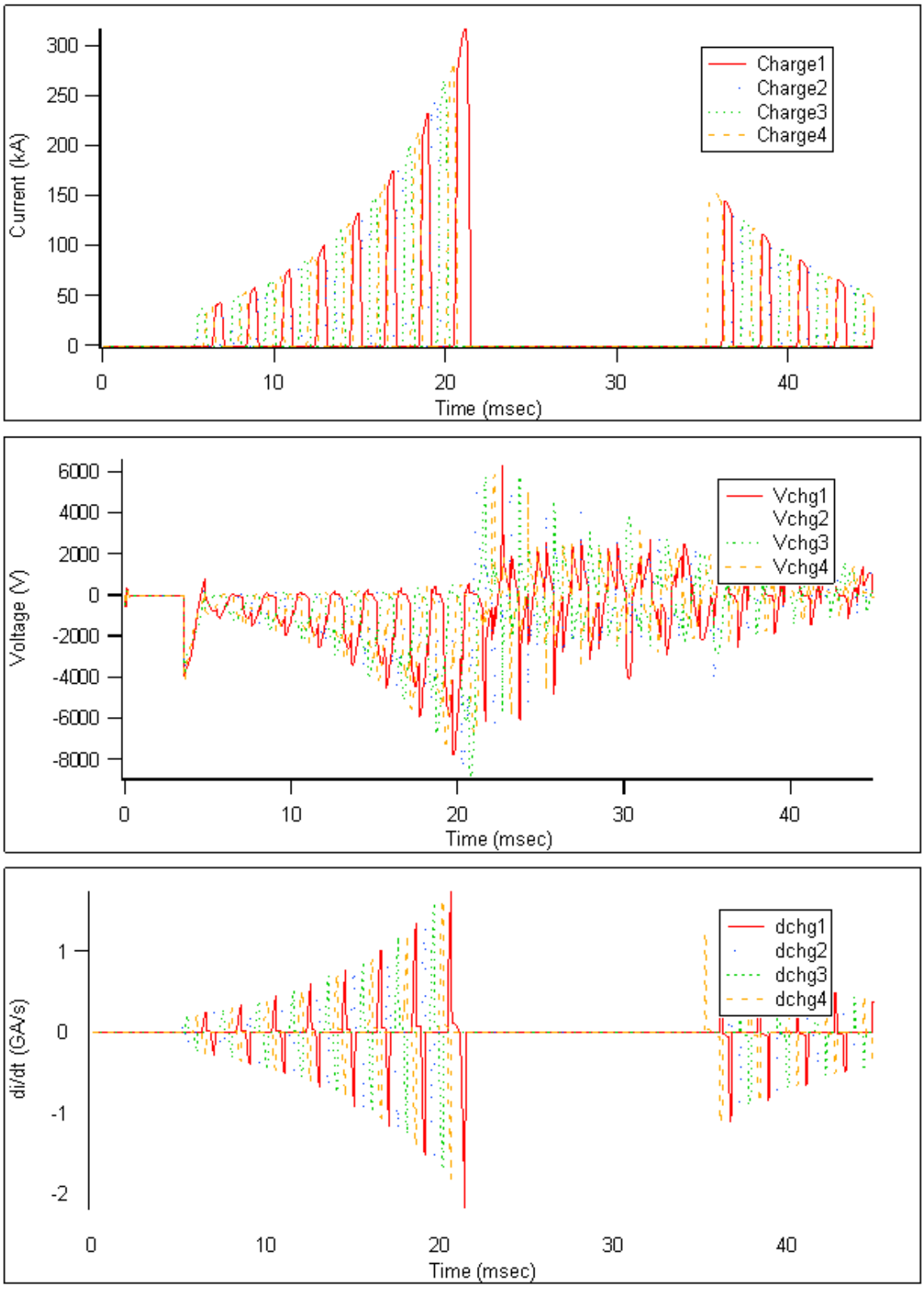

Figure C-27. Field Coil Converter Data Shot 6 (HE round)

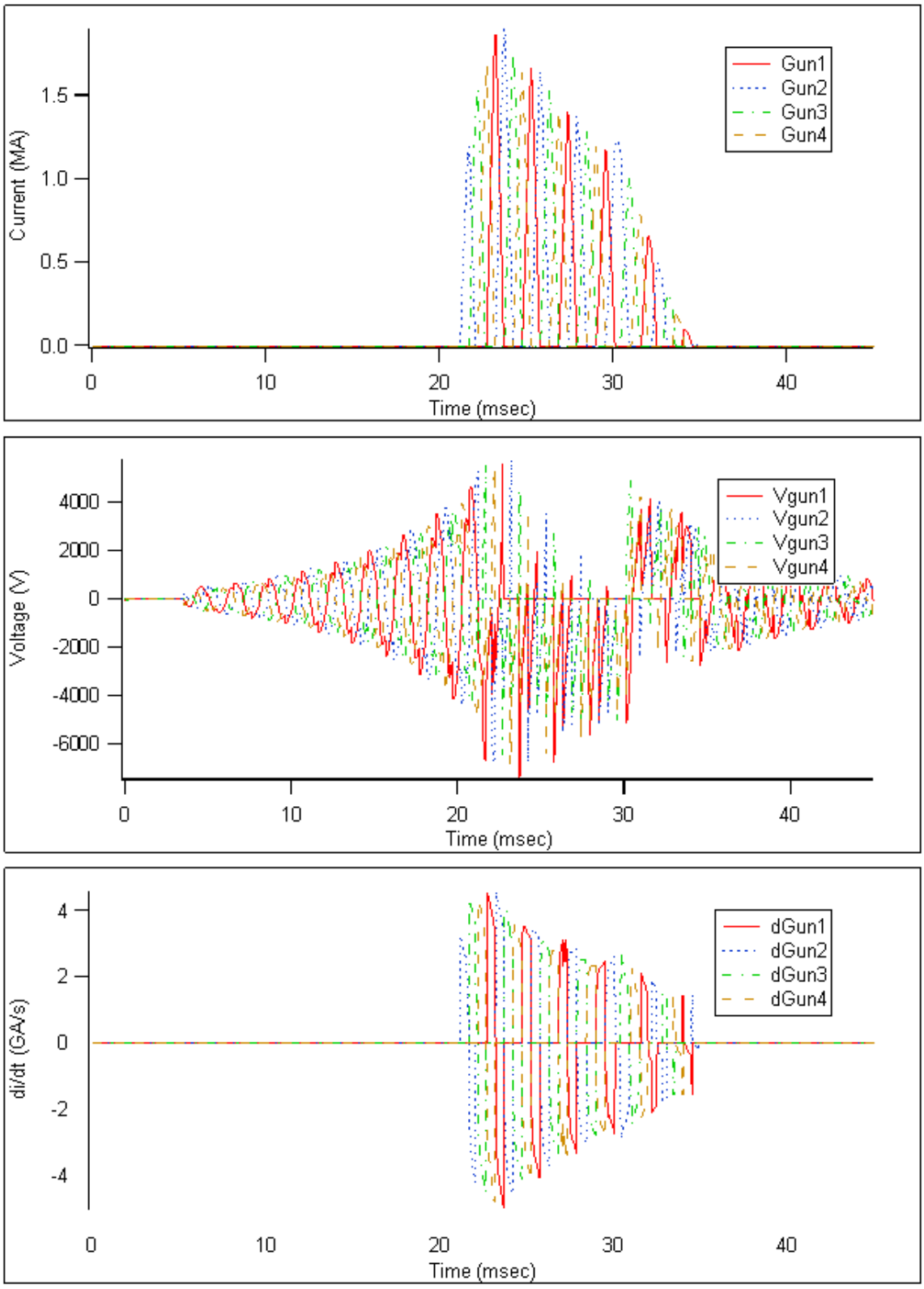

Figure C-28. Gun Switch Converter Data Shot 6 (HE round)

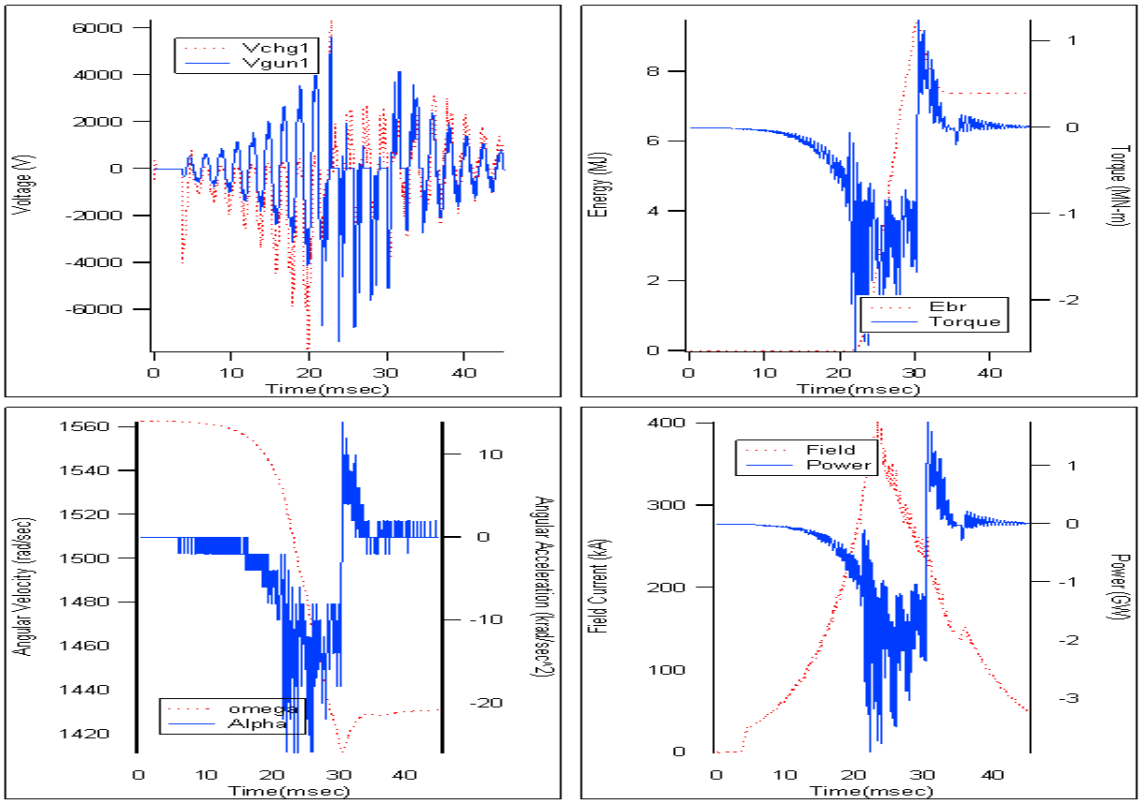

Figure C-29. Miscellaneous Data Shot 6 (HE round)

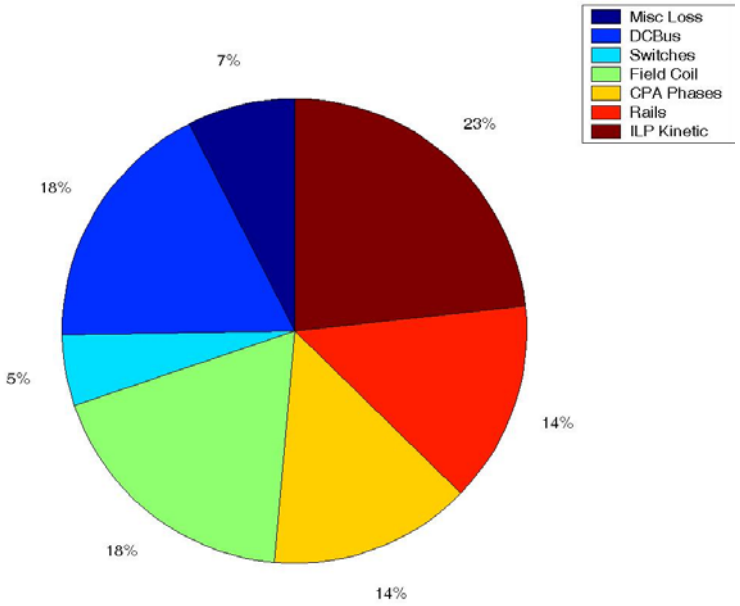

Figure C-30. PPS System Energy Balance and Efficiency (shot 6, HE round, 18.5 MJ used)

APPENDIX D: Device Scaling

Using SPT411A as basis:

Exterior Dimensions of SPT411A

Dimensions from data sheet

Outside diameter of package:

$$A_{411} := 162.7 \cdot mm$$

Inside diameter of pole:

$$B_{411} := 106.4 mm$$

Longitudinal thickness of outside insulator:

$$C_I := 20.12 \cdot mm$$

Height of pole from cup surface to longitudinal edge:

$$D_{411} := 7.71 \cdot mm$$

Radial Thickness of outside insulator

$$t_I := \frac{\left(A_{411} - B_{411}\right)}{2}$$

$$t_I = 28.15 \times 10^{-3} m$$

Measured Dimensions

Height of pole cup copper from cup surface:

$$h_{cup} := 3 \cdot mm$$

Radial length of cup copper from surface projection to edge:

$lip_{cup} := 6 \cdot mm$

Diameter of active silicon

$d_{as411} := 125 \cdot mm$

Dimensions of switch element:

Active silicon:

$t_{as411} := 0.0011 \cdot m$

$d_{as411} := 0.125 \cdot m$

$$A_{as411} := \pi \cdot \left(\frac{d_{as411}}{2} \right)^2$$

$$A_{as411} = 12.27 \times 10^{-3}\, m^2$$

Inactive silicon

$t_{is411} := t_{as411}$

$d_{is411} := d_{as411}$

Strain match element (tungsten):

$t_{sm411} := .76 \cdot mm$

$t_{w411} := 2 \cdot t_{as411} + t_{sm411}$

$$t_{w411} = 2.96 \times 10^{-3}\, m$$

Strain buffer (molybdenum)

$t_{sb} := 0.00076 \cdot m$

Measured masses of 402B (gross construction is the same as 411A)

Outside package of 402B including cups:

$mp := 79.18 \cdot gm + 182.53 \cdot gm$

$$m_P = 261.71 \times 10^{-3}\,kg$$

Strain buffer:

$$m_{sb} := 63.53 \cdot gm$$

Wafer with passivation:

$$m_W := 154.06 \cdot gm$$

$$mass_{measured} := m_P + m_{sb} + m_W$$

$$mass_{measured} = 479.3 \times 10^{-3}\,kg$$

Calculated masses and effective densities of individual components

Pole cup material is copper:

$$\rho_{cu} := 8913 \cdot \frac{kg}{m^3}$$

Thickness of cup copper:

$$t_{cup} := 0.001016 \cdot m$$

Diameter of cup copper is the pole diameter plus length of edge features:

$$m_{cup} := \frac{t_{cup} \cdot \rho_{cu} \cdot \pi \cdot \left[B_{411} + 2 \cdot \left(h_{cup} + lip_{cup} \right) \right]^2}{4}$$

$$m_{cup} = 110.06 \times 10^{-3}\,kg$$

Mass of exterior insulator:

$$m_I := m_P - m_{cup}$$

$$m_I = 151.65 \times 10^{-3}\,kg$$

Effective density of exterior insulator

$$\rho_I := 4 \cdot \frac{m_I}{C_I \cdot \pi \cdot \left(A_{411}^2 - B_{411}^2 \right)}$$

$$\rho_I = 633 \frac{kg}{m^3}$$

Effective density of switch wafer:

$$\rho_{sw} := 4 \cdot \frac{m_W}{\pi \cdot t_{w411} \cdot d_{as411}^2}$$

$$\rho_{sw} = 4.24 \times 10^3 \frac{kg}{m^3}$$

Effective density of the strain buffer (diameter of strain buffer is the same as B):

$$\rho_{sb} := 4 \cdot \frac{m_{sb}}{t_{sb} \cdot \pi \cdot B_{411}^2}$$

$$\rho_{sb} = 9.4 \times 10^3 \frac{kg}{m^3}$$

Electrical Specifications of base device (411A)

Electrical action:

$$A_{E411} := 25 \cdot 10^6 \cdot A^2 \cdot s$$

Rate of current rise at turn on:

$$dI_{411} := 25 \cdot 10^6 \cdot \frac{A}{s}$$

Maximum applied symmetrical voltage:

$$V_{411} := 5000 \cdot V$$

Scaling Example:

5 kV 125 mm device to 11 kV 150 mm device

$V := 11 \cdot kV$

$d_{as} := 150 \cdot mm$

Electrical action:

The action allowed is proportional to the square of the active area and inversely proportional to the wafer thickness (because of additional resistive loss). The thickness is proportional to the voltage.

Thickness of the wafer:

$$t_w := t_{sm411} + 2 \cdot t_{as411} \cdot \frac{V}{V_{411}}$$

$$t_w = 5.6 \times 10^{-3}\, m$$

Active area of wafer:

$$A_{as} := \pi \cdot \left(\frac{d_{as}}{2} \right)^2$$

$$A_{as} = 17.67 \times 10^{-3}\, m^2$$

$$A_E := A_{E411} \cdot \frac{A_{as}^{\,2} \cdot t_{w411}}{A_{as411}^{\,2} \cdot t_w}$$

$$A_E = 27.4 \times 10^{6}\, s A^2$$

Rate of current rise at turn on:

The rate of current rise at turn on is affected by geometrical and non-geometrical factors such as gate structure and power. Therefore, I will assume that the critical di/dt for this device is the same as for the 411A.

Dimensions of device:

Outside thickness at pole:

$$t_p := 2 \cdot t_{cup} + t_w + t_{sb}$$

$$t_p = 8.39 \times 10^{-3}\,\text{m}$$

Inside diameter of pole

$$B := d_{as} \cdot \frac{B_{411}}{d_{as411}}$$

$$B = 127.68 \times 10^{-3}\,\text{m}$$

Exterior insulator:

The exterior insulator consists of a molded insulating labyrinth. Its primary purpose is to prevent surface tracking along the outside edge of the device. The labyrinth effective length is approximately 100 mm and can therefore resist tracking at up to 100 to 300 kV. This estimate neglects corona effects, which should not be an issue at the voltages of interest. As a result, the device will break down through the wafer long before edge tracking can occur. Therefore, for the calculation of overall device diameter and thickness, the same insulator dimensions as the SPT411A will be used unscaled for all devices in the range of 5 kV to 15 kV.

Outside diameter of device:

$$A_o := B + 2 \cdot t_I$$

$$A_o = 183.98 \times 10^{-3}\,\text{m}$$

Height of device at exterior insulator:

$$C_I = 20.12 \times 10^{-3}\,\text{m}$$

Mass of device

Mass of wafer:

$$m_w := \rho_{sw} \cdot t_w \cdot \pi \cdot \frac{d_{as}^{\,2}}{4}$$

$$m_w = 419.71 \times 10^{-3}\,\text{kg}$$

Mass of strain buffer:

$$m_B := \rho_{sb} \cdot t_{sb} \cdot \pi \cdot \frac{B^2}{4}$$

$$m_B = 91.48 \times 10^{-3}\,kg$$

Mass of a pole cup:

$$m_{cup} := \frac{t_{cup} \cdot \rho_{cu} \cdot \pi \cdot \left[B + 2 \cdot \left(h_{cup} + lip_{cup} \right) \right]^2}{4}$$

$$m_{cup} = 150.94 \times 10^{-3}\,kg$$

Mass of exterior insulator:

$$m_I := \rho_I \cdot C_I \cdot \pi \cdot \frac{\left(A_o^2 - B^2 \right)}{4}$$

$$m_I = 175.63 \times 10^{-3}\,kg$$

Mass of assembled switch device:

$$m_D := m_w + m_B + 2 \cdot m_{cup} + m_I$$

$$m_D = 988.7 \times 10^{-3}\,kg$$

Scaling Example:

5 kV 125 mm device to 9 kV 125 mm device

$$V := 9 \cdot kV$$

$$d_{as} := 125 \cdot mm$$

Electrical action:

The action allowed is proportional to the square of the active area and inversely proportional to the wafer thickness (because of additional resistive loss). The thickness is proportional to the voltage.

Thickness of the wafer:

$$t_w := t_{sm411} + 2 \cdot t_{as411} \cdot \frac{V}{V_{411}}$$

$$t_w = 4.72 \times 10^{-3}\,\mathrm{m}$$

Active area of wafer:

$$A_{as} := \pi \cdot \left(\frac{d_{as}}{2} \right)^2$$

$$A_{as} = 12.27 \times 10^{-3}\,\mathrm{m}^2$$

$$A_E := A_{E411} \cdot \frac{A_{as}^{\,2} \cdot t_{w411}}{A_{as411}^{\,2} \cdot t_w}$$

$$A_E = 15.68 \times 10^{6}\,\mathrm{s\,A}^2$$

Rate of current rise at turn on:

The rate of current rise at turn on is affected by geometrical and non-geometrical factors such as gate structure and power. Therefore, I will assume that the critical di/dt for this device is the same as for the 411A.

Dimensions of device:

Outside thickness at pole:

$$t_p := 2 \cdot t_{cup} + t_w + t_{sb}$$

$$t_p = 7.51 \times 10^{-3}\,\mathrm{m}$$

Inside diameter of pole

$$B := d_{as} \cdot \frac{B_{411}}{d_{as411}}$$

$$B = 106.4 \times 10^{-3}\,\mathrm{m}$$

Exterior insulator:

The exterior insulator consists of a molded insulating labyrinth. Its primary purpose is to prevent surface tracking along the outside edge of the device. The labyrinth effective length is approximately 100 mm and can therefore resist tracking at up to 100 to 300 kV. This estimate neglects corona effects, which should not be an issue at the voltages of interest. As a result, the device will break down through the wafer long before edge tracking can occur. Therefore, for the calculation of overall device diameter and thickness, the same insulator dimensions as the SPT411A will be used unscaled for all devices in the range of 5 kV to 15 kV.

Outside diameter of device:

$$A_o := B + 2 \cdot t_I$$

$$A_o = 162.7 \times 10^{-3}\,\text{m}$$

Height of device at exterior insulator:

$$C_I = 20.12 \times 10^{-3}\,\text{m}$$

Mass of device

Mass of wafer:

$$m_w := \rho_{sw} \cdot t_w \cdot \pi \cdot \frac{d_{as}^{\,2}}{4}$$

$$m_w = 245.66 \times 10^{-3}\,\text{kg}$$

Mass of strain buffer:

$$m_B := \rho_{sb} \cdot t_{sb} \cdot \pi \cdot \frac{B^2}{4}$$

$$m_B = 63.53 \times 10^{-3}\,\text{kg}$$

Mass of a pole cup:

$$m_{cup} := \frac{t_{cup} \cdot \rho_{cu} \cdot \pi \cdot \left[B + 2 \cdot \left(h_{cup} + lip_{cup} \right) \right]^2}{4}$$

$$m_{cup} = 110.06 \times 10^{-3}\,kg$$

Mass of exterior insulator:

$$m_I := \rho_I \cdot C_I \cdot \pi \cdot \frac{\left(A_o^2 - B^2\right)}{4}$$

$$m_I = 151.65 \times 10^{-3}\,kg$$

Mass of assembled switch device:

$$m_D := m_W + m_B + 2 \cdot m_{cup} + m_I$$

$$m_D = 680.97 \times 10^{-3}\,kg$$

SiC Device Scaling

Scaling based on SPT411 properties and Silicon Carbide semiconductor property scaling fron silicon published in:: Development of SiC High Voltage Power Semiconductor Devices in KANSAI EPC, Yoshitaka Sugawara, Technical Research Center, The KANSAI Electric Power Company. Bonzai.

Properties of SiC semiconductor (SiC/Si)		Performance of SiC power device		Impact for equipment
Melting point	2X	High temperature operation	3X	Simple heat sink
Bandgap	3X	High breakdown voltage	10X	Device number reduction
Breakdown field	10X	Wide safe operation area	30X	Snubberless, Simple Protection circuit
Thermal conductivity	3X	High current density-Low loss	100X	Small size, High efficiency
Saturation carrier velocity	2X	High speed	10X	High speed, Small size

Largest SiC device tested under pulsed power conditions is 6 mm by 6 mm:

$$V := 11 \cdot kV$$

Action rating for a single wafer:

Assume that the voltage standoff of a practical device will be limited by existing passivation and device packaging materials and techniques as well as the break down strength of SiC. Therefore, the thickness of the wafer:

$$t_w := t_{sm411} + 2 \cdot t_{as411} \cdot \frac{V}{V_{411} \cdot 5}$$

$$t_w = 1.73 \times 10^{-3}\,\text{m}$$

Active area of wafer:

$$A_{as} := \left(6 \cdot 10^{-3} \cdot \text{m}\right)^2$$

$$A_{as} = 36 \times 10^{-6}\,\text{m}^2$$

The action rating will be governed by losses (thickness) allowable current density and allowable temperature rise. Assume that a practical device will be limited by the allowable temperature rise of the SiC and by packaging materials. The range from the table is a factor of 10 to 100 There fore limit rise over Si allowable to a factor of .

$$f := 10$$

$$A_E := f A_{E411} \cdot \frac{A_{as}^2 \cdot t_{w411}}{A_{as411}^2 \cdot t_w}$$

$$A_E = 3.69 \times 10^3\,\text{s}\,\text{A}^2$$

Rate of current rise at turn on will be limited by allowable temperature rise

$$Rise_{crit} := f \cdot 20000 \cdot 10^6 \cdot \frac{A}{s}$$

$$Rise_{crit} = 200 \times 10^9\,\frac{A}{s}$$

The 6 mm wafers are to be packaged in an array of 216 devices in a conventional package without individual equalization circuits. As a result, difference in device characteristics will cause unequal current sharing, and the device must be designed for the worst case condition.

$n := 216$

For perfect sharing, the allowable ratings are

$A_E := A_E \cdot n^2$

$A_E = 171.94 \times 10^6 \, sA^2$

$Rise_{crit} := Rise_{crit} \cdot n$

$Rise_{crit} = 43.2 \times 10^{12} \frac{A}{s}$

assume a tolerance in current sharing characteristics

$tol := .3$

The overall device must be derated by a factor DF

$$DF := \frac{[\,1 + tol + (n-1)\cdot(1-tol)\,]}{n\cdot(1+tol)}$$

$DF = 540.6 \times 10^{-3}$

$A_E := A_E \cdot DF$

$A_E = 92.95 \times 10^6 \, sA^2$

APPENDIX E: Adiabatic Temperature Rise Of Pole Pieces From Thyristor Electrical Loss

Field coil and Gun Switch Converters:

Data files hold the vectors containing the worst-case currents for each converter.

$I_{gsc} := I_{gsc} \cdot A$

$I_{fcc} := I_{fcc} \cdot A$

$dt := 2.5 \cdot 10^{-5} \cdot s$

Number of alternators in modeled pps

$n_a := 2$

Number of poles in a phase:

$n_{pole} := 4$

Number of parallel devices in a pole

$n_{gscp} := 3$

$n_{fccp} := 1$

Nominal current in a device

$$I_{gsc} := \frac{I_{gsc}}{n_a \cdot n_{pole} \cdot n_{gscp}}$$

$$I_{fcc} := \frac{I_{fcc}}{n_a \cdot n_{pole} \cdot n_{fccp}}$$

On-state voltage drop is defined by the behavior of an SPT411A

$V_{gscdev} := 168 \cdot 10^{-6} \cdot \Omega \cdot I_{gsc} + 0.7 \cdot V$

$$V_{fccdev} := 168 \cdot 10^{-6} \cdot \Omega \cdot I_{fcc} + 0.7 \cdot V$$

$$P_{gscdev} := \overrightarrow{\left(I_{gsc} \cdot V_{gscdev}\right)}$$

$$P_{fccdev} := \overrightarrow{\left(I_{fcc} \cdot V_{fccdev}\right)}$$

Differential energy loss per device per timestep:

$$E_{gscdev} := P_{gscdev} \cdot dt$$

$$E_{fccdev} := P_{fccdev} \cdot dt$$

Energy loss per device integrated over a shot:

$$\sum E_{gscdev} = 2.3 \times 10^{3} J$$

$$\sum E_{fccdev} = 1.4 \times 10^{3} J$$

In a combined FCC and GSC module, there are 12 thyristors, 7 connection-type pole pieces that weigh 0.77 kg and 8 pole pieces that weigh 0.72 kg. Definine an average pole piece mass per device:

$$m_{con} := 7 \cdot 0.77 \cdot kg$$

$$m_{pole} := 8 \cdot 0.72 \cdot kg$$

$$m_{dev} := \frac{\left(m_{con} + m_{pole}\right)}{12}$$

$$m_{dev} = 0.9\,kg$$

At 100 K:

$$c_{pAl} := 963 \cdot \frac{J}{kg \cdot K}$$

$$\Delta T_{gscdev} := \frac{\sum E_{gscdev}}{m_{dev} \cdot c_{pAl}}$$

$$\Delta T_{gscdev} = 2.6\,K$$

per shot

$$\Delta T_{fccdev} := \frac{\sum E_{fccdev}}{m_{dev} \cdot c_{pAl}}$$

$$\Delta T_{fccdev} = 1.6\,K$$

per shot

Free wheel leg:

$$I_{fwl} := I_{fwl} \cdot A$$

$$n_{fwlp} := 6$$

$$I_{fwl} := \frac{I_{fwl}}{n_a \cdot n_{fwlp}}$$

$$V_{fwldev} := 168 \cdot 10^{-6} \cdot \Omega \cdot I_{fwl} + 0.7 \cdot V$$

$$P_{fwldev} := \overrightarrow{\left(I_{fwl} \cdot V_{fwldev}\right)}$$

$$E_{fwldev} := P_{fwldev} \cdot dt$$

$$\sum E_{fwldev} = 3.1 \times 10^{3}\,J$$

The free wheel leg module has 12 thyristors (2 series by 6 parallel), 7 connection-type pole pieces that weigh 0.77 kg and 6 pole pieces that weigh 0.72 kg. Definine an average pole piece mass per device:

$$m_{con} := 7 \cdot 0.77 \cdot kg$$

$$m_{pole} := 6 \cdot 0.72 \cdot kg$$

$$m_{dev} := \frac{\left(m_{con} + m_{pole}\right)}{12}$$

$m_{dev} = 0.8\,kg$

$$\Delta T_{fwldev} := \frac{\sum E_{fwldev}}{m_{dev} \cdot c_{pAl}}$$

$\Delta T_{fwldev} = 3.9\,K$ per shot